TOHOKU GAKUIN UNIVERSITY

GRADUATE SCHOOL OF HUMAN INFORMATICS

LARGE SCALE LANDSLIDE RISK EVALUATION BY AERIAL PHOTOGRAPH INTERPRETATION AND INTEGRATED AHP APPROACH FOR HUMID TROPICAL REGION BASED ON JAPAN AND VIET NAM FIELD SURVEYS

LE HONG LUONG

Promoter: Prof. TOYOHIKO MIYAGI

SENDAI, MARCH 2016

LARGE SCALE LANDSLIDE RISK EVALUATION BY

AERIAL PHOTOGRAPH INTERPRETATION AND

INTEGRATED AHP APPROACH FOR HUMID TROPICAL REGION

BASED ON JAPAN AND VIET NAM FIELD SURVEYS

DISSERTATION

to obtain

the degree of doctor at the Tohoku Gakuin University

by

LE HONG LUONG

ACKNOWLEDGEMENT

CONTENTS

LIST OF FIGURES

LIST OF TABLES

CHAPTER 1. INTRODUCTION

According to Dr. David Varnes, "landslide" is defined as a downslope movement of a mass of rock, debris, or earth down a slope, under the influence of gravity (Varnes, 1978). Landslides are recognized as important "natural hazards" in many areas throughout the world (Crozier and Glade, 2005), probably results in thousands of deaths and tens of billions of dollars of damage each year..

Assessing landslide risk, the probability of landslide occurrence, is extremely important and useful for local residents and for decision makers responsible for land planning projects. They can understand the threats to human life and prepare necessary measures for emergencies.

1.1. Importance of the problem and research objectives

In tropical humid regions such as Vietnam, landslides are hazardous phenomena that occur frequently, destroying human life, damaging structures and infrastructure, and adversely affecting living conditions. Particularly in recent years, economic development and consequent rapid expansion of new settlement areas has occurred, along with expansion of infrastructure such as roads, bridges, and railroads into hazardous areas. Recognizing existing landslide areas and assessing landslide risks poses a difficult challenge for all Vietnamese scientists and civil managers.

Although landslides and related disasters occur frequently in Vietnam, few studies have been conducted to elucidate them. Most specifically examine mapping of landslide susceptibility. No studies devote attention to landforms formed by landslides, or to risk evaluation (probability of landslide occurrence).

Japan has a longer than 60-year history of landslides. Landslide mapping experience has therefore accumulated to a great degree. For aerial photograph interpretation, Japan has many sources of data such as color photographs at many scales and taken in several periods of years (five years or ten years). Therefore, features of landslide morphological forms are clearly identifiable. Japan also has published landslide inventory maps for all areas of the country based on aerial photograph interpretation. In Vietnam, accessing these data sources is extremely difficult. Sometimes it is impossible to use them for scientific work. At the time of this study, only aerial photographs of the 1990s were available. Based on the collected data, it would be beneficial to produce a landslide inventory map of the study area and to clarify the limitations and completeness when producing landslide inventory maps for Vietnam.

Landslide maps can be developed to identify landslide topographic areas with differing past conditions. Such maps are useful to ascertain the probability of landslide recurrence in each landslide topographic area. Such maps are the first step in ensuring that the landslide risk does not exceed an acceptable level in planning future land use. Interpretation of future landslide recurrence requires an understanding of the processes controlling landslides. That process supports risk evaluation. The Japan Landslide Society has developed an inspection sheet for risk evaluation in the Tohoku area. It incorporates geomorphic factors within and beyond landslides. This sheet does not mention geological and weathering features. Humid

tropical countries such as Vietnam have a richly diverse geologic composition. Geology and weathering must play important roles in landslide occurrence and risk evaluation. That inspection sheet must be modified to include perspectives of geological and weathering features.

Ambitions of this work include contributions to reduce landslide damage to communities and to provide scientific approaches for landslide inventory and for risk assessment in humid tropical regions.

1.2. Outline of the work

The thesis is presented in six chapters:

- Chapter 1 introduces the importance of the study, ambitions of the research, and an outline of the thesis.

- Chapter 2 specifically examines the study background. This chapter presents the current situation of landslide disasters and potential disasters in Vietnam, AHP methodology, as well as landslide mapping and history.

- Chapter 3 is a general description of the study areas and the reasons they were chosen this for study. This chapter describes the study areas (Japan and Vietnam) and provides general information related to the type and abundance of landslides and on the local setting, including geography, morphology, lithology, structure, climate, and other physiographic characteristics.

- Chapter 4 presents landslide mapping and discusses features used for landslide identification. Two locations of study areas (Japan and Vietnam) were chosen for landslide recognition through aerial photograph interpretation. At the study area in Japan (Fukayama pastureland), color aerial photographs taken in 1976 at 1/15,000 scale were used for interpretation. Many characteristics presumed to have been formed by landslides were observed around the study area. Field surveys were conducted to elucidate the mechanisms forming these topographic features. At the study area in Vietnam (area between Prao and Kham Duc in central provinces of Vietnam), topographic features such as main scarp, lateral scarp, and landslide body are discussed for recognition and classification. Monochromatic aerial photographs from 1999 were used for interpretation and for development of a landslide inventory map for the study area. Furthermore, this presentation describes the completeness of the landslide inventory maps and factors affecting the quality of landslide inventories between Japan and Vietnam.

- Chapter 5 emphasizes a discussion of risk evaluation and the application of Japan's inspection sheet to humid tropical regions such as Vietnam. Fieldwork was conducted to prove the relation between geologic conditions and landslide occurrences in the study area and to deduce regional characteristics of landslide in Vietnam. Based on fieldwork results geology should be described in an inspection sheet in addition to morphological features. This chapter proposes an initial new inspection sheet for application to Vietnam.

- Chapter 6 presents related discussions and conclusions. This chapter presents conclusions, with proposals and general recommendations for using landslide inventory maps and landslide risk evaluation using the new inspection sheet.

1.3. Personal contributions and positioning of published papers

This thesis presents results of Japan's experiential study and their application to Vietnam. The following list presents the main contributions to landslide studies in Vietnam:

– A large-scale landslide inventory map for area between Prao and Kham Duc in central provinces in Vietnam was produced, extending to 1000 km^2 for an area with approximately 20,000 residents. At each landslide, 13 characteristics were recorded and listed in an accompanying database table.

– Experiments assessing the application of Japan's inspection sheet for risk evaluation were conducted in 36 case studies in the study area.

– Fieldwork was conducted to demonstrate the influence of geologic conditions on landslide occurrences (type and patterns) in the study area.

– An initial inspection sheet for risk evaluation was proposed using the AHP approach in the case of humid tropical regions such as Vietnam. The sheet will combine morphology and geology.

Most work related to this thesis is discussed. In all, six papers have been published, with one poster presentation and accompaniment with many other papers from international journals, proceedings, and conferences. Those papers are the main contents of the study.

Chapter 2 mainly presents referenced data and field photographs and our related JICA project. Only a part of chapter 2.2 used reports No. 3 and No. 4. Chapter 3 is based mainly on data from papers No. 1, No. 2, No. 4, and No. 5. Additionally nationwide background data are referenced. Chapter 4 is based mainly on results reported in papers No. 1, No. 2, No. 5, and No. 6. Chapter 5 is based mainly on papers No. 2 and No. 6. Additionally, all used data and paragraphs include names and published age.

1. **Le Hong Luong**, Miyagi Toyohiko, Shinro Abe, Hamasaki Eisaku, Dinh Van Tien, (2014). Detection of active landslide zone from aerial photograph interpretation and field survey in central provinces of Vietnam. "*The International Programme on Landslides (IPL), Landslide Science for a Safer Geoenvironment*", Volume 1, pp. 435-441, Doi 10.1007/978-3-319-04999-1-61.

2. **Le Hong Luong**, Miyagi Toyohiko, Shinro Abe, Hamasaki Eisaku, Dinh Van Tien (2014). Landslide mapping and detection of active landslide area from aerial photograph interpretation and field survey in central provinces of Vietnam. "*Landslide Risk Assessment Technology - Proceedings of the SATREPS Workshop on Landslides*", pp. 42-49.

3. **Le Hong Luong** (2015). Overview of characteristics of landslide No.18 in Ho Chi Minh Road, Vietnam. "*Human information magazine No.20, Graduate School of Human informatics, Tohoku Gakuin University*", pp. 59-63.

4. **Le Hong Luong**, Miyagi Toyohiko, Shinro Abe, Hamasaki Eisaku and Pham Van Tien (2015). Landslide risk evaluation by combination of morphology, geology and simulation approach in tropical humid region. "*Proceedings of International Conference on Landslides and Slope Stability 2015*", pp. 244-250.

5. **Le Hong Luong**, Miyagi Toyohiko (2015). Hidden landslide: as the Caldera rim deformation at Fukayamadake plateau, at the foot slope of Kurikoma volcano, Kurihara, Japan. *"Proceedings of International Conference on Landslides and Slope Stability 2015"*, pp. 216-220.

6. **Le Hong Luong**, Miyagi Toyohiko, Pham Van Tien (2016). Mapping of large scale landslide topographic area by aerial photograph interpretation and possibilities for application to risk assessment for the Ho Chi Minh route – Vietnam. *"Transactions, Japanese Geomorphological Union"*, pp. 97-118.

7. **Le Hong Luong**, Miyagi Toyohiko (9/2014). Landslide mapping and risk evaluation by aerial photograph interpretation and field survey in central provinces of Vietnam - Poster presentation. *"The Inaugural Conference of IGU Commission on "Geomorphology & Society"*.

8. Ngo Doan Dung, Hamasaki Eisaku, Tatsuya Shibasaki, Miyagi Toyohiko, Hiromu Daimaru, Dinh Van Tien, **Le Hong Luong** (2014). Change the safety factors by the series of land deformation at a typical landslide along the National Road No.6, Vietnam. *"Landslide Risk Assessment Technology - Proceedings of the SATREPS Workshop on Landslides"*, pp. 119-122.

9. Miyagi Toyohiko, Hamasaki Eisaku, Dinh Van Tien, **Le Hong Luong**, Ngo Doan Dung (2014). Landslide mapping and the risk evaluation by aerial photo interpretation in Vietnam. *"Landslide Risk Assessment Technology - Proceedings of the SATREPS Workshop on Landslides"*, pp. 87-95.

10. Tien Pham, Tam Doan, **Luong Le** (2014). Overview of Landslide Phenomena along Arterial Transport System in Vietnam. *"Landslide Risk Assessment Technology - Proceedings of the SATREPS Workshop on Landslides"*, pp. 57-61.

11. P.V. Tien, K. Sassa, K. Takara, H.T. Binh, **L.H. Luong** (2015). Characteristics and failure mechanism of landslides in weathered granitic rocks in Hai Van mountain. *"Proceedings on International conference on landslides and slope stability 2015"*, pp. 165-172.

CHAPTER 2. BACKGROUND OF THE STUDY

2.1. Current situation of landslide disasters and potential disasters in Vietnam

Vietnam, a humid tropical country with 3/4 of its territory as mountainous area, has a richly diverse geologic composition. Landslides occur frequently, severely affecting living conditions, resulting in loss of human life and damage to infrastructure. Most landslides in Vietnam occur in mountainous areas during the rainy season (Doan, 2008). According to a landslide susceptibility map (Ngo, 2016), three regions have high risk of landslide occurrence: the Hoang Lien Son, Fansipan, Hoang Su Phi mountain ranges in northwestern Vietnam; the Truong Son mountain range in central provinces, which includes provinces from Thanh Hoa to Kom Tum; and the northern part of the central highlands from Kom Tum to Dak Nong province, including Ngoc Linh and Di Linh mountains. During the first stage (2012–2014) of state-funded projects (Investigation, assessment and warning zonation for landslides in the mountainous regions of Vietnam, 2015), 10,266 landslide locations in eight northern provinces and two central provinces of Vietnam were recognized and classified based on the landslide volume (Table 2.1). Most landslides are small-to-medium size (occupy 81%); 2.8% landslide locations are very large to huge.

Table 2.1 Numbers of landslide locations in some provinces in Vietnam (State-funded project – Investigation, assessment and warning zonation for landslides in the mountainous regions of Vietnam, 2015)

No	Province name	Total number of locations	Size of landslide location				
			Small (<200m³)	Medium (200 – 1,000 m³)	Big (1.000 – 100,000 m³)	Very big (100.000 – 1,000,000 m³)	Very huge (≥1,000,000 m³)
1	Bac Kan	700	285	281	123	9	2
2	Ha Giang	967	522	288	145	4	8
3	Yen Bai	2326	1165	580	385	187	9
4	Lao Cai	534	316	162	53	3	
5	Son La	1694	795	622	266	11	
6	Lai Chau	970	337	325	280	18	10
7	Dien Bien	673	335	181	139	12	6
8	Tuyen Quang	248	144	91	11	1	
9	Thanh Hoa	864	620	178	65		
10	Nghe An	1290	671	420	187	6	6
	Σ	10266	5190	3128	1654	251	41

This section briefly introduces current landslides at some locations in Vietnam.

2.2. Landslide disasters in Vietnam

Landslide at Coc Pai town, Xin Man district Ha Giang province

Coc Pai town is located in Xin Man district, Ha Giang provinces, in northern Vietnam. Its geology, which comprises schist and quartz schist, sericite schist and graphite gneiss of Ha Giang formation, exhibits a layered structure. The area is affected by strong weathering processes with depth of the weathering crust layer changing from 15 m to 35 m. A high weathering crust is about 10–25 m (Tran, 2009). A field survey conducted in 2009 revealed 46 landslide locations in this area. Most landslides occur at the high weathering crust and are classified as rotational slides. Figure 2.1 shows some images of landslide in this area. The most dangerous landslide (500 m long, 300 m wide) is in a downtown area, which has high population density. The town hall, monument, and numerous constructions are in the middle of this landslide body (Figure 2.2). Monitoring data showed that it moved 1.0 m during 2005–2010 (Tran, 2009).
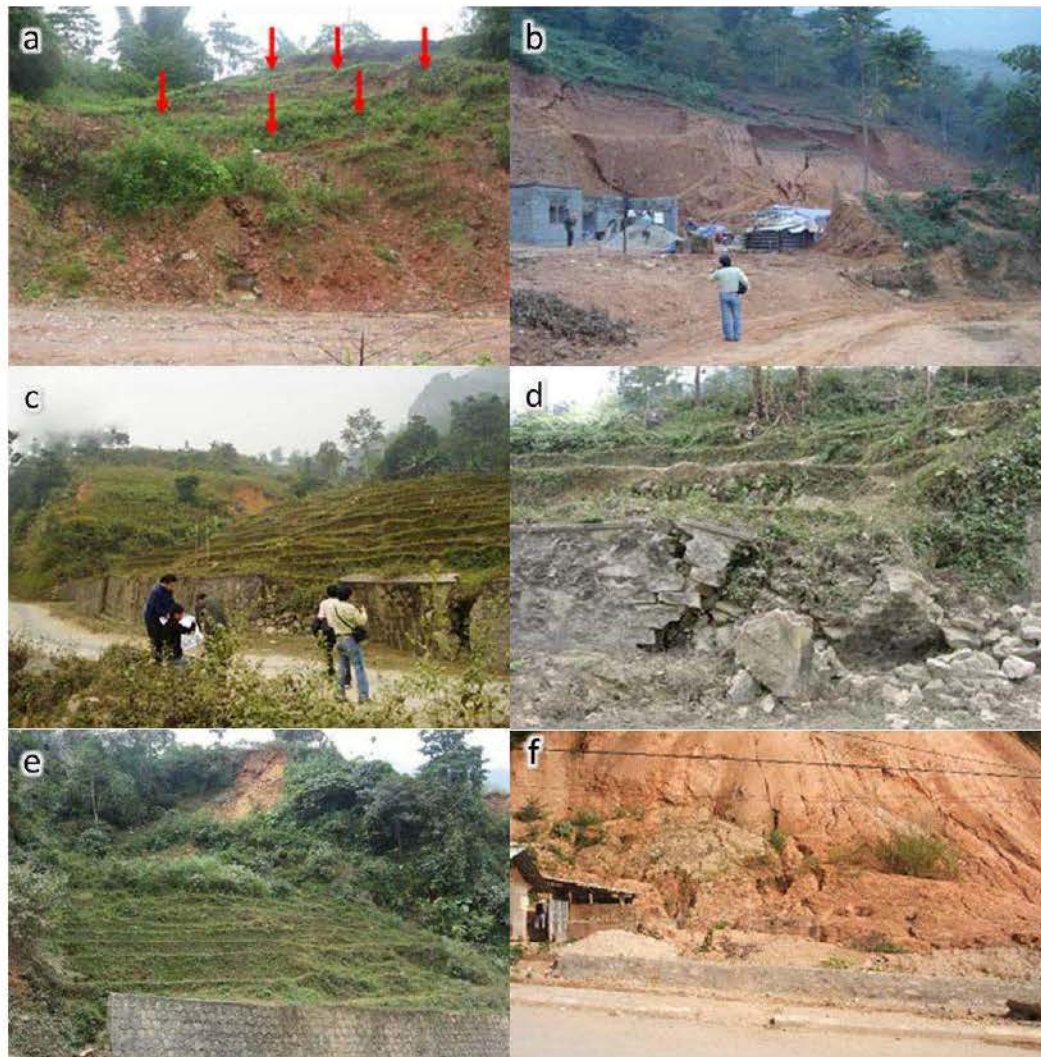
Figure 2.1 Some images of landslide at the Coc Pai town (Tran, 2009):
a: rotational slide next to the road; b, slope failure by slope cutting (two houses were demolished); c, d, e: landslide damage to retaining wall; and f: debris flow caused by weak and weathered materials

6

Figure 2.2 Landslide damage in Coc Pai downtown (Tran, 2009):
a: landslide-damaged monument; b: boundary of landslide cuts throughout the road; c: house
fence tilting because of landslide; and d: landslide movement of steps

Landslide along National road No. 37

National Road No. 37 passes through five provinces, starting from Sao Do (Hai Duong province) to Co Noi T-junction (Son La province). Along this road, slope failures and landslides occur frequently. The largest is located on Km 447+500 with 650 m wide and 950 m long (Figure 2.3). It first occurred during the rainy season 9/2008 and formed 10 m high main scarp. Subsequently, some minor slide appeared. We observed five scarps in this landslide and the road was depressed 0.2–0.5 m and moved 0.3–0.5 m to a river, but it still moves now despite the establishment of countermeasures.

Figure 2.3 Landslide at Km 447+900, National Road No. 37 (taken by Vinh, 2009):
a: overview of landslide; b: sedimentary rock bedding was bent because of intruded basalt; c:
bedding plane parallel to slope; d: conglomerate

7

Landslide along National Road No. 6

On National Road No. 6, landslides occur frequently every year during the rainy season. Most have occurred at section between Hoa Binh and Son La city, destroying houses and structures, blocking roads, and causing many deaths. During an intense storm on 10/2007, 400–500 mm of rain fell in 20 hr, inducing 20 landslides along the road, destroying many kilometers of roads, and killing two people, later blocking the road for 7 days. The government paid 200 billion VND for cleaning and countermeasures. However, landslides continued in 2012, when 30,000 m³ of mass collapsed on Km 138+750, producing traffic congestion for several days (Figure 2.4). Figure 2.5 depicts another example of a landslide along national Road No. 6.

Figure 2.4 Landslide at Km 138+750 (a, Pham, 2014; b, photograph by Le):
a: this picture was taken at the time the landslide occurred, 30,000 m³ debris fell after a period of heavy precipitation and caused traffic congestion in 7 days; and b: was taken two weeks after landslide occurrence

Figure 2.5 Some pictures of landslide along National Road No. 6 (photograph by Le):
(a: landslide at Km 141+200; b: rockfall and topple at Km 128+700; c: rotational slide at Km 111+850).

8

Landslide along National road No. 7

Along National Road No. 7, geologic structures are generally composed of sandstone, gritstone, shale, and schist of Song Ca formation belonging to the Silurian. It shows high folding structures. The area is very close to a large and deep-seated fault. Rock strength is rather high. Landslides do not often occur in hard rock areas, but they are abundant in this area. Most are concentrated along a deep-seated fault. We assume that the fault and folding are main factors promoting landslides in this area shown in Figure 2.6. According to a landslide inventory map along this road from Muong Xen (West) to Son Ha (East) (Dung, 2016), we can readily recognize most landslides occurring at the western area of the road; the eastern area has far fewer landslides. Figure 2.7 portrays some pictures of these landslides.

Figure 2.6 Typical example of landslide related to geology (Silurian) in National Road No. 7 (Le et al., 2015b):
a: road cut exposures fold and fault; b, c, d: road cut exposes folding structure. These fold, fault, and folding structures are main factors causing landslides in this area; e: landscape at National Road No. 7, this river is a fault.

9

Figure 2.7 Images of landslides along National Road No. 7 (photograph by Le):
a: retaining wall damaged by landslide; b: road was uplifted; c: ditch was bent; and d:
landslide damage to a road and retaining wall

Landslide along Ho Chi Minh route

Ho Chi Minh route is an important road in Vietnam running north–south with total length of 3,167 km slated for completion in 2020. After traffic operation, since 2004, many slope failures and landslides have occurred.

According to the Ho Chi Minh project management unit report (2010), 1600 landslides and slope failures have occurred, accounting for a total length of 146 km out of the current 2499-km-long Ho Chi Minh Road. These are concentrated mostly along the 1200 km from Quang Binh to Dak Lak province (central provinces of Vietnam), which can be divided into nine sections: Da Deo – Tay Gat section; U Bo Pass; Khu Dang Pass; Cong Troi Pass, Sa Mui Pass; Dak Rong – Ta Rut section; Hai Ham Pass; Song Bung Pass; and the Kham Duc – Lo Xo section. Many landslides result from the reactivity of aged landslides after slopes were cut for road construction. Most occur during the rainy season. Figure 2.8 and Figure 2.9 displays typical landslides in this area.

Figure 2.8 Some typical landslide in Ho Chi Minh Road (1)(a and b taken by Ngo; c: photograph by Le):
a: rotational slide; b: debris flow damaged a middle segment of retaining wall; c: old landslide next to Thanh My Bridge, with an extremely clear scarp and body

Figure 2.9 Typical landslides in Ho Chi Minh route (2) (Doan, 2008):
a, b: debris slide at Km 339; c: rotational slide at Da Deo Pass; and d: rotational at Km516+713 damage ditch at upper slope. These landslides reactivated after a period of heavy precipitation

11

These landslides can be classifiable into seven categories: rock fall, rotational slide, translational slide, debris slide, debris flows, earth flows, and wedge type. Field surveys show that these landslides are related closely to geology and weathering. For example, landslides in Song Bung Pass are formed in well bedded sedimentary rocks such as cuesta landforms. Lenses of a weak layer (coal layer and mudstone) are observed in this area (Le, 2015a). Most landslides occur along a bedding plane and weak layer as translation slides Figure 2.10.

Figure 2.10 Typical geology structure of Song Bung Pass (Le et al., 2015a and 2015d): a: well bedded layer structures; b: some weak layer between sedimentary rocks; and c: lenses of coal layer, it is also a slip surface.

Another example of wedge type occurs in metamorphic rocks (Hai Ham Pass area). Cracks and fractures are well developed with many dips and strikes in this rock. These allow water to penetrate, enhance weathering, and weaken a potential sliding layer. Wedge type failures occur often along fracture planes.
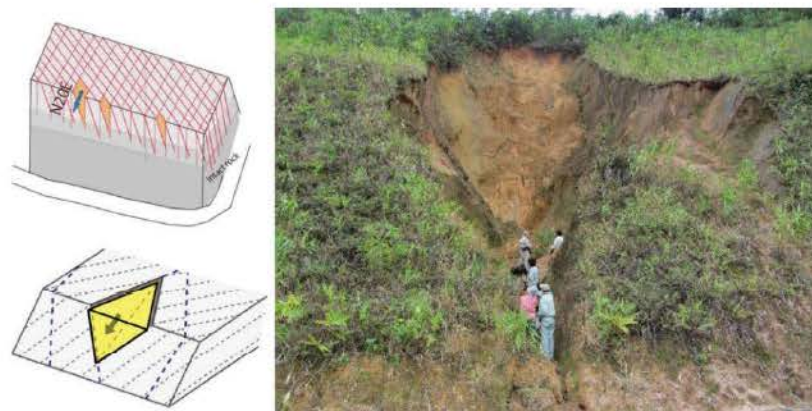
Figure 2.11 Wedge type in Ho Chi Minh route (N16°04'50.4", E107°29'17.2") (photograph by Ngo)

12

Landslide in Hai Van

The Hai Van mountainous area, located north of Da Nang city, is characterized by granite comprising biotite granite and two-mica granite. Granitic rocks are known to be very hard. They are not sensitive to landslide occurrence. Nevertheless, landslides in this area are abundant. We assume that weathered granitic material contributes to this landslide. Field surveys show that the granite has undergone intensive tropical weathering, creating weather profiles of various characteristics and thicknesses. Most landslides are associated with such weathered material. It is porous, friable, and inherits relict planes of weakness from the parent rock. Intensive and heavy rain saturated soils form slides. The porous, friable and weathered material enters the stream, forming a debris flow. These landslides directly threaten the operation of national roads and national railways. For example, 11 landslides occurred in November 1999, causing extensive damage to National Road No. 1. Truck and bus traffic was blocked for several weeks, causing severe economic losses. In October 2007, a railroad track (Figure 2.12-a) was severely damaged and blocked for one week by landslides. The budget for countermeasures and the damage repair reached 100 billion VND.

Figure 2.12 Some landslide at Hai Van (a, photograph by Dinh; b, Tien et al., 2015; c, photograph by Le):
a: overview landscape of old landslide at Hai Van railway station; b: rotational slide; c: landslide damaged retaining wall

13
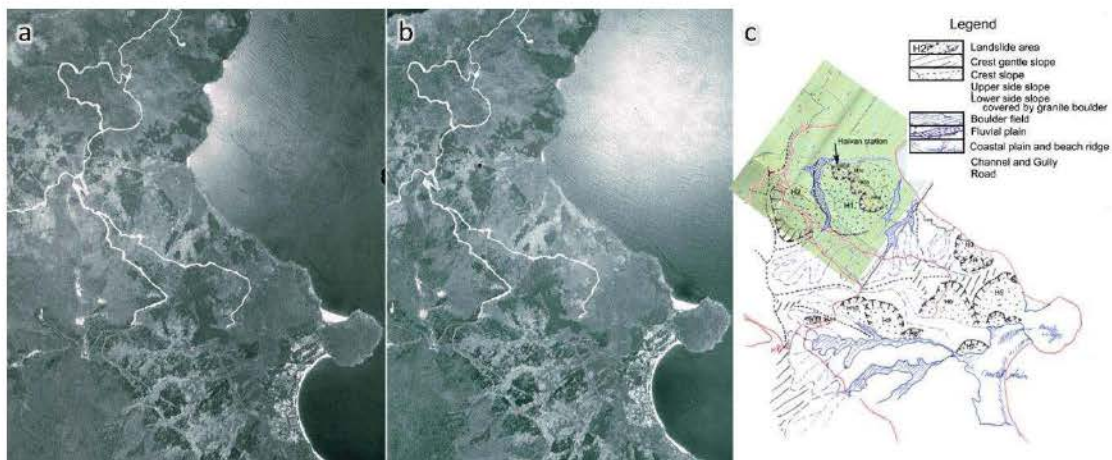
Figure 2.13 Aerial photograph and landslide inventory map at Ha Van Station area (established by Miyagi, 2014):
a and b: stereo pair aerial photograph shows Hai Van Station area; c: landslide inventory map at Hai Van Station

2.3. Some causes of landslides in Vietnam

Landslide mechanisms occur in terms of the relation between shear strength or resistance to sliding along surface of failure and the downslope gravity or shear force. This ratio defines as "Factor of Safety." As long as the shear strength does not exceeds the pull of gravity, the Factor of Safety is greater than 1. The block of material will remain in place. Landslides result from changes in the "Factor of Safety" of a block of overburden near a failure. Many factors induce landslides, such as geological structures, downslope dip of fracture and bedding, slope geometry, undercutting and surcharging slope, weathering, pore water pressure, and vegetation removal... For Vietnam, the main reasons are the following.

Human activities

Human activities include undercutting of slopes for construction of houses, roads, and other structures and infrastructure. Such activities remove the lateral support of the slope, increasing the shear force, thereby leading to slope failure. Deforestation is regarded as a main preparatory factor for landslides in Vietnam. Many studies show that deforestation decreases the safety factor in the rainy season. At such times, water penetrates and saturates the soil, increases pore water pressure, and promotes the slide. The absence of landslides under high forest cover on slopes with similar topographic and soil properties compared with other slopes in Vietnam proves this perspective.

Rainfall

During intense rain showers, it is apparent that roads, small footpaths, plot boundaries and runoff ditches concentrate large volumes of runoff water and direct this to restricted infiltration zones (hollows). When sloped areas become saturated completely by heavy rainfall landslides can occur many times. Without the aid of mechanical root support, the soil simply runs off when it contains too much water.

The discharge rate of water from unstable overburden is probably the most important hydrologic factor affecting slope movement. A perched groundwater table will form within the overburden if the subsurface flow rate is less than the infiltrating rates (from rainfall) for

14

extended periods of time. The height and persistence of the perched water table above an impermeable layer depends largely on the rainfall intensity, duration, and antecedent conditions of water infiltration rate at the site, in addition to the slope gradient, subsurface configuration of the bedrock, and the flow rate within the overburden. The infiltration rate often does not limit the recharge of unstable slopes: the infiltration rate is more than able to absorb incident rainfall. Therefore, the subsurface flow rate becomes the controlling hydrologic variable during most rainfall periods.

Geology and weathering

In humid tropical countries such as Vietnam, geology and weathering are extremely important factors causing landslides. Such factors are the type of rock (soft rock such as mudstone or hard rock such as limestone), jointing, faults, fractures, and orientation of bedding planes, the rock layer arrangement, and weathering processes.

Under tropical climatic conditions, many materials are susceptible to rapid weathering, such as medium to fine grained sedimentary rocks (siltstone, mudstones, claystone, poorly indurated shale, sandstone). Such materials develop a high degree of cohesion and mobility. They are prone to slope movements of the creep, slump, and earthflow types. Slopes underlain by more resistant coarse-grained intrusive (granites and diorites) typically have hard and dense sedimentary and metamorphic rocks (massive shale, sandstone and conglomerate, greenstone and limestone/marble), and a shallow overburden derived from these rock types are usually coarse grained and low in clay-sized particles. Such materials have low cohesion. They are most likely to develop slope movements of the debris avalanche and debris flow types.

Highly jointed or fractured bedrock slopes with principal joints and fracture surfaces parallel to or dipping with the slope provide little mechanical support to overlying materials. They create avenues for concentrated subsurface water movement. Jointing, which also provides avenues for deep penetration of surface and groundwater, results in the development of springs at remote sites on the slope. Excess hydrostatic pressures occur locally because of confining rock and overburden layers. At near-surface locations, joint and fracture planes are ready-made zones of weakness that provide potential failure surfaces along which overlying materials can slide. Downslope dipping surfaces constitute potential surfaces of failure. Conversely, horizontal bedding surfaces and those dipping into the slope might actually increase slope stability locally. However, if fractures are highly developed, rock fall or rotational slide will occur along these fractures.

In many places on steep slopes, metamorphic rocks fractured by faulting and folding are prone to fail as falls, topples, and translational slides. Such landslides are common along the Ho Chi Minh Road. Furthermore, along National Road No. 7, most landslides occur along deep seated faults. Faults and folding are the main factors controlling landslides in this area. As another example in Kham Duc area, slopes are underlain by weathered granite, which weathers into marble-sized grains of quartz and feldspar called gruss. When saturated by heavy precipitation in prolonged winter rains, gruss-covered slopes are prone to fail as debris flows or debris slides. Removal of vegetation by human activity exacerbates this situation.

15

2.4. Risk evaluation and AHP approach

On previous pages, we briefly introduced landslides in Vietnam. In Vietnam, we only know of landslides after they occur. Countermeasures must be quite simple because of lack of funds. They include retaining walls, surface water drainage works, and earth removal works. These countermeasures require large budgets, although the government cannot supply them sufficiently because disasters increase year by year. Therefore, risk evaluation is extremely important. We must ascertain the probability of landslide occurrence and take time to prepare sufficient necessary sources for reduction.

AHP methodology

Analytic Hierarchy Process (AHP) method is multiple-criteria decision-making method proposed by Thomas Saaty in 1980. In that time, Saaty was directing research projects for Arms Control and Disarmament at the US State Department. He had to surmount communication difficulties between scientists and lawyers with an apparent lack of practical systems for priority-setting and decision-making. After noting these difficulties, he attempted to develop a simple means of helping ordinary people make complex decisions (Saaty, 1980), choosing among a set of pre-specified alternatives. The decision-making process relies on information related to alternatives.

This method is useful where teams of people are working on a complex problem involving judgment. It aims to rank decision alternatives and select the best one for a complex multi-criteria decision-making problem using pairwise comparison of those criteria.

The decision situation to which the AHP is applicable includes the following six aspects (Zhang, 2010):

- Choice – Selection of one alternative from a given set of alternatives, usually with multiple decision criteria involved

- Rank – Arranging a set of alternatives from most to least desirable

- Priority – Determining the relative merit of members of a set of alternatives, as opposed to selecting a single one or merely ranking them

- Resource allocation – Apportioning resources among a set of alternatives

- Benchmark – Comparing the processes in one's own organization with those of other best-of-breed organizations

- Quality management – Dealing with the multidimensional aspects of quality and quality improvement

The AHP provides a comprehensive and rational framework for structuring a decision problem. The essence of the AHP process is to create a hierarchy based on the decomposition of a complex problem, with a goal at the top, criteria and/or sub-criteria at different levels, and decision alternatives at the bottom of Figure 2.14. Therefore, AHP was proposed. It is a simple method: people with no formal training can understand and participate in activities using it.
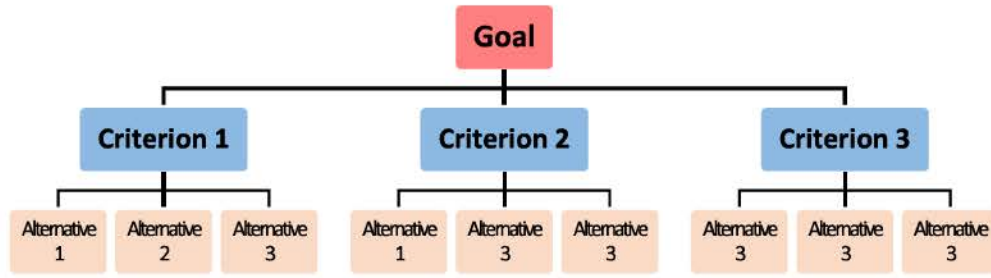
Figure 2.14 Structure of AHP (Zhang, 2010)

In this method, the number of criteria and the corresponding relative priority form judgment matrix A (reciprocal matrix), which contains pairwise comparison values.

$$A = \begin{bmatrix} a_{11} & a_{12} & \cdots & a_{1n} \\ a_{21} & a_{22} & \cdots & a_{2n} \\ \vdots & \vdots & \ddots & \vdots \\ a_{n1} & a_{n2} & \cdots & a_{nn} \end{bmatrix} = \begin{bmatrix} 1 & z_1/z_2 & \cdots & z_1/z_n \\ z_2/z_1 & 1 & \cdots & z_2/z_n \\ \vdots & \vdots & \ddots & \vdots \\ z_n/z_1 & z_n/z_2 & \cdots & 1 \end{bmatrix}$$

Therein, z_i denotes the element/criterion to be compared. a_{ij} is the pairwise comparison value of criteria z_i and z_j; $a_{ij} = 1/a_{ji}$ for $i \neq j$, and $a_{ii} = 1$. These values, which are given by each decision-maker, form a square matrix.

A priority vector can be calculated using the following formula:

$$w = \begin{bmatrix} w_1 \\ w_2 \\ \vdots \\ w_n \end{bmatrix} = \begin{bmatrix} (\prod_j^n a_{1j})^{1/n} \\ (\prod_j^n a_{2j})^{1/n} \\ \vdots \\ (\prod_j^n a_{nj})^{1/n} \end{bmatrix}$$

To check the consistency of the answer, it is necessary to calculate the principal eigenvalue (λ_{max}). The principal eigenvalue is obtained from the summation of products between each element of eigenvector and the sum of columns of the reciprocal matrix.

$$\lambda_{max} = w_1 * b_1 + w_2 * b_2 + \cdots + w_n * b_n$$

Therein, the following variables are used:

$$b_1 = a_{11} + a_{21} + \cdots + a_{n1}$$
$$b_2 = a_{12} + a_{22} + \cdots + a_{n2}$$
$$b_1 = a_{1n} + a_{2n} + \cdots + a_{nn}$$

Saaty proved that, for consistent reciprocal matrix, the largest eigenvalue is equal to the comparison matrix size, or $\lambda_{max} = n$. For a measure of consistency, called Consistency Index as deviation or degree of consistency using the following formula:

$$CI = \frac{\lambda_{max} - n}{n - 1}$$

Saaty also proposes consistency ratio, which is a comparison between the Consistency Index and the Random Consistency Index, as in the following equation:

$$CR = \frac{CI}{RI}$$

The inconsistency is acceptable if the value of the consistency ratio (CR) is less than or equal to 10%. It is necessary to revise the subjective judgment if the consistency ratio is greater than 10%. The Random Consistency Index can be referred from Table 2.2.

Table 2.2 Random Consistency Index (RI)

n	1	2	3	4	5	6	7	8	9	10
RI	0	0	0.58	0.4	1.12	1.24	1.32	1.41	1.45	1.49

Using AHP for landslide risk evaluation

The Japan landslide society (JPS) first used AHP for landslide risk evaluation in 2002. At that time, they wanted to evaluate the probability of landslide occurrence by interpreting aerial photographs (Hamasaki, 2013). This work was implemented through several times discussion at the working group according to the following flowchart (Figure 2.15):
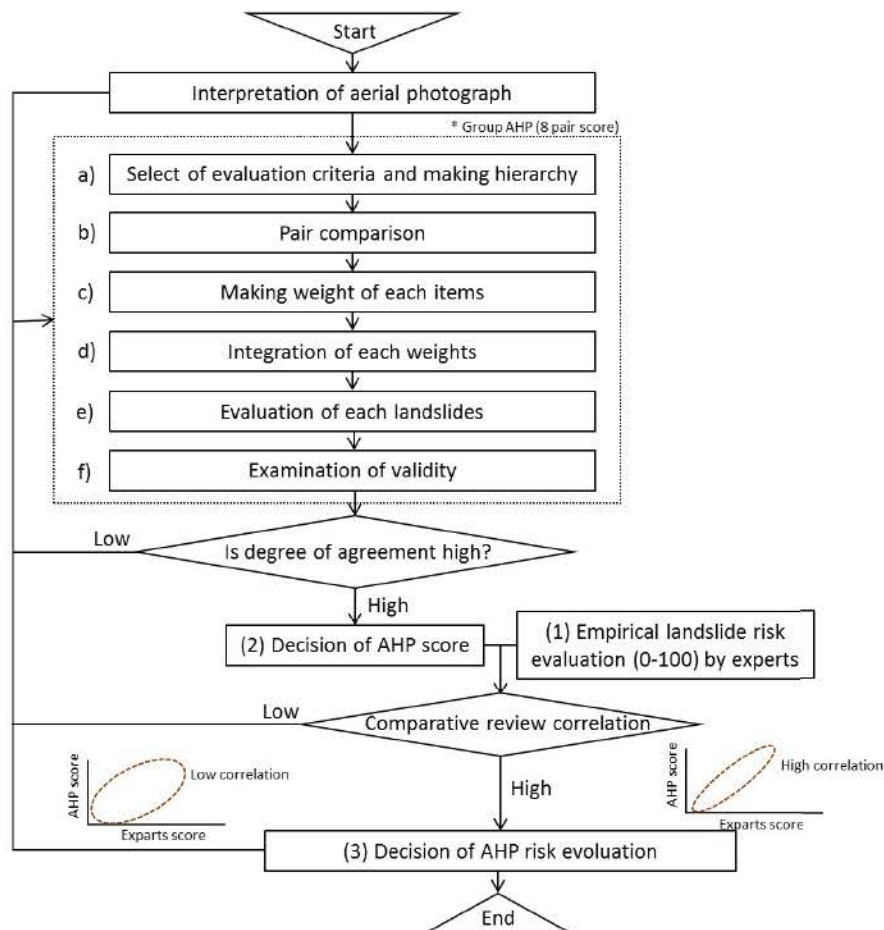
Figure 2.15 Flow chart showing the determination process for the Analytic Hierarchy Process score (Hamasaki, 2013)

First, the working groups separate evaluation criteria items into three main categories: (1) "landslide body micro-topography" as an index related to movement characteristics; (2): "landslide body boundary" as an index related to time elapsed; and (3) "topography surrounding the landslide body" as an index related to the topographic area.

18

Further subdivision can be made into six intermediate elements: a) mode of movement, b) landslide body micro-topography, c) head boundary, d) toe boundary, e) tip of landslide body tip, and f) potential (Hamasaki, 2013).

Created categories (minor elements) for the intermediate elements that will be the check indexes of the actual chart, and which will use the Analytic Hierarchy Process (AHP) method to make paired comparisons for each of the major elements, intermediate elements, and minor elements. For practical purposes, the categories presented in Figure 2.16 are arranged by intermediate items so that the risk level increases from bottom to top (Hamasaki, 2013).

To facilitate understanding of topography formation mechanisms, these items were organized from left to right when the chart was created. Incidentally, this structure permits the position of checks for categories to be placed between categories. In other words, in Figure 2.16, if item F was determined to be between "talus" and "large scale talus," then a check can be placed between the two.

However, when it is clear that multiple categories exist, the contribution of that with the most weight is assigned priority.

Each person in the working group implements Analytic Hierarchy Process evaluations. The results are used as a springboard for creating the group's Analytic Hierarchy Process weights. Here, we have set the Analytic Hierarchy Process paired comparison values as described below (Hamasaki, 2013):

1: Both elements are about equally important

3: A previous element is slightly more important than the following one

5: A previous element is slightly more important than the following one

7: A previous element is much more important than the following one

(Other: 2, 4, 6, and 8 are interpolative values)

When finding the final weight for each category, JPS used this formula: *Final weight of minor element category = general AHP weight x intermediate AHP weight x minor AHP weight.*

Among the coefficients obtained from integrating the weights, when checking the highest categories for intermediate items a–f, compensating coefficients are added so that the total will be 100 (Hamasaki, 2013).

On the chart, the total of these check scores is designated as the Analytic Hierarchy Process scores (total of model weight coefficients). In other words, the following holds.

$$\text{AHP score} = \alpha * \sum X(A \sim I)$$

α: is the compensating coefficient

Paired comparison and weight determination methods

Specific steps for determining the weight are the following.

(1) Paired comparison of "general categories" related to risk estimation.

At this stage, 3×3 paired comparisons are made, based on the following.

I. Landslide body micro-topography

II. Landslide body boundary

III. Landslide body and surrounding environment

For example, a matrix is shown below for paired comparisons assuming that "landslide body micro-topography is three times more important for risk evaluation than the landslide body boundary."

In the Analytic Hierarchy Process method, paired comparisons are conducted in the same way for all elements. Then geometric means are found for the horizontals of the matrix. These ratios are converted into weights.
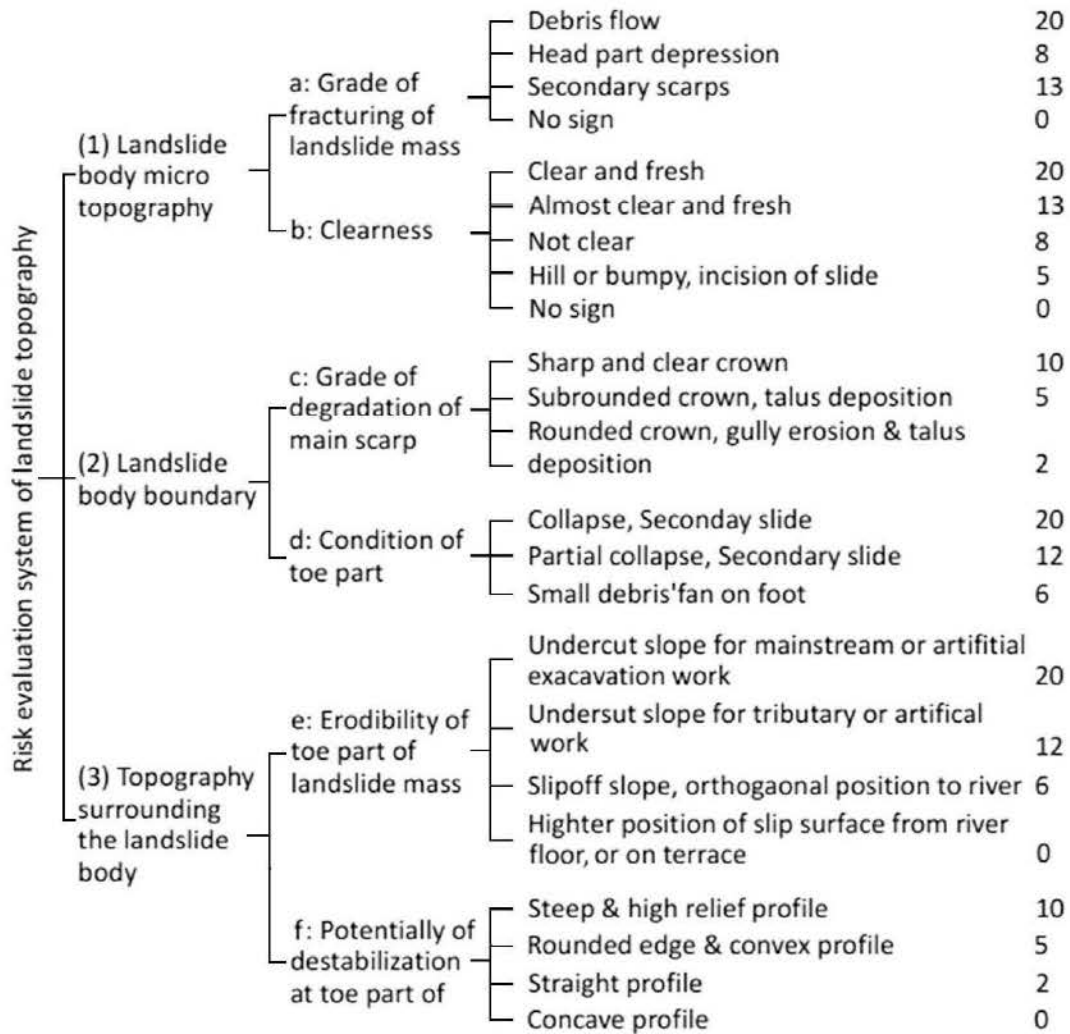
Figure 2.16 Risk evaluation criteria (Miyagi et al., 2004)

Figure 2.17 depicts an example of inspection sheet for the Okamizawa landslide in Japan. The total AHP score is 78, meaning that this landslide has a high probability of re-activation.
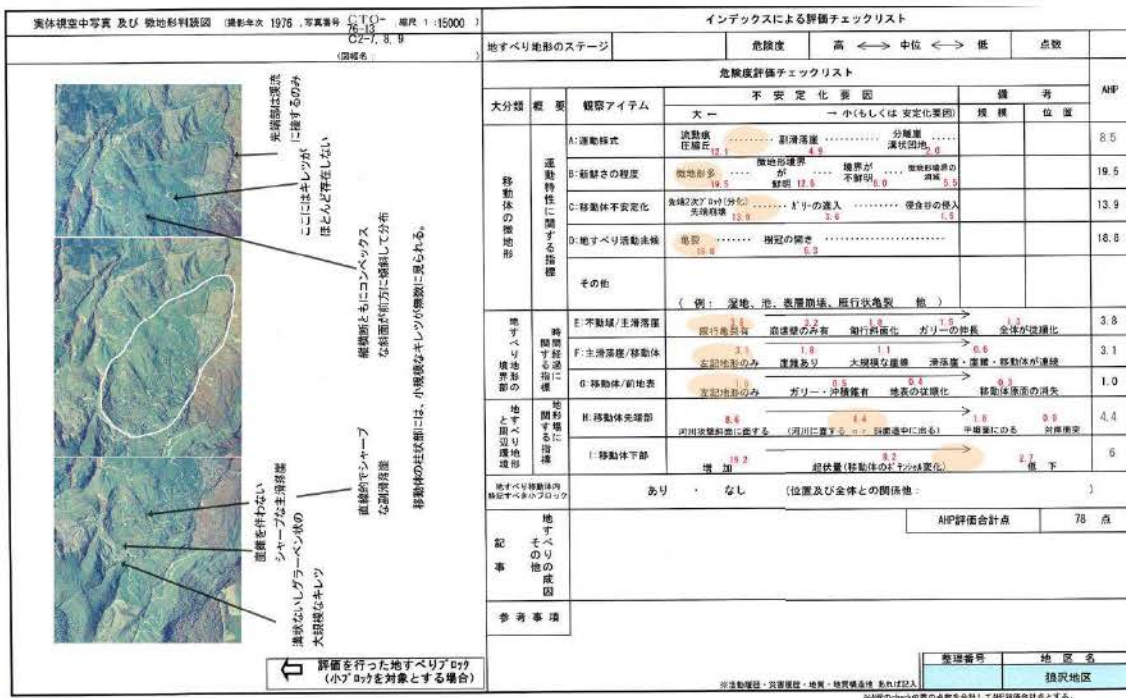
Figure 2.17 Example of inspection sheet for Okamizawa in Tohoku, Japan (Miyagi, 2014a): (Left side shows a pair of aerial photograph, right side shows risk evaluation criteria).

2.5. Large-scale landslide mapping

To assess landslide hazards or evaluate landslide risks, one must start with collection of information related to where landslides are located: this is the goal of landslide mapping. The simplest form of landslide mapping is a landslide inventory map, defined as a map recording the locations. It might show the dimensions, geographical extent of respective landslides, types of mass movements, and states of activity. This dataset might represent a single event, a regional event, or multiple events. It might be very helpful for predicting the hazard for an area. In most cases however, not all this information is available because most of the existing inventories include only a subset of the required data. Based on the type of mapping, landslide inventory maps are classifiable as archive or geomorphological inventories (Guzzetti, 2005; Malamud *et al.*, 2004b). An archive inventory presents information related to landslides obtained from the literature, or other archive sources (Guzzetti, 2005; Reichenbach *et al.*, 1998; Salvati *et al.*, 2003; Taylor and Brabb, 1986). Geomorphological inventories can be classified further as historical, event, seasonal or multi-temporal inventories.

Landslide susceptibility displays the probability of occurrence of landslides of a particular type at a given location. This spatial probability, either qualitatively or quantitatively determined, is usually expressed on maps in qualitative terms (e.g. nil or low, medium, high) and depicted as zones (polygons in digital maps) filled in with colors ranging from cold hues representing lower landslide susceptibility to warm hues for higher landslide susceptibility zones.

Landslide hazard maps specifically depict the probability of occurrence of landslides of a particular type and magnitude at a given location within a reference period of time. Therefore landslide hazard assessment differs from susceptibility assessment by consideration also of the event magnitude, and more importantly, the frequency of occurrence or reactivation.

Landslide risk maps generally show the probability (often expressed annually) of landslides causing casualties, damage to property and infrastructure, and interruption of services and economic activities. In landslide risk assessment, the exposure (as the amount and value of the elements at risk, such as population, buildings, a road or railway, or a vehicle or a train passing by) and vulnerability (as the degree of loss of these elements) are usually considered in addition to the landslide hazard.

Among these landslide maps, susceptibility maps are the most abundant worldwide, but an inventory map is the simplest form of landslide mapping. Regarding the history of landslide mapping, the first idea of systematically collecting historical information related to landslides was conducted in Italy in 1907–1910. Geographer Roberto Almagià published two volumes of maps at 1:500,000 scale. In them, landslides were shown as points. The maps depicted hundreds of landslides in the Apennines. Since then, many efforts have been conducted to update the database and search for new data related to historical landslide events. The landslide inventory map engendered great changes in sketching and preparing. In 2004, a landslide susceptibility and landslide inventory map was basically produced for Japan. Italy and America produced such maps in 2011. In recent years, GIS technology has been widely used for preparing landslide mapping. In the next two sub-sections, an overview of landslide mapping of Japan and Vietnam (mainly landslide inventories and susceptibility or hazard maps) will be introduced.

2.5.1. Landslide mapping in Japan

Landslide mapping in Japan has a long history extending more than 60 years. It started in risk evaluation in some projects, giving it the longest history in the world. In the 1960s, Tohoku University's research laboratory for geography used 1/40,000 monochrome aerial photographs taken by the US military. This was done to analyze aerial photography and land classification in national land surveys. Around 1965, various scholars pointed out that "landslide topography" formed through landslides can be recognized using aerial photography analysis (Ichise, 1964; Miyagi, 2014a). Furthermore, applying aerial photograph interpretation in terrain surveys for dam construction, cases of unexpected unstable ground "resampling landslides" were pointed out. In 1971, Hatano analyzed the "Sendai" area using a 1/200,000 topographical map and provided a map highlighting various slope terrains possibly created through landslides (Hatano, 1974). He was probably the first person in Japan to describe the distribution conditions of large-terrain landslides. Since Hatano's revelations, other investigators such as Terado (1978), Miyagi (1979), Shimizu *et al.* (1982–1988), and the Japan Landslide Society Tohoku Branch (1992) have put forward distribution maps of landslide terrains for various areas in Japan (Miyagi *et al.*, 2014a, b).

Analysis of landslides through aerial photograph interpretation (Figure 2.18) enables us to distinguish topographical areas created through landslides from those which did not result from landslides. Landslide terrain is clearly demarcated from general slopes through the landslide scarps (Varnes, 1978). The main part of a landslide is surrounded by slips and is recognized as consisting of moving objects such as the landslide body. Landslide topography is constituted by slip surface so-called surface of rupture and moving material called the landslide body. Various shapes and inclinations of slip precipices exist. Moreover, the moving parts

themselves undergo various changes in form and substance in the process of movement, which appear in the form of micro-topographical features at the surface of the moving part.

Naturally, the topography caused by the effects of landslides creates particular landslide topographies. Furthermore, it has been pointed out that the micro-topography formed through landslide topography corresponds to the material characteristics and movement of landslides (Miyagi, 1979; Yagi, 2003). Landslide topography includes a host of basic units of topography. Each topographic unit is formed by peculiar processes. Consequently, it has been suggested that by understanding the formation of micro-topographies, one can investigate the form of movement and the location of the slide structure, as well as the formation processes of landslide topographies, and the landslide mechanisms (Kimata, 1985).

Figure 2.18 Picture of aerial photo interpretation (Miyagi, 2013)
(performed using aerial photograph, stereoscope for aerial photography (mirror type), simple stereoscope, topography map, geological map, writing materials, etc.) The series of aerial photographs should be arranged as shown above, and be examined from directly above. The gap separating photographs differs depending on the person; fine tune the image by moving the photographs slightly until the image is clearly visible (Miyagi, 2013)
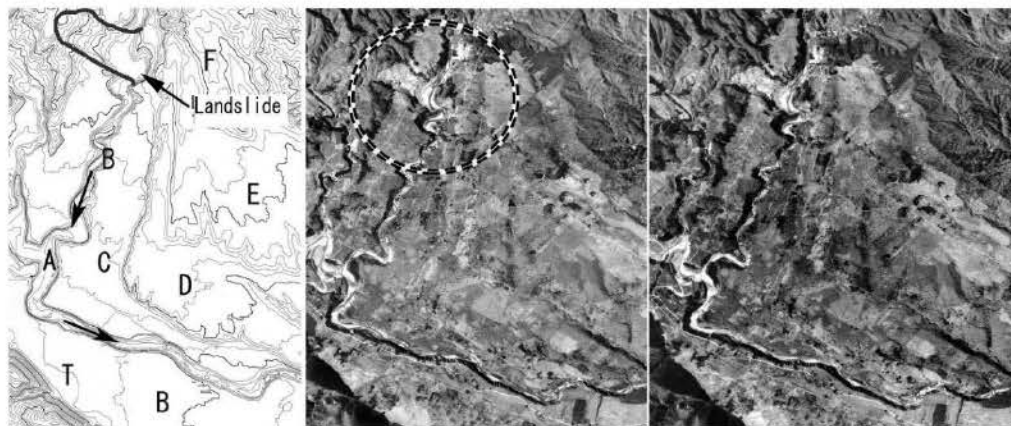
Figure 2.19 Example of Stereo pair image and the topographical map (left) (Miyagi et al., 2004): A: river; B–F: river terraces; T: alluvial cone. Landslides distributed at the upper part. The landslide cut the river terraces.

23

In 2015, the National Research Institute of Earth Sciences and Disaster (NIED) established landslide inventory maps for all of Japan, which amounts to over 400,000 landslide topographic locations.

Analysis of the discovery of landslide topography was conducted with great scientific interest in important geomorphological questions of "how slopes develop." Aerial photo-interpretation has advanced research on quaternary tectonic movements. The development of topography has specifically examined the recognition of terraces and active faults. The recognition of landslides was advanced, addressing the question of how to locate mass movement as a factor in explaining the topographical development of slopes (Miyagi, 2013).
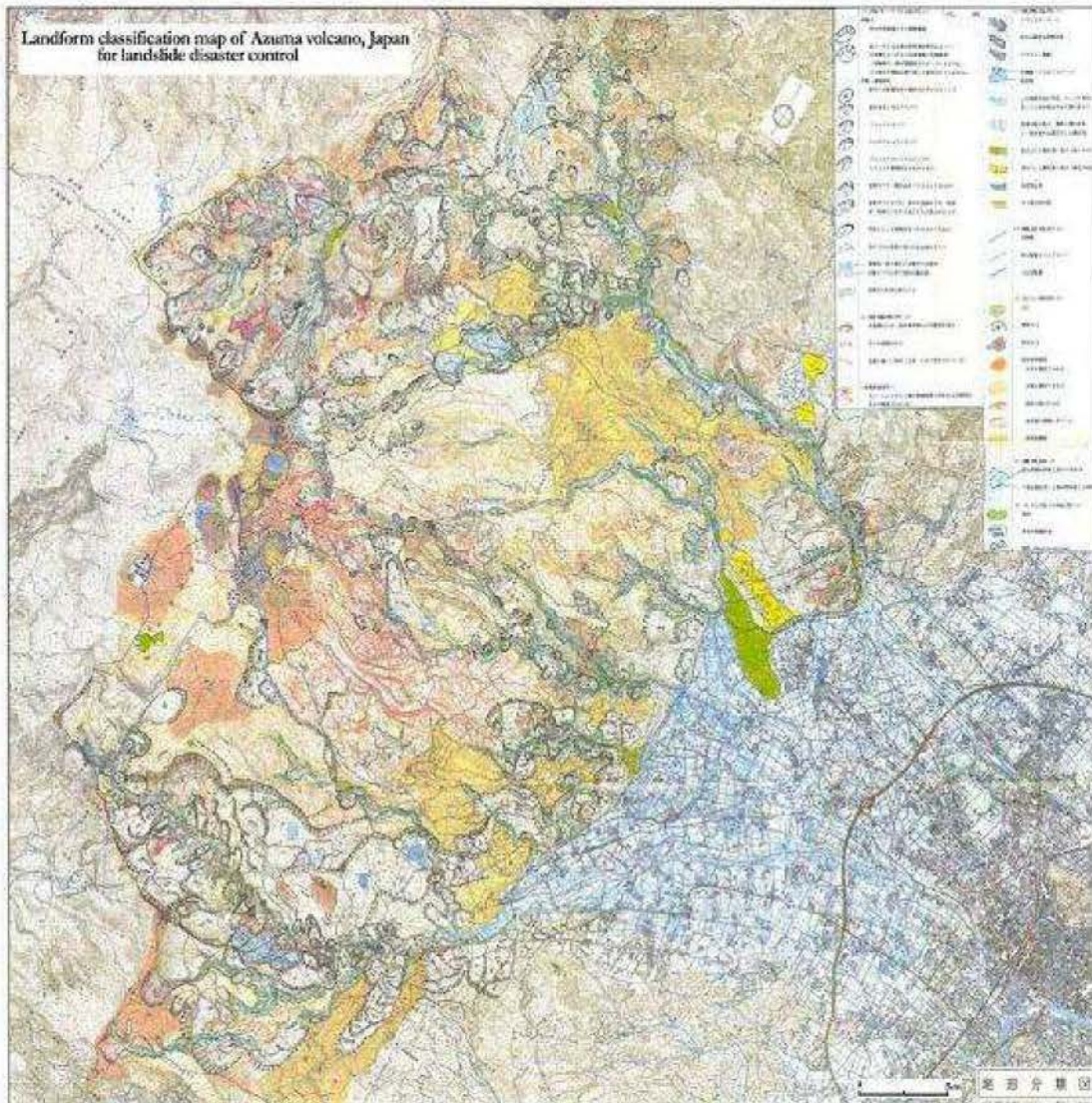
Figure 2.20 Azuma volcanic region landform classification map (top) (Miyagi, 2013) rendered as a 1:25,000 scale topography map. It depicts the landslide topography (the movement type is also classified), volcanic slope, accumulation topography of the mountain foot, and a convex break line (corrosion line) allowing estimation of the landslide topography distribution, as well as the relation between the landslide area and volcanic slope, and potential sediment yield per watershed. Aerial photograph: 1:20,000 scale monochrome adhesive photograph (Miyagi, 2013)
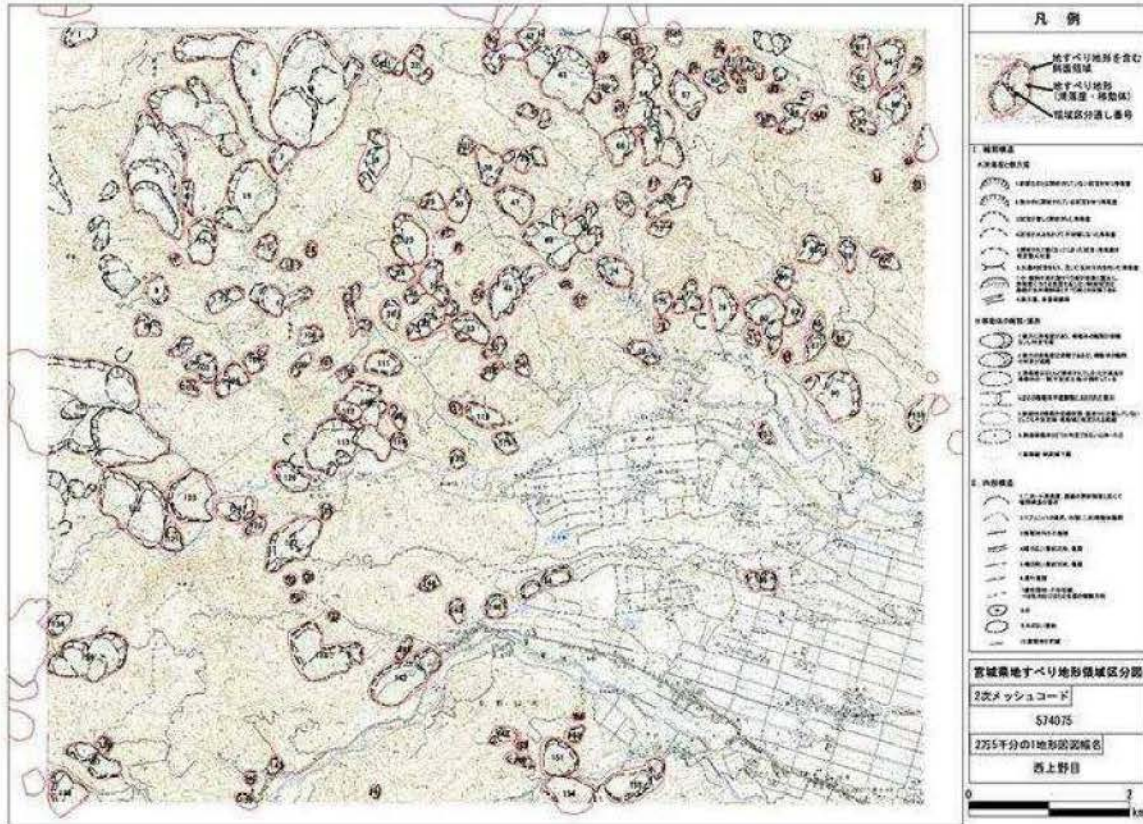
Figure 2.21 Landslide topography distribution map (created at the request of the Japan Landslide Society) (Miyagi, 2013)
Landslide topography derived from aerial photograph interpretation in a 1:25,000 scale topography map. Here, maps are annotated according to the legend on the right. The minimum landslide fluctuation range has been determined. The main scarp is shown by heavy lines and hatch marks. The actual landslide body shape is shown with thin lines. For large-scale landslide topography, if large-scale internal structures on a scale that permits interpretation within the landslide body are confirmed, then these too are noted. The main scarp and its surroundings, the height difference at the top part of the slope, and fissures, have probability indicators suggesting instability. They are noted with extreme caution. The aerial photographs used were 1:20,000 scale monochrome adhesive photographs from the Nishikaminome region of northwestern Miyagi Prefecture. Each landslide topography map is assigned an ID number linked to relevant information. The creation of these distribution data began in the 1980s, and comprises a 1:50,000 scale map of recent information covering all of Japan (Miyagi, 2013)
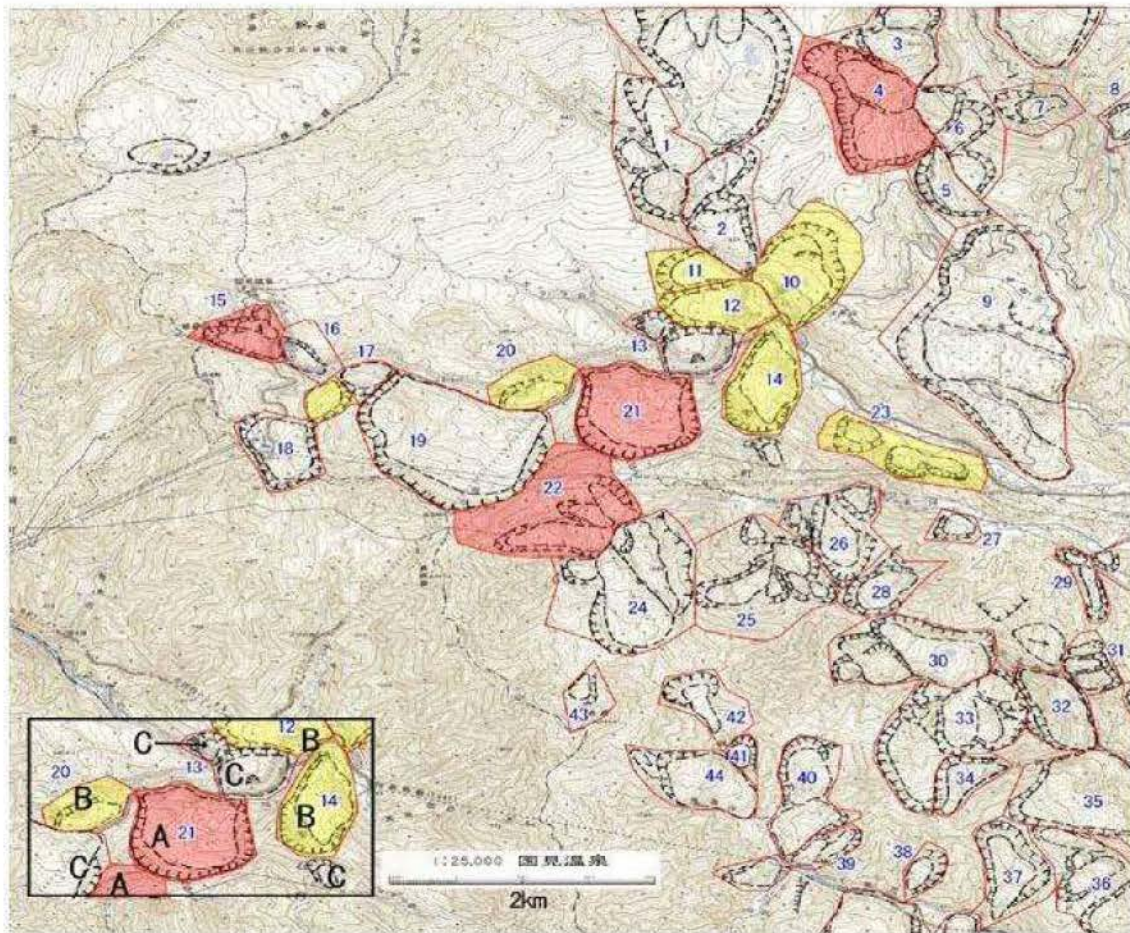
Figure 2.22 Landslide topography distribution and risk level chart (Miyagi, 2013)
Stereo pair interpretation was conducted of the distribution map from Figure 2.18 and the images recorded in the interpretation evaluation chart. Landslide risk was evaluated using AHP. Hamasaki provides an explanation of this. The evaluation points obtained through interpretation do not constitute a rigorous scale (e.g., no significant difference was found between scores of 60–65). They are divided into three general ranks: A-rank areas, which have an AHP score of 80 or higher if synthesized with AHP evaluations in actual disaster countermeasure case studies, can be judged to be fundamentally active. B-rank areas have a score of 60 or higher. Caution is necessary when surveying them. C-rank areas have been judged to be fundamentally unmoving, but caution is necessary as the landslide body itself has sustained damage from the landslide, and actions such as tearing might lower the landslide body's stability. Relevant evaluation is done using aerial photograph interpretation alone; use of estimated values is legitimate. It is extremely useful as a draft map for various plans. It is the basis for assigning priority to the implementation of field surveys (Miyagi, 2013)

26
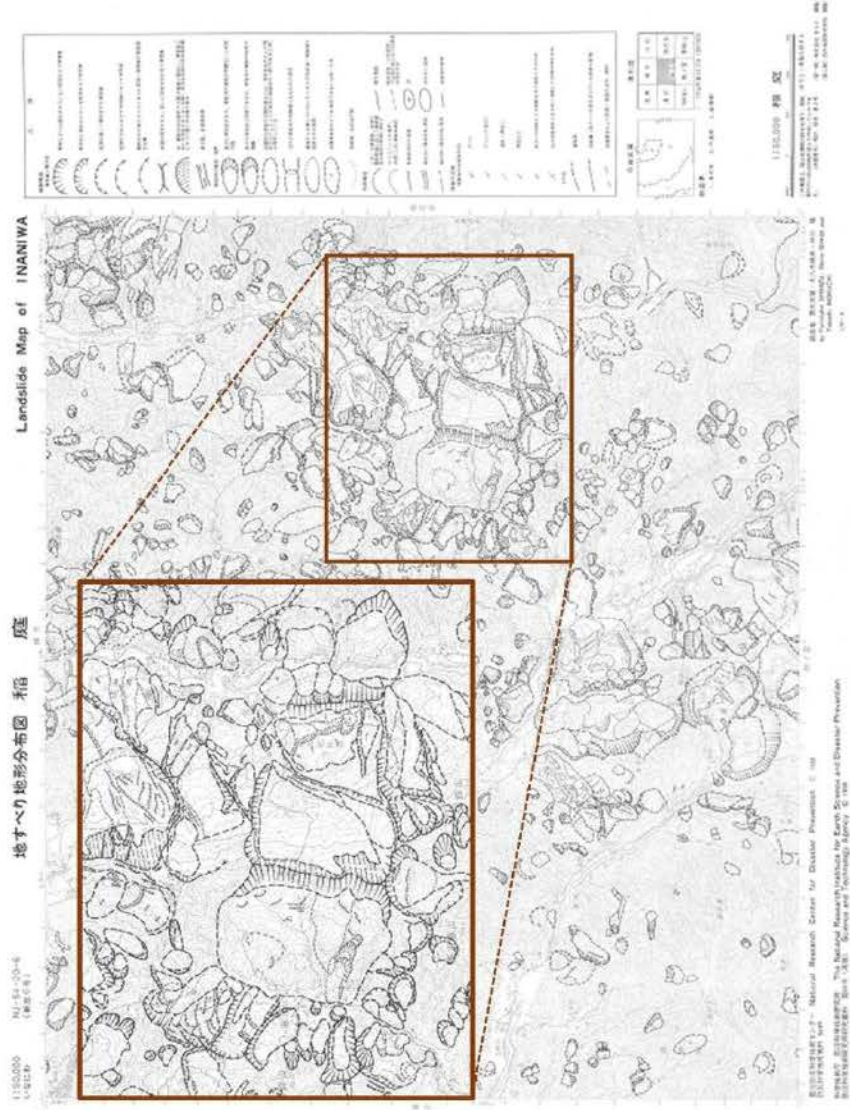
Figure 2.23 Landslide inventory map 1982 at Inaniwa (NIED, 1982)
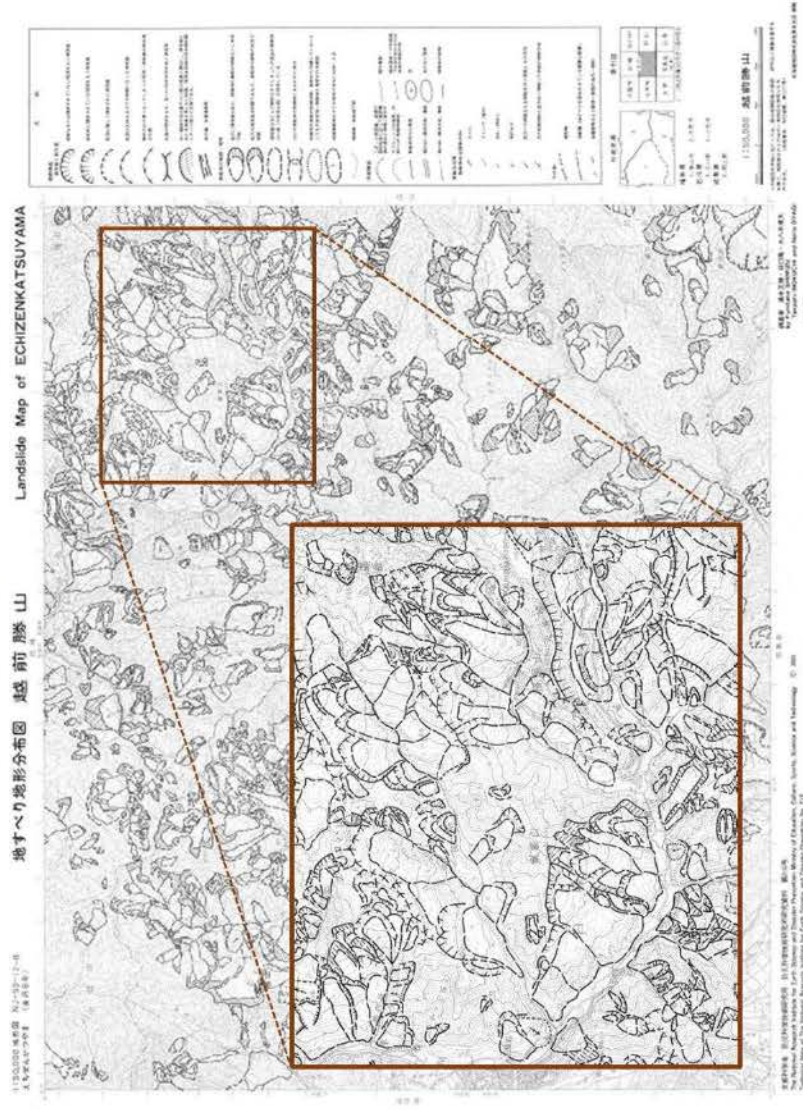
Figure 2.24 Landslide inventory map 2000 at Echizenkatsuyama (NIED, 2000)

27

2.5.2. Landslide mapping in Vietnam

In Vietnam, landslide studies started in 1974 by Prof. Ho Chat, but landslide mapping (Figure 2.25) was first developed in 1994 by Dao Van Thinh and Nguyen Phuong Dong (Doan, 2008) for northwestern provinces of Vietnam. It is a susceptibility map by nature, indicating low, moderate, high, and very highly landslide susceptible locations. Landslide locations are shown only as points on the map.
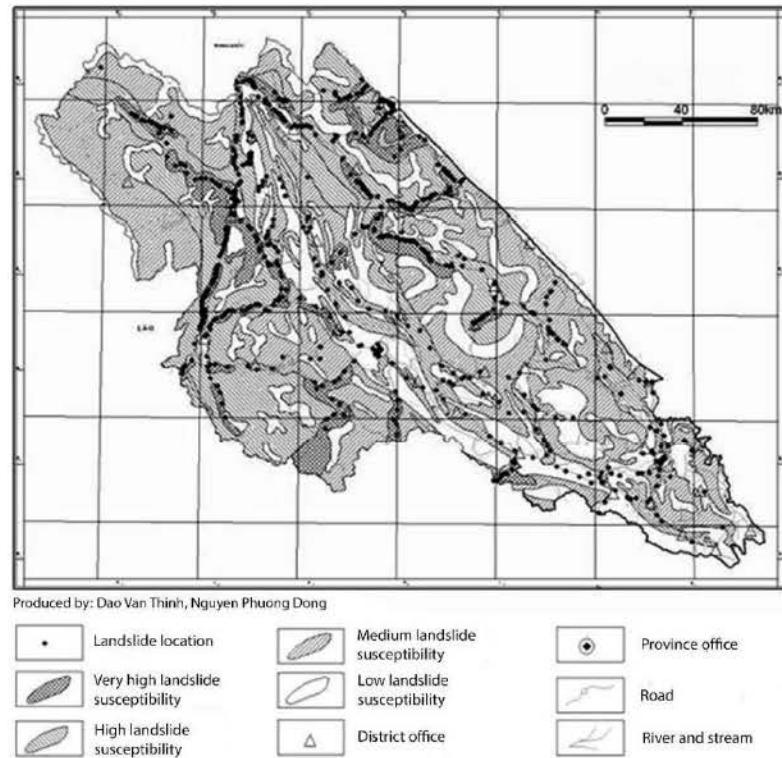
Figure 2.25 Susceptibility map for northwestern provinces of Vietnam (produced by Dao Van Thanh and Nguyen Phuong Dong)

During 1990–2010, many studies of landslide mapping were conducted. Many landslide susceptibility maps were done severally for different areas. Landslides were described on these maps and were divided into five types (Table 2.3) depending on their volumes, as proposed by Lomtadze (Lomtadze, 1997), e.g. a landslide inventory map of Tran Tan Van (Tran, 2006) for Truong Son commune, Quang Ninh district, and Quang Binh province (Figure 2.26).

Table 2.3 Quantitative landslide classification (Lomtadze, 1997)

Classification	Size	Volume (m3)
I	Small	< 200
II	Moderately large	200 -1,000
III	Large	1,000 -100,000
IV	Very large	100,000 -1,000,000
V	Extremely large	> 1,000,000
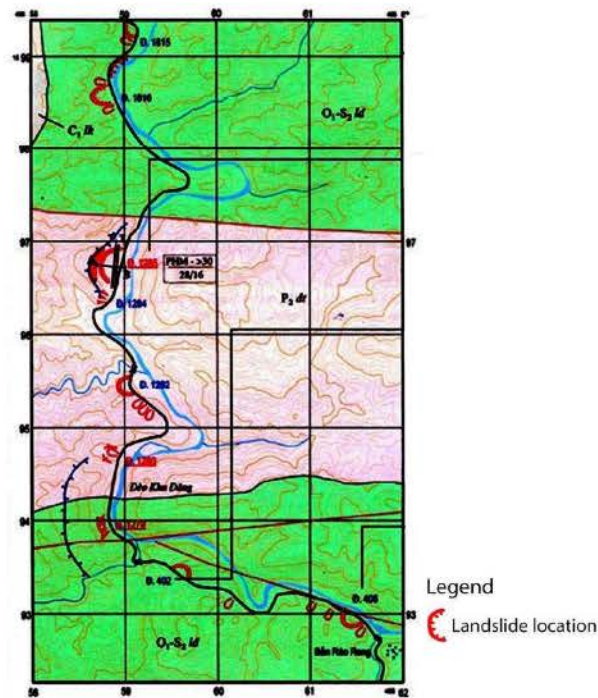
Figure 2.26 Landslide inventory map for Truong Son commune, Quang Ninh district, Quang Binh province (Tran, 2006): (in this map, the landslide location was described as the red arc. Its size denotes the volume of landslide

In 2008, Nguyen Quoc Khanh developed a landslide inventory map for Muong Lay district, Son La province (Figure 2.27). 88 landslides were sketched, representing point features with different symbols and depending on old or new landslides. For no landslide is there a description of triggering factors information.
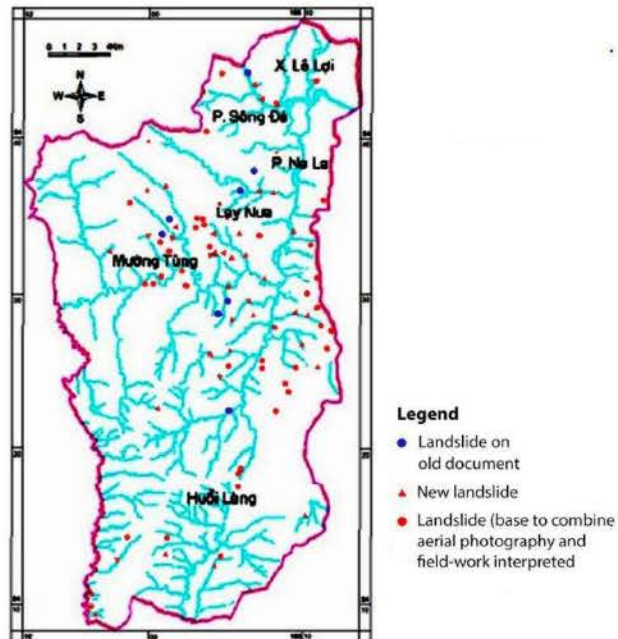
Figure 2.27 Landslide inventory map of Muong Lay district, Son La province (Nguyen, 2008): landslide location was represented as point features with different symbols and depending on whether it is an old or new landslide.

29

In 2009, Nguyen Thanh Long produced an inventory of landslides for A Luoi district, including 181 landslides and landslides described as a region (Figure 2.28), but it is extremely difficult to recognize scarps indicating a landslide body.
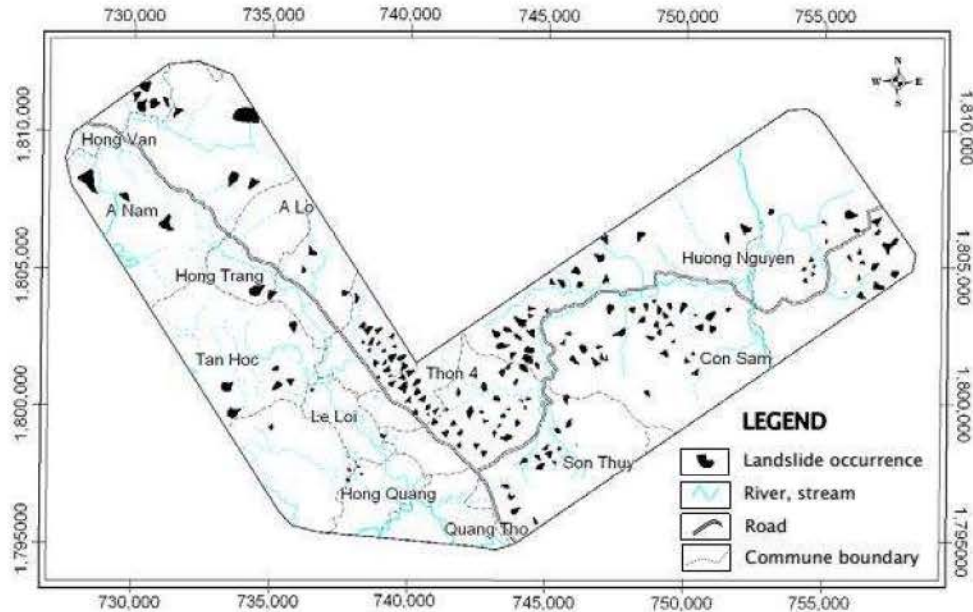
Figure 2.28 Landslide inventory map of A Luoi district, Thua Thien Hue province (Nguyen, 2009):
landslide topographic area was represented as a black region, but it does not mention scarp and landslide bodies

Actually, all maps above were published by individuals. Vietnam has no organization responsible for collecting and producing landslide mapping. No law exists for landslide databases and maps. All studies above are separate works, specifically examining small/local areas, range districts, and provinces. In 2012, a state-funded project, "Investigation, assessment and warning zonation for landslides in the mountainous regions of Vietnam" established a standard national database of landslides and generated landslide hazard maps, landslide inventory maps at scales of 1:50,000 and 1:10,000 for 37 provinces in Vietnam. However, the project is not well organized, according to the project report, the first stage (2012–2016) has been completed, but the web page (www.canhbaotruotlo.vn) cannot be accessed now, allowing no comments. Landslide hazard maps and landslide inventory maps have been produced for eight northern provinces and two central provinces of Vietnam, but landslide inventory maps are still very poor. Figure 2.30 portrays an example at 1:50,000 scale. In this map, brownish brick hatches represent areas prone to slides; red dot hatching and red cross hatching represent areas where landslides have occurred. Landslide locations are denoted by the symbol "↯". The symbol size denotes the landslide volume. Five categories are displayed on this map: small (<200 m³), moderately large (200–1000 m³), large (1000–20,000 m³), and very large (20,000–100,000 m³).
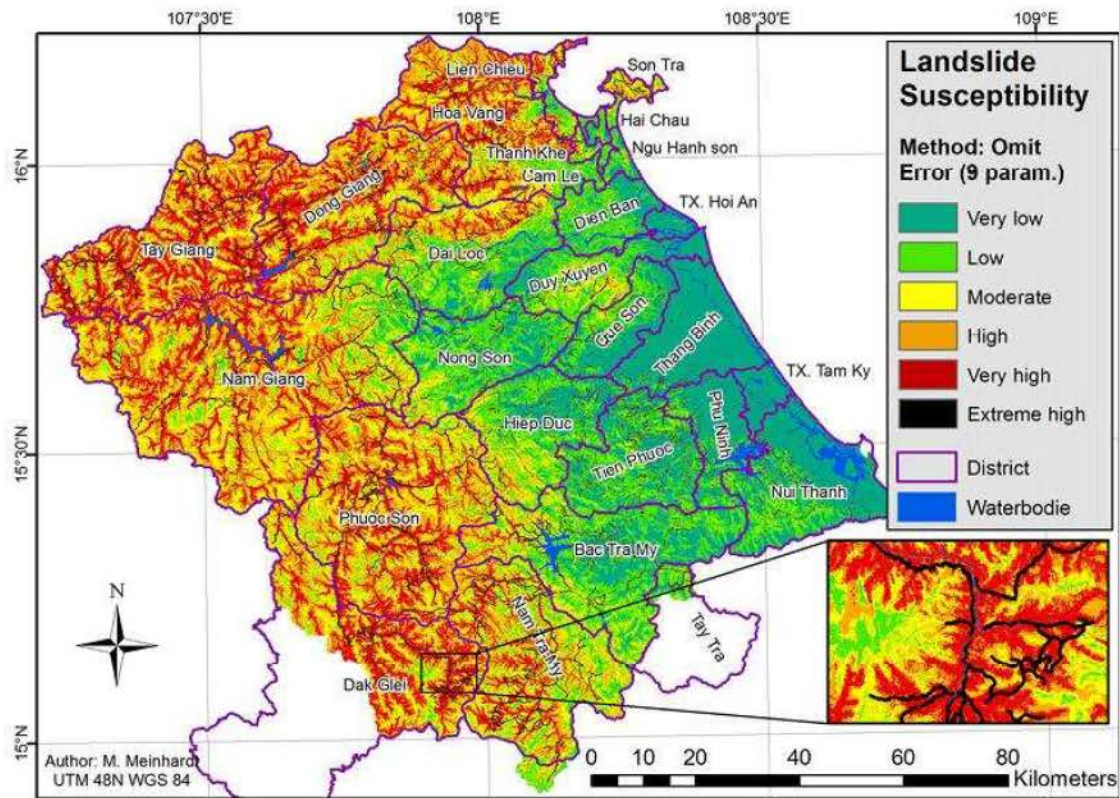
Figure 2.29 Example of landslide susceptibility maps for Quang Nam province (Markus, 2015): The level of landslide susceptibility is represented by the color tone: black represents extreme high landslide susceptibility, red represents very high landslide susceptibility, green denotes very low landslide susceptibility
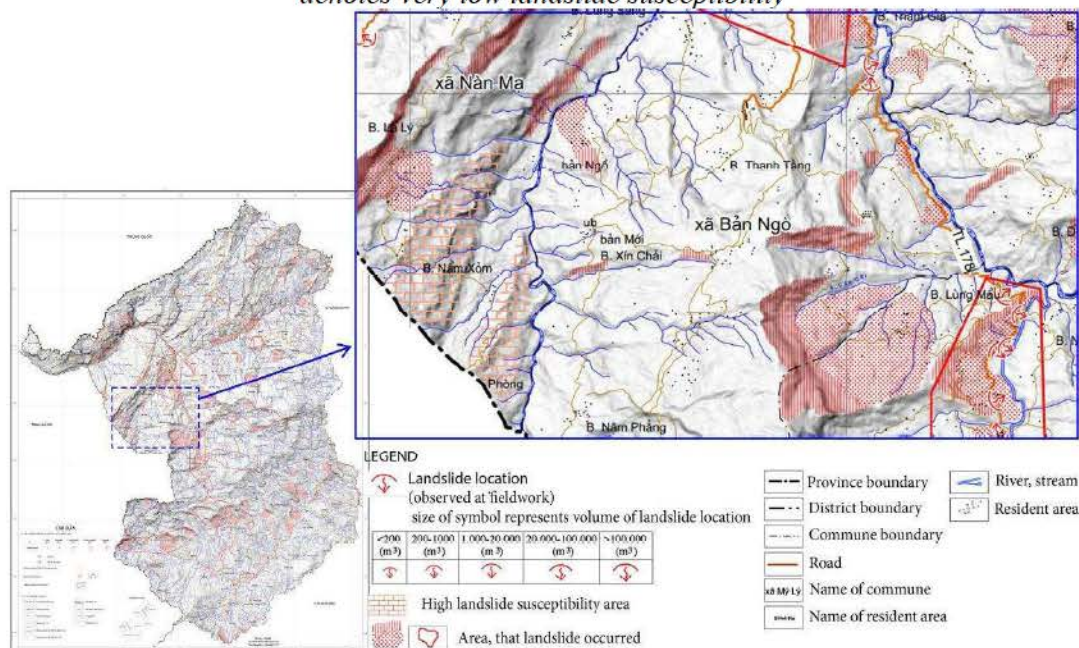
Figure 2.30 Landslide inventory map of Xin Man district, Ha Giang province (produced by State-Funded Landslide Project – Investigation, Assessment and Warning Zonation for Landslides in the Mountainous Regions of Vietnam, 2015)

In general, landslide susceptibility maps are abundant in Vietnam. They have played important roles for spatial planners and risk management in Vietnam. However, landslide

31

inventory mapping is still poorly done. Information related to landslides is not systematic: mostly it is organized by location. The area of extension and type of process are not represented. We lack systems and methods for collecting data and publishing consultation.

2.6. Possibility and limit of aerial photograph interpretation in Japan and Vietnam

As described above, although Japan has a history of 60 years of landslide research by aerial photograph interpretation, progress is still being made in the research of landslide phenomena. In other countries such as Vietnam, landslides are observed as a main mechanism related to development of a slope. The distribution and development are supported by the usefulness of aerial photographic interpretation.

In Japan, aerial photographs of various kinds of a scale have been taken and have been released repeatedly. Aerial photographs have been taken repeatedly at time intervals of less than ten years, with scales of 1/5000 – 1/40,000. For this reason, land can be observed for arbitrary parts in Japan by various details. Changes of geographical features over time have also been checked. Detailed fine micro-landform feature interpretation has become possible and even commonplace from color aerial photography on a large scale (mountain regions of 1/15000 and plains at 1/1000 and 1/8000) taken in the 1970s.

Photograph decipherment technology has progressed. Its application to danger evaluation has been tried. Risk evaluation related to re-activity possibility of the landslide topographic area based on the technology of aerial photograph interpretation was connected with a judgment technique called AHP (Sarty, 2000), and became a settled technology. Miyagi *et al.* (2004) reported outlines and examples of interpretation. Although the author has mastered the technology of aerial photograph interpretation in Japan, some practical difficulties remain for adaptation to Vietnam.

In Vietnam, acquisition of an aerial photographs or a precise topographical map entails some difficulty. The aerial photographs that are useful daily are 1/33000 monochrome images, which is not a good scale for observation of micro-landform features in detail. Moreover, the interpreted landslide topography must be copied into a topographical map, and must be used as a landslide topographic map. However, it is not so high resolution as the accuracy of the contour indicated on topographical maps that show fine landform features.

First, interpretation of the micro-landform features enables observation of the inside of a landslide place. It presents landslide topographic features from creation of a distribution map of landslide topography.

Such a state is not restricted to Vietnam. Many countries can also benefit from aerial photograph decipherment, which is very effective for grasping landslide topography itself in many countries which have aerial photograph resources. If 1/33000 aerial photographs are used, then main slide scarps can show an outline of the landslide topographic area. Moreover, a landslide body and its position, the main movement direction, and other points can be fully deciphered, but micro-landform features are not easy to recognize

In Japan, the Japanese landslide topography distribution map (NIED, 1985–2015) was created using 1/40,000 of monochrome aerial photographs. However, it is not necessarily easy to decipher micro-landform features from 1/33,000 aerial photographs. The micro-landform of the landslide that area exceeds 0.5 km² and for which activity is very high is also large-scale,

and it is the target of interpretation. It is inapplicable to the general subject of "re-activity risk evaluation of landslide topography" if this fine geographical feature cannot show almost all landslide topography features.

Contents

35

CHAPTER 3. GENERAL DESCRIPTION OF THE STUDY AREA

3.1. General environment of Japan regarding potential for landslide disasters

The Japanese Islands are emerged areas of volcanic island arcs extending to about 3000 km and located in a part of circum-Pacific orogenic zone which comprises 10% of the earthquakes. The area accounts for 10% of active volcanoes in the world. Its geology is very young and fragile (Figure 3.1). Japan has four main islands: Hokkaido, Honshu, Shikoku, Kyushu. Among them, Honshu is the largest island, on which the capital (Tokyo) is situated. On the Pacific Ocean side, trenches run parallel to these islands, including the Kuril Trench, Japan Trench, Izu-Bonin Trench, Nankai Trough, and Ryukyu Trench (Figure 3.2).

The Japanese archipelago is located at the meeting point of four plates: the Pacific Ocean plate, the Philippine ocean plate, the Eurasia Continental plate and the North America Continental Plate. The Pacific Plate moves W–NW at a rate of about 8 cm/year, subducting beneath the Kuril Arc and the Izu-Bonin. The Kuril Trench, the Japan Trench and the IzuBonin Trench are deeper than 6000 m in the region where the Pacific Plate is subducted. Quaternary volcanoes lie parallel to these trenches, forming a "volcanic front." In the north, subduction of the Pacific Plate is oblique to the Kuril Trench, causing a strike-slip movement along the Kuril Arc, which results in a local collision zone within the Okhotsk Plate in central Hokkaido (NUMO, 2004).

The Philippine Sea Plate moves NW at a rate of approximately 5 cm/year, subducting beneath SW Japan and the Ryukyu Arc. In southwestern Japan, the volcanic front lies parallel to the Ryukyu Trench and the Nankai Trough. The volcanic front becomes less pronounced in the central areas of Honshu and in Shikoku. To the south, the Philippine Sea Plate is also subducting obliquely to the Nankai Trough, constituting a tectonic sliver moving westward along the strike-slip "Median Tectonic Line" (NUMO, 2004). The tectonic situation is complicated in the area where the North American/Okhotsk Plate, Eurasian/Amurian Plate, and Philippine Sea Plate converge (NUMO, 2004).

The Tohoku district is located at the subduction zone of the Pacific Ocean plate as a place of a typical Island arc and trench system (Figure 3.2, Figure 3.4). The Japan Trench, Ohu Backbone Range, volcanoes, basins, and the earthquake zone stretch parallel: north–south. For this reason, we usually produce an image using an east to west cross section.
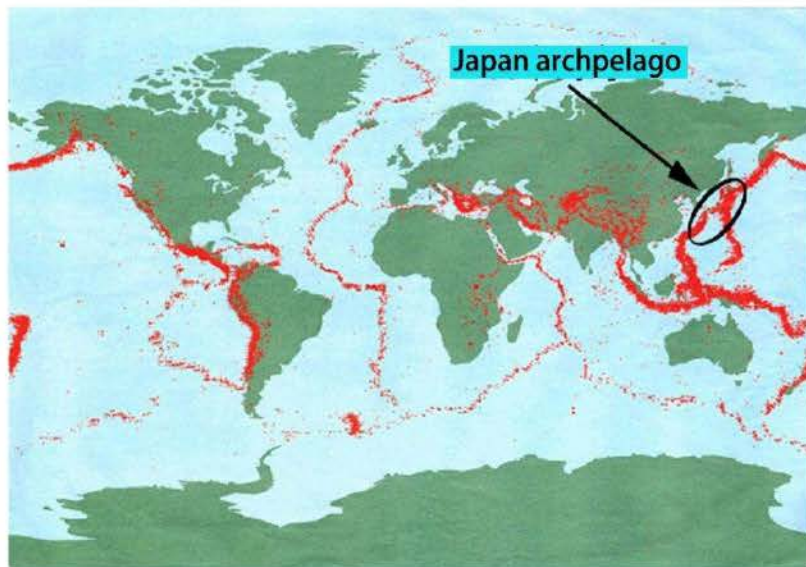
Figure 3.1 World earthquake distribution map (modified from data from headquarters of Research Promotion of Earthquake and Volcanic Disasters in Japan)
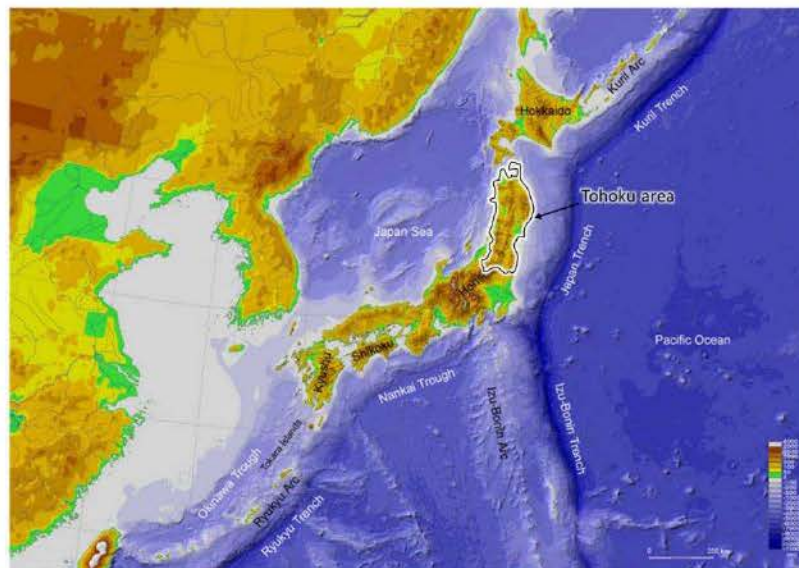
Figure 3.2 Topography and main geographical regions of Japan (NUMO, 2004)
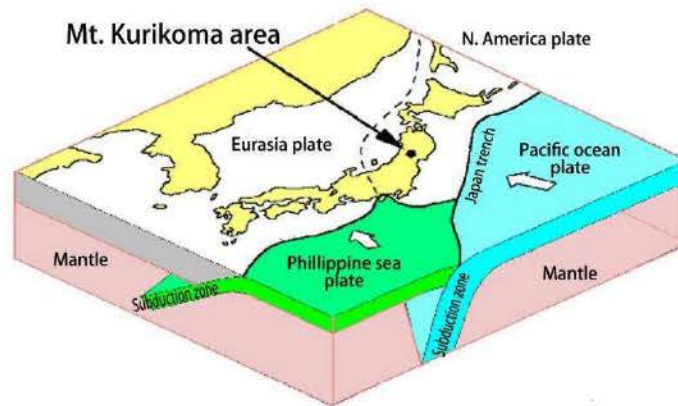
Figure 3.3 Four main plates of Japan (modified from data from the headquarters of Research Promotion of Earthquake and Volcanic Disasters in Japan)

Figure 3.4 shows a cross section of the Tohoku district. The typical island arc and trench system is established by the relations of the subduction of the Pacific Ocean Plate to under the North American Continental Plate. This system generates earthquakes of four types: at the plate boundary, at the subduction, shallow earthquakes at the continental plate, and earthquakes related to volcanism. In 2010, over 1300 earthquakes were sensed in Japan. The frequency of magnitude (M) ≥5 aftershocks during the two weeks after the main shock of M 9 earthquake in eastern Japan in 2011 was greater than 400.
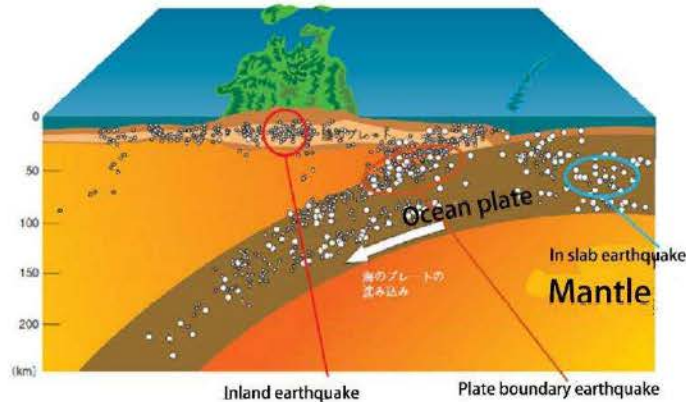
Figure 3.4 Cross section of the Tohoku district (modified from data of the headquarters of Research Promotion of Earthquake and Volcanic Disasters in Japan)

Figure 3.5 presents an outline of the schematic cross profile of the eastern half of the Tohoku District and the main landslide phenomenon in the area of interest (Miyagi *et al.*, 2011). In this area, volcanic sediment is deposited on a Tertiary structure forming the foundational ground and the sediment such as lava, pyroclastic flow sediment, and mudflow sediment, various substantially in scale, consolidation, specific gravity, composition and other characteristics. Geological caldera structures occur in the foothills, which are thought to have been formed from the end of the Tertiary to middle of the Quaternary. These are partly filled with thick, weak lacustrine sediment.
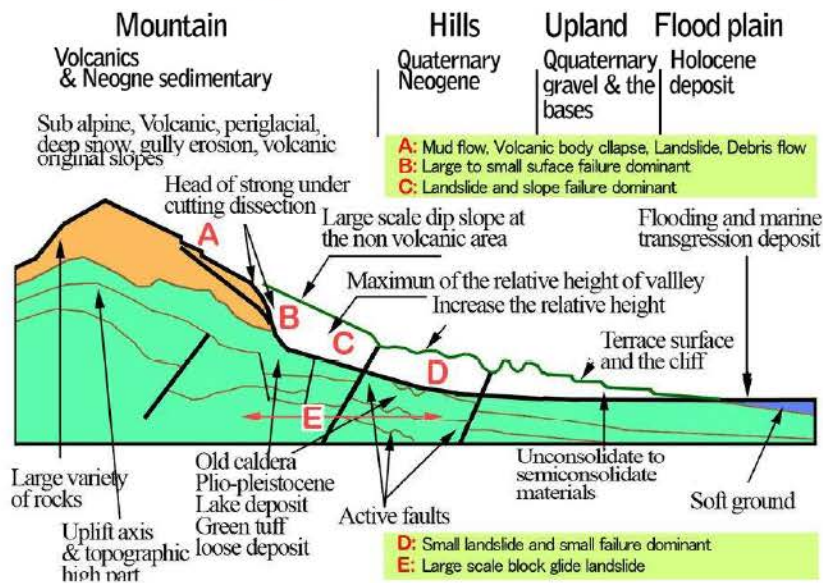
Figure 3.5 Outline of the schematic cross profile of the eastern Tohoku District (Miyagi et al., 2011)

36

Regarding climate, the area of Japan archipelago has typical temperate monsoon climate and characterized as the high precipitation. The Pacific Ocean High Pressure in the southeastern area brings strong typhoon activity at the southern part of Japan. The cold and dry northwestern winds blow in winter and bring heavy snowfall, contrasting against the wet and hot southeastern winds blowing in summer (Figure 3.6). Furthermore, typhoons usually hit during summer. Figure 3.7 shows typical weather satellite Himawari images in summer. Strong typhoon activity brings heavy rainfall causing torrential rains in and around Japan. Figure 3.8 presents a typical weather satellite Himawari image in winter. Cold air flows across Japan, bringing heavy snowfall to its Sea of Japan coast.
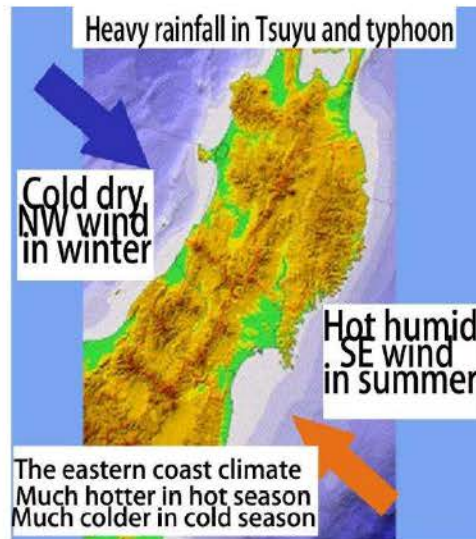
Figure 3.6 Schematic showing Siberian High Pressure on Northwestern and the Pacific Ocean High Pressure on southeastern areas
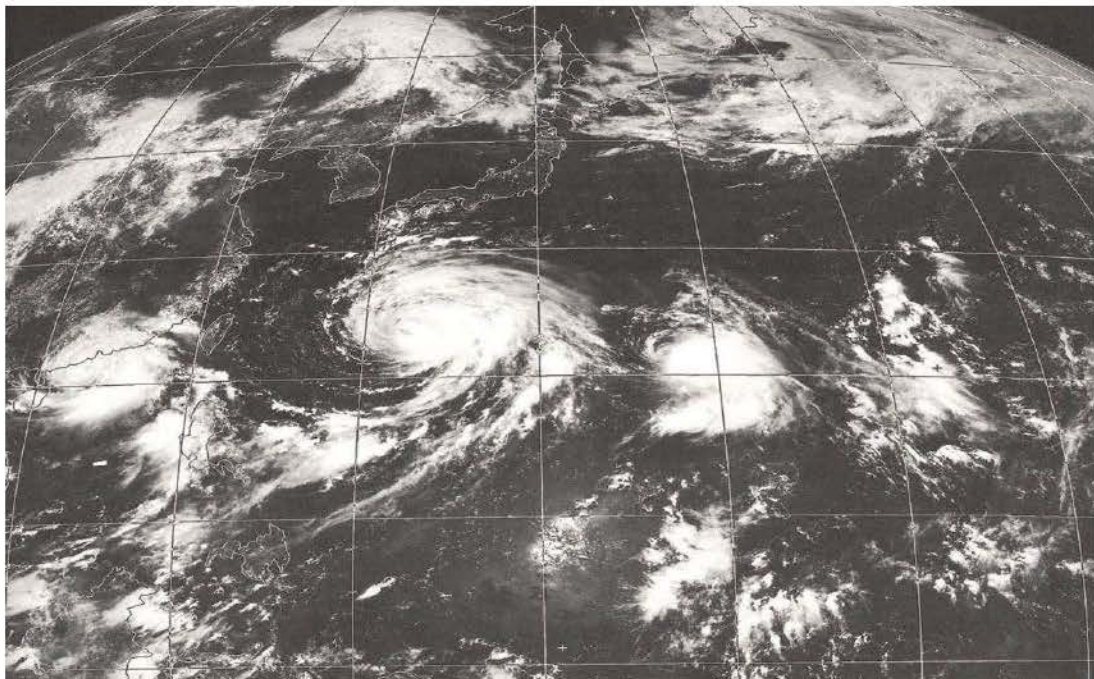
Figure 3.7 Typical weather satellite Himawari image in summer (strong typhoons bring heavy rainfall) (Takahashi, 1982)
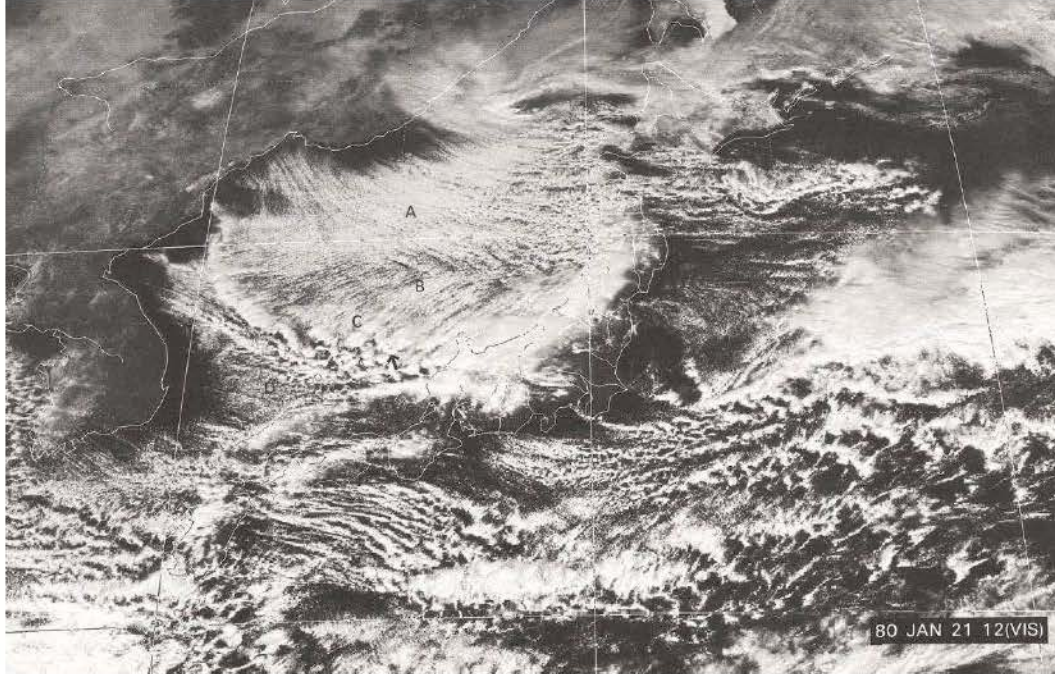
Figure 3.8 Typical weather satellite Himawari image in winter (cold air flowed across Japan, bringing heavy snowfall to its Sea of Japan side) (Takahashi, 1982)

Regarding geology, the Japan region has been in a zone of subduction-related accretionary tectonics since the Permo-Jurassic (>295–135 Ma). It is also situated in a volcanic zone on the Pacific Ring of Fire. Therefore, Japan, especially the Tohoku district, is characterized by a very active orogenic zone. This environmental condition leads to the severe background of landslide disasters in the district.

3.2. Landslide disasters around the study area

Japan, especially the Tohoku district, is characterized by a very active orogenic zone and typical monsoon climate. This set of environmental conditions leads to a severe background for landslide disasters in the district, with landslides of various types such as surface failures, shallow landslides, deep failures, deep-seated landslides, and rock falls (Miyagi *et al.*, 2011). Earthquakes are a main factor affecting landslides in this area. At 8:43 am on June 16, 2008, an earthquake of M7.2 (Richter scale) with a focal depth of 8 km struck in the southern part of interior of Iwate prefecture. The main shock and after-shocks occurred in an area stretching in a NNE–SSW direction, approximately 45 km long and 15 km wide. The main shock occurred almost in the middle of the area (Forestry Agency Japan, 2015). The earthquake was characterized by intense acceleration and extremely short-period shaking on the hanging-wall side of the source fault. Among the seismic waveforms observed at the station around the epicenter, the long-period acceleration waveform (1 s to 2 s), which can cause damage to structures such as houses, is displayed on Figure 3.10 and is overlapped with those of past earthquakes (Forestry Agency Japan, 2015).
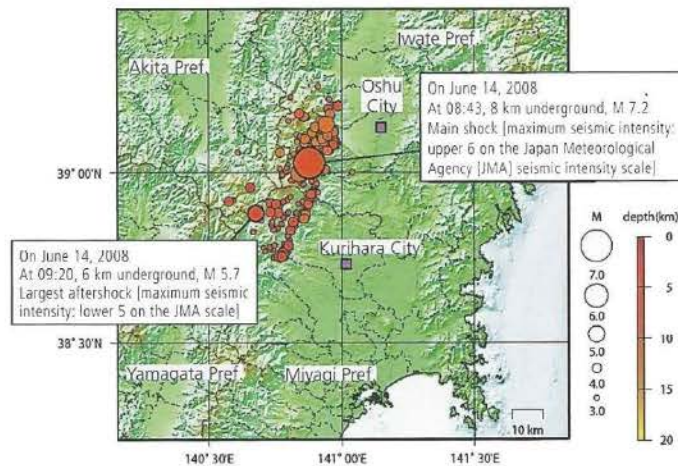
Figure 3.9 Epicenter distribution map on and after the June 14, 2008 earthquake (Forestry Agency Japan, 2015)

The peak acceleration of this earthquake was about half that of The Southern Hyogo Prefecture Earthquake in 1995 and the mid-Niigata Prefecture Earthquake in 2004. Therefore, the effects on structures such as houses are believed to have been limited (Forestry Agency Japan, 2015).

However, the short-period acceleration waveform (0.3-s) was predominant, so that characteristics of damage are believed to have been mainly ground failures in mountainous regions with smaller layers of sediment, which can absorb seismic ground motion (Forestry Agency Japan, 2015).
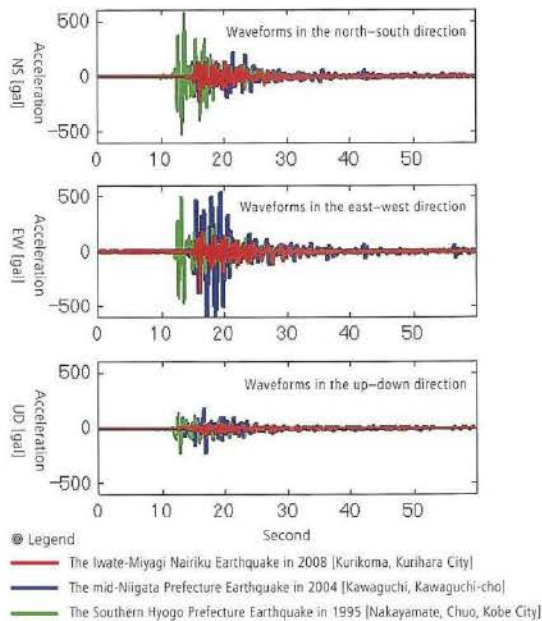
Figure 3.10 Comparison of seismic waveforms in Iwate–Miyagi 2008, Niigata 2004, and Southern Hyogo 1995 earthquake (Forestry Agency Japan, 2015)

Figure 3.11 shows the Shizumikurasawa deep-seated landslide at the upper reaches of Nihasamagawa, which occurred during the 2008 earthquake, with geology that is characterized

by pumice tuff and welded tuff distributed on alternating layers of sandstone and mud stone (Forestry Agency Japan, 2015).

Figure 3.11 Shizumikurasawa deep-seated landslide in the upper reaches of Nihasamagawa (Forestry Agency Japan, 2015)

Figure 3.12 shows the Kawaragoyasawa surface landslide at the Ichihasamagawa River Basin, which occurred in welded tuff distributed on pumice tuff and tuff breccia. In this area, 751 slope failures were observed. The amount of unstable debris reached approximately 14,670,000 m³ (Forestry Agency Japan, 2015).

Figure 3.12 Slope failure (Surface landslide) at Ichihasamagawa River Basin (Forestry Agency Japan, 2015)

Figure 3.13 shows an earthflow that occurred at Dozousawa, located at Mt. Kurikoma, characterized geologically by mudflow sediment overlain by pumice tuff distributed on welded tuff. In this area, large-scale slope failures occurred at first, later turning into debris or flow. In all, 137 slope failures were observed in this area. The amount of unstable debris reached 1,690,000 m³.

Figure 3.13 Earthflow at Dozousawa (Forestry Agency Japan, 2015)

Figure 3.14 presents a bird eye view of Aratozawa landslide before and the after landslide event. This landslide was located at a gentle slope at the southeastern part of Kurikoma mountain, about 4 km far from the study area. It was the largest landslide among mountain disasters caused by the Iwate–Miyagi earthquake. It was also the largest landslide in Japan. It was 900 m wide and 1,300 m long, with area of 98 ha and a maximum drop of the main scarp of 150 m. Observed data show that the angle of inclination of the slip surface is extremely gentle (1° and 2°) (Figure 3.15). The geology consists of pumiceous tuff and welded tuff distributed on lacustrine sediment of geological caldera (Forestry Agency Japan, 2015).

Figure 3.14 Bird's eye view of Aratozawa landslide before and after the landslide event
(Miyagi et al., 2011)
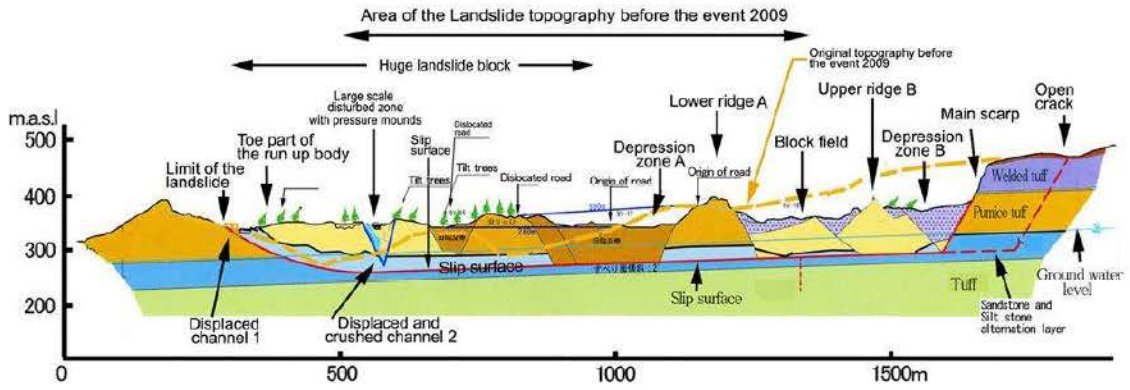
Figure 3.15 Typical cross profile of the Aratozawa landslide (Miyagi et al., 2011)

Figure 3.16, Figure 3.17 show the Oikubo landslide, which occurred because of heavy rainfall.

Figure 3.16 Oikubo landslide (a: aerial photograph after the movement; b: prefectural road cut and transformed about 30 m; c: overview of the upper part of landslide (Higaki et al., 2008)
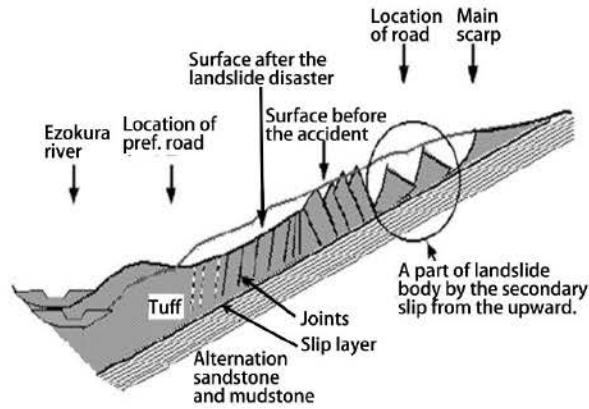
Figure 3.17 Cross section of the landslide of the Oikubo landslide (Higaki et al., 2008)
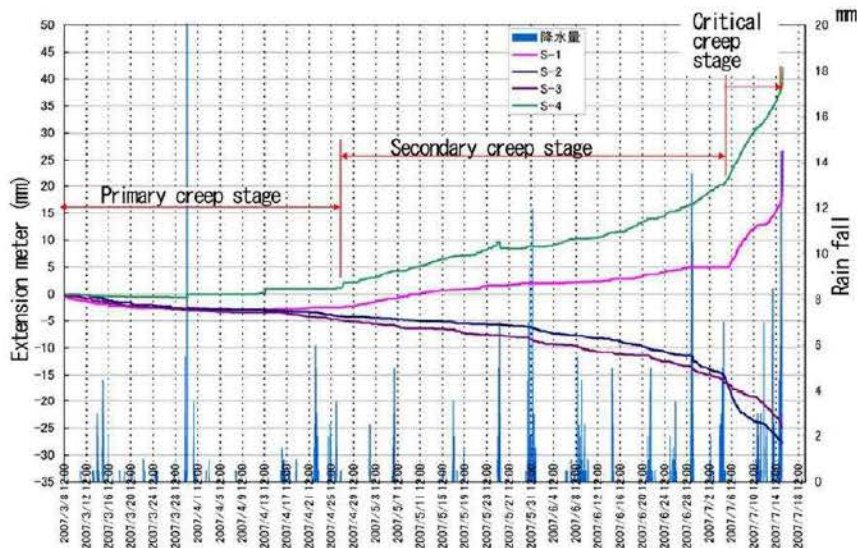
Figure 3.18 Rainfall record and the deformation sequences of the extension meter at the Oikubo landslide (Higaki et al., 2008)

3.3. Japan study site at Fukayamadake area

3.3.1. General environment and study area selection

The study area, Fukayamadake, is located south–southeastward of Mt. Kurikoma (Figure 3.21), a volcano in the Ohu mountain range. The area is between 38°52'30.92" and 38°51'2.1198" North latitude, between 140°49'40.97" and 140°51'41.57" East longitude. It belongs to the Tohoku area and the Japan archipelago.

The study area is just 4 km distant from the Aratozawa landslide, the largest landslide in the Tohoku area. From its center spreads a gentle pasture called the Fukayama pastureland. This pasture is a low relief surface with elevation around 550 m, bordered by the Onomatsuzawa Valley, a branch of the Nihasama River on the northern side, and by the Tozawa River on the south. The relative height between the Onomatsuzawa Valley and the Fukayama pastureland is about 100 m. Mt. Hitsugaori has elevation of 700 m, rising high over the east side.

The study area sustains severe rains caused by the temperate monsoon climate and typhoons. Average annual rainfall is about 1,285 mm; average annual temperature is about 11.08°C. Rivers that dissect the upheaving mountain slopes have caused violent down-cutting, which has developed ubiquitous gorges with relative height of more than 100 m. Developed gorges of a relative height near 150 m are observed also around this study region, such as in the upper stream of the Ichihasama River and the Osawa Valley on the Nihasama River. A huge dip slope structure formed by volcanic sedimentary rocks such as the Neogene green tuffs and Quaternary volcanic rocks has been cut deeply into an erosional valley to form a large-scale landslide. Many caldera structures were developed in the Tohoku district in the middle of the young orogenic movement. Oyagi (2008) pointed out that the existence of a lacustrine deposit aggrading this caldera is an important factor affecting formation of a large-scale landslide concentrated in the Tohoku district.
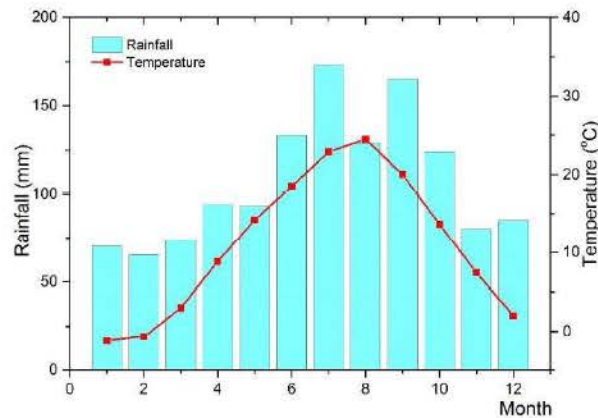
Figure 3.19 Average rainfall and temperature of study area; last 30 years from 2014 (data from www.climate-data.org at Kurikoma city weather station).

When the 2008 Iwate–Miyagi Nairiku Earthquake struck, more than 3,000 slope disasters occurred, such as landslides and slope failures, in the foothills of Mt. Kurikoma. Among these, multiple huge landslides took place near this study region, including the huge and destructive Aratozawa landslide, the largest in Japan. For this area, Landslide Distribution Maps are available from the National Research Institute for Disaster Prevention (NIED). The risk evaluation of reactivation of landslide topographic areas by Miyagi Prefecture has also been implemented. Repeated surveys of landslides and landslide topographic areas in this area have promoted wide understanding that large-scale landslides occur frequently in this area because of a caldera on the southern foothills of Mt. Kurikoma. However, it is not correct to infer that landslides rarely take place outside the caldera. The Landslide Distribution Maps by NIED also describe multiple large-scale landslides outside the caldera. Not long ago, a large-scale landslide occurred in the Kanisawa area.

Figure 3.20 Typical landscape of the study area: Fukayamadake Pastureland and Mt. Kurikoma Volcano (Le and Miyagi, 2015c)
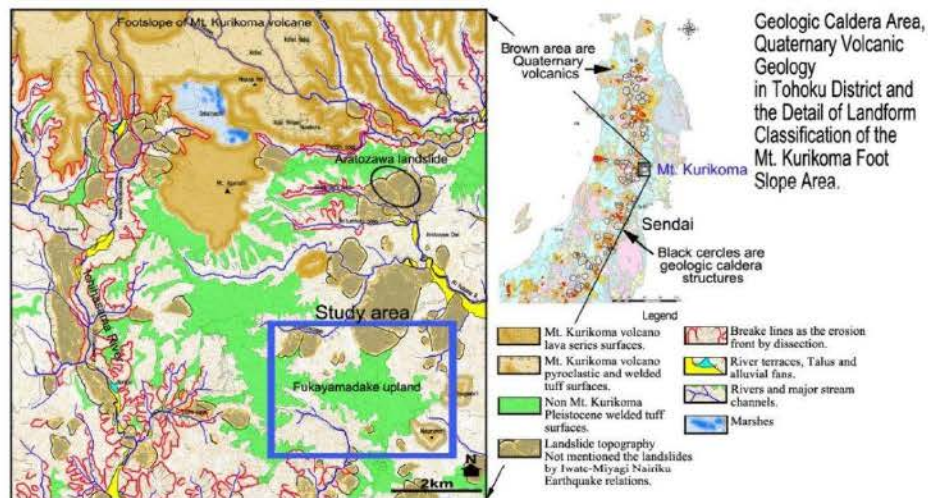
Figure 3.21 Study area and distribution of the geologic caldera structures and Quaternary volcanics in Tohoku district northeastern Japan (right up) (Le and Miyagi, 2015c) Landform classification map includes landslide topography. Landslide topographies referenced from NIED Data

3.3.2. General description of topography, geological features, weathering crust features, geomorphologic features

Geological features of this region were presented in the Database of Neogene Geology in Tohoku Main Arc, edited by Kitamura (1986), followed by the seamless digital geological map of Japan compiled by the Geological Survey of Japan of the National Institute of Advanced Industrial Science and Technology (AIST). Oba *et al.* (2009) reports the latest search results, which show that caldera sediments of the Pliocene designated as the Onomatsuzawa formation prevail over the whole neighborhood in the north of the Fukayama pastureland, and the Hosokura formation of the Miocene dominates the south. Mt. Hitsugaori to the east comprises andesitic lava. The entire area of Fukayama pastureland and Onomatsuzawa Valley has been believed to be caldera sediments. However, the age of the

45

lacustrine deposits of the caldera is estimated by Oba *et al.* (2009) as younger. It has also been believed that the low relief surface of the Fukayama pastureland comprises Kitagawa dacites (welded tuffs). However, its stratigraphic view was reorganized drastically by Oba *et al.* (2009): sediments on the low relief surface are an ejection related to the formation of the Onikobe and Naruko calderas, and comprise the Ikezuki welded tuffs (semi-consolidated), the Shimoyamasato tuffs (about 250,000 years ago), the Nisaka tuffs (60,000–80,000 years ago), and the Yanagisawa tuffs (40,000–50,000 years ago), from the bottom. The geological features exposed to both north–south foothills of the Fukayama pastureland differ greatly. This is considered to be true because a caldera rim is hidden underground of the Fukayama pastureland. Gravity anomaly measurements by AIST revealed a clear and sudden change from positive to negative at the north edge section of the Fukayama pastureland, which is regarded as corresponding to a part of the south rim of the caldera on the south foothills of Mt. Kurikoma. Most regions in the Fukayamadake area comprise the Hosokura formation of the Miocene, with Lacustrine deposits such as the Onomatsuzawa formation piled up on the lake basin formed by the caldera deformation of this Hosokura formation. Then, the hilly area composed of the Hosokura formation and the Onomatsuzawa formation had been filled since several hundred thousands of years earlier by sedimentation of the Ikezuki welded tuffs and previously described layers to form the present low-relief surface.

The whole study region has been eroded severely by dissection by branches such as the Onomatsuzawa Valley after the formation of the low relief surface. Erosion is progressing by an arborescent river system. Under these circumstances, the role of the landslide is attracting attention in the erosion activities of areas in which many landslide topographic areas are distributed. Especially, the existence of large-scale landslide topographic areas flowing down toward the Aratozawa Dam and the Onomatsuzawa Valley in the northwestern part of the area has attracted attention.
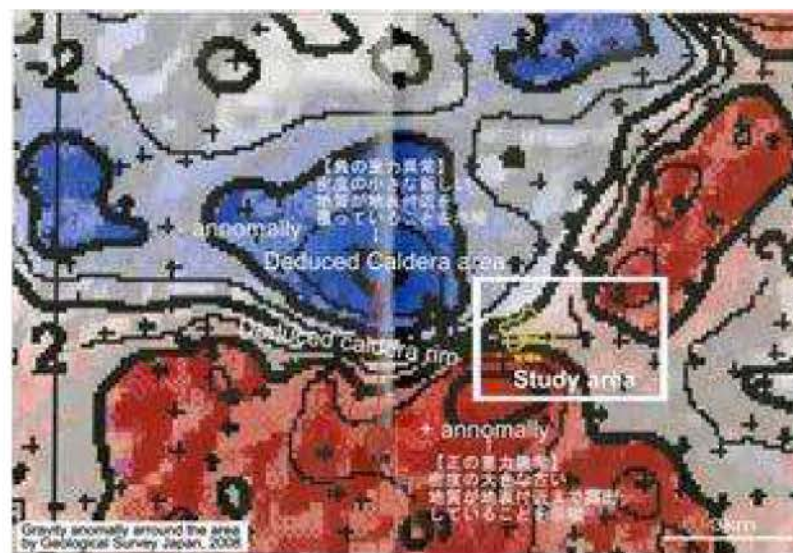
Figure 3.22 Gravity anomaly of the Caldera structure area by Geological Survey of Japan (Le and Miyagi 2015c)

46
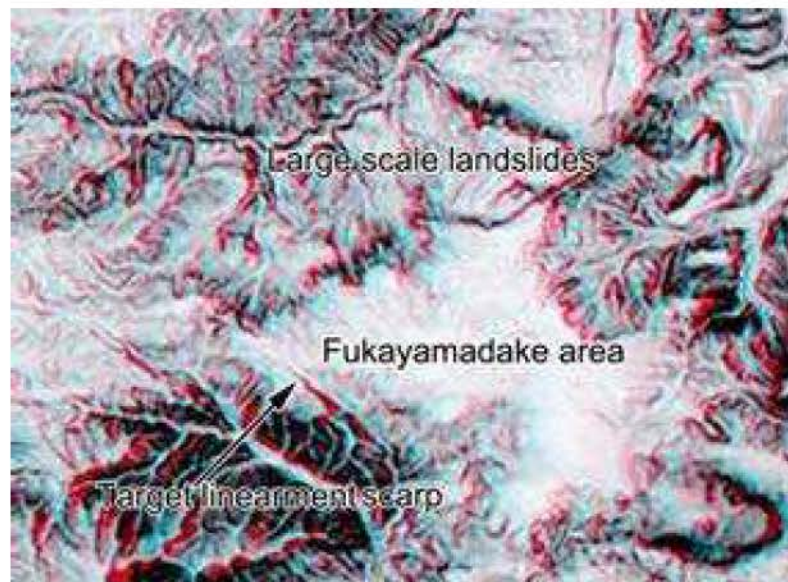
Figure 3.23 Shadow image of the study area, established by 5 meter DEM (Le and Miyagi 2015c)

3.4. General environment of Vietnam and study area

The study area is located in central Vietnam along Ho Chi Minh road, covering between 15°59'57.1" and 15°22'26.5" North latitude, and between 107°37'36" and 107°52'37' East longitude. Its altitude is about 400–1000 m above sea level. The study area comprises four districts (Dong Giang, Nam Giang, Phuoc Son, Dai Loc), covering an area of 1000 km² with around 20,000 residents.

The study area has monsoon tropical climate. Every year, there are around 2,000 hours of sunshine on average. The sunny season is April–August, average annual temperatures are about 25.91°C. The highest temperature is over 39°C in April, May, or June. The cold season only lasts for 3 months: December, January, and February. The hot season lasts for 6 months from April through September.

Average annual rainfall is about 2,043 mm, although the highest rainfall was reported as high as 3,800 mm. The rainy season lasts from September through November. Particularly, during the past 50 years (1961–2008), more than 44 typhoons have affected the study area. Peak storm frequency has been reported for October and November.

Table 3-1 Number of typhoons in study area (QCVN 02: 2009/BXD - Vietnam Building Code Natural Physical and Climatic Data for Construction)

Periods	Number of storms	Periods	Number of storms
1961-1970	8	1991-2000	5
1971-1980	11	2001-2008	6
1981-1990	14		

47
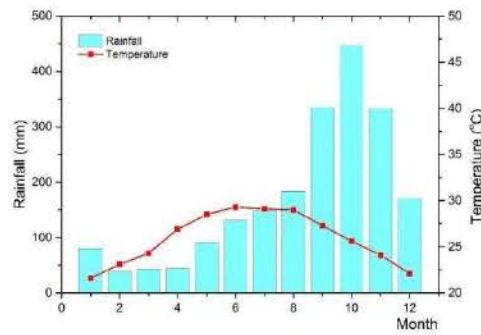
Figure 3.24 Average rainfall and temperature of the study area: last 30 years from 2014 (data from www.climate-data.org - at Thanh My weather station)

3.5. General description of topography, geological features, weathering crust features, geomorphologic features of the study area in Vietnam

Topography

The study area has topography of generally high relief, dominated by landforms of high undulating mountains. The altitude decreases gradually from north to south and is classifiable into three parts: mountainous, hilly, and plain areas. Mountainous areas occupy most of the total area (80%) although smaller shares of terrain are hills and plains. The northern part of this area is strongly dissected and steep, characterized by high mountainous relief with altitudes of 600–1500 m. The highest mountains are 1674 m. The southern part altitudes are 200–600 m, with relief features such as hills and various alluvial plains. The hills are dispersed between the mountains and the plains. Surface materials range from stones through silts and clays.

River and stream systems have short lengths and steep longitudinal morphometries, which abruptly change into gentle slopes in the plains. The study area has four main rivers: A Vuong, Bung, Giang and Cai River.
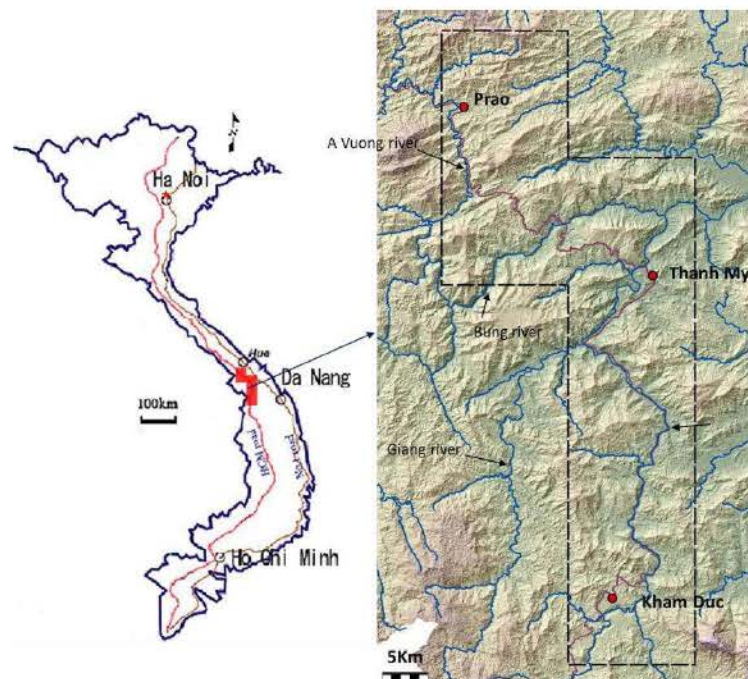
Figure 3.25 Study area and distribution of land elevation throughout the study area (detail relief established from DEM data in ITST)

48

Geological features

Geological features in the study area shown in Figure 3.26 c are divisible into four main groups as described below:
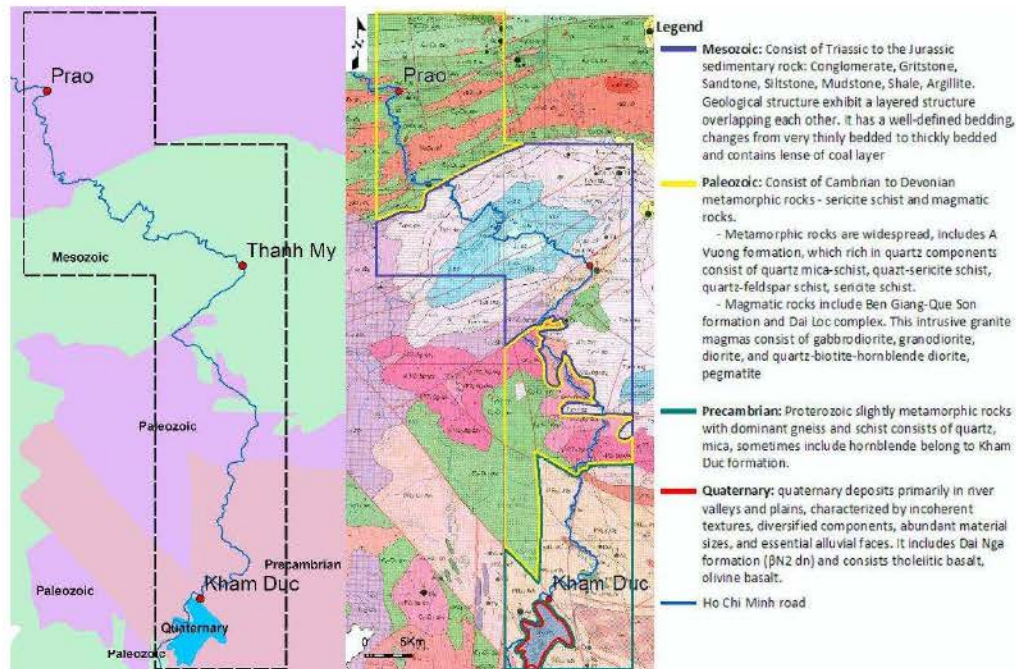
Figure 3.26 Simplified geological map of study area (Ho Chi Minh road) (modified from Le et al, 2015d)

Mesozoic: This area includes Nong Son, Ban Co, Khe ren, Huu Chanh, and Song Bung, with Song Bung formations and Cha Val, Hai Van, Deo Ca complexes. It has Triassic to Jurassic sedimentary rock: conglomerate, gritstone, sandstone, siltstone, mudstone, shale, Argillite. Geological structures exhibit mutually overlapping layered structures. It has a well-defined bedding, changing from very thinly bedded (2 cm mudstone) to thickly bedded (3 m sandstone). It consists of conglomerate, gritstone, sandstone, siltstone, mudstone, shale, and Argillite layers, containing lenses of coal layers. The sandstone is generally fine to coarse grained, containing high contents of quartz and mica (Le *et al.*, 2015b).

Paleozoic: This area includes A Vuong, Tan Lam, Long Dai, Ben Giang - Que Son formations, and Dai Loc complexes. It consists of metamorphic rock: sericite schist and granite (Le *et al.*, 2015b).

Geology in this area is divisible into two groups: metamorphic rocks and magmatic rocks.

- Metamorphic rocks are widespread. They are included in Long Dai, A Vuong, and Nui Vu formations, which are rich in quartz components consisting of quartz mica-schist, quartz-sericite schist, quartz-feldspar schist, and sericite schist.

- Magmatic rocks include the Ben Giang-Que Son formation and the Dai Loc complex. These intrusive granite magmas consist of gabbrodiorite, granodiorite, diorite, and quartz-biotite-hornblende diorite, as well as pegmatite.

Precambrian: This area includes Kham Duc formations. They consist of hornblende, quartz-mica, and biotite. Kham Duc formation's granite occupies almost all of this area, consisting of medium to coarse-grained. The medium to coarse-grained granite consists mainly of quartz, mica and biotite, sometimes with hornblende. The region is characterized by a very thick layer of residual soil and completely weathered material with 2–10 m depth. It is overlain over high and moderate weathered material, at bottom of the river, granite breaks into small to medium blocks. This structure is prone to slide behaviors (Le *et al.*, 2015b).

Quaternary: This area includes quaternary deposits primarily in river valleys and plains, characterized by incoherent textures, diverse components, abundant material sizes, and fundamental alluvial facies. It includes the Dai Nga formation (βN_2 dn) and consists of Tholeiitic basalt and olivine basalt (Le *et al.*, 2015b).

Weathering crust features

The study area has a tropical climate, which strongly influences the weathering process. Weathered materials are also strongly involved in landslides because rapid weathering processes that occur under humid conditions strongly weaken and degrade regolith covers.

According to Tran Tan Van (Tran, 2006), the weathered crusts in area show high diversity deep, texture, landform, chemical–mineral components, geochemical characteristics, and origin. The reasons include the many different processes that create such weathering crusts such as climate (tropical monsoon climate, hot and wet condition, long time of rainfall), topography (mountains and hills, paleo planation surface, weathering traces), geology (existences of various geological structures), time effects in generation, and development of weathering crusts there.

In each weathering zone, weathering products typically have mineral components, structures, and textures that reflect the origin and the creation conditions of the weathering zone.

The Mesozoic zone becomes slightly to moderately weathered, with shallow to moderate depth depending on lithology. The depth of the weathering crust layer is changeable from 10 m to 30 m. Sedimentary rocks break into small to medium blocks. Joints and fractures are well developed. These cracks combine with bedding plane openings to provide moderate to high permeability (Le *et al.*, 2015b).

The Paleozoic zone has differences of weathering among areas. The area between Prao town has high weathering, surficial soil layer that is brown with high contents of clay and fresh rocks observed at the bottom of the slope next to the river, it is quartz-sericite schist and biotite schist, belonging to the A Vuong formation. The depth of the high weathering crust is about 10–20 m. At other metamorphic rock areas, the degree of weathering is not as high as in the Prao town area, schists are visible at the slope. In this area, shallow debris slides, wedge type slides and rock falls are frequent. For magmatic rocks, fractures and cracks are moderately developed. The upper parts of rocks mass have changed to soil. The depth of this layer is diverse, from 1 m to 3 m. Lower parts of rocks show a loss of strength, with discoloration appeared. Fractures and cracks are moderately developed with irregular spacing (Le *et al.*, 2015b).

The Precambrian zone has high weathering. A surficial weathered material layer is reddish brown and is silty to sandy grained. It rapidly loosens with increasing amounts of water. Granite rock masses break into small to medium blocks, which are only observed at a river with depth of 10–30 m lower than surface. Therefore, the depth of the high weathering crust is greater than 30 m (Le *et al.*, 2015b).

The Quaternary zone has lake deposits (black reddish brown color with a weathering level that is not so deep), with a boundary of the volcanic and lake deposits (black deeply weathered material, and many holes because of the lava gas. Lake sediments are deeply weathered and have changed to clayey materials (Le *et al.*, 2015b).

Geomorphologic features

The study area is an end of the Truong Son range and the connection area of the Kom Tum massif. The northern part of the nation belongs to the Truong Son range, which is primarily an ancient crystalline platform. During Paleozoic and early Mesozoic orogenetic movements, this solid platform was not folded, but rather dissected into a number of blocks uplifted into separate plateau of varying elevations. This zone is characterized by very steep eastern slopes, resulting from an extensive geological fault that split the solid crystalline blocks of the ancient plateau during the Triassic age about 200 million years ago. In some places, faults represent vertical cliffs that are more than 100 m high. This area is also characterized by narrow, highly eroded canyons of ancient eroded crystalline rocks (mainly granite and gneiss). Rivers of this area are rather short and rapidly draining.

The southern areas are characterized by a wide plateau, consisting of Dai Hong, Dai Chanh, Dai Thanh and Que Ninh wards, and Kham Duc town. Altitudes are reduced from 800–950 m to 400–500 m ranging from 600–800 m. Natural slopes are fairly steep. This zone represents a peneplain of leveled Hercynian folding of old schist and sandstone, largely overlain by basalts of various ages (Tran, 2006).

3.6. Landslide disasters in the study area and surrounding

The study area has a richly varied geologic composition with many stratigraphic unit and strata, rock have been found from Cambrian to Quaternary and has also a tropical climate. These features promote intense chemical weathering. The weathering crust is extremely thick and has highly diverse deep, texture, landform, chemical-mineral components, geotechnical characteristics and differences among areas. In each weathering zone, weathering products typically have structure, texture, and mineral components and reflect original rocks and creation conditions of weathering zones.

These features play an important role in causing and promoting landslides in the study area. For example, in the Mesozoic zone (between Prao and Thanh My), geology consists of well-bedded sedimentary rocks and lenses of a weak layer (coal layer and mudstone layer). Most landslides have occurred as translational slides along the bedding plane and the weak layer. These weak layers are key factors controlling landslides in this area.

In the Quaternary zone, located on Kham Duc town, geological structures are usually flat, including lake deposits with extremely weak layers such as organic rich, peat and clayey layers, and volcanic rocks: with intruded basalt consolidate hard and heavy rock. The lake

deposits are black reddish brown but the weathering level is not so deep. The boundary of the volcanic and lake deposits is black deeply weathered material, with many holes because of the lava gas. Lake sediments are deeply weathered and changed to clayey materials. Landslides occur as rotational slides along river side slopes, with a complex of small to surface landslides and soil creeps.

In Paleozoic: The geology of this area is divisible into two groups: metamorphic rocks and magmatic rocks.

– Metamorphic rocks are widespread, included Long Dai, A Vuong, and Nui Vu formations, which are rich in quartz components consisting of quartz mica-schist, quartz-sericite schist, quartz-feldspar schist, and sericite schist.

– Magmatic rocks include the Ben Giang-Que Son formation and Dai Loc complex. These intrusive granite magmas consist of gabbro-diorite, granodiorite, diorite, and quartz-biotite-hornblende diorite, pegmatite.

Characteristics of landslides in this area depend on the degree of weathering. On the metamorphic rock area, which has high weathering, most landslides occur at high and deep weathering layers and are classified as slumps. At moderate weathering areas and magmatic rocks, landslides are small. They might be classified as shallow debris slides or debris flows and wedge type slides. Debris slides occur at the top of the weathering crust: reddish brown soil and has high content of clay. The landslide at N15°55'59.3" E107°32'17.4" is typical of this type. A wedge type slide occurs at slightly weathered rocks. In that layer, there are many cracks in different directions. The landslide at N16°04'50.4" E107°29'17.2" (Fig. 2.11) is typical of this landslide type. The landslide at N16°05'11.8" E107°28'16.6" is a complex combination of multiple wedge slides.

In the Precambrian zone: This zone is formed by granite rock, belonging to the Kham Duc formation, of the Precambrian age. Granite has undergone intensive tropical weathering process, creating a profile with various characteristics and thicknesses. Surficial weathered material layer is reddish brown and is silty to sandy grained. It rapidly loosens with increasing amounts of water. Granite rock masses break into small to medium blocks, these blocks are only observed at rivers with depth that is 10–30 m lower than the surface. Therefore, the depth of the high weathering crust is greater than 30 m.

Most landslides in this area are small to medium size. They are strongly associated with weathered material. These types of landslides are rotational slide and debris flow slides, occurring in intense and heavy rains. During that time, it saturates residual soil. Landslide material is porous and friable. It enters streams, forming a debris flow. In the rotational slide, the main scarp has a tendency to be vertical.

Generally, landslides are abundant in this study area. Field surveys have revealed numerous landslides. They are classifiable into six types: rock falls, rotational slides, translational slides, debris slides, debris flows and earth flows, and wedge type slides.

Rock falls

Rock falls are abrupt movements of masses of geologic materials, such as rocks and boulders, which become detached from steep slopes or cliffs (http://pubs.usgs.gov). Separation

occurs along discontinuities such as fractures, joints, and bedding planes. Movement occurs by free-fall, bouncing, and rolling. Rock falls are very rapid to extremely rapid mass movements (from m/min to m/s). Rock falls are influenced strongly by gravity, mechanical weathering, and the presence of interstitial water. In the study area, rock falls were found in Paleozoic zone.

Figure 3.27 Rock fall (photograph by Le)

Rotational slides

Rotational slides occur where the surface of rupture is curved concavely upward and the slide movement is roughly rotational about an axis that is parallel to the ground surface and transverse across the slide. These often involve combined processes of earth movement (rotation of a block of overburden over a broadly concave slip surface, or slump). Rates of movement range from extremely slow (mm/year) to rapid (m/s). In the study area, we usually observe this type in a high weathering zone.

Figure 3.28 Rotational slide (photograph by Le)

Translational slides

Translational slides occur where the landslide mass moves along a roughly planar surface with little rotation or backward-tilting. A block slide is a translational slide in which the moving mass consists of a single unit or a few closely related units that move downslope as a

coherent mass. Movement rates range from rapid (m/min) to extremely rapid (m/s) and are usually initiated below the surface. Most slides of this type occur in the Mesozoic zone.

Figure 3.29 Translational slide (photograph by Le)

Debris flows

A debris flow is a form of rapid mass movement in which a combination of loose soil, rock, organic matter, air, and water mobilize as a slurry that flows downslope. Debris flows include <50% fines. Debris flows are commonly caused by intense surface-water flow, because of heavy precipitation, that erodes and mobilizes loose soil or rock on steep slopes. Debris flows also commonly mobilize from other types of landslides that occur on steep slopes, are nearly saturated, and consist of a large proportion of silt-sized and sand-sized material. Debris-flow source areas are often associated with steep gullies, and debris-flow deposits are usually indicated by the presence of debris fans at the mouths of gullies. Fires that denude slopes of vegetation intensify the susceptibility of slopes to debris flows.

Debris flows commonly follow existing drainage ways or linear slope depressions created by past landslide activity, although not necessarily. Debris flows tend to increase in volume downstream. Rates of movement range from rapid (m/min) to extremely rapid (m/s).

Figure 3.30 Debris flow (photograph by Le)

Debris slides

Debris slides are defined as low or rapid flow-like movement of loose dry, moist or subaqueous, sorted or unsorted granular material, involving or not involving excess pore-pressure or liquefaction of material originating from the landslide source. The material might range from loose sand to loose debris (fill or mine waste), loess, and silt.

Debris slides are rapid, shallow landslides from steep hillslopes. Movement begins when the overburden slides along bedrock or along other layers within the overburden, having higher strength and lower permeability. Debris avalanches become debris flows if sufficient water is present. Such avalanches cause the rapid downslope transport of a slurry of soil, rocks, and organic material (collectively called debris) directly to the valley floor and occasionally to stream channels.

Wedge type slides

Wedge type slides are defined as sliding of a mass of rock on a planar rupture surface, or a wedge of two planes with downslope-oriented intersection. The rupture surface might be stepped. No internal deformation occurs. The slide head might be separate from stable rock along a deep, vertical tension crack. Usually, it occurs very rapidly. Figure 2.11 is typical of this type. Figure 3.32 is large scale wedge type, which combines multiple small wedge types.

Figure 3.31 Debris slide (photograph by Le)

Figure 3.32 Wedge type (photograph by Le)

Contents

CHAPTER 4. LANDSLIDE INVENTORY AND MAPPING

4.1. Theoretical framework

Before discussing landslide inventory maps, one must defined one: a terrain map showing a distribution of existing landslides. Such maps can include diverse data related to past landslide occurrence, such as location, date of occurrence, activity, and physical properties of landslides in a region (Fell, 2008; Pasek, 1975). These maps play a key role in disaster management and risk assessment. They might provide scientific data for applied landslide research.

According to Guzzetti (Guzzetti, 2005), identification and mapping of landslides should derive from all of the following assumptions.

i)   When landslides occur, they leave discernible signs, most of which can be recognized, classified, and mapped from aerial photograph interpretation. These morphological signs refer to changes in form, position or appearance of the topographic surface. Other signs induced by a slope failure might reflect lithological, geological, land use, or other types of surface or sub-surface changes.

ii) Morphological signs of landslide depend on the type and rate of movement. In general, the same type of landslide will produce similar signs. The morphological signs left by a landslide can be interpreted to ascertain the extent of slope failure and to infer the type of movement. From the appearance of a landslide, an expert or morphologist can also infer qualitative information of the probability of landslide re-occurrence.

iii) Landslides do not occur randomly. Slope failures represent the result of the interplay of physical process.

iv) For landslides, we can adopt a principle that follows from uniformitarianism. The principle implies that slope failures in the future will be more likely to occur under the conditions which led to past and present instability. Mapping recent slope failures is important to elucidate the geographical distribution and arrangement of past landslides. Landslide inventory maps are fundamental information to help forecast the future occurrence of landslides.

4.2. Landslide recognition

Aerial photographs have long been used to provide land-use information and topographic information for many engineering purposes. Landslide topographic area recognition achieved wide recognition as a source of landslide information. Landslide landform information of many kinds can be obtained from aerial photographs.

Landslides can be recognized and mapped using various techniques and tools. In this study, interpretation of stereoscopic aerial photographs is used to identify and map landslides because it is an intuitive process that requires no sophisticated technological skill. The

technology and tools necessary to interpret aerial photographs are simple and inexpensive compared to those of other methods (Guzzetti, 2005). Furthermore, when landslides occur, they alter the local topography of the land surface and leave discernible signs in comparison to the surrounding areas. Most such signs are morphological, involving changes in the shape or appearance of the topographic surface. They can be recognized, classified and mapped through the interpretation of (stereoscopic) aerial photographs (Rib and Liang, 1978; Hansen, 1984a, 1984b; Hutchinson, 1988; Baum, 1999; Guzzetti *et al.*, 2012). A skilled aerial photograph interpreter, by observing various elements on a photograph, can identify numerous ground conditions (e.g.., material type, drainage) that are indicative of potential or present landslides.

Numerous features discernible on aerial photographs also aid in the identification and interpretation of landslides and landslide processes. Some of these are the following: scarps; irregular or hummocky topography below scarps, at the body; bare linear tracks oriented downslope; fresh rock exposure; fresh rock accumulation at the slope base; disordered vegetation and disarranged drainage. Aerial photograph examples and a list of basic features are useful for identifying landslides and terrain that might slide.

Figure 4.1 presents typical aspects of each part constituting the landslide topography. They help interpreter and morphologists can understand and interpret the morphological signature left by the landslide. Of course, landslide topography is diverse and is adjusted by time and erosion processes (Figure 4.2). Observational data from aerial photograph interpretation range from obvious to subtle. Morphologists must classify landslide morphological forms based on experience and based on the analysis of characteristics (signatures) that are identifiable on the images.
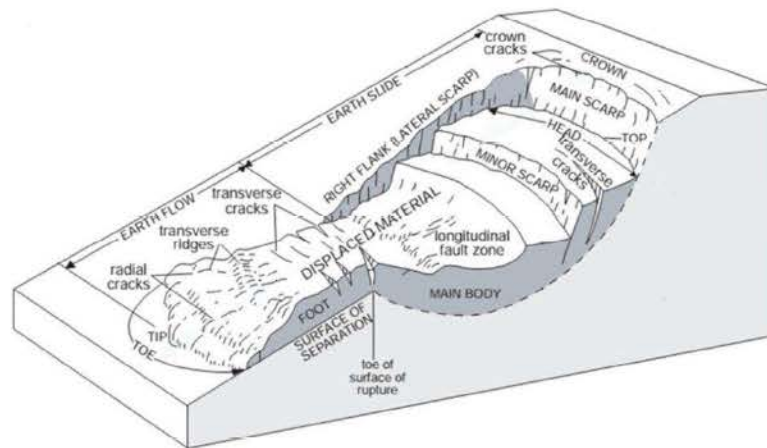
Figure 4.1 Typical of each part which constitutes landslide topography (Varnes, 1978): This figure shows typical aspects of each part constituting landslide topography
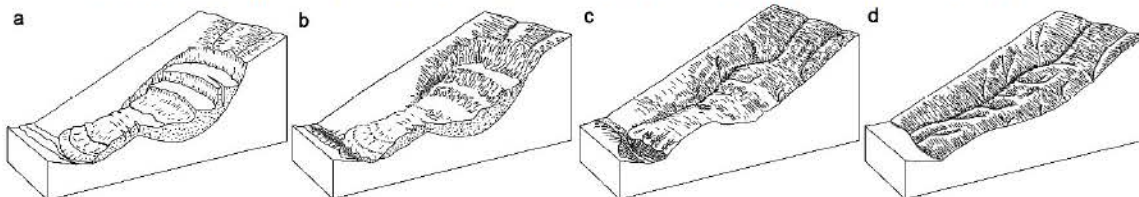
Figure 4.2 Landslide topography was adjusted by time and erosion process (Karl, 2006).

Morphological changes of landslide topography over time, at the first stage when landslide occurred morphological features are very clear (a), and by time and erosion process morphological features become to be more vague (b→d)

Herein, we will outline the basic features used for identifying landslides and potential terrain slides. Interpretation will begin with observation, identification, and measurement of features on photographs. When examining aerial photographs, the significant recognition elements are the relative photographic tone, color, texture, pattern, and shape, in addition to the association of features. Therefore, we must use these elements to recognize existing landslide topographic areas. They are commonly identified based on morphology, vetgetation cover characteristics and drainage characteristics

Regarding to morphology: Identifying the landform-morphology commonly identifies the natural process that formed it. It is the first element used to recognize existing landslide. Features related to these elements are concave–convex slopes, hummocky relief, step-like morphology, back tilting of slope faces, semicircular niches, and steep slopes (Figure 4.3). For example, in a plan including landslide blocks, clear scarp, and depressions behind blocks, a block may be back-tilted with an intermediate scarp or cracks in the middle of the body (Figure 4.3-c); In profile, it is a concave–convex slope. Therefore, it must be a rotational slide. When a landslide occurs, landforms at the landslide body are disordered, producing hummocky relief. These features are extremely important to recognize existing landslides. Alternatively, when there is a sudden change in gradient of slope (Figure 4.3-f); it might be a scarp: a landslide feature. Cracks might be observed on aerial photograph interpretation (Figure 4.3-e) based on changing of the graphic color and tone.
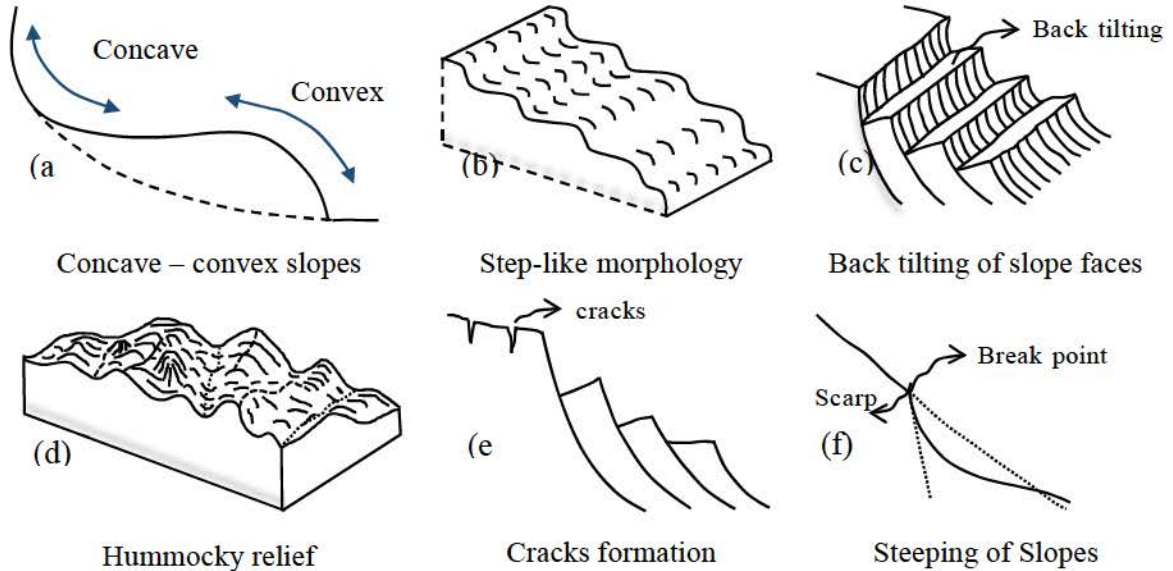
Figure 4.3 Morphological characteristics of landslides (modified from referenced data)

Vegetation characteristics: These include disorder of vegetation, partly dead vegetation, differences of vegetation inside and outside of the landslide area, and disrupted vegetation across a slope. Compared with morphology and drainage characteristics, vegetation as an element has been regarded as difficult to interpret because it is influenced by climatic factors and the soil type. For example where abrupt changes in soil conditions exist, vegetation changes will also occur. However, distribution patterns of trees and shrubs contribute to

landslide interpretation. These characteristics demand attention when interpreting aerial photographs: disorder of vegetation, partly dead vegetation, differences of vegetation inside and outside of landslide, and disrupted vegetation cover across a slope.

Drainage characteristics: These include disarranged drainage and anomalies in a drainage patterns, zones with stagnated water, seepage zones or well appearance, excessively drained masses. These are easy to recognize from aerial photographs because they contrast with not failed slopes. At first, we view the drainage arrangement, a drainage line broken or a zone of stagnated water making pond at slope means that the area probably is a landslide. Another example is slopes dissected by gullies or canyons, which usually indicates linear features. Such areas are susceptible to debris flows.

Landslide and landslide topographic areas are general terms involving downslope movement under gravitational influence of soil and rock materials. According to Cruden and Varnes classification (Varnes, 1978) (Table 4-1), landslides of 16 types are classified based on type of movement and type of material. In this classification, many kinds of material are involved with different modes of movement. In this study, it was difficult to determine the material type using aerial photographs so the categorization of slope movements is not as detailed as per the Cruden and Varnes classifications system. Details of each classification will be discussed in the following parts of this thesis.

Table 4-1 Summary of Cruden and Varnes 1978 classification system

Type of movement		Type of material		
		Bedrock	Engineering soils	
			Predominantly coarse	Predominantly fine
Falls		Rock fall	Debris fall	Earth fall
Topples		Rock topple	Debris topple	Earth topple
Slide	Rotational	Rock slide	Debris slide	Earth slide
	Translational			
Lateral spreads		Rock spread	Debris spread	Earth spread
Flows		Rock flow	Debris flow	Earth flow
Complex		Combination of two or more principal types of movement		

4.3. Results of landslide mapping at Fukayamadake area, Japan

The stereopsis interpretation of a color aerial photography filmed in 1976 of the slope movement situation was conducted in this whole area. From it, a slope movement situation prediction chart was prepared. The reason for adopting the photographs taken in 1976 is the following. The Landslide Distribution Maps compiled by NIED are contact-printed images of 1/40,000 scale from monochrome films taken by the U.S. military; they are unsuitable for interpretation and extraction of small-scale landslides (Oyagi *et al.* 2014). However, contact-printed color photographs taken in 1976 are presumed to have been taken soon after the vegetation of the whole Fukayamadake area was modified into a pasture. In addition, because they had a scale of 1/10,000, microtopographic features were regarded as easy to comprehend. Furthermore, Google Earth[R] images and the information of the 5 m Digital Elevation Model (DEM) by the Geospatial Information Authority of Japan were used properly to elucidate fine characteristics of ground surface conditions.

Many characteristics presumed to have been formed by landslides were observed around the Fukayama pastureland, which were recognized as landslide topographic areas. Many lineaments were also found on the south slope of the pastureland. Although all local areas show intrusion by arborescent dissection valleys, the relative age of topographic areas was determined by the degree of erosion of landslides and lineament topographic areas by a dissection valley. The interpretation results are presented in Figure 4.4. Its outline is presented below.

4.3.1. Distribution of landslide topographic areas

No landslide deformation structure was observed in the whole area of Mt. Hitsugamori located in the easternmost end of the whole pastureland, except at the southern slope. However, most other slopes around the pastureland are covered with landslide deformation. The scale and morphological characteristics of each landslide deformation is widely diverse. The largest-scale landslide topographic area in the whole study region is in the northeastern area of the pastureland (LS1). This landslide was the largest in many large-scale landslides concentrated around the Aratozawa Dam, which has an area of about 2.0 km^2. Presumably, the lower half moved east–northeastward, i.e., toward the Aratozawa Dam and the Onomatsuzawa Valley, whereas the upper half moved mostly northward in the direction of the Onomatsuzawa Valley (Le and Miyagi, 2015c). On the outbreak of the Iwate–Miyagi Nairiku Earthquake (hereinafter, the Nairiku Earthquake) in 2008, surface failure occurred at landslide scarps at its tip and bottom half. The end of this landslide is in contact with the Aratozawa Dam lake and the Onomatsuzawa Valley, where secondary deformation occurred frequently. This landslide topographic area is an object for landslide hazard assessment by Miyagi Prefecture, which assigned 82 points as its risk score. This value suggests that this landslide is still in motion.

In some spots where landslides concentrate also on the south of the study region (LS 2-4), these landslide topographic areas are of a scale of several hectares or less. Their intensity is as great as severe failure of the valley side slopes of a dissection valley. A landslide occurs occasionally in the south valley of the pastureland. Interviews with community residents reveal that it is geologically weak. Moreover, a field survey confirmed steep landslide scarps and small-scale falling, which suggests recent movement.

Distributed sites are concentrated by large-scale landslide topographical areas (LS 5–7) and small-scale landslide topographic areas (LS 8–10) on other neighboring slopes of the pastureland. It is noteworthy that LS 5–10 is not shown in the Landslide Distribution Maps by NIED, and that LS 11–13 are landslide groups regarded as active at present.

LS 5–7 are areas where an arborescent dissection valley is prominent. Nevertheless interpretation using the aerial photograph of a large-scale reveals characteristic microtopographies everywhere. Microtopography is an isolated and small-scale hill. Presumably, it is a moving block split by a landslide because erosion by a dissection valley never forms an isolated topography in the middle of a slope. Such isolated blocks are denoted in the figure as a point. LS 5–7 are presumed as an old landslide topography subdivided by a dissection valley.

LS 8–9 are landslide topography groups of small and medium scale covered with a forest, although they are difficult to observe. These landslide topographic areas are moving toward the dissection valley of a lineament representing the moving direction.

60

4.3.2. Distribution of lineaments

Numerous lineaments with a longitudinal axis along the northwest–southeast have developed in the southwest half of a low relief surface that constitutes the pastureland. Because a lineament is a mere linear morphology, it is important to ascertain what each linear topography signifies. Characteristics of these lineaments are presented below.

L1, the most prominent lineament in the region, comprises extremely straight ridges: valleys, slopes, and mountain streams that extend along the northwest–southeast. This lineament is characterized by a valley side slope on the left bank of a mountain stream, the dissecting valley of which has remained almost unaffected by erosion except for very small-scale surface failure. The mountain stream also flows almost straight. The mountain stream of an extension of about 2 km is the trace of the lineament. Relative height of about 40 m of the valley side slope at the southeast end of the downstream declines gradually northwestward, eventually disappearing. It is noteworthy that landslides occur frequently on the northwestern extension of this lineament.

L2 is a dissection valley extending southward from LI. This dissection valley is extended on a longitudinal axis along the northwest–southeast, is mostly parallel to L1, and is longer than L1 by about 1 km. Many developed dissection valleys join the mountain stream of the extension where the secondary deformation by the erosion after lineament formation is prominent.

L3–L8 are small-scale level differences where neither a mountain stream nor an erosional valley is observed. Photographic interpretation raises suspicion of small-scale artificial modification.
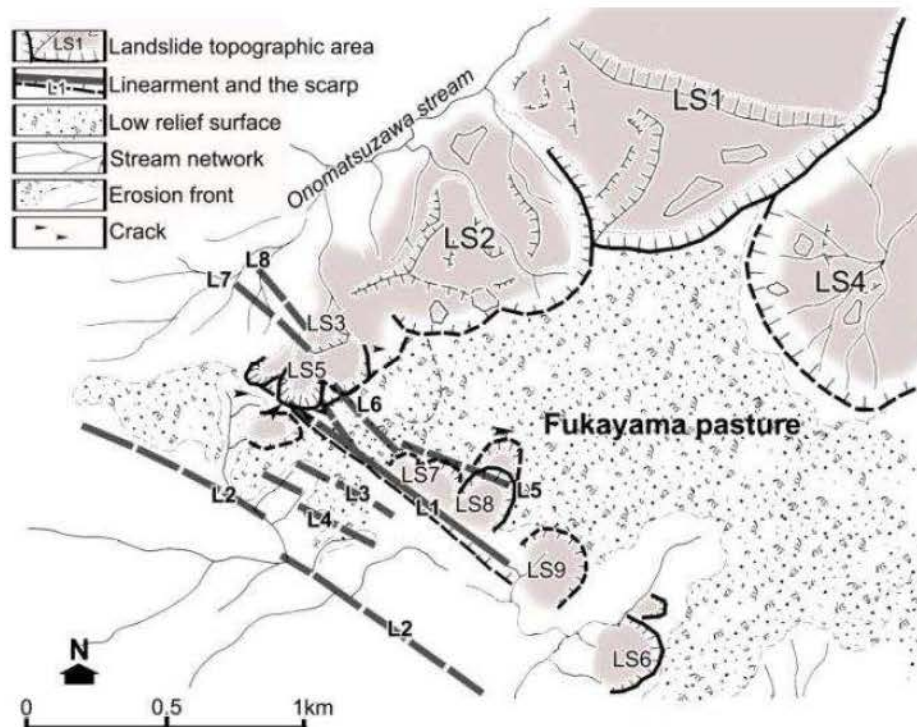
Figure 4.4 Distribution of landslide topography, lineament, and cracks at the area of Fukayamadake plateau, Mt. Kurikoma foot slope, Miyagi Prefecture, northeastern Japan (Le and Miyagi, 2015c)

61

Figure 4.5 Stereo aerial photograph pair (CTO-76-13-17B-23 & 24) showing landslide LS1 in Figure 4.4

Figure 4.6 Aerial photograph of the study area presented in Figure 4.4

4.3.3. Cracks

Several cracks exist at two locations. One is immediately above the LS 8 and L 8. One of two open cracks is a typical circular crack open to the LS 8. It is 2 m long, 5 cm wide, and more than 1 m deep. Apparently, the phenomenon of the early stage of land deformation is the extension of LS 8 (Figure 4.7-6; 4.7-7). The other concentrated area is located between the LS 5 and L 1. Five cracks can be found there. A small bog is also located at L 1. The largest crack is 20 m long, 20 cm wide, and more than 1 m deep. It stretches northwest to southeast in parallel with L1.
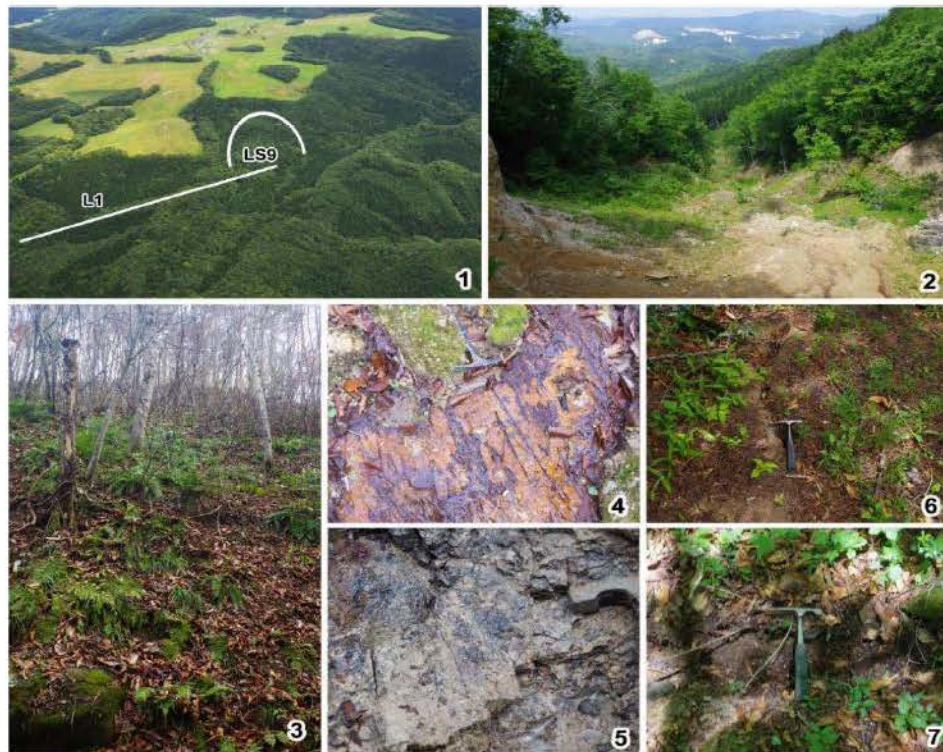
Figure 4.7 Field evidence of the landslide related features at Fukayamadake area (Le and Miyagi, 2015c):
1: Aerial view of the target area. L1 and LS9 marked of the photograph; 2: LS5 landslide; 3: southwestern side scarp of L1; 4: slip surface of LS5 (also former slip surface); 5: slip surface of LS8; and 6 and 7: cracks on the plateau near LS5 and LS6

4.3.4. Discussion of landslide development with special reference to the caldera rim

Landforms of the study area are characterized by low relief surfaces, landslide topography, lineaments, and cracks. A series of field surveys was conducted to elucidate the mechanisms forming these topographic features

After the earthquake at this site in 2008, small surface failures were observed (Yagi *et al.*, 2008). However about 1 year later, there occurred a landslide of 50 m width, 50 m depth, and 15 m thickness in pumice tuffs. The landslide body was crushed severely to flow down for several hundred meters as a mudflow.

The LS 5 landslide looks as a fresh landslide triggered by the earthquake. However observation over the slip surface reveals a rusty reddish thin layer with innumerable extensively developed linear grooves or gouges. Therefore, this landslide is presumed to be formed by a process by which iron was accumulated near a slip plane in an earlier landslide. The uncrushed portion of the landslide body was reactivated and subdivided after the earthquake. Such a small-scale landslide occurred also adjacent to LS 5, so that many cracks are observed all part of behinds of LS 5. Some cracks are not connected directly with LS 5, but extend along the northwest–southeast. It is located on the northwestern extension of lineament L1.

Distribution of a series of phenomena explained above in the ground surface state suggests interesting landslide phenomena in relation with the caldera rim modification (Le and Miyagi, 2015c).

63

Topographic and geological cross sections across landslides and lineament L1

Many lineaments are observed to extend along the northwest–southeast in the westernmost end of the study region. The sharpest and largest is L1; L2 is to its south and parallel to it. It has become a path of a mountain stream. Moreover, it is affected by the secondary deformation of a dissection valley. L3–L8 are on the slope between L1 and the low relief surface. All are small-scale and ambiguous. However, some might be related to the expansion of LS 5 or a landslide generation in the neighborhood. Accordingly, two topographic cross sections from L1 to the low relief surface are assumed. For deeper understanding, the observed microtopography is associated with conditions such as a lineament, a crack, and change in ground surfaces.

Cross section A–B

Figure 4.8 presents a topographical and geological cross section passing from L1 through LS 3,5. The topography was prepared from the 5 m DEM. The cross section of L1 is recognized as the linear channel, but the side slope is presumed to be extremely unsymmetrical, as described above. The right side slope has a smooth but steep slope consisting of hard lapilli tuffs with relative height of 25–30 m. In contrast, the left bank is a gentle slope of 15 deg or less and hummocky. This slope is so overly humid that gullies and subsoil water are observed everywhere. A part of the slope is accompanied by a small-scale horseshoe-shaped cliff with radius of about 50 m.

The geology of pastureland is assumed by the well boring core. The top 10 m layer is Pleistocene weathered pumice tuff, with andesitic welded tuffs. There are tuffs underneath, with interstitial siltstone at several depths. The tuff breccia as the hard tuffs and volcanic rocks underneath correspond to the Hosokura formation as the member of Miocene marked to about 100 m deep. The slope of the north side of pastureland comprises lacustrine deposits, tuffs, and pumice tuffs deposited. The lacustrine one is a typical sediment of the caldera. This portion meets the slopes of LS3 and LS5.

The L1 is presumed as the huge crack or a main scarp of large scale landslide. Actually, L1 is established by the large scale mass movement, but is linear down cutting the channel. It is therefore considered unreasonable to assume that "There is no occurrence of surface condition change such as a landslide on the south of the caldera wall because of its strong geological features".
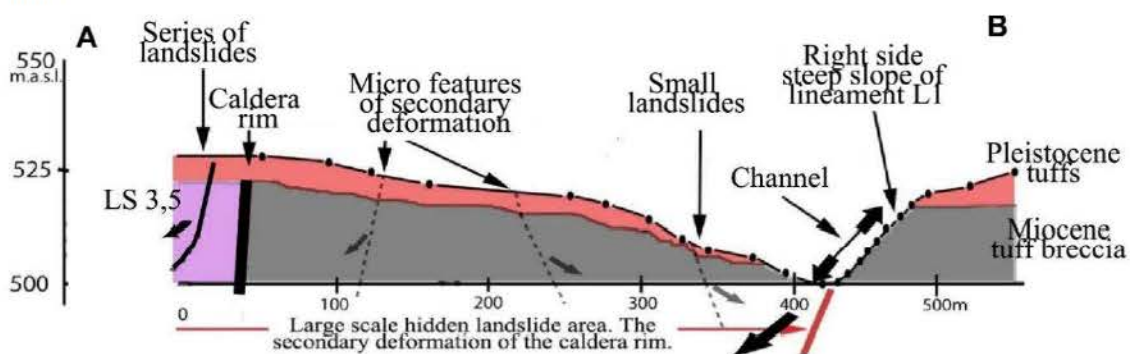
Figure 4.8 Topographical and geological cross section passing from L1 through LS 3,5 (Le and Miyagi, 2015c)

Cross section C–D

A characteristic microtopography is assumed to be tension cracks aligned north–south on the west of the low relief surface of the pastureland. No noticeable landslide topography was confirmed in the neighborhood. However cracks and two horseshoe-shaped cliffs assumed to be a landslide revealed by the aerial photograph interpretation and field survey. Figure 8 portrays the survey result. At the toe slope of LS8, the slip surfaces and flow mound was also identified. These findings suggest that the left bank slope was formed by the frequent occurrence of small-scale and shallow landslides. The LS 8 is a typical case. The L1 right bank of L1 channel retains a steep slope with no secondary modification, but the slope size increases to 40 m.

This cross section revealed topographical and geological phenomena similar to those on the A–B cross section: slopes on both sides of L1 are extremely unsymmetrical. The slope adjacent to the right bank is a very smooth and steep slope, with a relative height of as much as 40 m and an inclination of 40–45 deg. However, the left bank comprises a typical landslide-type half-crushed rock lump. The landslide and related phenomena are distributed widely. Furthermore, the low relief surface of the pastureland is above the upper landslide topography. A small and clear crack on the slope side of this low relief surface is regarded as having been formed by tensile stress forces.
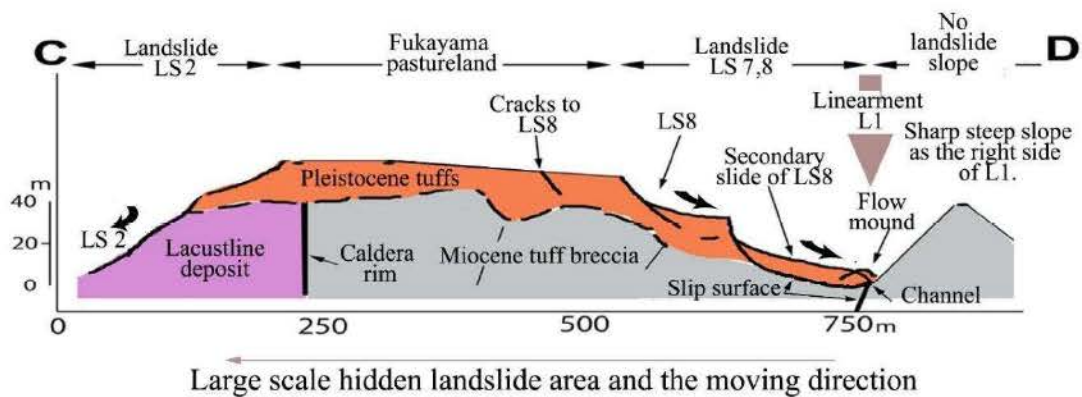
Figure 4.9 Cross profile at LS 7,8 areas

4.4. Results of landslide inventory map in Vietnam between Prao and Kham Duc

4.4.1. Landslide topographic area identified and its mapping

In this study area, we recognized and classified the mass movements of flowing five types: (i) rotational slide (RS), (ii) translational slide (TS), (iii) complex/compound slide (CS), (iv) debris slide (DS), and (v) debris flow (DF). Among these types, there are three types (rotational slide, translational slide, compound slide) that are classifiable by their topographic features: main scarp, lateral scarp, and landslide body. Two other types (debris slide, debris flow) can be identified only by the topographic features of the body of the feature in Figure 4.10 (Le *et al.*, 2016).

65
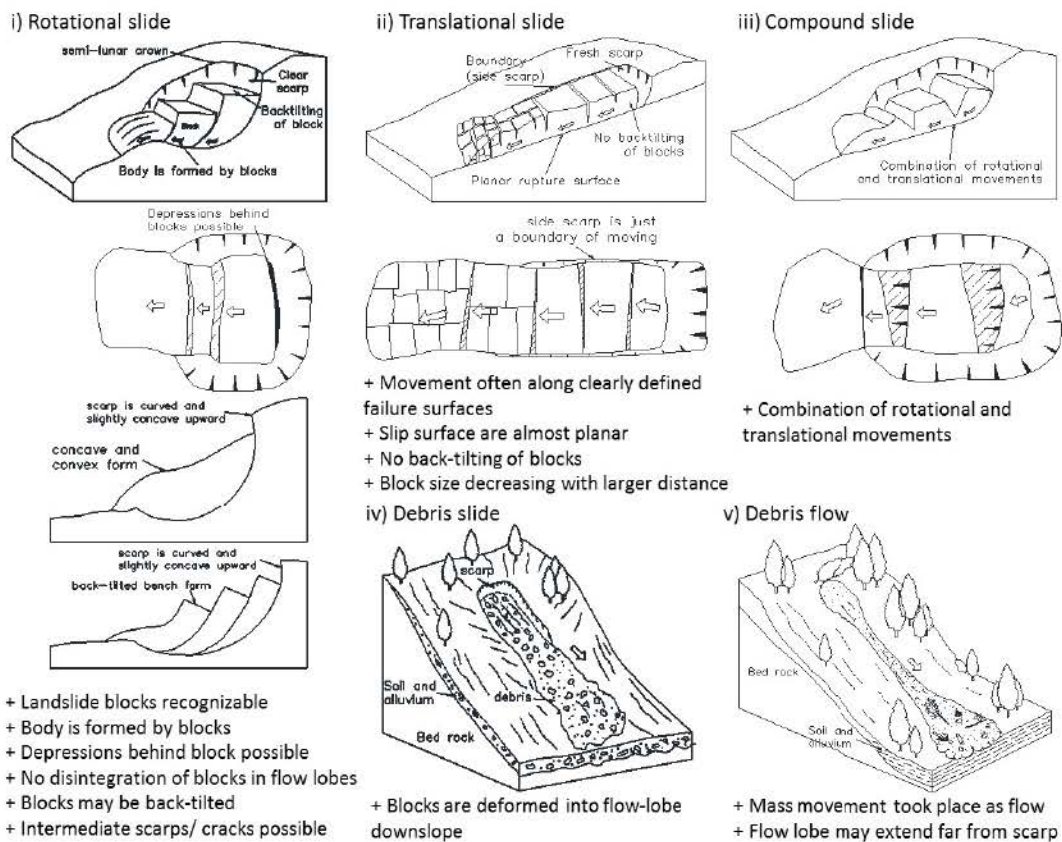
Figure 4.10 Features for landslide typology in study area (modified from Westen, 1996)

To identify and classify each type of landslide, here I described the geomorphological features of five types that have enabled us to classify mass movements of different types in the study area:

Rotational slide: A rotational slide is defined as a sliding of a mass of weak rock, soil on a cylindrical or other rotational rupture surface (Oldrich Hungr, 2013). The slide movement is more or less rotational about an axis that is parallel to the contour of the slope. The body is formed by blocks and is generally easily recognizable. There is no disintegration of blocks in the flow lobes. They include spoon-shaped irregular landforms. The morphology is characterized by a prominent main scarp and a characteristic back-tilted bench formed at the head of the slide. In the stereo-pair image from the aerial photographs (shown in Figure 4.10-i), the block is extremely clear, hitting and blocking the stream. Depressions exist behind the block, with ponding in niches of the back-tilting area.

Of course, not all landslides have these features attributable to postevent weathering, erosion processes, and the type of landslide material. For landslide No. 95 (Figure 4.11), this has a semilunar crown and lobate frontal part. The scarp is curved and slightly concave upward and the slope is characterized by concave (niche) – convex (run-out lobe) forms. These morphological features are specific characteristics of a rotational slide.

66
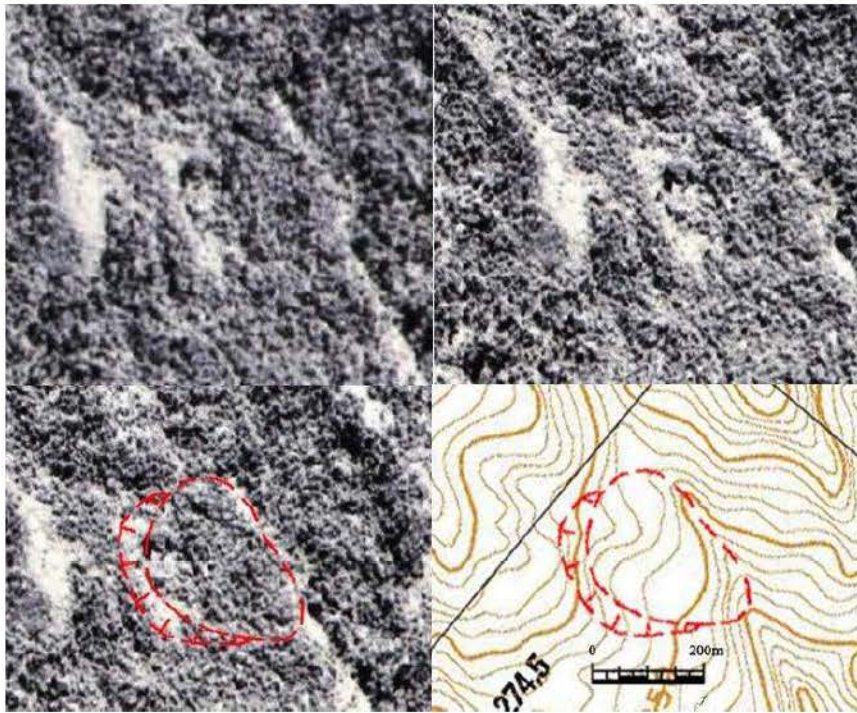
Figure 4.11 Stereo pair aerial photograph (D2-99-06-415 & 416) showing a typical rotational slide (Le et al., 2016):
the upper panel shows stereoscopic image of landslide; the lower panel is a sketch of landslide on photographs and topographic maps

Translational slide: A translational slide is a sliding mass of rock or block of cohesive soil that moves across one or more inclined planar rupture surfaces (Oldrich Hungr, 2013). In the case of rock, planar slides usually involve dip slopes that have been undercut by erosion or excavation. The slide head might be separating from stable rock along a deep vertical tension crack. In the case of a soil planar slide, it is likely controlled by a weak layer, inclined at an angle exceeding the angle of repose. Before total failure, tension cracks often form during initial disturbance. During and after the failure event, the sliding mass separates from stable soil along these tension cracks and leaves a fresh scarp, thereby forming a graben (Le *et al.*, 2016).

The main scarp is not a slip surface. The side scarp is just a boundary of movement because that is a detachment between the body and the stable zone (Figure 4.10-ii). The slip surface is shallow, the run-out hummocky rather chaotic relief, with the block size decreasing with distance (Le *et al.*, 2016).

In the source area and along the movement pathway, the vegetation is denuded, often with lineation in the direction of movement. In comparison with a rotational slide, no ponding exists below the crown; surface drainage is either disordered or absent on the body (Soeters and Van Westen, 1996). The scarp is clear and is often elongated with no back tilting of blocks. Figure 4.12 shows a typical translational slide in which a weak layer overlays a planar rock formation. At the head of slide, the separate stable soil and sliding area can be recognized easily. The slip surface is almost planar. Debris accumulates at the bottom of slope deforming the river (Le *et al.*, 2016)..

67
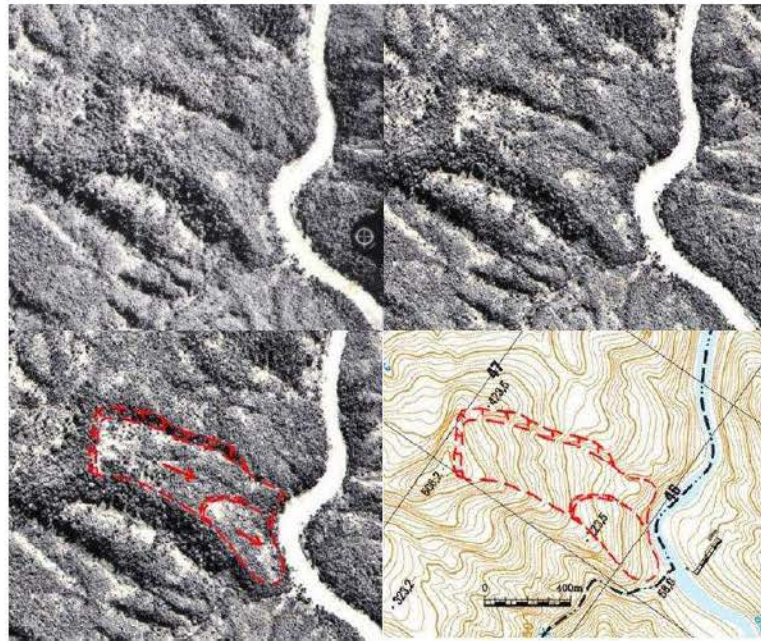
Figure 4.12 Stereo aerial photograph pair (D2-99-06-415 & 416) showing a typical translational slide (Le et al., 2016): the upper panel shows stereoscopic image of landslide; the lower panel is sketch of landslide on photographs and topographic maps

Compound slide: A compound slide is a sliding mass of rock, soil on a rupture surface consisting of several planes or an irregular rupture surface consisting of several randomly oriented joints. When a landslide occurs as a compound slide, it creates a concave–convex slope morphology. Concavity is often associated with a linear graben-like depression. There is no clear run-out but there is a gentle convex/bulging frontal lobe. Back-tilting facets are associated with (small) antithetic faults (Soeters and Van Westen, 1996). Figure 4.13 presents typical features of a slide of this type (Le *et al.*, 2016).
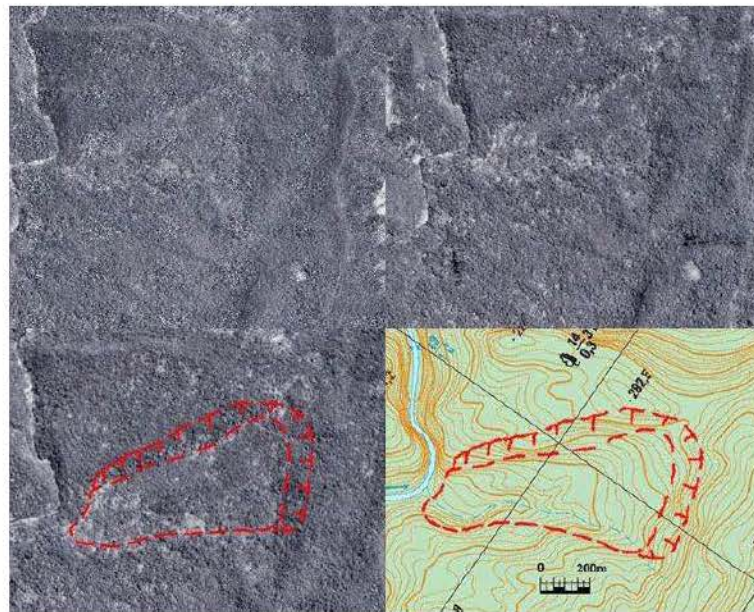
Figure 4.13 Stereo pair aerial photograph (D2-99-04-226 & 227) show typical of compound slide (Le et al., 2016): the upper panel shows stereoscopic image of landslide; the lower panel is a sketch of a landslide on a photograph and a topographical map

Debris slide: A debris slide involves the movement of a mass of unconsolidated material along a steeply sloping, planar surface parallel to the ground. Usually, the sliding mass is a veneer of colluvium, weathered soil or pyroclastic deposits sliding over a stronger substrate. Many debris slides become flow-like after moving from tens to hundreds of meters and might transform into extremely rapid debris avalanches (Oldrich Hungr, 2013) and accumulate downslope. Based on this definition, we can infer morphological characteristics belonging to this type: blocks (landslide body) are deformed into flow-lobes downslope. They display clear flow-structures with a lobate convex frontal section. The flow-lobe is usually larger than the initial blocks (landslide body). Figure 4.10-iv presents these features (Le *et al.*, 2016).

Vegetation on the scar and body is highly disturbed and is clearly distinguishable from the surroundings. Drainage conditions include ponding or disturbed drainage towards the rear and deflected or blocked drainage at the frontal lobe.
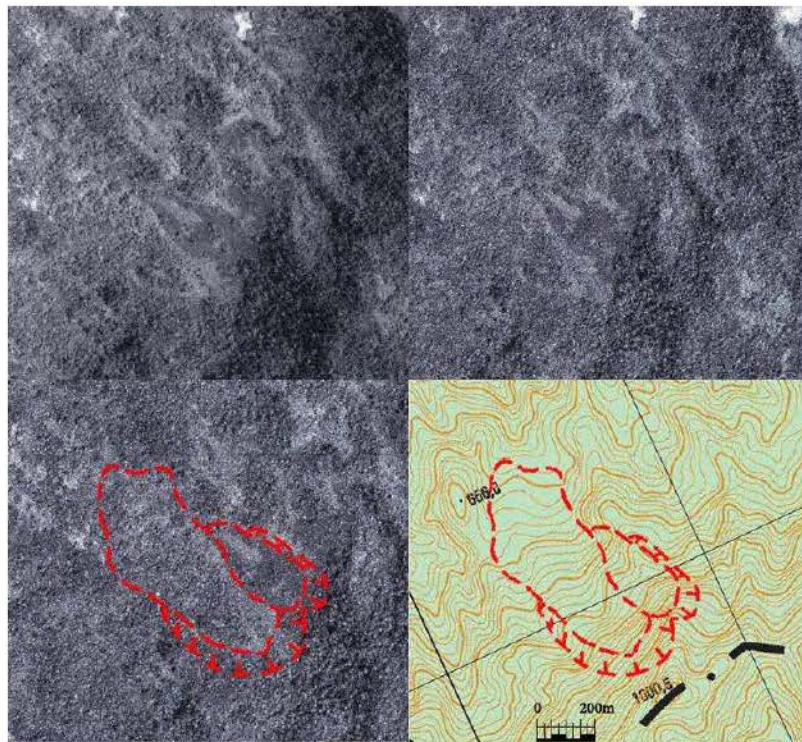
Figure 4.14 Stereo pair aerial photograph (D2-99-03-244 & 245) show typical of debris slide (Le et al., 2016):
the upper panel is a stereoscopic image of the landslide; the lower panel is a sketch of the landslide on a photograph and topographical map

Debris flows: A debris flow involves movement of loose soil or gravel on a steep slope. It often occurs simultaneously with heavy rainfall and is initiated by a slide, debris avalanche, or rock fall from a steep bank or spontaneous instability in a steeply sloping stream bed (Oldrich Hungr, 2013). Under such conditions, these materials can liquefy or be subject to a great increase in pore-pressure and flow downslope. Morphological features associated with this type of landslide typically include numerous small concavities) or one major scar characterizing the source area. Almost complete destruction occurs along the movement pathway, sometimes marked by depositional levees. Figure 4.15 shows a typical debris flow feature in the study area (Le *et al.*, 2016).
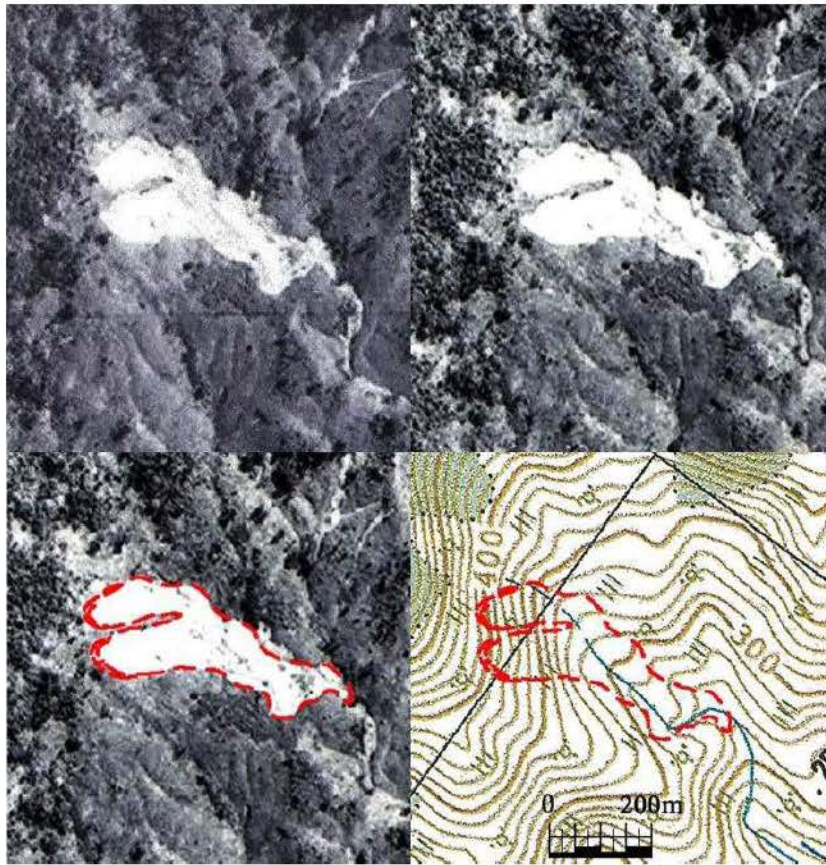
Figure 4.15 Stereo pair aerial photograph (D2-99-06-127 & 128) show typical of debris flow (Le et al., 2016):
the upper panel is a stereoscopic image of a landslide; the lower panel is sketch of a landslide on photograph and topographic map

4.4.2. Large-scale landslide topography mapping in central Vietnam

Using methods described above, a landslide inventory map has been produced for the area between Prao and Kham Duc. The inventory was prepared by interpreting landslides observed in 1999 from over 100 aerial photographs at a scale of 1:33,500. We used these photographs because, at the time of this study, only the 1999 aerial photographs are available. Interpretation of aerial photographs was locally aided by field checks. Thereby, all the unstable areas were mapped onto topographical maps at a scale of 1:25,000. This map (Figure 4.16) was transferred to GIS and includes 685 landslides, corresponding to an average density of 0.6 landslides per square kilometer. Landslides range in size from 3071 m^2 to 3.08 km^2. The most frequent (abundant) landslide has an area of about 25,400 m^2. They were classified into five categories, 324 of which are classified as rotational slide, 66 are classified as translational slide, 4 are classified as compound slide, 275 are classified as debris slide, and 16 are classified as debris flow. For each landslide, 13 characteristics were recorded and listed in the accompanying database table (see at appendix). Combined with geological maps, among 685 landslides that were mapped, 314 landslide topographies are Mesozoic; 178 landslide units are Paleozoic; 171 landslide units are Precambrian; and 22 landslide units are Quaternary. Most landslides occur in the Mesozoic zone, accounting for 46% of recorded landslides (Le *et al.*, 2016).

70
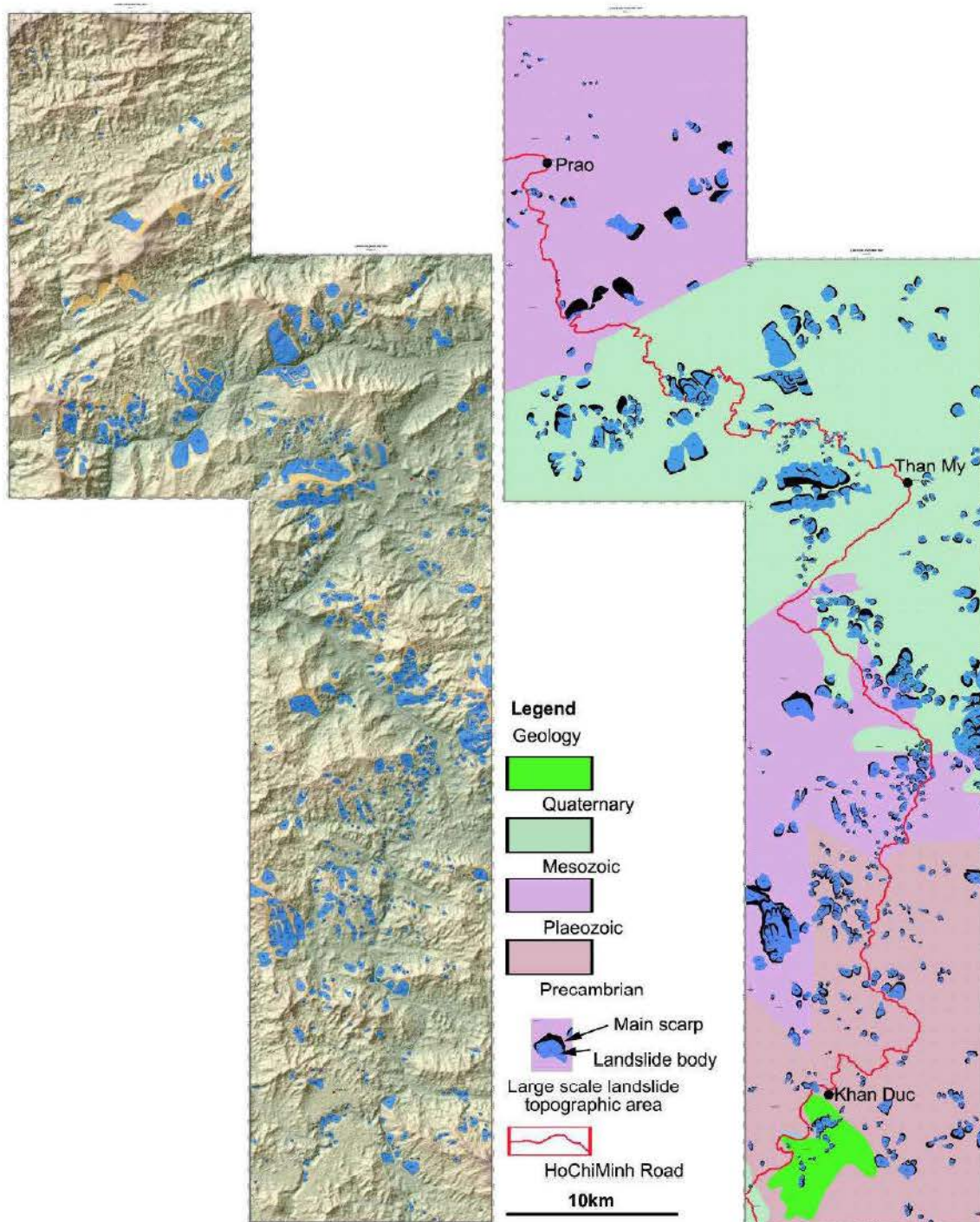
Figure 4.16 Maps of landslide topographic area from Prao to Khan Duc along the Ho Chi Minh Road, central Vietnam (Le et al., 2016):
this map is a combination of six sheets of scale of 1:25,000

The maps portray interesting distribution features: 1) the spatial distribution seems to have some relation with geological periods. The large-scale landslide topography concentrates to the area of the Mesozoic geology. The Paleozoic geology has few large-scale landslides except in areas of plutonic rocks such as gabbro and granitic rocks. Especially, the largest landslide topography is located at the gabbro. The Quaternary and Precambrian geology also have several characteristics. Details are presented in Chapter 5. 2) The movement features are

71

categorized to five types: Rotational slide, Translational slide, Compound slide, Debris slide, and Debris flow (Le *et al.*, 2016).

However, an interesting characteristic was observed at Thon A So in the study area. This was located at the part of northward homoclinal slope at a southern part of the major Mesozoic syncline. I observed numerous distributed landslides and scars, with very remarkable topographic features identified, the scars are distributed at the northward dip slope. Many types of landslide topographies are located in the other direction of the slope. The landslides are small, but are easy to identify in size. Such landslides and scar distribution are strongly reflective of the geology structure. In cases of the landslide distribution, the type in case of the Mesozoic sedimentary rock influences characteristics (Le *et al.*, 2014b).
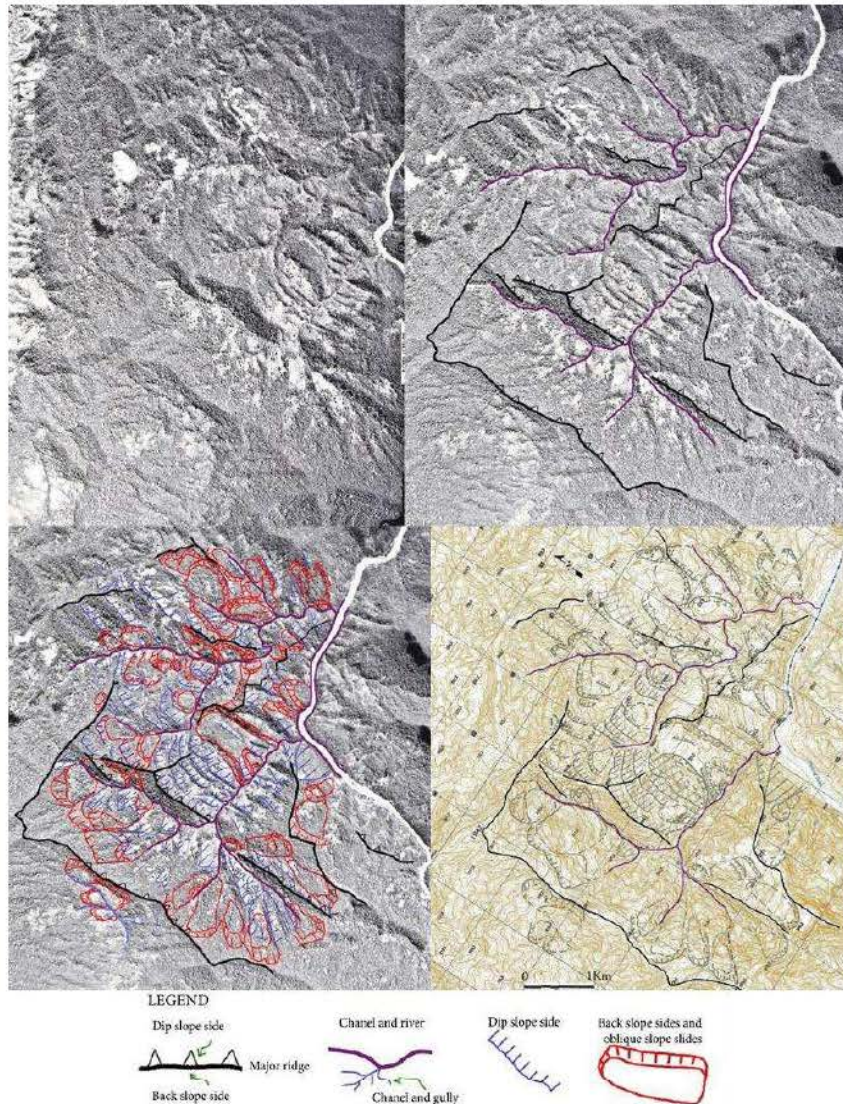
*Figure 4.17 Stereo pair aerial photograph (D2-99-06-415 & 416) show main joint plane and bedding plane having tendency to parallel to or dipping with slope (Le et al., 2014b):
the upper panel shows stereoscopic image of landslide; the lower panel shows a sketch of landslide and micro-landform features on photograph and topographic map*
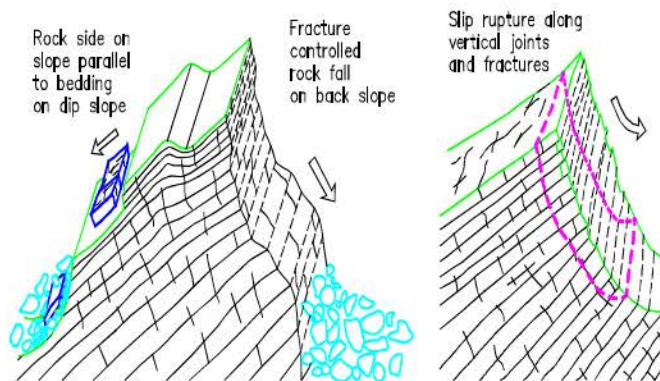
Figure 4.18 Parallel bedding in rock causing slides (Le et al., 2014b)

4.5. Comprehensive landslide inventory maps and factors affecting landslide inventory quality

Interpretation of aerial photographs has proved to be a widely available method to identify landslide and risk evaluation because it requires no sophisticated technical tools and provides an investigator or interpreter clear visual stereoscopic image of landslides. However, images remain a challenging task. It is extremely difficult to give out a formal standard for identification. The interpreter classifies landslide morphological forms based on experience, and on the analysis of a set of characteristics (signatures) that is identifiable on the images. Quality of photographs and original data strongly influence to quality of recognition. Comparing Japan and Vietnam, it is clear that Japan used photographs are color photography of many scales. They might have been taken over several s years (five years or ten years), so there are diverse data for the shape, features of landslides, and morphological forms are clearly identifiable. For example, Figure 4.19 shows landslide inventory map at Fukayamadake, this map was established by NIED on 1984 based on a scale of 1/40,000. Therefore, there are some limits of identification. Only large-scale landslides were mapped in the Fukayamadake area. In 2009, the Japan Geographical agency established landslide inventory map in the same area. They used color photography at the scale of 1/15,000. Therefore, the landslide topographic areas were recognized as having more detail than NIED maps (Figure 4.20).
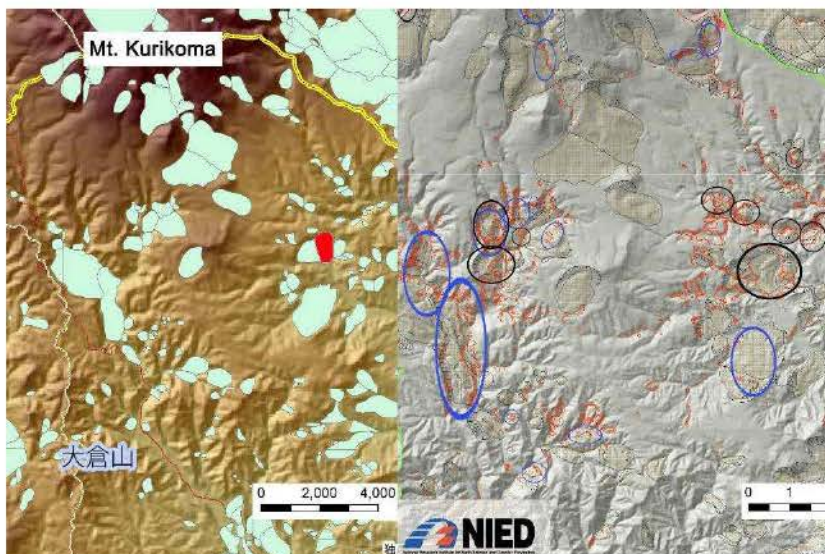
Figure 4.19 Landslide inventory map at Fukayamadake (established by NIED, 2008)

73
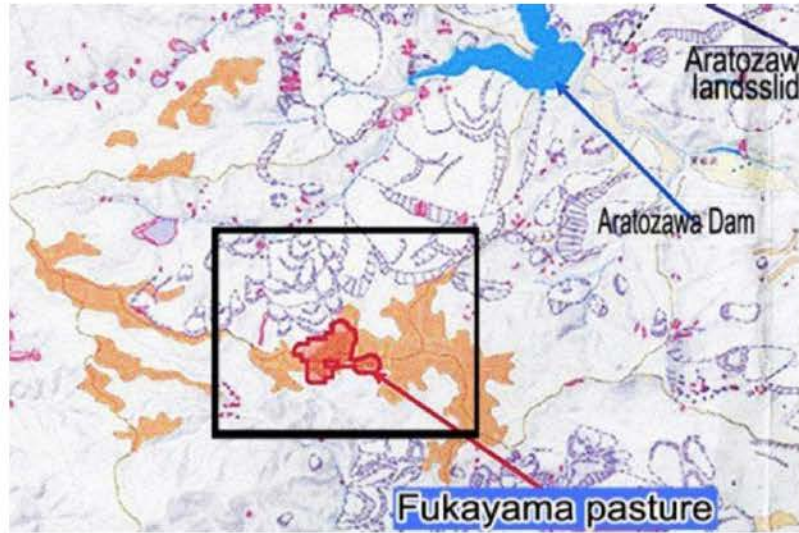
Figure 4.20 Landslide inventory map at of Fukayamadake (established by Japan Geographical Agency, 2008)

In Vietnam, aerial photograph interpretation is difficult because of limitations of original data (aerial photographs). First, is the scale of aerial photographs. All interpreters agree that the best scale for interpreting is smaller than 1/15,000. However, all aerial photographs in Vietnam are available at a scale of 1/33,000 (pixel size of 1 m). This will affect the accuracy of the object's size. It is important in the interpretation of associated features. From small-scale photographs, associated features might be easily interpreted because of their size with regard to other features. Large-scale photographs show that direct identification might be made because photographic details are not readily visible. Sometimes, some objects are confused with others. The landslide (0.295 km long, 0.301 wide) as shown in Figure 4.11 is typical of this case. Another example is shown in Figure 4.21 (landslide No.18). The lower part is divided into 3–4 sub landslides, but they are not easily recognizable. With the scale of 1:33.500, one can infer a landslide larger than 150–200 m wide.
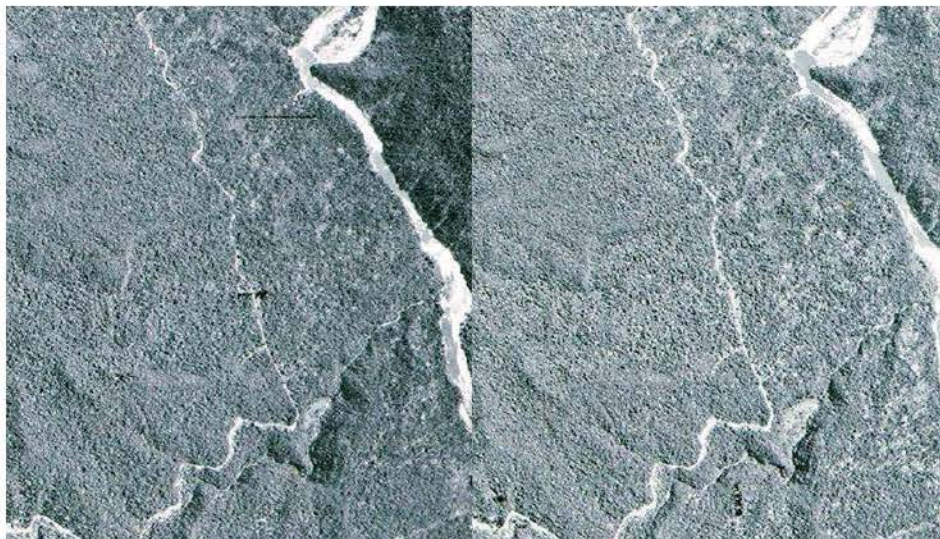
Figure 4.21 Stereo pair aerial photograph (D2-99-06-166 & 167) showing landslide No. 18 (Le et al., 2016)

74

The second difficulty is the quality of aerial photographs: landslide phenomena are variable. Not all landslides are clearly and easily recognizable from the aerial photographs. Aerial photograph interpretation is a cognitive process involving the inherent characteristics of the landslide on photograph, such as the color, tone, texture, contrast, shape, texture, shadow, and pattern. Color as a recognition element is a useful criterion for interpretive purposes. However, all aerial photography images are black and white. Therefore, it will permit a lesser amount detail to be recognized and interpreted. Some other elements are not clear, for example in Figure 4.15, an intensely white area exists. We cannot explain why it has this tone. It might be a debris slide or error of photographic tone.

Finally, the study area has high forest cover. For this reason, microlandforms such as irregular slope surfaces (Figure 4.21, Figure 4.22-a, b), cracks are not clearly distinguishable on an aerial photograph. We must identify it through a crown of trees. In this case, the boundary and main scarp of landslides can be identified based on the abrupt change of color tone of photographs (Figure 4.21, Figure 4.22-c), We can infer microlandforms through different tones and colors of aerial photographs, but it might be correct or incorrect. Landslide No. 18 (Figure 4.21) is an example of the present situation. We readily identify boundaries of landslides, but at the lower part of the landslide body, it is extremely difficult to infer the material type of the slope, cracks, and other microfeatures. That is not useful to predict the probability of landslide occurrence in the future using an inspection sheet.
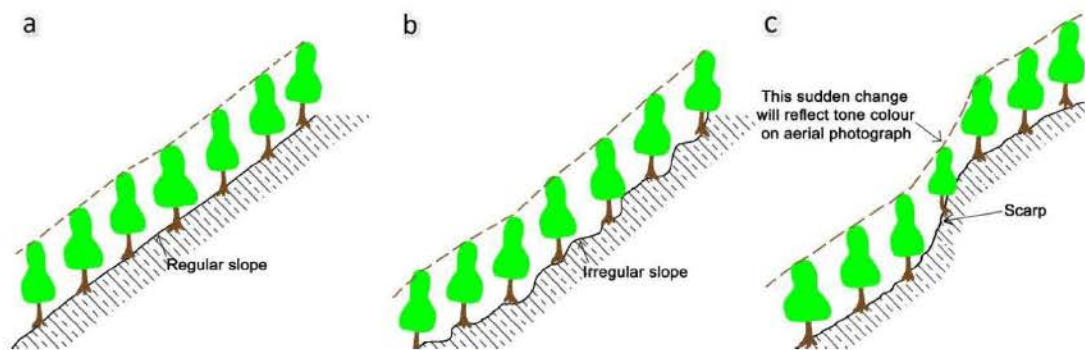
Figure 4.22 Schematic views of regular/irregular slopes (Le et al., 2016):
Identifying irregular slope is extremely difficult because of high vegetation cover if there is
sudden change of slope such as a scarp. It is shown as tone color that can be easily identified
on aerial photographs

Generally, for Vietnam, limits of data sources make it difficult to identify landslides.

4.6. Summary of achieved results and discussion

This chapter accomplished the following:

i)   The landslide topographic area of Caldera Rim at the Footslope of Mt. Kurikoma is presented and discussed using aerial photographic interpretation and field surveys. The Fukayamadake area and its surroundings constitute the southern edge of the caldera on the south footslopes of Mt. Kurikoma. Phenomena were observed everywhere throughout these sites: welded tuffs and pumice weathered tuffs sediments in the caldera and it formed a cap rock structure. A landslide severely eroded the inside of the caldera toward the Onomatsuzawa Valley. However, rocks constituting the caldera rim were originally hard rocks such as tuff breccia. They are presumed to have brought about movement to deform the caldera rim

gradually, as observed in lineaments such as L1 and L2. Especially, the deformation of L1 was triggered geologically very recently. That movement is presumed to be ongoing. The reasons are that an erosional valley or the weathering and secondary land modification of topography is only slightly observed, whereas lineament L1 is connected directly to cracks and landslides such as LS 5 on its northwestern extension. The discussion presented above suggests that L1 is a deep-seated landslide. It also is a process of caldera rim extension to the outside of the current rim. The trace of L1 is a principal landslide scarp. Although this landslide encourages the expansion of a caldera rim, its formation occurred much later than that of the caldera body of the Pleistocene, millions of years ago. The mechanism by which this landslide contributes to the deformation above is presumed as a load increase by a series of volcanic products, such as the welded tuffs and pumice tuffs, covering the caldera rim, as well as stress release to the radial direction of the rim. The trace of L1 is a large-scale cliff in the southeastern part, where the Ikezuki welded tuffs present a typical cap rock structure, but it turns to a crack in the northwestern part where the distribution of this welded tuffs becomes ambiguous. This inclined deformation structure is regarded as attributable to the unequal distribution of a vertical load. Consequently, the ground was presumably loosened on the north side of L1 (on the left bank of the mountain stream) in connection with this deformation of L1. It is reasonable to conclude that this deformation is still in action quietly. We assume that this deformation has loosened the left bank of the mountain stream. Thereby, many landslides have occurred along the left bank of the mountain stream. The Fukayama pastureland provides a seemingly very moderate landscape. Nevertheless, it is presumed that both a large slope movement and a surface landslide movement are still in progress underground.

ii) An inventory map of study areas in central provinces of Vietnam was produced through aerial photograph interpretation and established a table of attribute description for each landslide unit in Vietnam. However, because of the complexity, inventory map can be prepared only for area of limited extent.

iii) Limitations of photograph interpretation were explained for the case of Vietnam. Those are limitations of original data, (aerial photograph), scale and quality of aerial photographs, and high forest cover at the study area. In Vietnam, access to aerial photograph sources is extremely difficult. Sometimes it is impossible for scientific work. At the time of this study, only 1999 monochromatic aerial photographs were available. Limitations of data sources make it difficult to identify landslides.

iv) Interesting landslide distribution features of study area in Vietnam were shown, with a relation between spatial landslide distribution and geology. The large-scale landslide topography concentrates to the area of the Mesozoic geology. The Paleozoic geology has few large-scale landslides, except in areas of plutonic rocks such as gabbro and granitic rocks. Especially, the largest landslide topography is located at the gabbro. Quaternary and Precambrian geology also have several characteristics. The movement features are categorized to five types: rotational slide, translational slide, compound slide, debris slide, and debris flow.

Contents

78

CHAPTER 5. RISK EVALUATION AND APPROACHES FOR HUMID TROPICAL REGION

5.1. Introduction of Japan's inspection sheet for risk evaluation

Landslide maps were developed to identify areas with differing past landslide topographic areas. It is useful to know the probability of landslide re-occurrence for each landslide topographic areas. This is the first step in ensuring that the landslide risk does not exceed an acceptable level when planning future land use. Interpretation of future landslide re-occurrence requires elucidation of the processes controlling landslides.

According to Miyagi (Miyagi *et al.*, 2004) various stages exist in a sequence of a landslide development: the primary stage, the active stage and periods of differentiation, the expansion stage, and the suspension and the dissolution stage. The series of these stages is presented in Figure 5.1. The micro-topography of each stage reflects the characteristics of autonomous destruction processes and comprises distinct micro-landform units. Each stage is made up of distinct micro-landform units. In the initial (stage) period of occurrence, a landslide has been gradually differentiated, becoming vulnerable because some internal transformation is deformed repeatedly. However, variation processes proceed intermittently and repeatedly over time. Geomorphologic processes of two types occur: an intermittent landslide action and a normal process in landslide area. The landslide hazard risk evaluation must distinguish these two processes. Determining the stage of a landslide activity and interpreting direct indexes of the risk and landslide risk evaluation will be the following (Miyagi *et al.*, 2004):

1) Landslide topography is identified and illustrated through aerial photograph interpretation and through development of the landslide topography distribution map.

2) Micro-topographies are identified through photograph interpretation. The items are checked on a card. The card is constructed on the system of item arrangement.

3) The total score of the checked items indicates the risk level. The score of items is estimated by AHP. Each landslide topography is identified as high risk (70–100), moderate risk (30–70), and low risk (0–30).

Risk evaluation can be conducted by analyzing landslide topographies because most landslide processes result from reactivity of aged landslide topographies. Risk evaluation is therefore based on the following assumptions (Miyagi *et al.*, 2004):

1) Fundamental factors for the evaluation are limited to topographical information interpreted from aerial photographs.

2) Scale or characteristics of interpretable landforms and landslide phenomena are often affected by the aerial photograph accuracy.

3) Factors such as rainfall are not objects for evaluation.

Disintregating scarp

scarp due to gullies development

Cracks

Crack

Scarp

Scarp

Alluvial cone floating masses

Debris flow

Gully formation

Debris flow on lower scetion of active landslide body

Toe of surface rupture

Compression layer of mudflow deposit

...ks developed on ...llies are active ...pe of body is ...bulging.
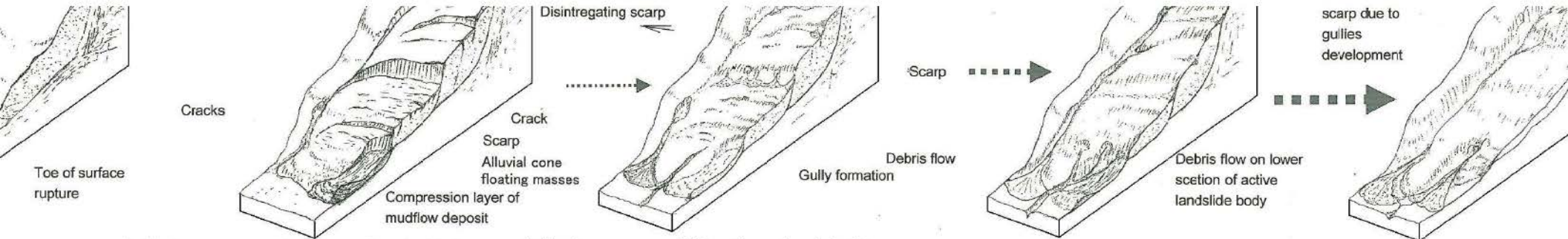
In this stage upper mass is sliding as dissecting blocks, cracks are in advance stage on crow and body. Scarps have sharply developed in the upper section, debris flow is accumullateding as copmressing layers at lower section, surface rupture is clearly defined, all these factors are fresh and in active stage.

In this stage scarps are disintegrating and eroded, all the mass of unstable sections of scarp eroded, modifyed sharp edge, talus developed on scarp foot. The gullies are in advance stage at lower slope that are develping upward and making debris flow fan at lower section. Channels have not well stablished

In this stage blocks have already deformed, channels are weddining as well as deepening and reached on head of body and gullies are still in active and in advansce stages

In this stage gulies are in stabilizing order, the unstab... removed, reactivated by gullies development, sliding completely removed, channel net work are developed surfacial material has remained still weak

Active landslide > scarp develcpe by sliding blocks

II - 1 : Landslide deformed into several numbers of sliding blocks at upper section and mudflow accumulation at lower section

II - 2 : Last stage of landslide

...is active and in enlargment, moving mass ...several blocks

Multi slump

Colluvial deposit

Slurry of mud flow

Debris flow source

Mudflow acumullation

...sses of lower section of ...dslide body is becoming ...stable and moving as mudflow

In this stage landslide body deformed into several numbers of sliding blocks at upper section that converted devris flow accumlation at the lower section

Most of the slicing masses have already m... stage and formed large debris fan on foot

III-1:Translation types of block slide

III - 2 :Discontinuation active landslide

Depression

Minor scarps

Cracks

Pressure ridge

...on the slopes, ...the lower section, ...xpanding or bulging

In this stage several clear cracks appeared. Several transverse and minor scarps have dissected the body into blocks and small debris slides and pressure ridgse have developed at the lower section due to load pressure of upper moving blocks, this is known as active stage of translational type of block slide,

In this stage landslide is subsiding toward the scarp on head and depression formed, talus formed on the foot of scarp by eroding unstable mass of scarp and debris flow fan developed at lower body of landslide, sharp scarp are modified by eroding process.

Primary factors increasin... stabilizing stage

Primary fctors increasing... unstabilzing stage

Risk evaluation is a probability of landslide re-occurrence within a given area. Risk evaluation can be conducted by analyzing landslide topographies because most landslide processes result from reactivity of aged landslide topographies. Wherever landslides occur, the unit of risk evaluation should be the whole area of the landslide topography. When conducting risk evaluations, the following points should be noted:

1) Occurrence of landslides caused by artificial influences such as anthropogenic alternation is not an object for evaluation.

2) Risk is a probability of landslide occurrence. It is not a magnitude of occurrence or behavior of destruction on the surrounding area in movement.

3) If the whole area of a landslide topography is evaluated based on an unstable area within it, then an interpretation map should represent the area and mention the existence of such an area, its position within the landslide topography and relative relation to other.

For purposes of systematic and objective risk evaluation, the Japan landslide society has developed an inspection sheet (Figure 5.2) incorporating geomorphic factors within and beyond landslides (Miyagi *et al.*, 2004). In this sheet, geomorphic factors are classified into large, medium, and small categories. The first major category includes characteristics of types of movement, material, and critical features of action. Micro-landforms of various types and their spatial arrangement indicate activities of landslides distributed mainly within the domain of the landslide body. The second major category involves aging factors, time processes, and clearness of the top edge of the main scarp and the sharpness between the main scarp and the landslide body. The third involves the potential energy of the slip body caused by the last action. It can change the instability of the landslide body, and increasing or decreasing their geomorphic setting such as the body face attached to the slope of a river. Focusing on these geomorphic settings, one can predict the prospective transition of stability. Each major category above was classified into smaller classifications. The larger classifications include (1) the micro-landforms features in landslide body as an item of the characteristics of movement, (2) the boundary of major landslide landform component as an item of the time process, and (3) the landslide topography and the adjoining environment as in index of geomorphic setting. The smaller classifications include eight categories: A, type of movement; B, level of clearness and micro-landform components within the landslide body; C, level of instability of the landslide body; D, direct features of movement; E, between the top edge of the main scarp and the upper slope; F, between the main scarp and the body; G, between the landslide body and the frontal slope; H, toe part of the landslide body; and I, lower part of the landslide body. The items of the medium classifications are further divided into smaller categories, which will be checked and evaluated using aerial photograph interpretation. Characteristics and features of each small classification are described as follows by Miyagi *et al.* (2004):

A) Type of movement

Movement of each type will produce a distinct micro-landform, such as flow mound, pressure ridge which caused by mud flow and debris flow. Clay debris flows to mud flow type landslide are fairly unstable because of the strongly weathered clayey materials. It will increase the recurrence of landslides (Miyagi *et al.*, 2004).

B) Level of clarity and micro-landform components in the body

By processes occurring over time, weathering and erosion, micro-landform units within the landslide body (e.g., cracks, minor scarps, graven, depression, and pressure ridge) have been modified and have lost their original shape. The landslide body is divided into small parts changing toward the active stage. The micro-landform density indicates some level of destruction (Miyagi *et al.*, 2004).

C) Level of stable (Stability of landslide body)

The landslide body often becomes unstable by sustaining head block separation from the lower part and slight failure at the toe and lateral portions. Such inversion phenomena often become triggers of a large slide reoccurrence. If the landslide faces a suspended stage, the process that causes the invasion of gullies and erosion valleys can be regarded as an erosion process leading to its disappearance (Miyagi *et al.*, 2004).

D) Direct features of movement

Generally, if a crack is clear, then it can be inferred that little time has passed after the landslide occurrence. Sometimes, it is difficult to recognize the crack existence from aerial photographs. However, cracks are often recognized as an indirect feature such as a systematic deformation of the forest crown (Miyagi *et al.*, 2004).

E) Boundary of the landslide main scarp and upper normal slope

At the top edge of a main scarp after landslide action that includes lateral stress situation, there remain some unstable materials. Consequently, several echelon cracks and lateral cracks develop at the top edge of the main scarp. After the action, the stability increases gradually and is modified by creep. Furthermore, the weathering process deforms the initial topography and decreases the edge sharpness. If the suspending condition holds for a long time, then the area of creep and gully erosion will develop. Typical topographic characteristics of the landslide main scarp will disappear (Miyagi *et al.*, 2004).

F) Boundary of the main scarp and landslide body

This boundary is very clear, like an edge of the main scarp, which is formed immediately after the action. Plenty of materials fall from the scarp and accumulate at the boundary. Such materials develop talus topography. The development of talus accompanies aging. The spatial ratio of the talus indicates the time process after the event (Miyagi *et al.*, 2004).

G) Boundary of the stable slope and landslide body

This boundary is very clear after the action. The landslide body is deformed and dissected by weathering process and linear erosion such as gully erosion, which leads to the development of a gully, a channel at the body and small alluvial cones develop in front of the landslide body. Therefore, such components of micro-landforms are also indicators of time processes after the landslide action (Miyagi *et al.*, 2004).

H) Landslide body toe (Toe part of the landslide body)

If a mountain stream creates an erosion situation, then it will be identified as equal to attack the face to a river. However, the front part of a body might become unstable by the partial abutment to the opposite bank of the mountain stream (Miyagi *et al.*, 2004).

I) Change of the potential of instability at lower part of body (lower part of the landslide body)

An increase or decrease of relief energy will engender a change of the potential of the landslide body (Miyagi *et al.*, 2004). Although we can recognize multiple items in a landslide body, we must mark only one item at each category box. In such cases we should mark those items as much unstable ones.

All the items above were put into a card (Figure 5.2). Each classification is compared as a pair of items based on AHP. For convenience of practices, the categories are arranged to decrease the risk from the left to the right, enabling clarification of the landform formation mechanisms. In addition, a category can be checked between some categories. For example, in the item F in Table 5.1. If a category is judged as being between "Talus" and "Large-scale talus", then one can check these categories. However, if more than one category exists, the heavy one should be contributed to the calculation (Miyagi *et al.*, 2004).

The score of the card is calculated intuitively based on the experiences of a geomorphologist. In this way, landslides are classified from special high risk to low risk (high probability of landslide occurrence) based on the AHP score evaluation. The landslide's morphometric signs appeared fresh on aerial photographs if the score's evaluation is high. In contrast, morphometric signs are extremely vague. A score of 70–100 signifies high probability of landslide occurrence; 30–70 stands for the probability of landslide occurrence; and 0–30 denotes no probability of landslide (Miyagi *et al.*, 2004).

5.2. Application of Japan's Landslide inspection sheet for risk evaluation in Vietnam

The primary application of this landslide inventory is to ascertain areas that are best avoided in highway route facilities, infrastructure, and other similar works. However, not all landslides have high risk of re-occurrence. Some of them have high risk; others might be stable. Therefore, we must ascertain the risk or probability of landslide re-occurrence within these old landslides.

To ascertain the landslide risk, we used the inspection sheet developed by the Japan Landslide Society. It incorporates geomorphic factors within and beyond landslides (Miyagi, 2004). In this way, landslides are classified from high risk to low risk (high probability of landslide occurrence) based on the AHP score evaluation. The landslide's morphometric signs appeared fresh on aerial photographs if the score's evaluation is high. In contrast, morphometric signs are extremely vague.

Table 5.1 Weight value of each morphological item for risk evaluation (Miyagi et al., 2004)

Major classification	Medium classification	Small classification	Weight value

81

Major classification	Medium classification	Small classification		Weight value
(1) Micro landform features in landslide body (as an item of the characteristics of movement)	A: Type of movement	1	Flow mound and pressure ridge	12.5
		2	Minor scarp	4.9
		3	Separation scarp, Depression, Trenches	2.0
	B: Level of clearness and micro landform components within landslide body	1	Huge no. of deformed blocks and clear micro topographic boundary	19.5
		2	Clear micro-topography of smooth boundary	12.5
		3	Unclear deformed block	6.0
		4	Smooth boundary	5.5
	C: Level of instability of landslide body	1	Head block separates from the lower part	13.9
		2	Gullies development	3.6
		3	Linear erosion development	1.5
	D: Direct features of movement	1	Cracks and scares	18.8
		2	Tree crown deformation	6.3
(2) The boundary of major landslide landform (as an item of the time process)	E: Between top edge of main scarp and the upper slope	1	Echelon	3.8
		2	Main scarp	3.2
		3	Creeping slope	1.8
		4	Gullies extension	1.5
		5	Modified to smooth slope	1.3
	F: Between the main scarp and the body	1	Non deposition	3.1
		2	Talus	1.8
		3	Large-scale talus	1.1
		4	Smooth deformed by creeping and talus development	0.6
	G: Between the landslide body and the frontal slope	1	Non deformed landslide body	1.0
		2	Gully, debris cone	0.5
		3	Smooth surface topography	0.4
		4	Disappeared surface	0.3
(3) Landslide topography and the adjoining environment (as in index of geomorphic setting)	H: Toe part of landslide body	1	Face to the undercutting slope of river	8.6
		2	Face to the river	4.4
		3	On the flat plain	1.6
		4	Hit to opposite slope	0.9
	I: The lower part of landslide body	1	Increasing toward the active condition	19.2
		2	Moderate the change of relief energy	9.2
		3	Decreasing	2.7

Figure 5.2 Example of inspection sheet (Le et al., 2014a):
the left side panel shows a pair of aerial photographs and a sketch of landslide on topographic map; the right side panel shows criteria for risk evaluation

To illustrate the potential of this method, 32 landslide units were chosen for evaluation. Results of evaluation are shown at Table 5.2. Figure 4.21 shows a stereo pair of aerial photographs of landslide No. 18. This landslide is very large: 2.3 km long and 0.99 km wide. Aerial photographs show that the main scarp and side scarp are clear. There is no talus deposit and no weathering shape modification at the boundary of the scarp and the landslide body. The lower part is divided into 3–4 sub landslides. The slide type changes to debris slide or rotational slide. Therefore, with these features, we assigned an AHP score of landslide morphometric signs as shown in Figure 5.2. The total score is 70, meaning that it has high probability of landslide occurrence.

Figure 5.3 Stereo pair of aerial photographs (D2-99-04-228 & 229) showing landslide No. 163

Figure 5.3 shows a stereo pair of aerial photographs of landslide No. 163 (1.345 km long and 0.867 km wide). It has clear micro-topography: several minor scarps were observed.

At the boundary, many materials fall and accumulate, forming a slightly talus topography. Large landslides are classified as a translational slide, but minor slides are classified as rotational slides. A part of landslide body material was eroded, forming a gully. To these morphometric features, we assigned respective scores of 5.5, 16, 9, 8, 3.3, 1.6, 0.5, 4.4, and 9 for A) type of movement, B) level of clearness and micro-landform components within LS body, C) level of stable, D) direct features of movement, E) top edge of main scarp, F) boundary of the main scarp, G) boundary of landslide body and the front slope, H) landslide body toe, and I) change of the potential of instability at lower half of body. The total score is 57.3. This landslide is classified as having a medium probability of landslide occurrence.

Figure 5.4 shows a stereo pair aerial photograph of landslide No. 102. This is a typical rotational slide that is 0.295 km long and 0.301 km. The block is very clear, with hits and blocks of the stream. A depression is apparent behind the block, with ponding in niches of the back-tilting area. The boundary is extremely clear. The total score is 70.2. This landslide is classified as having high probability of landslide occurrence.

Figure 5.4 Stereo pair of aerial photographs (D2-99-06-415 & 416) showing landslide No. 102 (Le et al., 2016)

Table 5.2 Results of AHP score for 36 landslide units (Le et al., 2016)

LS No.	AHP score	LS No.	AHP score	LS No.	AHP score	LS No.	AHP score
3	46.2	134	62.46	381	33.9	626	65.7
15	47.3	139	64.2	510	41.3	631	54.1
18	70	140	66.1	516	47	633	57.7
95	35.65	141	70.2	517	46.8	636	57.75
102	70.2	144	59.5	541	56.65	647	37.2
113	38.4	163	57.3	570	58.3	648	36.6
125	54.15	171	54.8	571	54.8	655	22.5
127	58.3	174	42.1	620	25.45	662	20.6
128	58.9	371	25.25	625	69.5	668	25.35

5.3. Limitation of Japan's Landslide inspection sheet when applied in Vietnam and the importance of geologic conditions in risk evaluation for humid tropical region

5.3.1. Limitation of Japan's Landslide inspection sheet when applied in Vietnam

Aside from challenging tasks with regard to source data, such as quality, scale of aerial photographs, high forest cover at the study area as described in chapter 4, one remains. The sheet shows morphological factor only, it does not mention geologic factors. In Vietnam, which has a richly varied geologic composition, rocks have been found from Precambrian to Quaternary. Fieldwork shows that geologic conditions must play an important role in landslide occurrences in Vietnam and other humid tropical regions. For example, non-cohesive materials promote landslides such as debris flow or debris slide. Cohesive materials have high contents of clay mineralogy. When they are dry, shear strength and angle friction are usually high, water therefore deforms these materials and causes failure. Bedrock is directly susceptible to weathering. Sometimes at some slopes, shallow weathered materials are coarse grained and have low cohesion. They are likely to develop movement. High joints and fractures allow water to penetrate and weaken under a soft layer and make it prone to slide. Bedding planes parallel to slope provide little mechanical support and are prone to slope movement. In the following chapter, the author explains and clarifies actual relations between landslide occurrences and geologic conditions in the study area.

5.3.2. Importance of geological structure and weathering in risk evaluation for humid tropical region

The study area was divided into four geological zones. According to the database of a large-scale landslide topographic area (Fig. 3.8), geologic maps (Fig. 5), and based on field investigations, clear mutual relations are apparent. This chapter clarifies the actual relations among them. Furthermore, one must consider the causative mechanisms of landslide processes at each geological stage.

At Quaternary zone

Quaternary deposits are located mainly in river valleys and plains, characterized by non-consolidate sediment, diverse components, abundant material sizes, and fundamental alluvial faces. They include the Dai Nga formation ($\beta N2\ dn$) and include tholeiitic basalt and olivine basalt.

Weathering features: Geological structures are usually flat, including non-consolidated lake deposits with some weak layers such as organic rich, peat, and clayey layers. Volcanic rocks include intruded basalt consolidated with hard and heavy rock. They include lake deposits (dark reddish brown color but weak weathering) and the boundary of the volcanic and lake deposits (dark deeply weathered material, with many holes because of the lava gas), and lake sediments, which are deeply weathered and changed to clayey materials.

Landslide characteristics: Landslides occur as rotational slides along river-side slopes and concentrate at the basalt cap rock area (Figure 5.5). However, large scale landslide topography consists of numerous shallow and small landslides (Figure 5.5-f).

At Mesozoic zone

These include Nong Son, Ban Co, Khe Ren, Huu Chanh, Song Bung, Song Bung formations and Cha Val, Hai Van, and Deo Ca complexes. They consist of Triassic to Jurassic sedimentary rock: conglomerate, gritstone, sandstone, siltstone, mudstone, shale, and Argillite. The geological structure exhibits a mutually overlapping layered structure (cuesta landform). It has a well-defined bedding, changing from very thinly bedded (2 cm of mudstone) to thickly bedded (larger than 3 m of sandstone), containing a lens of weak layer such as coal layer and mudstone. The sandstone is generally fine to coarse-grained, containing high contents of quartz and mica.

Weathering features: Field surveys show that the top surficial soil is about 0.5–1 m thick. Therefore, we assume that the zone becomes slightly to moderately weathered compared with Paleozoic and Precambrian. At the sedimentary rock, joints and fractures are well developed, making sedimentary rocks break into small to medium blocks. These cracks combine with bedding plane openings to provide moderate to high permeability. Along joints of reddish sandstone (containing iron and manganese), chemical weathering alters hard unstable minerals into softer minerals such as iron to clay (Le and Miyagi, 2015c).

Landslide characteristics: Following the inventory map, we identify landslides in this area that tend to be larger than in the Paleozoic zone. At the forward slope, landslides occur along the bedding plane and weak layers. These weak layers such as mudstone and lens of coal layer are key factors controlling landslides in this area (Figure 5.6). Numerous landslides in this area are classified as translation slides (Figure 5.6). At the reverse slope, landslides occur as rocks fall or rotationally slide along joints and fractures (Figure 5.7) (Le and Miyagi, 2015c).

Figure 5.5 Typical example of landslide related to geology in the Quaternary zone (Le et al., 2015b):

a, b, c: dark reddish brown color lake deposit; d: intruded basalt; e: holes caused by the lava gas; f: example of landslide inventory map (large-scale landslide consists of numerous shallow and small landslides)
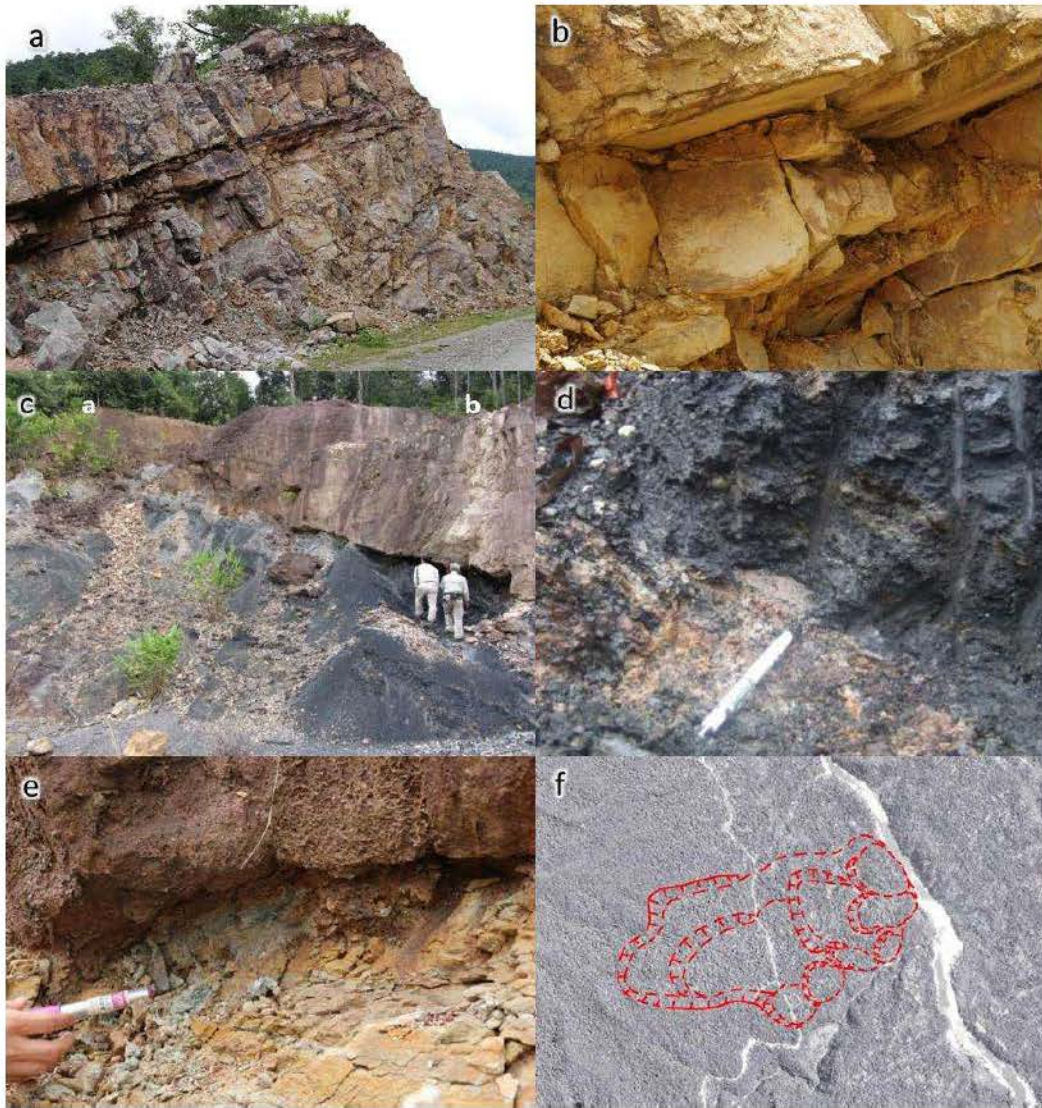
Figure 5.6 Typical example of landslide with emphasis on geology in the Mesozoic (Le et al., 2015b)
a: bedding plane parallel to slope; b: fractures of sedimentary rock; c: lens of coal layer; d, e: slip surface at weak layer; f: aerial photograph of landslide
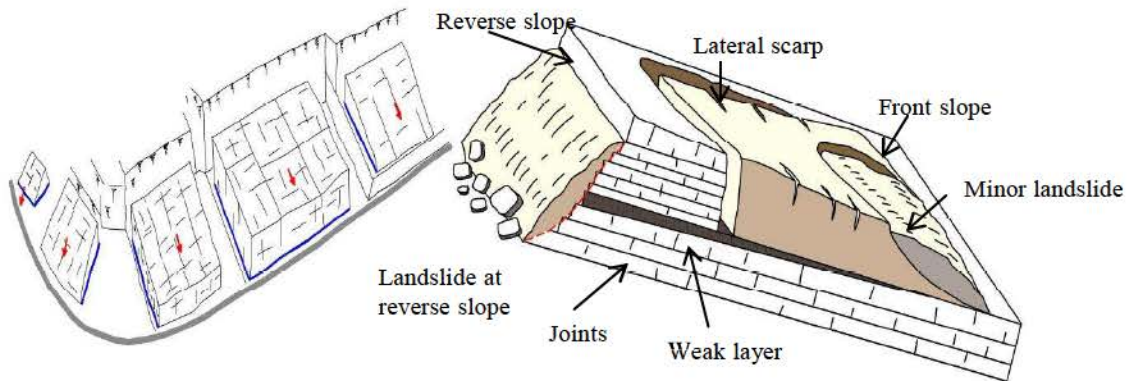
Figure 5.7 Translational rocks slide at Mesozoic zone (Le et et al., 2016)

88

At Paleozoic zone

These include A Vuong and Ben Giang-Que Son formations, and Dai Loc complexes. They consist of Cambrian to Devonian metamorphic rocks: sericite schist and magmatic rocks.

- Metamorphic rocks are widespread, including A Vuong formation, which is rich in quartz components consisting of quartz mica-schist, quartz-sericite schist, quartz-feldspar schist, and sericite schist.

- Magmatic rocks include the Ben Giang-Que Son formation and Dai Loc complex. These intrusive granite magmas consist of gabbrodiorite, granodiorite, diorite, quartz-biotite-hornblende diorite, and pegmatite.

Weathering features and landslide characteristics: This zone shows different weathering among areas. The area around Prao town has a highly weathered, surficial soil layer that is brown with high contents of clay, with fresh rocks observed at the river. Therefore the depth of the highly weathered crust is about 10–20 m. Landslides in this area are almost all surficial slides. Shallow landslides occur as debris slides, debris flows, and rotational slides. Large-scale landslides occur as combinations of numerous small landslides (Figure 5.9).

At areas with less weathering, outcrops of weathering rocks are visible along Ho Chi Minh road. The upper part of weathering rocks has changed to soil. The soil layer thickness varies: 0.5–1.5 m. The lower parts of rocks show loss of strength, with discoloration. Fractures and cracks are moderately developed. Water and other weathered elements can penetrate following fractures, cracks, and weakening of the face (Figure 5.8, Figure 5.9-b, c, d). Therefore, wedge slide types are abundant in this area, but the size of this type is small to medium. It is therefore not mapped (Le *et al.*, 2016).

Field surveys show that most landslides in this area are surficial, with shallow landslides. Following the inventory map, landslides in this Paleozoic zone are not as numerous as those in the Mesozoic zone. Among 178 landslides with recorded topography, 77 landslides were classified as debris slides; 67 landslides were classified as rotational slides (Le *et al.*, 2015d).
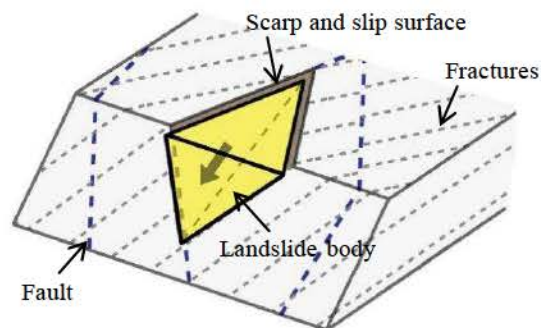
Figure 5.8 Schematic diagram of joints and fractures cause wedge slide type (Le et al., 2016)
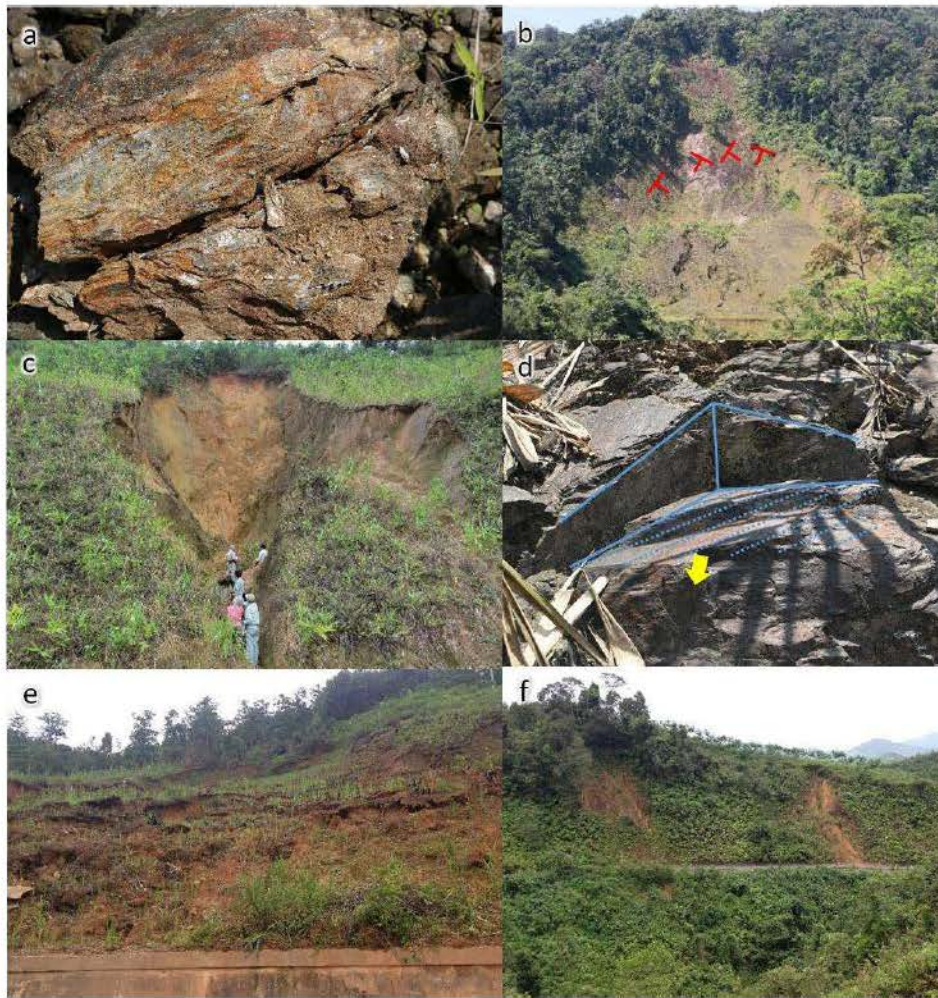
Figure 5.9 Typical example of landslide emphasizing geology in Paleozoic (Le et al., 2015b): a: weathered schist stone; b, c, d: wedge type; e: slump type; f: debris slide

At Precambrian zone

Proterozoic slightly metamorphic rocks exposed at the river occupy almost all of this area, with dominant gneiss and schist consisting of quartz, mica, and sometimes including hornblende belonging to the Kham Duc formation. The region is characterized by a very thick layer of residual soil and completely weathered material of 100 m depth (Figure 5.10-c, d).

Weathering features: The area formed by gneiss and schist rocks has undertaken intensive tropical weathering processes, creating a profile with various characteristics and thicknesses with a history of weathering (Figure 5.11). Two deep weathering layers were observed at this zone (old and new weathering). The upper portion is new weathering consisting of reddish brown soil. It is rich in iron minerals. The strength at the outcrop is easily crushable by fingers. It has highly clayey minerals (Figure 5.10-d). In contrast, at the lower portion is another feature of weathering that is identifiable. It characterizes the skeleton structure. It has a dark reddish brown color, semi-consolidated in spite of original geological structure remains. The skeletal structure seems to result from melting out of some parts of materials (such as an orthoclase, plagioclase, Figure 5.10-a, b, c). These weathering characteristics are established during a long period. Therefore, this zone is said to have old weathering.

Landslide characteristics: Most observed landslides in this area are small to medium size and are strongly associated with weathered material. They develop only at the weathering zone. Types of landslides are slump and debris flow slides, occurring in intense and heavy rains. During that time, it saturates residual soil, which is porous and friable and enters the stream forming a slump and a debris flow slide (Le *et al.*, 2016).

At other areas, we identified the relation between the landslide direction and geological structures. Landslides are strongly affected by geological structures. However, the directions of movement in this area are various, e.g., at the Ba Hai channel area (Figure 5.11-a). Combined with geological structures and weathering, we deduced that the geological structure is not relative to landslide compared with the weakness of surface geology because of two-layer-deep weathering (Le *et al.*, 2016).

Figure 5.10 History of weathering at Precambrian (Le et al., 2016):
a: gneiss, b: medium weathering gneiss, c: weathered gneiss; d: highly weathered granite

New weathering: reddish brown soil, highly content clay minerals and easily crush by fingers

Old weathering: dark reddish brown colour, semi consolidate and characterize by skeleton structure

Fresh rock: gneiss and schist consists of quartz, mica
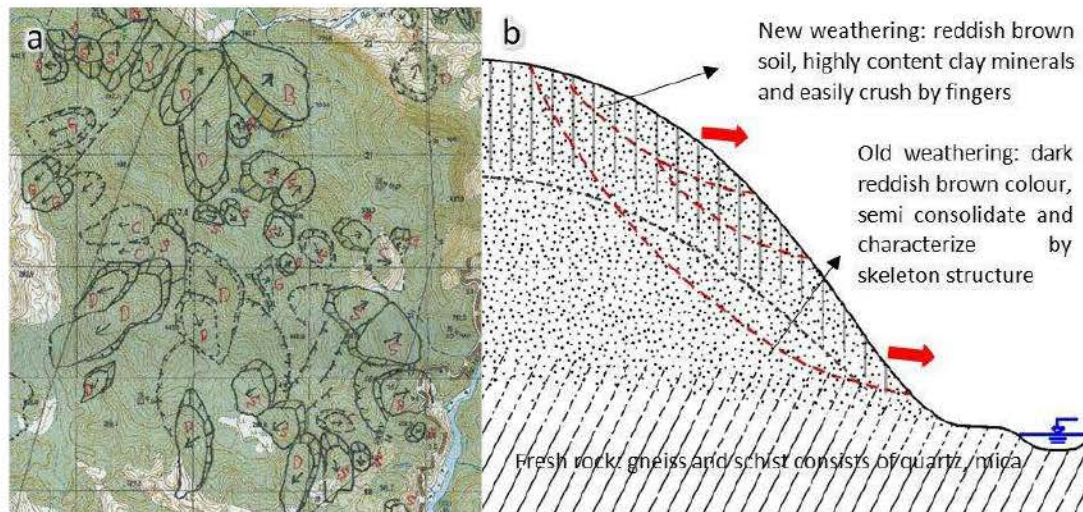
Figure 5.11 Landslide inventory map at Ba Hai channel area (Le et al., 2016) (a); typical
cross section of Precambrian weathering (b)

5.4. Regional characteristics of landslides in relation to geological structure and weathering

Based on the discussions presented above, we inferred the regional characteristics of landslide in Vietnam with explanation of the two following points related directly to geological structure and weathering:

Geological structures

Geological structures such as joints, fractures, bedding planes, and rock types can strongly influence the spatial and temporal distribution of mass movements across a landscape in many ways. Several geologic factors identified in this study area appear to account for the spatial distribution of many of the identified landslides. For example, weak rock is more likely to slide than strong rock. On the slope, strong rock overlying weak rocks will increase potential sliding as a translational slide. In the Mesozoic zone, a cuesta landform (Figure 5.7) was observed, with large-scale landslides that are abundant in this area. Numerous landslides occurred as translational slides along the bedding plane and weak layer (mudstone and coal layer). The landslide size is a function of the slope size and coal layer depth. Landslide No. 18 is a typical one, characterized by well-bedded sedimentary rocks with high presence of coal layer lenses, cracks, and fractures (Figure 5.12). These characteristics promote water penetration and are prone to landslides. Field surveys show these features in landslide areas and also indicate that the recent landslide is a reactivation of an older slide (Figure 5.12).

Other examples of landslides exist at less weathered metamorphic rock in the Paleozoic zone. Landslides occur as translational wedge slide along joints and fractures when water penetrates and weakens the face (Figure 5.8, Figure 5.9-b, c, d). Most landslides are small. Sometimes large landslides occur by combinations of multiple small wedge slides. In these cases, joints and fractures are the main factors causing landslides.

Figure 5.12 Some evidence of landslide action was observed at a part of landslide No. 18 (Le, 2015a)

Weathering

Weathering has a prominent role in the formation of landslides in humid tropical regions such as Vietnam. It is an extremely important factor. In an area that received high weathering processes (Paleozoic, Precambrian zone), surficial weathered material layers turned to a loose and reddish brown clayey material that is silty with a sandy grained particle size. It rapidly loosens with increasing amounts of water. With rainfall, surficial soil saturates, forming a landslide as a debris slide or debris flow (Figure 5.9-e, f; Figure 5.11; Figure 5.13).

Figure 5.13 Debris slide at highly weathered Paleozoic river valley side slope (Le et al., 2016)

In areas with weaker weathering processes, such as at magmatic rocks of Paleozoic areas, the surficial crust is a moderately weathered rock with many cracks and fractures in different directions. Landslides occur as wedge type slides along joint and fracture planes. The landslide size changes greatly from small to large depending on fractures (Figure 5.8; Figure 5.9-c, f).

At the Ba Hai channel area, landslides occur in many directions (Figure 5.11). That characteristic is explainable by geology structure. It is not so much influent to the landslide. It influences topography and weathered material. Main factors contributing to these landslides include the weakness of surface weathered material.

Based on the analysis described above, geology structure and weathering have played important roles in landslide occurrence. Risk evaluation is expected to include geology and weathering factors. The methodology will be discussed based on the accumulation of field data and the limitation of aerial photograph interpretation because of the lack of good quality photographs. The microtopography in the landslide area has some difficult realization. Therefore, it is ultimately necessary to improve the inspection sheet for application to humid tropical regions. That includes geomorphology and geology.

5.5. Integrated risk evaluation sheet by combination of morphology and geology for humid tropical regions

5.5.1. Integrated risk evaluation sheet

Based on AHP approach, the author presumes that a new integrated inspection sheet will combine two components: The first is morphology, as mentioned in the old version. The

second is geologic conditions. With this component, it is also classified into large, medium, and small categories. Based on the results of aerial photograph interpretation and fieldwork, we infer that the large category will include the following: (1) geologic age, (2) bedrock lithology and structure, (3) surficial geology, and (4) level of weathering. Each major category above was also classified into medium and small classifications. The first major category is related to identification of the dominant minerals or parent rock types and the geological unit. This category can be divided further into smaller classifications as Quarternary, Mesozoic, Precambrian, and Paleozoic, which correspond with river soil sediment; Triassic to the Jurassic sedimentary rock (conglomerate, gritstone, sandstone, siltstone); schist and granite gneiss; and schist, quartz-sericite schist. The second major category is related to the attitude of bedding: joints, cracks, fractures of rocks and stratigraphy such as sensitive layer between rocks. The category includes three medium categories: attitude of beds; presence and degree of fractures, joints, and foliation and stratigraphy. Attitudes of beds are divided into two small classifications: beds of rock that parallel or dip in the same direction as the slope and beds that dip into the slope. Presence and degree of fractures, joints, and foliation are divided into three small classifications base on distance between fractures, joints, and foliation; less than 20 cm; 20 cm – 50 cm; and greater than 50 cm. Stratigraphy (Sensitive key layer) has three minor classifications: hard beds overlying softer rock (coal); hard beds overlying softer rock (mudstone); and massive. It is the third major concerned with the level of weathering. It was divided into four small classifications corresponding with degree of weathering: completely weathered, highly weathered, moderately weathered, and slightly weathered.

To put the AHP score in the new inspection sheet, we must create a score system for the new integrated inspection sheet. First we must evaluate the degree of contribution of each morphology and geology to risk evaluation. To carry out this evaluation between two objects, AHP method was used. Geomorphology was deduced as two times more important than geology and the matrix (Table 5.3). Results show that, of the total AHP score, geomorphology will account for 44.44% and geology will account for 55.56%.

Table 5.3 Reciprocal matrix of paired comparison between geomorphology and geology

Paired comparison	Geomorphology	Geology	Weight vector	Eigenvector / AHP score
Geomorphology	1.0	0.8	0.89	44.44
Geology	1.250	1.0	1.12	55.56
Σ	2.25	1.8	2.01	100

To compute and compare five medium categories (Primary geologic unit (Rock type); Attitude of beds; Presence and degree of fractures, joints, and foliation; Stratigraphy (Sensitive key layer); Degree of weathering), a paired comparison of each object was set up. No standard method exists to make a pairwise comparison between these objects. The author's judgment based on the results collecting from landslide inventory map and fieldwork is that the primary geologic unit (rock type) is more important than the bed attitude. The primary geologic unit is not less important than the presence and degree of fractures, joints, and foliation and stratigraphy. The primary geologic unit is not far more important than the degree of weathering. Therefore, in the matrix, those are rated as 2.0, 0.25, 0.333, and 0.2. The same judgments were made of relative objects and forms of the completed matrix (Table 5.4). We obtained

94

eigenvectors as 7.90, 8.57, 40.63, 10.29, and 32.62. The sum of all elements in the eigenvector is 100. The eigenvector represents relative weights among the factors that we compare. In this study, geology comprises 55.56%, so maximum AHP scores are the following: Primary geologic unit (Rock type) is 4.39; Attitude of beds is 4.76; Presence and degree of fractures, joints, and foliation is 22.57; Stratigraphy (Sensitive key layer) is 5.72; and Degree of weathering is 18.12.

To verify the consistency of the evaluation, the consistency index (CI) was calculated as the deviation or degree of consistency using the following formula (as described in Chapter 1).

λmax = 5.335 (about 2.4% error)

n: comparison matrix size (n=5)

Therefore, the consistency index: $CI = \frac{\lambda_{max}-n}{n-1} = 0.084$

Consistency ratio, $CR = \frac{CI}{RI} = 6.98\%$. It is smaller than 10%, thereby the author's evaluation of geology elements is consistent.

Doing the same with for small classifications in each medium category yields the AHP scores corresponding with respective elements, as presented in Tables 5.4, 5.5, 5.6, 5.7, 5.8, and 5.9.

Table 5.4 Reciprocal matrix of paired comparison: Primary geologic unit; Attitude of beds; Presence and degree of fractures, joints, and foliation; Stratigraphy; and Degree of weathering

Paired comparison	Primary geologic unit (Rock type)	Attitude of beds	Presence and degree of fractures, joints, and foliation	Stratigraphy	Degree of weathering	weight vector	Eigen-vector	AHP Score
Primary geologic unit (Rock type)	1.00	2.00	0.25	0.33	0.20	0.506	7.90	4.39
Attitude of beds	0.50	1.00	0.20	2.00	0.25	0.549	8.57	4.76
Presence and degree of fractures, joints, and foliation	4.00	5.00	1.00	3.00	2.00	2.605	40.63	22.57
Stratigraphy	3.00	0.50	0.33	1.00	0.25	0.660	10.29	5.72
Degree of weathering	5.00	4.00	0.50	4.00	1.00	2.091	32.62	18.12
Σ	13.50	12.50	2.28	10.33	3.70	6.412	100.0	

Table 5.5 Reciprocal matrix of paired comparison: Quarternary; Precambrian; Paleozoic; and Mesozoic

Paired comparison	Quaternary	Precambrian	Paleozoic	Mesozoic	weight factor	Eigenvector	Score
Quaternary	1.00	2.00	3.00	1.00	1.57	34.45	3.97

Paired comparison	Quaternary	Precambrian	Paleozoic	Mesozoic	weight factor	Eigenvector	Score
Precambrian	0.50	1.00	2.00	0.33	0.76	16.73	1.93
Paleozoic	0.33	0.50	1.00	0.33	0.49	10.69	1.23
Mesozoic	1.00	3.00	3.00	1.00	1.73	38.13	4.39
Σ	2.83	6.50	9.00	2.67	4.54	100.0	

λ max = 4.042

CI = 0.014

CR = 1.56 % < 10%

Table 5.6 Reciprocal matrix of paired comparison between beds of rock that parallel or dip in the same direction as the slope and beds that dip into the slope

Paired comparison	Beds of rock that parallel or dip in the same direction as the slope	Beds that dip into the slope	Weight factor	Eigenvector	AHP Score
Beds of rock that parallel or dip in the same direction as the slope	1.00	3.00	1.73	75.00	4.76
Beds that dip into the slope	0.33	1.00	0.58	25.00	1.59
Σ	1.33	4.00	2.31	100.00	

λ max = 2.00

CI = 0.000

CR = 0.00 % < 10%

Table 5.7 Reciprocal matrix of paired comparison between distances of fractures, joints, foliation

Paired comparison	Numerous (distance less than 20cm)	Few (distance ranging from 20cm to 50cm)	Very few (distance greater than 50cm)	Weight factor	Eigenvector	Score
Numerous (distance between less than 20cm)	1.00	2.00	3.00	1.82	53.96	22.57
Few (distance ranging from 20cm to 50cm)	0.50	1.00	2.00	1.00	29.70	12.42
Very few (distance greater than 50cm)	0.33	0.50	1.00	0.55	16.34	6.84
Σ	1.83	3.50	6.00	3.37	100.00	

λ max = 3.009

CI = 0.005

CR = 0.79 % < 10%

Table 5.8 Reciprocal matrix of paired comparison between hard beds overlaying softer rock
(coal); hard beds overlaying softer rock (mudstone); massive

Paired comparison	Hard beds overlaying softer rock (coal..)	Hard beds overlaying softer rock (mudstone..)	Massive	Weight factor	Eigenve ctor	Score
Hard beds overlaying softer rock (coal..)	1.00	0.90	4.00	1.53	44.25	5.72
Hard beds overlaying softer rock (mudstone..)	1.11	1.00	3.00	1.49	43.13	5.57
Massive	0.25	0.33	1.00	0.44	12.61	1.63
Σ	2.36	2.23	8.00	3.46	100.00	

λ max = 3.017

CI = 0.009

CR = 1.48 % < 10%

Table 5.9 Reciprocal matrix of paired comparison between completely weathered, highly
weathered, moderately weathered, and slightly weathered

Paired comparison	Completely weathered	Highly weathered	Moderately weathered	Slightly weathered	Weight factor	Eigenvector	Score
Completely weathered	1.00	3.00	5.00	7.00	3.20	56.69	18.12
Highly weathered	0.33	1.00	3.00	5.00	1.50	26.48	8.46
Moderately weathered	0.20	0.33	1.00	2.00	0.60	10.70	3.42
Slightly weathered	0.14	0.20	0.50	1.00	0.35	6.12	1.96
Σ	1.68	4.53	9.50	15.00	5.65	100.00	

Finally, develop the new integrated inspection sheet as shown in Figure 5.14

Integrated Inspection sheet for landslide risk evaluation for humid tropical region　　LS No:

Element	Major division	Main factor	Observation theme	Unstable factor (Large and unstable ⟷ Small and stable)	Scale	Location	AHP score
Morphology	Micro-landform features in landslide body / Characteristics of active landslide		A: Type of movement	Flow mound and pressure ridge 8.33 — Minor scarp 3.27 — Separation scarp, Depression, Trenches 1.3			
			B: Level of clearness and micro landform components within landslide body	Huge no. of deformed blocks and clear micro topographic boundary 13.0 — Clear micro-topography of smooth boundary 8.33 — Unlear deformed block 4.0 — Smooth boundary 3.67			
			C: Level of instability of landslide body	Head block separates from the lower part 9.27 — Gullies development 2.4 — Linear erosion development 1.0			
			D: Direct features of movement	Cracks and scares 12.53 — Tree crown deformation 4.2			
			Other minor features	(Causes: Swamped land, Pond surface, Deformed development, Crack, Change?)			
	Level of after movie deformation at major boundaries / Age distribution		E: Between top edge of main scarp and the upper slope	Echelon 2.53 — Main scarp 2.13 — Creeping slope 1.2 — Gullies extension 1.0 — Modified to smooth slope 0.87			
			F: Between the main scarp and the body	Non deposition 2.07 — Talus 1.2 — Large-scale talus 0.73 — Smooth deformed by creeping and Talus development 0.4			
			G: Between the landslide body and the frontal slope	Non deformed landslide body 0.67 — Gully, debris cone 0.35 — Smooth surface topography 0.27 — Disappeared surface 0.2			
	Landslide and adjacent environment / Geomorphic setting		H: Toe part of landslide body	Face to the undercutting slope of river 5.73 — Face to the river 2.93 — On the flat plain 1.07 — Hit to opposite slope 0.6			
			I: The lower part of landslide body	Increasing toward the active condition 12.8 — Moderate the change of relief energy 6.13 — Decreasing 1.8			
			Particularly removable deformed block in landslide	Yes — Non — (Total No. small blocks)			
	Un-classifiable matters / Unexpected landform of landslide						
Geology	Geologic age / Geology age		Primary geologic unit (Rock type)	Mesozoic (Triassic to the Jurassic sedimentary rock: Conglomerate, Gritstone,) 1.63 — Quarternary (River soil sediment) 2.38 — Precambrian (Schist and Granit gneiss) 1.16 — Paleozoic (Schist, Quazt-sericite Schist, …) 0.74			
	Bedrock Lithology and Structure	Bedrock Lithology and Structure	Attitude of beds	Beds of rock that parallel or dip in the same direction as the slope 2.86 — Beds that dip into the slope 0.95			
			Presence and degree of fractures, joints, and foliation	Numerous |distance between fractures, joints, and foliation less than 20cm| 13.84 — Few |distance between fractures, joints, and foliation ranging from 20cm to 50cm| 7.45 — Few |distance between fractures, joints, and foliation greater than 50cm| 4.10			
			Tratigraphy (Sensitive key layer)	Hard beds overlaying softer rock (coal..) 3.43 — Hard beds overlaying softer rock (mudstone..) 3.34 — Massive 0.98			
	Level of weathering / Level of weathering		Degree of weathering	Completely weathered 10.87 — Highly 5.08 — Moderately weathered 2.05 — Slightly weathered 1.17			
			Risk of landslide occurrence base on your experience	Large → Middle → Small	Total points of AHP assessment: ………. scores		
			Comment and view of each selection		Score by own inspector: ………. scores		

Figure 5.14 Example of new inspection sheet for humid tropical regions

5.5.2. Case study applications and discussion

For application, landslide (LS) No. 18; LS No. 3; LS No. 163, LS No. 171, and LS No. 371 were recomputed. Results are presented in Table 5.10. Few differences are apparent between the two results when applying Japan's inspection sheet and the integrated inspection sheet.

Table 5.10 Result of risk evaluation by two inspection sheets

Landslide number	AHP score when use Japan's inspection sheet	AHP score when use integrated inspection sheet	Level of risk
03	46.20	42.92	Medium risk
18	70.00	71.20	High risk
163	57.30	62.35	Medium risk
171	54.80	61.24	Medium risk

| 371 | 25.25 | 32.31 | Medium risk |

This sheet was developed based on an AHP approach, the author's fieldwork, and the author's opinion. Few collected data are related to soil characteristics, relations between geologic conditions, and landslide occurrences. The sheet also has not been much discussed. For that reason, one cannot define the degree of agreement when applying this sheet. It is an initial sheet that includes numerous limitations. Nevertheless, further discussion of this matter seems unnecessary.

5.6. Summary of achieved results and discussion

This chapter has accomplished the following:

a) Japan's inspection sheet was applied for risk evaluation in 35 case studies in the study area. In each case study, the total risk level was evaluated.

b) The relation between geologic conditions and landslide occurrences (type, pattern) was shown strongly in the study area. The area was classified into four geological zones (Quaternary, Mesozoic, Paleozoic, and Precambrian). In each geological zone, landslide occurrences have their own characteristics in relation to geology.

c) Japan's inspection sheet was shown to have some limitations when applied to humid tropical regions such as Vietnam. It should be modified because geology is not described in risk evaluation.

d) Using the AHP approach, the author produced and proposed an integrated inspection sheet for humid tropical regions. This includes geological factors and reevaluation using an AHP approach. It remains in the initial stage of development, presenting some limitations and requiring more discussion because it has been not discussed much.

Contents

CHAPTER 6. DISCUSSION AND CONCLUSIONS

This study is intended to contribute to knowledge related to landslide problems in Vietnam by recognizing existing landslides from aerial photograph interpretation and by assessing the probability of landslide occurrence. Japan has achieved success in this area, but that success must be translated to Vietnam and other humid tropical regions.

In the last five chapters, results were discussed. Several conclusions were obtained. In these sections, the main discussions and conclusions are related to the key points corresponding to the initial objectives of this study. Finally, some recommendations were made for additional work.

6.1. Landslide mapping

A landslide inventory map is the basic for geomorphological analysis and risk assessment. During the course of this study, a landslide inventory was mapped using aerial photograph interpretation. Using this method, landslides and mass movement features were classified and mapped based on the morphological signatures left by the landslides:

+ In the study area of Japan, small-scale aerial photographs were used. Therefore, micro-topographic features left by landslides are clearly identifiable. Fieldwork was conducted to elucidate the mechanisms forming these features.

+ In the study area of Vietnam, we established six sheets of the landslide inventory map with 685 identified landslide areas. Then we transferred them to GIS. However, surfaces and small landslides were not identifiable because of source data limitations. Therefore, inventory maps only clarify large-scale landslides. By combination of fieldwork and geological maps, distribution tendencies of large scale landslide topography were characterized clearly with geological features.

A landslide inventory map of the study area was produced using aerial photograph interpretation. This map is extremely useful for people to define the spatial locations of landslide sites. The map is a basic data source for applied landslide research and management efforts to improve strategies for industrial and infrastructural risk management.

In Vietnam, detection and mapping of landslides using aerial images presents a challenging task that depends strongly on the quality of source data and experiences of morphologist and interpreter. Formal standards for identification do not exist. The interpreter classifies landslide morphological forms based on experience, and on analysis of a set of characteristics (signatures) that are identifiable on the images.

For landslides examined in this study, mass movement features have been classified and mapped based on the morphological signatures left by the features. These signatures are unique to the type of movement observed.

For developing countries such as Vietnam, data acquisition in the field is usually extremely expensive. Often in cases of large-scale landslides, that process is unaffordable. In

such cases, using aerial photographs for landslide study proved to be extremely useful to present a general view of landslides.

6.2. Landslide risk evaluation

For translating Japan's inspection sheet, which involves geomorphic features within and outside of landslides into Vietnam's situation, the author attempted application for 35 case studies. Some micro-features were found to be difficult to identify because of the scale of photographs. High-quality photographs are not available at the moment. Therefore, it is one reason for the necessity to modify the sheet in the future.

The author conducted fieldwork and recognized that the characteristics between landslide distribution and geology, including weathering features, can be summarized as explained below:

- Quaternary: Geology limited to areas near Kham Duc town. Landslides occur along river side slopes. Large-scale landslides are combinations of numerous small surface landslides. Topographic features are of a size that strongly affects the basal lava covering structures such as a caprock.

- Mesozoic: Landslide distributions are extremely common. The size also shows great diversity. Causative factors of landslides should be regarded as a deep slope established by geological structures along with distribution of weak layers such as coal and sericite fine materials. Weathering processes make a very poor contribution here.

– Paleozoic: Landslides in this area have a typical distribution. A few large-scale landslides have occurred, but numerous small landslides were observed in the field. Small landslides are affected strongly by weathering and geological structures such as surface and shallow landslides distributed at weathering slopes. Wedge type slides can occur at some partially deep weathering joints.

– Precambrian. Precambrian geology is characterized by widely various landslide distributions. However, a poor relation is shown with geological structures. The landslide and direction are apparently influenced by the topographic features. The Precambrian geology receives very deep and strong weathering processes. Therefore, landslide deformation and distribution might result from material weaknesses that are related directly to deep weathering.

Based on the factors described above, risk evaluation should include geology and weathering factors. The methodology will be discussed based on the accumulation of field data and the limitations of aerial photograph interpretation because of the lack of high-quality photographs. The micro-topography in the landslide area has some difficult realization. Therefore, it is ultimately necessary to improve the inspection sheet for application to humid tropical regions. Geology should be described in the inspection sheet along with morphological features.

To produce the integrated inspection sheet, the AHP approach was used. Criteria were put into a matrix. Every pairwise or degree of contribution of criterion was compared and judged. A score system was established corresponding to each criterion. An integrated inspection sheet for humid tropical region was produced involving morphology and geology. The AHP score arrangement was restructured into a new inspection sheet. It is in the initial

stage of development: it retains some limitations and requires more discussion because it has been little discussed to date.

6.3. Recommendations for additional work

The lack of source data in Vietnam has led to difficulties related to this study. Therefore, a key recommendation for this point is to keep inventory updated more often. Furthermore, greater study and discussion are needed to produce a high-quality landslide inventory.

The integrated inspection sheet should be discussed much more. Experts on geology, morphology, and landslide mechanics can gather and discuss each parameter in the sheet

By analyzing and applying landslide mapping and risk evaluation, it is the author's hope that this study will contribute to landslide hazard reduction in Vietnam.

Contents

No table of figures entries found.

No table of figures entries found.

LIST OF REFERENCES

Baum, R.L., Schuster, R.L., Godt, J.W., 1999. Map showing locations of damaging land-slides in Santa Cruz County, California, resulting from 1997 to 1998 ElNino rain-storms. U.S. Geo-logical Survey Miscellaneous Field Studies Map, MF-2325-D, scale 1:125,000

Crozier, M.J., and Glade, T., 2005. Landslide Hazard and risk: Issues, concepts, and approach. In: Glade, T., Anderson, M., and Crozier, M. (eds): Landslide hazard and risk. Wiley, Chichester, pp.1-40

Dinh Van Tien, Shinro Abe, Hiroyuki Yoshimatsu, Tatsuya Shibasaki, Miyagi Toyohiko, 2015. Geological mechanisms of landslide generation along Ho Chi Minh route in central Viet Nam. Journal of the Japan landslide society, July 2015, pp. 25-35

Doan Minh Tam, 2008. Research study on countermeasure technology for landslide prevetion along national road in Viet Nam. Institute of transport science and technology

Fell R, C. J, 2008. Guidelines for landslide susceptibility, hazard and risk zoning for land-use planning. Eng Geol 102 (3-4), pp. 99-111

Geological and mineral resources map of Viet Nam on 1:200,000, 1996. Geological survey of Viet Nam, Ha Noi, 1996

Guzzetti Fausto, 2005. Thesis - Landslide hazard and risk assessment. Rheinischen Friedrich-Wilhelms-Univestität Bonn

Guzzetti Fausto, Alessandro Cesare Mondini, Mauro Cardinali, Federica Fiorucci, Michele Santangeloa, Kang-Tsung Chang, 2012. Landslide inventory maps: New tools for an old problem. Earth-Science Reviews 112, pp. 42–66

Hamaski Eisaku, Miyagi Toyohiko, 2013. Risk Evaluation using the Analytic Hierarchy Process (AHP) - Introduction to the process concept. ICL Landslide Teaching Tools, pp36-49

Hansen, A., 1984a. Engineering geomorphology: the application of an Evolutionary model of Hong Kong. Zeitschrift für Geomorphologies 51, pp. 39–50

Hansen, A., 1984b. Strategies for classification of landslides. In: Brunsden, D., Prior, D.B. (Eds.), Slope Instability. Wiley, New York, pp. 523–602

Hatano S, 1974. Landforms of rapid massmovement origin (Recent progress in geomorphology 8) art-2. Soil Mech Found Eng (Tsuchi to Kiso) 22(11), pp. 85–93, in Japanese

Hutchinson, J.N., 1988. General report: morphological and geotechnical parameters of landslides in relation to geology and hydrology. In: Bonnard, C. (Ed.), Proceedings 5th International Symposium on Landslides, Lausanne, Switzerland. Balkema, Rotterdam, Netherlands, 1, pp. 3–35

Ichise Y, 1964. Landslide identification by the areial photo interpreta-tion. Bull Nat Resour Res 62, pp. 13–22, in Japanese

Karl W. Wegmann, 2006. Digital Landslide Inventory for the Cowlitz County Urban Corridor, Washington. Washington division of Geology and Earth resources - Report of Investigations 35 – Washington State department of Natural Resources

Kimata R, Miyagi T, 1985. Basic components of landslide topography. J Landslide Soc 21(4), pp. 1–9, in Japanese

NIED, 1982 - 2015. Landslide maps. National research Institute for Earth Science and Disaster Prevention, Japan (NIED)

Le Hong Luong, Miyagi Toyohiko, Shinro Abe, Hamasaki Eisaku, Dinh Van Tien, 2014a. Detection of active landslide zone from aerial photograph interpretation and field survey in central provinces of Vietnam. Volume 1 - The International Programme on Landslides (IPL), Landslide Science for a Safer Geoenvironment, 2014, pp. 435-441. Doi 10.1007/978-3-319-04999-1-61

Le Hong Luong, Miyagi Toyohiko, Shinro Abe, Hamasaki Eisaku, Dinh Van Tien, 2014b. Landslide mapping and detection of active landslide area from aerial photograph interpretation and field survey in central provinces of Vietnam. Landslide Risk Assessment Technology, Proceedings of the SATREPS Workshop on Landslides in Vietnam, pp. 42-49

Le Hong Luong, Miyagi Toyohiko, 2014c. Landslide mapping and risk evaluation by aerial photograph interpretation and field survey in central provinces of Vietnam, Poster presentation. The Inaugural conference of IGU commission on "Geomorphology & Society" 9/2014

Le Hong Luong, 2015a. Overview of characteristics of landslide No.18 in Ho Chi Minh road, Viet Nam. Human information magazine No.20, Graduate school of human informatics, Tohoku Gakuin university, pp. 59-63

Le Hong Luong, Miyagi Toyohiko, Shinro Abe, Hamasaki Eisaku and Pham Van Tien, 2015b. Landslide risk evaluation by combination of morphology, geology and simulation approach in tropical humid region. Proceedings on International conference on landslides and slope stability 2015, pp. 244-250

Le Hong Luong, Miyagi Toyohiko, 2015c. Hidden landslide: as the Caldera rim deformation at Fukayamadake plateau, at the foot slope of Kurikoma volcano, Kurihara, Japan. Proceedings on International conference on landslides and slope stability 2015, pp. 216-220

Le Hong Luong, Miyagi Toyohiko, Pham Van Tien, 2016. Mapping of large scale landslide topographic area by aerial photograph interpretation and possibilities for application to risk assessment for the Ho Chi Minh route – Vietnam. Transactions, Japanese Geomorphological Union, pp. 97-118

Le Quoc Hung, 2014. Investigation, assessment and warning zonation for landslides in the mountainous regions of Vietnam. Ha Noi - Institute of geosciences and mineral resources

Lomtadze V.D., 1997. Geoengineering - tectonical geoengineering. Moskva: Nedra Publishing House

Malamud, B.D., Turcotte, D.L., Guzzetti, F. and Reichenbach, P. (2004b) Landslides, earthquakes and erosion. Earth and Planetary Science Letters, 229, pp. 45-59

Miyagi T, 1979. Landslide in Miyagi Prefecture. Sci Rep Res Tohoku Univ, Ser 7 (geography) 29, pp. 91–101

Miyagi Toyohiko, Gyawali B. Prasad, Charlchai Tanavud, Aniruth Potichan and Eisaku Hamasaki, (2004). Landslide Risk Evaluation and Mapping - Manual of Aerial Photo Interpretation for Landslide Topography and Risk Management. Report of the National Research Institute for Earth Science and Disaster Prevention, pp. 75-137

Miyagi Toyohiko, Shinichi Yamashina, Fumitoshi Esaka, Shinro Abe, 2011. Massive landslide triggered by 2008 Iwate-Miyagi inland earthquake in the Aratozawa Dam area, tohoku, Japan. Landslide journal, pp. 99-108, Doi 10.1007/s10346-010-0226-8

Miyagi Toyohiko, 2013. TXT-tool 1.081-2.1 Landslide topography mapping through aerial photo interpretation. ICL Landslide Teaching Tools, pp. 36-49

Miyagi Toyohiko, Hamasaki Eisaku, 2014a. Risk Evaluation of Landslide Topographic Area by Aerial Photointerpretation. Landslide Science for a Safer Geoenvironment, Volume 2: Methods of Landslide Studies, WLF3, pp. 491-497, Doi 10.1007/978-3-319-05050-8_76

Miyagi Toyohiko, Hamasaki Eisaku, Dinh Van Tien, Le Hong Luong, Ngo Doan Dung, 2014b. Landslide mapping and the risk evaluation by aerial photo interpretation in Vietnam. Landslide Risk Assessment Technology, Proceedings of the SATREPS Workshop on Landslides in Vietnam, pp. 87-95

Markus Meinhardt, Manfred Fink, Hannes Tünschel, 2015. Landslide susceptibility analysis in central Vietnam based on an incomplete landslide inventory: Comparison of a new method to calculate weighting factors by means of bivariate statistics. Geomorphology journal - Volume 234, pp. 80-97, Doi:10.1016/j.geomorph.2014.12.042

Higaki Daisuke, Noriyuki Chiba, Jun Umemura, 2008. Phenomena and the mechanism of Oikubo landslide disaster in Shiroishi, Miyagi Pref. on July15, 2007 - Comparison with the result of susceptibility assessment for landslide disaster. Journal of the Japan Landslide Society, Vol. 45 (2008) No. 3, pp. 227-233

Ngo Doan Dung, Hamasaki Eisaku, Tatsuya Shibasaki, Miyagi Toyohiko, Hiromu Daimaru, Dinh Van Tien, Le Hong Luong, 2014. Change the safety factors by the series of land deformation at a typical landslide along the National Road No.6, Vietnam. Landslide Risk Assessment Technology, Proceedings of the SATREPS Workshop on Landslides in Vietnam

Nguyen Khanh Van, Nguyen Thi Hien, Phan Ke Loc, Nguyen Tien Hiep, 2000. Bioclimatic diagrams of Viet Nam. Ha Noi, Viet Nam National University, pp. 126, in Vietnamese

Nguyen Quoc Khanh, 2009. Thesis - Landslide hazard assessmentin Muong Lay, Viet Nam applying GIS and remote sensing. Faculty of Mathematics and Natural Sciences, Ernst-Moritz-Arndt-University Greifswald

Nguyen Thanh Long, 2008. Thesis - Landslide susceptibility mapping of the mountainous area in A Luoi district, Thua Thien Hue province, Viet Nam. Department of Hydrology and Hydraulic Engineering, Vrije Universitteit Brussel

NUMO-TR-04-04, 2004. Evaluating Site Suitability for a HLW Repository, Scientific Background and Practical Application of NUMO's Siting Factors, Nuclear Waste Management Organization of Japan (NUMO)

Ngo Doan Dung, Dinh Van Tien, Nguyen Xuan Khang, 2016. The current manuals and standards for the survey and design works for landslide prevention in Viet Nam. Transactions, Japanese Geomorphological Union 37-1, pp. 5-31

Oldrich Hungr, Serge Leroueil, Luciano Picarelli, 2013. The Varnes classification of landslide types, an update. Landslide journal april 2014, pp. 167-195. Doi 10.1007/s10346-013-0436-y

Oyagi, N., S. Uchiyama, A Sano., M. Ogura and S. Doshida, 2014. Landslide Maps, Series 57 "Island of Okinawa Prefecture" Explanation of Landslide Distribution Maps. National research institute for Earth Science and Disaster Prevention, Japan. No. 389, pp. 1-14

Takahashi, K., H. Yamashita, K. Tsuchiya and K. Nakamura eds. 1982. Meteorology of Japan by satellite images. Iwanamishoten, 158ps

Tien. P.V, K. Sassa, K. Takara, H.T. Binh, L.H. Luong, 2015. Characteristics and failure mechanism of landslides in weathered granitic rocks in Hai Van mountain. *"Proceedings on International conference on landslides and slope stability 2015"*, pp. 165-172

Pasek, 1975. Landslide inventory. International Association Engineering Geologist Bulletin, pp. 73-74

Reichenbach, P., Cardinali M., De Vita, L. and Guzzetti, F. ,1998. Regional hydrological thresholds for landslides and floods in the Tiber River basin (Central Italy). Environmental Geology, 35:2-3, pp. 146-159

Reichenbach, P., Guzzetti, F. and Cardinali, M. , 1998. Map of sites historically affected by landslides and floods in Italy, 2nd edition. CNR Gruppo Nazionale per la Difesa dalle Catastrofi Idrogeologiche Publication n. 1786, scale 1:1,200,000

Report on Investigation, assessment and warning zonation for landslides in the mountainous regions of Vietnam, 2015. State-Funded Landslide Project. Viet Nam institute of geosciences ad mineral resources, in Viet Namese

Rib, H.T., Liang, T., 1978. Recognition and identification. In: Schuster, R.L., Krizek, R.J. (Eds.), Landslide Analysis and Control.: Transportation Research Board Special Report, 176. National Academy of Sciences, Washington, pp. 34–80

Richard G.Ray, 1960. Aerial Photographs in Geologic Interpretation and Mapping, Geological survey professional paper 373, United states government printing office, Washington : 1960

Ritchie, A. M., 1958, Recognition and identification of landslides, in Landslides and engineering practice: Natl. Research Council, Highway Research Board Spec. Rept. no. 29, pp. 48-68

Saaty, T., 1980. The Analytic Hierarchy Process. McGraw Hill International

Salvati, P., Guzzetti, F., Reichenbach, P., Cardinali, M. and Stark, C.P. , 2003. Map of landslides and floods with human consequences in Italy. CNR Gruppo Nazionale per la Difesa dalle Catastrofi Idrogeologiche Publication n. 2822, scale 1:1,200,000

Shimizu F, Oyagi N, Inoguchi T, 1982–1988. The maps of landslide topography. National Res Inst Disaster Sci Japan, vol 1–6 (in Japanese)

Soeters, Cees Van Westen, 1996. Slope instability recognition, analysis, and zonation. In: Land-slides, investigation and mitigation / ed. by. A.K. Turner and R.L. Schuster. Washington, D.C. National Academy Press, 1996. ISBN 0-309-06151-2. (Transportation Research Board, National Research Council, Special Report; 247) pp. 129 - 177

Taylor, F. and Brabb, E.E. , 1986. Map showing landslides in California that have caused fatalities or at least $1,000,000 in damages from 1906 to 1984. U.S. Geological Survey Miscellaneous Field Studies Map, MF-1867

Terado T, 1978. Large scale mass movements in central part of the Ohou Back borne range. Q J Geogr 30, pp. 189-198, in Japanese

The chronicle of a mountain disaster, Iwate-Miyagi Nairiku earthquake in 2008, 3/2015. Japan Forestry agency, Tohoku regional forest office

Tien Pham, Tam Doan, Luong Le, 2014. Overview of Landslide Phenomena along Arterial Transport System in Vietnam, Landslide Risk Assessment Technology, Proceedings of the SATREPS Workshop on Landslides in Vietnam

Tran Tan Van, 2006. Investigate, evaluate current landslides along Ho Chi Minh, National road No.1 and propose countermeasure for mitagating. Ha Noi: Institute of geosciences and mineral resources

Tran Trong Hue, 2009. Landslide study and proposing countermeasure in Coc Pai, Xin Man, Ha Giang. Ha Noi. Viet Nam institute of geosciences ad mineral resources.

Varnes, D.J, 1978. Slope movements: types and processes. In: Schuster, R.L. and Krizek, R.J. (eds.) Landslide analysis and control, National Academy of Sciences, Transportation Research Board Special Report 176, Washington, pp.11-33

Yagi R, 2003. Micro topography in the landslide body and the devel-oping processes. Geomorphol J 24(3), pp. 261–294, in Japanese

Zhang L, 2010. Thesis-Comparison of classical analytic hierarchy process (AHP) approach and fuzzy AHP approach in multiple-criteria decision making for commercial vehicle information systems and networks (CVISN) project. University of Nebraska-Lincoln

APPENDIX A: LANDSLIDE INVENTORY MAP
KHAM DUC

Legend

- Town
- Landslide body
- Landslide scarp
- Ho Chi Minh road

0   0,5   1   2 Km

APPENDIX A: LANDSLIDE INVENTORY MAP
KHOM 9

N

PING
THON A SO
THANH MY
KHOM 9
PA PONG
KHAM DUC

Legend
● Town
Landslide body
Landslide scarp
Ho Chi Minh road
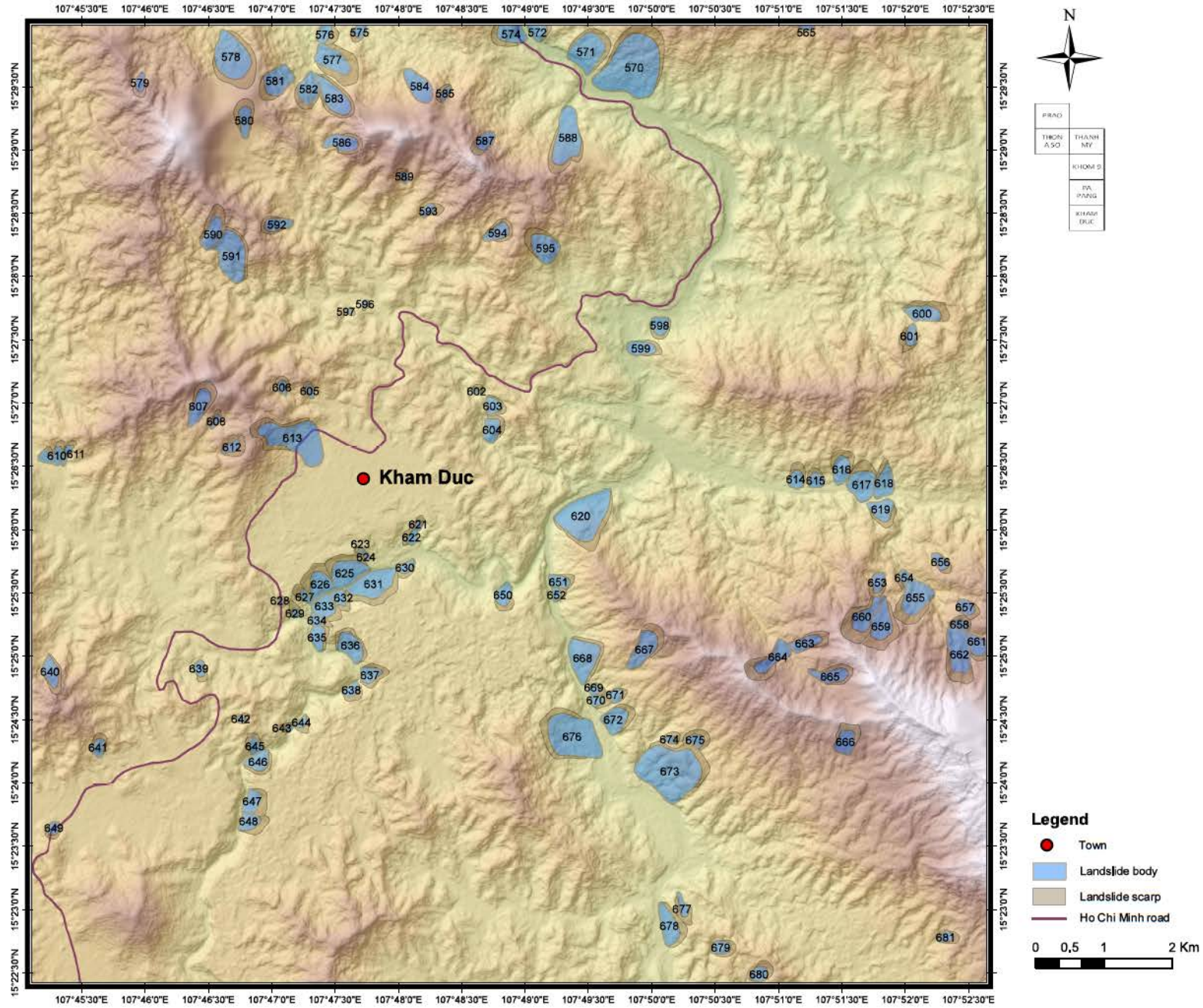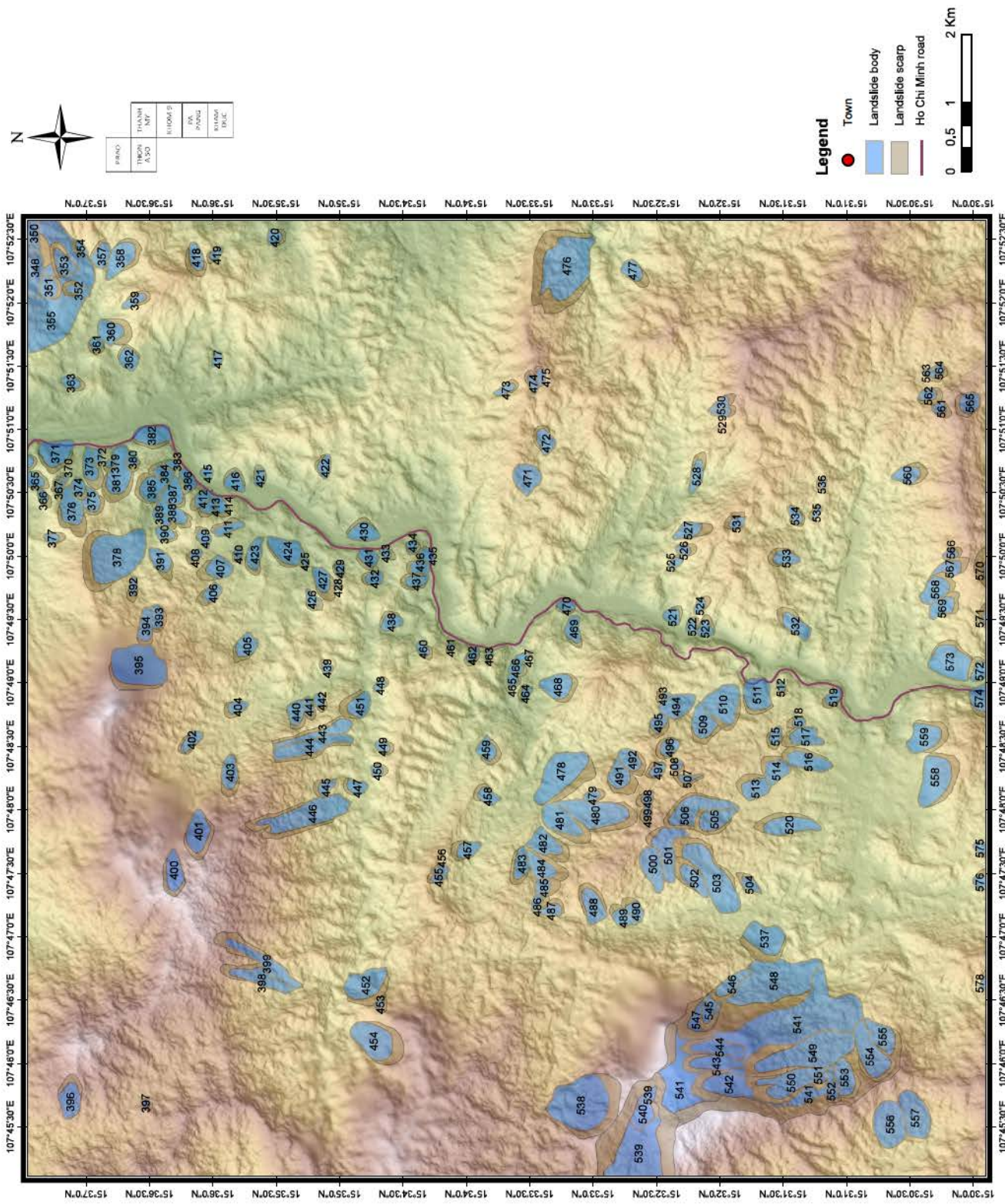
0 0.5 1 2 Km

APPENDIX A: LANDSLIDE INVENTORY MAP
PA PANG

Legend

- Town
- Landslide body
- Landslide scarp
- Ho Chi Minh road

0 0.5 1 2 Km

APPENDIX A: LANDSLIDE INVENTORY MAP
PRAO

Legend

● Town

Landslide body

Landslide scarp

Ho Chi Minh road
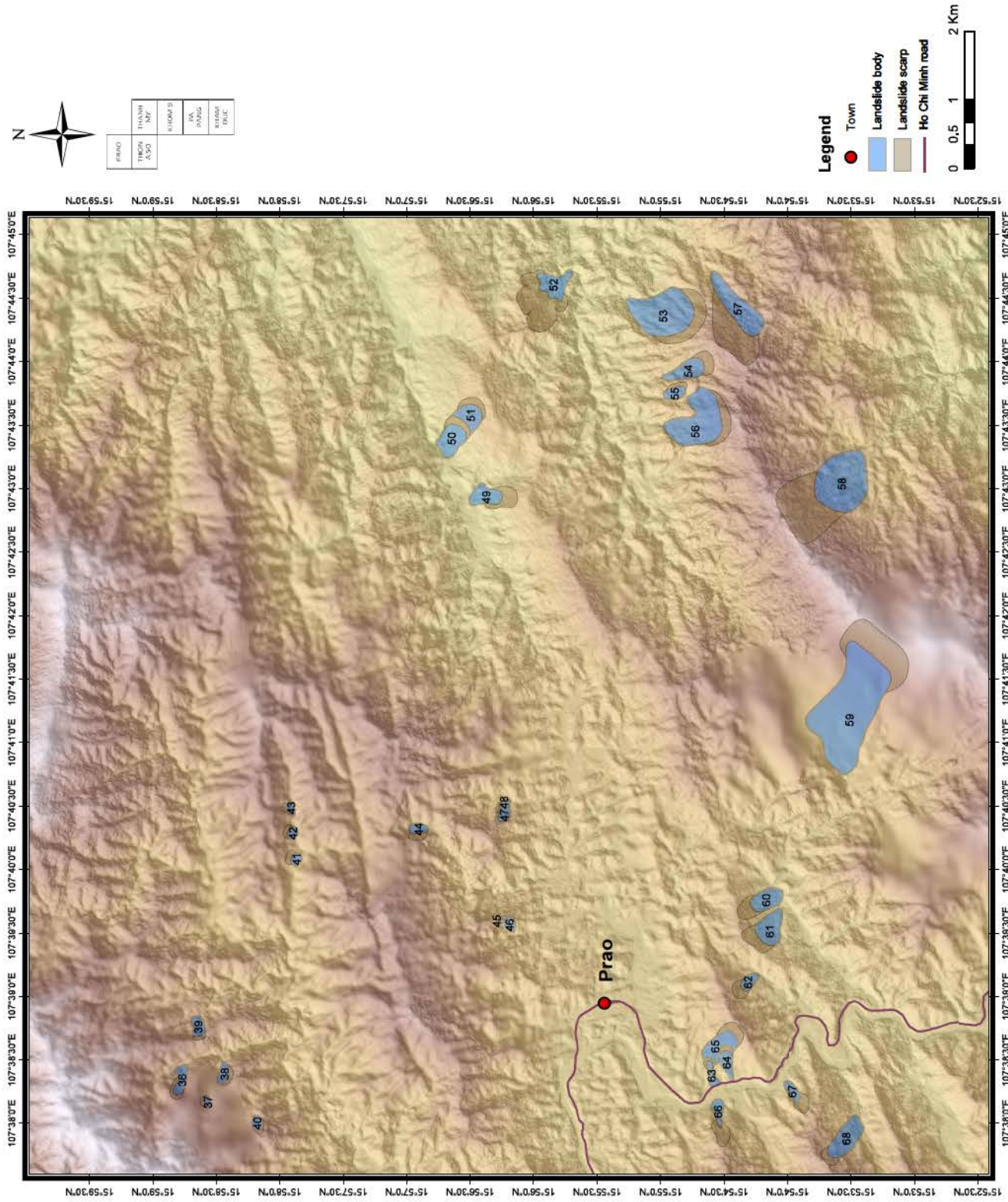
0 0.5 1 2 Km

APPENDIX A: LANDSLIDE INVENTORY MAP

THANH MY
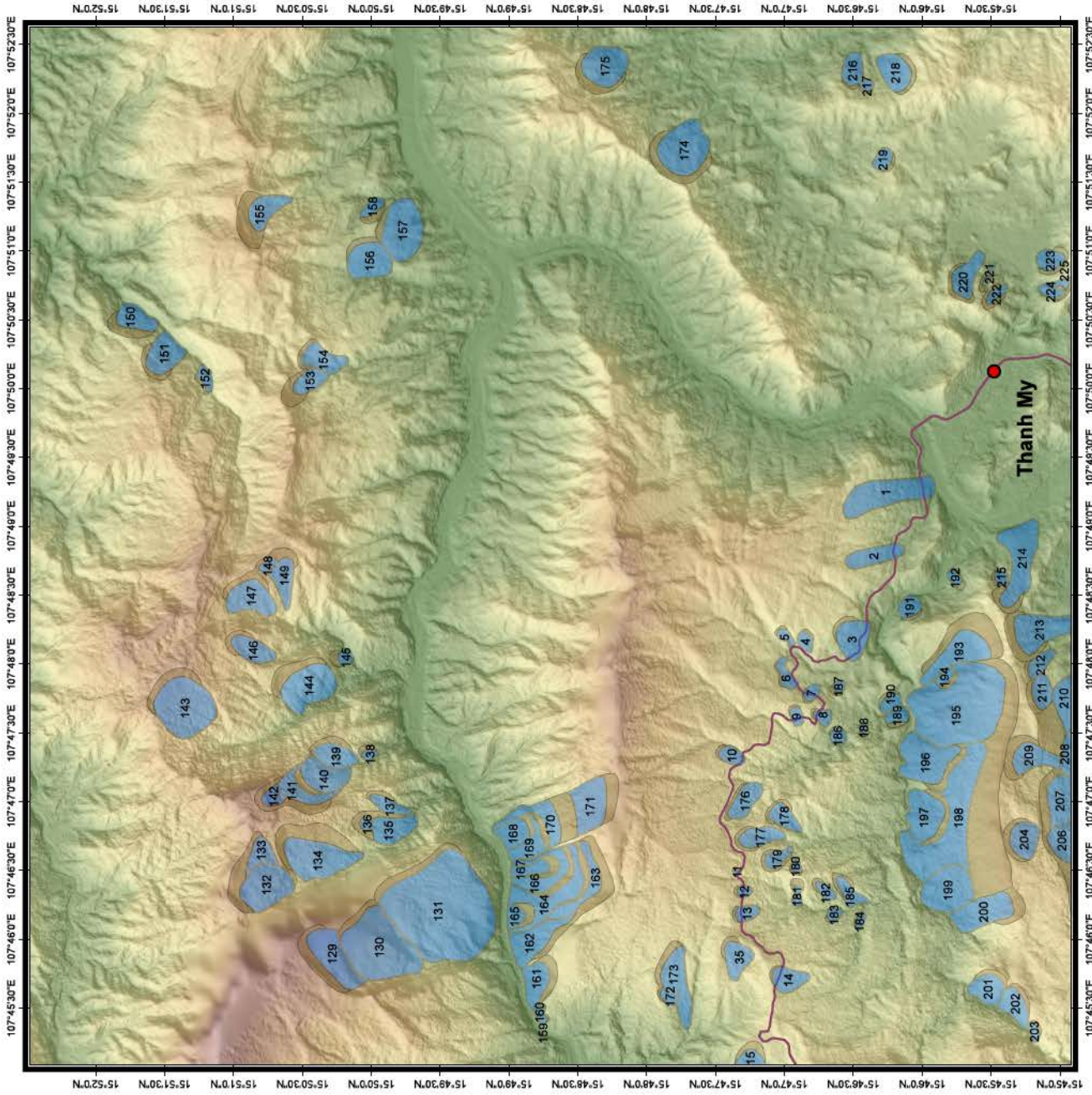
Legend

● Town

Landslide body

Landslide scarp

Ho Chi Minh road

0   0.5   1   2 Km

APPENDIX A: LANDSLIDE INVENTORY MAP

THON A SO

Legend

- City
- Landslide body
- Landslide scarp
- Ho Chi Minh road

0   0,5   1   2 Km
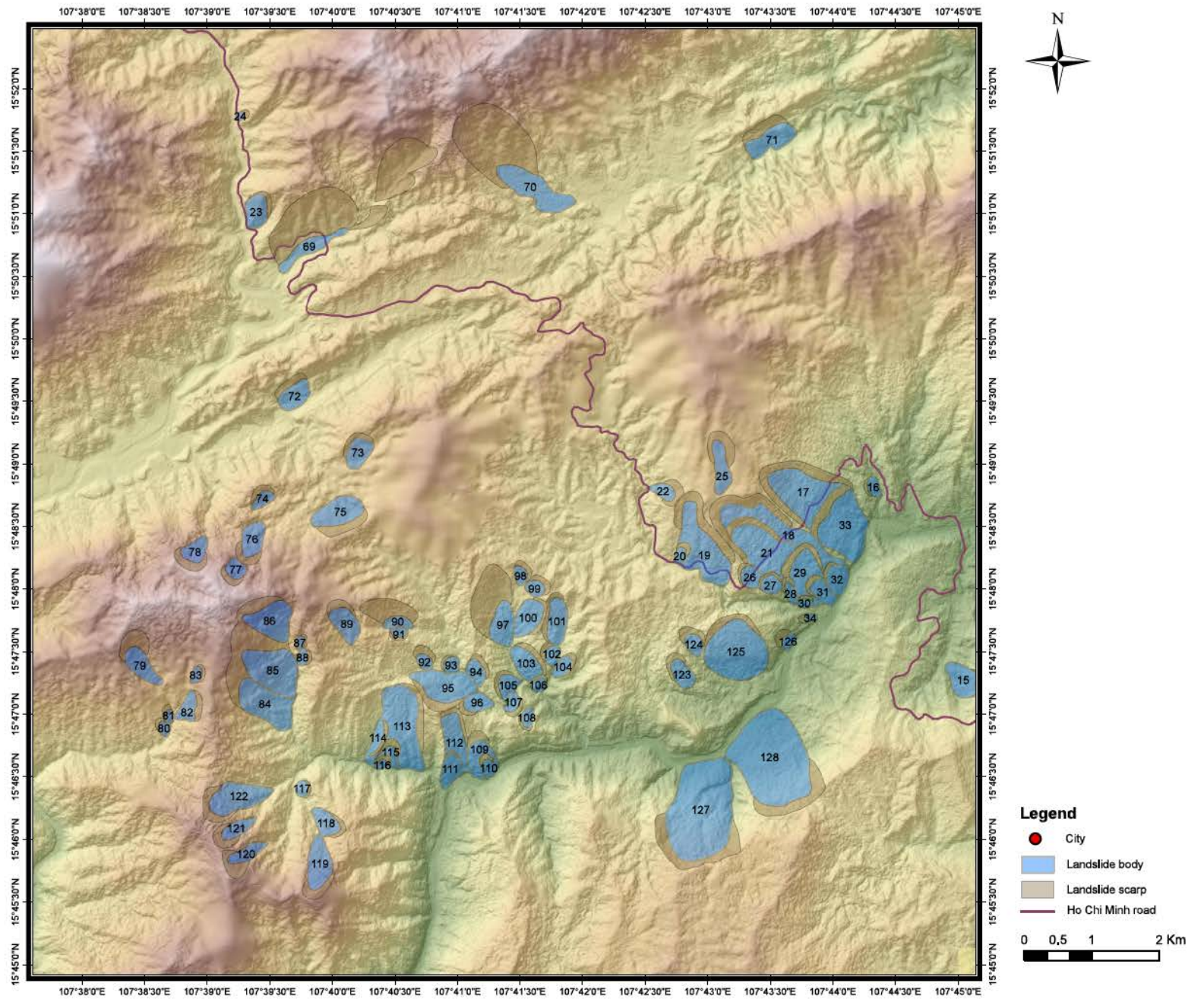
APPENDIX B: DATABASE ATTRIBUTE DESCRIPTIONS FOR LANDSLIDE INVENTORY MAP

Landslide Number (1)	Longtitude (2)	Latitude (3)	Length (m) (4)	Width (m) (5)	Area (km2) (6)	Landslide type (7)	Movement direction (8)	Face to river (9)	Bedrock (10)	Formation (11)	Geology age (12)	Affect to Road (13)	Affect to House (14)
1	107° 49' 13.728" E	15° 46' 15.753" N	1269	333	0.38	Rotational Slide	S9.5E	Yes	Sandstone, siltstone, conglomerate	Nong Son formation – Upper Subformation	Mesozoic	Yes	No
2	107° 48' 47.045" E	15° 46' 21.021" N	818	210	0.16	Translational Slide	S14.6E	No	Sandstone, siltstone, conglomerate	Nong Son formation – Upper Subformation	Mesozoic	Yes	No
3	107° 48' 11.100" E	15° 46' 30.178" N	495	470	0.21	Rotational Slide	W55.5S	No	Conglomerate, sandstone, siltstone	Ban Co formation	Mesozoic	Yes	No
4	107° 48' 9.653" E	15° 46' 50.959" N	248	218	0.07	Rotational Slide	N74W	No	Conglomerate, sandstone, siltstone	Ban Co formation	Mesozoic	Yes	No
5	107° 48' 11.651" E	15° 46' 59.395" N	308	162	0.04	Rotational Slide	W43S	No	Siltstone, sandstone	Khe Ren formation	Mesozoic	Yes	No
6	107° 47' 55.252" E	15° 46' 59.425" N	175	390	0.07	Translational Slide	S19E	No	Siltstone, sandstone	Khe Ren formation	Mesozoic	Yes	No
7	107° 47' 47.461" E	15° 46' 48.153" N	293	178	0.04	Rotational Slide	S51.28E	No	Siltstone, sandstone	Khe Ren formation	Mesozoic	Yes	No
8	107° 47' 36.808" E	15° 46' 43.172" N	286	166	0.04	Rotational Slide	W61.44S	No	Siltstone, sandstone	Khe Ren formation	Mesozoic	Yes	No
9	107° 47' 37.262" E	15° 46' 54.776" N	266	156	0.04	Rotational Slide	W19.2S	No	Siltstone, sandstone	Khe Ren formation	Mesozoic	Yes	No
10	107° 47' 20.025" E	15° 47' 22.970" N	395	223	0.07	Rotational Slide	W58.5S	No	Siltstone, sandstone	Huu Chanh formation	Mesozoic	Yes	No
11	107° 46' 29.390" E	15° 47' 20.672" N	118	66	0.01	Rotational Slide	W49.5S	No	Siltstone, sandstone	Huu Chanh formation	Mesozoic	Yes	No
12	107° 46' 20.609" E	15° 47' 17.560" N	214	143	0.03	Rotational Slide	S7.02E	No	Siltstone, sandstone	Huu Chanh formation	Mesozoic	Yes	No
13	107° 46' 11.176" E	15° 47' 16.418" N	372	287	0.06	Rotational Slide	S15E	No	Siltstone, sandstone	Huu Chanh formation	Mesozoic	Yes	No
14	107° 45' 42.431" E	15° 46' 58.294" N	432	312	0.13	Rotational Slide	W64.8S	No	Siltstone, sandstone	Huu Chanh formation	Mesozoic	Yes	No
15	107° 45' 2.550" E	15° 47' 16.281" N	573	421	0.23	Rotational Slide	N85W	No	Siltstone, sandstone	Huu Chanh formation	Mesozoic	No	No
16	107° 44' 19.699" E	15° 48' 48.901" N	217	301	0.06	Rotational Slide	E9.36N	Yes	Conglomerate, sandstone, siltstone	Ban Co formation	Mesozoic	Yes	No
17	107° 43' 44.853" E	15° 48' 46.472" N	1805	904	1.34	Rotational Slide	S53.4E	Yes	Conglomerate, sandstone, siltstone	Ban Co formation	Mesozoic	Yes	No
18	107° 43' 33.455" E	15° 48' 28.519" N	2288	986	1.95	Rotational Slide	S56E	Yes	Conglomerate, sandstone, siltstone	Ban Co formation	Mesozoic	Yes	No
19	107° 42' 57.333" E	15° 48' 18.827" N	730	841	0.74	Debris slide	W77.55S	Yes	Sandstone, siltstone, conglomerate	Nong Son formation – Upper Subformation	Mesozoic	Yes	No
20	107° 42' 46.482" E	15° 48' 15.838" N	326	144	0.05	Rotational Slide	W69.5S	Yes	Sandstone, siltstone, conglomerate	Nong Son formation – Upper Subformation	Mesozoic	Yes	No
21	107° 43' 25.929" E	15° 48' 19.218" N	1730	703	0.89	Rotational Slide	S55E	Yes	Conglomerate, sandstone, siltstone	Ban Co formation	Mesozoic	Yes	No
22	107° 42' 38.727" E	15° 48' 46.991" N	500	240	0.12	Debris slide	N74.6W	Yes	Sandstone, siltstone, conglomerate	Nong Son formation – Upper Subformation	Mesozoic	Yes	No
23	107° 39' 23.472" E	15° 51' 0.926" N	456	427	0.16	Translational Slide	W38S	Yes	Gneissogranite	Dai Loc complex – Phase 1	Paleozoic	Yes	No
24	107° 39' 15.902" E	15° 51' 46.905" N	204	110	0.02	Translational Slide	W29S	Yes	Gneissogranite	Dai Loc complex – Phase 1	Paleozoic	Yes	No
25	107° 43' 6.093" E	15° 48' 58.203" N	907	214	0.25	Debris Slide	S9.05E	No	Sandstone, siltstone, conglomerate	Nong Son formation – Upper Subformation	Mesozoic	No	No
26	107° 43' 20.394" E	15° 48' 5.611" N	390	318	0.10	Rotational Slide	S75E	No	Conglomerate, sandstone, siltstone	Ban Co formation	Mesozoic	Yes	No
27	107° 43' 30.235" E	15° 48' 1.788" N	316	307	0.08	Rotational Slide	S4E	No	Conglomerate, sandstone, siltstone	Ban Co formation	Mesozoic	No	No
28	107° 43' 39.662" E	15° 47' 57.839" N	405	146	0.06	Rotational Slide	S21E	No	Conglomerate, sandstone, siltstone	Ban Co formation	Mesozoic	No	No
29	107° 43' 46.460" E	15° 48' 7.232" N	826	552	0.44	Rotational Slide	S38E	No	Conglomerate, sandstone, siltstone	Ban Co formation	Mesozoic	No	No
30	107° 43' 46.486" E	15° 47' 53.185" N	181	227	0.04	Rotational Slide	W85S	No	Conglomerate, sandstone, siltstone	Ban Co formation	Mesozoic	No	No
31	107° 43' 55.342" E	15° 47' 58.321" N	512	237	0.12	Rotational Slide	S46E	Yes	Conglomerate, sandstone, siltstone	Ban Co formation	Mesozoic	No	No
32	107° 44' 2.392" E	15° 48' 4.754" N	359	394	0.13	Rotational Slide	S65E	Yes	Conglomerate, sandstone, siltstone	Ban Co formation	Mesozoic	No	No
33	107° 44' 5.586" E	15° 48' 29.284" N	817	774	0.61	Rotational Slide	S52.4E	Yes	Conglomerate, sandstone, siltstone	Ban Co formation	Mesozoic	No	No

(1)	(2)	(3)	(4)	(5)	(6)	(7)	(8)	(9)	(10)	(11)	(12)	(13)	(14)
34	107° 43' 49.294" E	15° 47' 46.124" N	275	98	0.03	Debris Slide	E10.05N	No	Conglomerate, sandstone, siltstone	Ban Co formation	Mesozoic	No	No
35	107° 45' 51.420" E	15° 47' 20.609" N	441	315	0.15	Translational Slide	W45.75S	No	Siltstone, sandstone	Khe Ren formation	Mesozoic	No	No
36	107° 38' 20.470" E	15° 58' 47.018" N	475	120	0.08	Rotational Slide	S76E	No	Sandstone, Schist	A Vuong formation – Middle Subformation	Paleozoic	No	No
37	107° 38' 10.147" E	15° 58' 34.005" N	140	163	0.02	Debris Slide	S10E	No	Sandstone, Schist	A Vuong formation – Middle Subformation	Paleozoic	No	No
38	107° 38' 23.329" E	15° 58' 26.468" N	210	282	0.05	Translational Slide	E58N	No	Schist	A Vuong formation – Upper Subformation	Paleozoic	No	No
39	107° 38' 45.465" E	15° 58' 38.581" N	335	184	0.06	Rotational Slide	E14N	No	Schist and gneiss	Kham Duc formation – Upper Subformation	Paleozoic	No	No
40	107° 37' 59.920" E	15° 58' 10.763" N	194	190	0.03	Debris Slide	E55N	No	Schist	A Vuong formation – Upper Subformation	Paleozoic	No	No
41	107° 40' 4.882" E	15° 57' 52.151" N	231	186	0.04	Rotational Slide	W63S	Yes	Schist	A Vuong formation – Upper Subformation	Paleozoic	No	No
42	107° 40' 17.169" E	15° 57' 53.912" N	202	184	0.03	Debris Slide	W67S	Yes	Schist	A Vuong formation – Upper Subformation	Paleozoic	No	No
43	107° 40' 28.715" E	15° 57' 54.739" N	172	173	0.02	Debris Slide	W89S	Yes	Schist	A Vuong formation – Upper Subformation	Paleozoic	No	No
44	107° 40' 19.021" E	15° 56' 54.547" N	239	251	0.06	Translational Slide	S79E	No	Schist	A Vuong formation – Lower Subformation	Paleozoic	No	No
45	107° 39' 35.535" E	15° 56' 14.895" N	94	68	0.01	Translational Slide	W17S	No	Schist	A Vuong formation – Lower Subformation	Paleozoic	No	No
46	107° 39' 33.792" E	15° 56' 11.302" N	241	134	0.03	Translational Slide	W18S	No	Schist	A Vuong formation – Lower Subformation	Paleozoic	No	No
47	107° 40' 25.700" E	15° 56' 13.878" N	239	148	0.04	Translational Slide	S29E	No	Schist	A Vuong formation – Lower Subformation	Paleozoic	No	No
48	107° 40' 30.387" E	15° 56' 13.980" N	250	87	0.02	Rotational Slide	S38E	No	Schist	A Vuong formation – Lower Subformation	Paleozoic	No	No
49	107° 42' 56.234" E	15° 56' 22.883" N	651	220	0.18	Debris Slide	E76N	Yes	Schist	A Vuong formation – Lower Subformation	Paleozoic	No	No
50	107° 43' 22.817" E	15° 56' 38.928" N	531	323	0.17	Debris Slide	N51W	Yes	Schist	A Vuong formation – Lower Subformation	Paleozoic	No	No
51	107° 43' 34.045" E	15° 56' 30.295" N	597	385	0.32	Debris Slide	N50W	Yes	Schist	A Vuong formation – Lower Subformation	Paleozoic	No	No
52	107° 44' 36.377" E	15° 55' 50.081" N	930	280	0.48	Debris Slide	S47E	Yes	Gneissogranite	Dai Loc complex – Phase 1	Paleozoic	No	No
53	107° 44' 22.994" E	15° 54' 58.772" N	753	769	0.64	Debris Slide	E40N	No	Schist	A Vuong formation – Lower Subformation	Paleozoic	No	No
54	107° 43' 55.815" E	15° 54' 47.770" N	778	272	0.18	Debris Slide	N22W	No	Schist	A Vuong formation – Lower Subformation	Paleozoic	No	No
55	107° 43' 45.024" E	15° 54' 53.280" N	299	288	0.06	Rotational Slide	N56W	No	Schist	A Vuong formation – Lower Subformation	Paleozoic	No	No
56	107° 43' 31.803" E	15° 54' 42.534" N	767	759	0.52	Debris Slide	E74N	No	Schist	A Vuong formation – Lower Subformation	Paleozoic	No	No
57	107° 44' 25.646" E	15° 54' 23.629" N	713	272	0.60	Translational Slide	S27E	No	Gneissogranite	Dai Loc complex – Phase 1	Paleozoic	No	No
58	107° 43' 2.975" E	15° 53' 34.410" N	1390	768	1.05	Translational Slide	S35E	No	Gneissogranite	Dai Loc complex – Phase 1	Paleozoic	No	No
59	107° 41' 16.274" E	15° 53' 30.642" N	1871	694	1.58	Rotational Slide	N59W	No	Gneissogranite	Dai Loc complex – Phase 1	Paleozoic	No	No
60	107° 39' 45.574" E	15° 54' 10.046" N	717	265	0.18	Rotational Slide	S28E	Yes	Schist	A Vuong formation – Lower Subformation	Paleozoic	No	No
61	107° 39' 31.956" E	15° 54' 8.489" N	600	394	0.21	Debris Slide	S37E	No	Schist	A Vuong formation – Lower Subformation	Paleozoic	No	No
62	107° 39' 6.750" E	15° 54' 18.271" N	456	165	0.08	Rotational Slide	S43E	No	Schist	A Vuong formation – Lower Subformation	Paleozoic	No	No
63	107° 38' 22.600" E	15° 54' 35.611" N	417	75	0.05	Debris Flow	W13S	Yes	Schist	A Vuong formation – Lower Subformation	Paleozoic	No	No
64	107° 38' 28.517" E	15° 54' 28.783" N	501	185	0.07	Debris Flow	W15S	Yes	Schist	A Vuong formation – Lower Subformation	Paleozoic	No	No

(1)	(2)	(3)	(4)	(5)	(6)	(7)	(8)	(9)	(10)	(11)	(12)	(13)	(14)
65	107° 38' 36.468" E	15° 54' 32.233" N	676	333	0.17	Debris Slide	N41W	No	Schist	A Vuong formation – Lower Subformation	Paleozoic	No	No
66	107° 38' 5.692" E	15° 54' 32.816" N	662	124	0.10	Debris Flow	E13N	Yes	Schist	A Vuong formation – Lower Subformation	Paleozoic	No	No
67	107° 38' 14.994" E	15° 53' 57.861" N	512	120	0.08	Debris Flow	E36N	Yes	Schist	A Vuong formation – Lower Subformation	Paleozoic	No	No
68	107° 37' 52.880" E	15° 53' 32.599" N	761	275	0.20	Debris Flow	S50E	Yes	Schist	A Vuong formation – Lower Subformation	Paleozoic	No	No
69	107° 39' 48.970" E	15° 50' 43.337" N	2000	222	1.51	Debris Flow	W28S	Yes	Schist	A Vuong formation – Lower Subformation	Paleozoic	Yes	No
70	107° 41' 36.688" E	15° 51' 11.845" N	2016	398	1.28	Debris Flow	S53.8E	Yes	Schist	A Vuong formation – Lower Subformation	Paleozoic	No	No
71	107° 43' 30.104" E	15° 51' 35.499" N	400	720	0.30	Translational Slide	S31.33E	Yes	Schist	A Vuong formation – Lower Subformation	Paleozoic	No	No
72	107° 39' 41.802" E	15° 49' 32.779" N	420	514	0.19	Rotational Slide	S23E	Yes	Schist	A Vuong formation – Lower Subformation	Paleozoic	No	No
73	107° 40' 12.625" E	15° 49' 5.538" N	410	469	0.16	Debris Slide	S31.55E	No	Schist	A Vuong formation – Lower Subformation	Paleozoic	No	No
74	107° 39' 26.576" E	15° 48' 43.016" N	293	343	0.09	Rotational Slide	S19.38E	No	Conglomerate, sandstone, siltstone	Nong Son formation – Lower Subformation	Mesozoic	No	No
75	107° 40' 2.877" E	15° 48' 37.049" N	519	714	0.34	Rotational Slide	N42.68W	No	Conglomerate, sandstone, siltstone	Nong Son formation – Lower Subformation	Mesozoic	No	No
76	107° 39' 21.741" E	15° 48' 24.039" N	662	305	0.20	Rotational Slide	E78.45N	No	Conglomerate, sandstone, siltstone	Nong Son formation – Lower Subformation	Mesozoic	No	No
77	107° 39' 13.581" E	15° 48' 9.451" N	350	320	0.11	Translational Slide	E57.76N	No	Conglomerate, sandstone, siltstone	Nong Son formation – Lower Subformation	Mesozoic	No	No
78	107° 38' 54.169" E	15° 48' 18.416" N	540	310	0.17	Translational Slide	E56.28N	No	Conglomerate, sandstone, siltstone	Nong Son formation – Lower Subformation	Mesozoic	No	No
79	107° 38' 28.221" E	15° 47' 23.350" N	858	285	0.26	Debris Slide	S42E	No	Conglomerate, sandstone, siltstone	Nong Son formation – Lower Subformation	Mesozoic	No	No
80	107° 38' 39.296" E	15° 46' 53.315" N	262	183	0.04	Translational Slide	S51E	No	Sandstone	Song Bung formation – Upper Subformation	Mesozoic	No	No
81	107° 38' 41.569" E	15° 46' 59.079" N	256	168	0.03	Translational Slide	S35E	No	Sandstone	Song Bung formation – Upper Subformation	Mesozoic	No	No
82	107° 38' 50.432" E	15° 47' 3.111" N	317	463	0.12	Debris Slide	N89W	No	Sandstone	Song Bung formation – Upper Subformation	Mesozoic	No	No
83	107° 38' 54.478" E	15° 47' 18.795" N	204	240	0.04	Rotational Slide	W1S	No	Conglomerate, sandstone, siltstone	Nong Son formation – Lower Subformation	Mesozoic	No	No
84	107° 39' 27.943" E	15° 47' 4.874" N	1032	508	0.50	Translational Slide	S66E	No	Conglomerate, sandstone, siltstone	Nong Son formation – Lower Subformation	Mesozoic	No	No
85	107° 39' 31.324" E	15° 47' 21.140" N	1022	620	0.62	Translational Slide	S70E	No	Conglomerate, sandstone, siltstone	Nong Son formation – Lower Subformation	Mesozoic	No	No
86	107° 39' 30.862" E	15° 47' 44.783" N	750	630	0.40	Translational Slide	S85E	No	Conglomerate, sandstone, siltstone	Nong Son formation – Lower Subformation	Mesozoic	No	No
87	107° 39' 44.434" E	15° 47' 34.312" N	212	172	0.03	Debris Slide	W49.3S	No	Conglomerate, sandstone, siltstone	Nong Son formation – Lower Subformation	Mesozoic	No	No
88	107° 39' 45.566" E	15° 47' 27.260" N	261	214	0.05	Debris Slide	W43S	No	Conglomerate, sandstone, siltstone	Nong Son formation – Lower Subformation	Mesozoic	No	No
89	107° 40' 6.371" E	15° 47' 43.337" N	647	316	0.20	Translational Slide	S36.65E	No	Conglomerate, sandstone, siltstone	Nong Son formation – Lower Subformation	Mesozoic	No	No
90	107° 40' 31.324" E	15° 47' 43.862" N	396	412	0.26	Translational Slide	S5E	No	Sandstone, siltstone, conglomerate	Nong Son formation – Upper Subformation	Mesozoic	No	No
91	107° 40' 31.840" E	15° 47' 39.472" N	194	256	0.04	Rotational Slide	N2.31W	No	Sandstone, siltstone, conglomerate	Nong Son formation – Upper Subformation	Mesozoic	No	No
92	107° 40' 44.136" E	15° 47' 25.105" N	361	256	0.08	Rotational Slide	W89S	Yes	Sandstone, siltstone, conglomerate	Nong Son formation – Upper Subformation	Mesozoic	No	No
93	107° 40' 57.034" E	15° 47' 23.522" N	268	245	0.06	Rotational Slide	S57E	Yes	Sandstone, siltstone, conglomerate	Nong Son formation – Upper Subformation	Mesozoic	No	No
94	107° 41' 9.004" E	15° 47' 20.310" N	320	335	0.10	Translational Slide	W57S	Yes	Sandstone, siltstone, conglomerate	Nong Son formation – Upper Subformation	Mesozoic	No	No

(1)	(2)	(3)	(4)	(5)	(6)	(7)	(8)	(9)	(10)	(11)	(12)	(13)	(14)
95	107° 40' 54.139" E	15° 47' 13.949" N	591	850	0.40	Rotational Slide	E74N	Yes	Sandstone, siltstone, conglomerate	Nong Son formation – Upper Subformation	Mesozoic	No	No
96	107° 41' 9.565" E	15° 47' 5.658" N	438	274	0.11	Translational Slide	E32N	Yes	Sandstone, siltstone, conglomerate	Nong Son formation – Upper Subformation	Mesozoic	No	No
97	107° 41' 21.632" E	15° 47' 42.912" N	714	596	0.56	Translational Slide	S45E	No	Sandstone, siltstone, conglomerate	Nong Son formation – Upper Subformation	Mesozoic	No	No
98	107° 41' 30.047" E	15° 48' 6.433" N	335	256	0.07	Debris Slide	W77S	No	Sandstone, siltstone, conglomerate	Nong Son formation – Upper Subformation	Mesozoic	No	No
99	107° 41' 37.122" E	15° 48' 0.277" N	307	278	0.08	Debris Slide	W47S	No	Sandstone, siltstone, conglomerate	Nong Son formation – Upper Subformation	Mesozoic	No	No
100	107° 41' 33.744" E	15° 47' 46.309" N	450	530	0.20	Rotational Slide	N88W	No	Sandstone, siltstone, conglomerate	Nong Son formation – Upper Subformation	Mesozoic	No	No
101	107° 41' 47.590" E	15° 47' 44.580" N	329	677	0.21	Rotational Slide	S69E	No	Sandstone, siltstone, conglomerate	Nong Son formation – Upper Subformation	Mesozoic	No	No
102	107° 41' 45.374" E	15° 47' 28.228" N	295	301	0.07	Rotational Slide	S60E	No	Sandstone, siltstone, conglomerate	Nong Son formation – Upper Subformation	Mesozoic	No	No
103	107° 41' 32.579" E	15° 47' 24.461" N	388	553	0.19	Rotational Slide	W39S	No	Sandstone, siltstone, conglomerate	Nong Son formation – Upper Subformation	Mesozoic	No	No
104	107° 41' 50.285" E	15° 47' 22.755" N	361	292	0.08	Rotational Slide	W26S	No	Sandstone, siltstone, conglomerate	Nong Son formation – Upper Subformation	Mesozoic	No	No
105	107° 41' 24.146" E	15° 47' 13.860" N	346	379	0.11	Rotational Slide	S50E	Yes	Sandstone, siltstone, conglomerate	Nong Son formation – Upper Subformation	Mesozoic	No	No
106	107° 41' 38.691" E	15° 47' 14.023" N	254	199	0.05	Rotational Slide	W80S	Yes	Sandstone, siltstone, conglomerate	Nong Son formation – Upper Subformation	Mesozoic	No	No
107	107° 41' 26.286" E	15° 47' 5.728" N	250	300	0.07	Rotational Slide	N45W	Yes	Sandstone, siltstone, conglomerate	Nong Son formation – Upper Subformation	Mesozoic	No	No
108	107° 41' 33.555" E	15° 46' 58.366" N	316	193	0.05	Debris Slide	E61N	No	Sandstone, siltstone, conglomerate	Nong Son formation – Upper Subformation	Mesozoic	No	No
109	107° 41' 10.525" E	15° 46' 39.138" N	720	336	0.24	Rotational Slide	S19E	Yes	Sandstone, siltstone, conglomerate	Nong Son formation – Upper Subformation	Mesozoic	No	No
110	107° 41' 14.993" E	15° 46' 34.314" N	331	215	0.06	Debris Slide	S28E	Yes	Sandstone, siltstone, conglomerate	Nong Son formation – Upper Subformation	Mesozoic	No	No
111	107° 40' 56.670" E	15° 46' 33.158" N	452	302	0.12	Translational Slide	S2E	Yes	Sandstone, siltstone, conglomerate	Nong Son formation – Upper Subformation	Mesozoic	No	No
112	107° 40' 58.795" E	15° 46' 48.521" N	975	328	0.23	Translational Slide	S10E	Yes	Sandstone, siltstone, conglomerate	Nong Son formation – Upper Subformation	Mesozoic	No	No
113	107° 40' 33.166" E	15° 46' 54.279" N	1258	572	0.83	Rotational Slide	W85S	Yes	Sandstone, siltstone, conglomerate	Nong Son formation – Upper Subformation	Mesozoic	No	No
114	107° 40' 21.252" E	15° 46' 48.839" N	175	570	0.09	Debris Slide	N67W	No	Sandstone, siltstone, conglomerate	Nong Son formation – Upper Subformation	Mesozoic	No	No
115	107° 40' 27.879" E	15° 46' 39.680" N	445	275	0.08	Rotational Slide	W84S	Yes	Sandstone, siltstone, conglomerate	Nong Son formation – Upper Subformation	Mesozoic	No	No
116	107° 40' 23.739" E	15° 46' 36.048" N	207	180	0.04	Debris Slide	W81S	Yes	Sandstone, siltstone, conglomerate	Nong Son formation – Upper Subformation	Mesozoic	No	No
117	107° 39' 45.401" E	15° 46' 24.457" N	227	240	0.05	Rotational Slide	N83.8W	No	Conglomerate, sandstone, siltstone	Nong Son formation – Lower Subformation	Mesozoic	No	No
118	107° 39' 56.983" E	15° 46' 8.386" N	425	403	0.14	Debris Slide	N86W	No	Conglomerate, sandstone, siltstone	Nong Son formation – Lower Subformation	Mesozoic	No	No
119	107° 39' 53.663" E	15° 45' 48.319" N	910	354	0.29	Translational Slide	N4.67W	No	Conglomerate, sandstone, siltstone	Nong Son formation – Lower Subformation	Mesozoic	No	No
120	107° 39' 18.581" E	15° 45' 53.495" N	689	207	0.18	Translational Slide	E30.65N	No	Conglomerate, sandstone, siltstone	Nong Son formation – Lower Subformation	Mesozoic	No	No
121	107° 39' 14.345" E	15° 46' 5.413" N	685	214	0.15	Translational Slide	E29.6N	No	Conglomerate, sandstone, siltstone	Nong Son formation – Lower Subformation	Mesozoic	No	No
122	107° 39' 14.189" E	15° 46' 20.108" N	1018	394	0.38	Translational Slide	E13.32N	No	Conglomerate, sandstone, siltstone	Nong Son formation – Lower Subformation	Mesozoic	No	No
123	107° 42' 47.661" E	15° 47' 19.201" N	561	263	0.14	Rotational Slide	S38E	No	Conglomerate, sandstone, siltstone	Ban Co formation	Mesozoic	No	No
124	107° 42' 53.371" E	15° 47' 33.492" N	385	274	0.11	Rotational Slide	W89S	No	Conglomerate, sandstone, siltstone	Ban Co formation	Mesozoic	No	No

(1)	(2)	(3)	(4)	(5)	(6)	(7)	(8)	(9)	(10)	(11)	(12)	(13)	(14)
125	107° 43' 13.646" E	15° 47' 29.946" N	956	843	0.69	Rotational Slide	S5E	No	Conglomerate, sandstone, siltstone	Ban Co formation	Mesozoic	No	No
126	107° 43' 38.743" E	15° 47' 34.922" N	286	245	0.07	Translational Slide	S56E	Yes	Conglomerate, sandstone, siltstone	Ban Co formation	Mesozoic	No	No
127	107° 42' 56.769" E	15° 46' 14.117" N	1629	945	1.43	Rotational Slide	E81N	Yes	Conglomerate, sandstone, siltstone	Ban Co formation	Mesozoic	No	No
128	107° 43' 30.709" E	15° 46' 38.602" N	1473	966	1.40	Rotational Slide	N29W	Yes	Conglomerate, sandstone, siltstone	Ban Co formation	Mesozoic	No	No
129	107° 45' 51.856" E	15° 50' 16.138" N	555	938	0.43	Compound slide	S15E	No	Conglomerate, sandstone, siltstone	Ban Co formation	Mesozoic	No	No
130	107° 45' 56.045" E	15° 49' 56.304" N	1006	835	0.73	Compound slide	W41S	No	Conglomerate, sandstone, siltstone	Ban Co formation	Mesozoic	No	No
131	107° 46' 12.742" E	15° 49' 28.720" N	1457	1260	1.65	Compound slide	W38S	No	Conglomerate, sandstone, siltstone	Ban Co formation	Mesozoic	No	No
132	107° 46' 22.720" E	15° 50' 45.621" N	840	600	0.42	Rotational Slide	W43S	Yes	Sandstone, siltstone, conglomerate	Nong Son formation – Upper Subformation	Mesozoic	No	No
133	107° 46' 36.714" E	15° 50' 47.993" N	440	380	0.17	Rotational Slide	W45S	No	Sandstone, siltstone, conglomerate	Nong Son formation – Upper Subformation	Mesozoic	No	No
134	107° 46' 35.079" E	15° 50' 23.331" N	845	699	0.62	Rotational Slide	W45S	Yes	Conglomerate, sandstone, siltstone	Ban Co formation	Mesozoic	No	No
135	107° 46' 47.989" E	15° 49' 50.527" N	736	489	0.23	Rotational Slide	W73S	Yes	Conglomerate, sandstone, siltstone	Ban Co formation	Mesozoic	No	No
136	107° 46' 50.120" E	15° 50' 1.928" N	263	167	0.05	Rotational Slide	W85S	No	Conglomerate, sandstone, siltstone	Ban Co formation	Mesozoic	No	No
137	107° 46' 58.080" E	15° 49' 52.048" N	530	23	0.10	Rotational Slide	W51S	No	Conglomerate, sandstone, siltstone	Ban Co formation	Mesozoic	No	No
138	107° 47' 20.650" E	15° 50' 0.604" N	200	184	0.04	Translational Slide	W35S	No	Sandstone, siltstone, conglomerate	Nong Son formation – Upper Subformation	Mesozoic	No	No
139	107° 47' 19.735" E	15° 50' 15.394" N	515	450	0.20	Rotational Slide	W50S	No	Sandstone, siltstone, conglomerate	Nong Son formation – Upper Subformation	Mesozoic	No	No
140	107° 47' 11.081" E	15° 50' 20.684" N	591	569	0.24	Rotational Slide	S36E	No	Conglomerate, sandstone, siltstone	Ban Co formation	Mesozoic	No	No
141	107° 47' 4.688" E	15° 50' 30.167" N	862	645	0.47	Rotational Slide	S41E	No	Conglomerate, sandstone, siltstone	Ban Co formation	Mesozoic	No	No
142	107° 47' 1.743" E	15° 50' 42.623" N	413	245	0.11	Rotational Slide	S34E	No	Sandstone, siltstone, conglomerate	Nong Son formation – Upper Subformation	Mesozoic	No	No
143	107° 47' 41.104" E	15° 51' 21.262" N	878	691	0.58	Translational Slide	W43S	No	Sandstone, siltstone, conglomerate	Nong Son formation – Upper Subformation	Mesozoic	No	No
144	107° 47' 49.840" E	15° 50' 27.121" N	644	742	0.44	Rotational Slide	W39S	Yes	Sandstone, siltstone, conglomerate	Nong Son formation – Upper Subformation	Mesozoic	No	No
145	107° 48' 2.787" E	15° 50' 11.222" N	298	180	0.05	Rotational Slide	S10E	Yes	Sandstone, siltstone, conglomerate	Nong Son formation – Upper Subformation	Mesozoic	No	No
146	107° 48' 6.072" E	15° 50' 51.513" N	650	290	0.18	Debris Flow	W60S	No	Sandstone, siltstone, conglomerate	Nong Son formation – Upper Subformation	Mesozoic	No	No
147	107° 48' 28.397" E	15° 50' 52.291" N	530	567	0.29	Rotational Slide	W20S	No	Sandstone, siltstone, conglomerate	Nong Son formation – Upper Subformation	Mesozoic	No	No
148	107° 48' 42.693" E	15° 50' 44.699" N	221	232	0.06	Debris Slide	W7S	No	Sandstone, siltstone, conglomerate	Nong Son formation – Upper Subformation	Mesozoic	No	No
149	107° 48' 36.791" E	15° 50' 37.954" N	799	309	0.17	Debris Slide	W3S	No	Sandstone, siltstone, conglomerate	Nong Son formation – Upper Subformation	Mesozoic	No	No
150	107° 50' 30.272" E	15° 51' 42.777" N	428	557	0.21	Rotational Slide	S67E	No	Sandstone, siltstone, conglomerate	Nong Son formation – Upper Subformation	Mesozoic	No	No
151	107° 50' 14.622" E	15° 51' 30.210" N	568	402	0.24	Rotational Slide	S50E	No	Sandstone, siltstone, conglomerate	Nong Son formation – Upper Subformation	Mesozoic	No	No
152	107° 50' 4.425" E	15° 51' 12.252" N	207	290	0.06	Rotational Slide	S51E	No	Sandstone, siltstone, conglomerate	Nong Son formation – Upper Subformation	Mesozoic	No	No
153	107° 50' 3.125" E	15° 50' 26.592" N	686	240	0.18	Debris Flow	S40E	No	Sandstone, siltstone, conglomerate	Nong Son formation – Upper Subformation	Mesozoic	No	No
154	107° 50' 12.464" E	15° 50' 21.005" N	590	240	0.17	Debris Flow	W65S	No	Sandstone, siltstone, conglomerate	Nong Son formation – Upper Subformation	Mesozoic	No	No

(1)	(2)	(3)	(4)	(5)	(6)	(7)	(8)	(9)	(10)	(11)	(12)	(13)	(14)
155	107° 51' 17.761" E	15° 50' 45.765" N	808	379	0.31	Rotational Slide	S45E	No	Sandstone, siltstone, conglomerate	Nong Son formation – Upper Subformation	Mesozoic	No	No
156	107° 50' 55.256" E	15° 50' 0.848" N	537	563	0.27	Rotational Slide	W18S	No	Sandstone, siltstone, conglomerate	Nong Son formation – Upper Subformation	Mesozoic	No	No
157	107° 51' 8.815" E	15° 49' 46.221" N	632	711	0.39	Rotational Slide	W81S	No	Conglomerate, sandstone, siltstone	Nong Son formation – Lower Subformation	Mesozoic	No	No
158	107° 51' 18.837" E	15° 49' 59.395" N	306	340	0.08	Rotational Slide	E7.64N	No	Sandstone, siltstone, conglomerate	Nong Son formation – Upper Subformation	Mesozoic	No	No
159	107° 45' 24.940" E	15° 48' 45.144" N	178	125	0.01	Rotational Slide	N40W	Yes	Conglomerate, sandstone, siltstone	Ban Co formation	Mesozoic	Yes	No
160	107° 45' 28.225" E	15° 48' 46.728" N	141	97	0.02	Rotational Slide	N25W	Yes	Conglomerate, sandstone, siltstone	Ban Co formation	Mesozoic	Yes	No
161	107° 45' 41.000" E	15° 48' 48.547" N	547	498	0.22	Rotational Slide	N36W	Yes	Conglomerate, sandstone, siltstone	Ban Co formation	Mesozoic	Yes	No
162	107° 45' 59.641" E	15° 48' 49.061" N	749	585	0.34	Translational Slide	N18W	Yes	Conglomerate, sandstone, siltstone	Ban Co formation	Mesozoic	Yes	No
163	107° 46' 22.418" E	15° 48' 28.503" N	1345	867	1.17	Translational Slide	N15W	Yes	Conglomerate, sandstone, siltstone	Ban Co formation	Mesozoic	Yes	No
164	107° 46' 19.535" E	15° 48' 42.098" N	1110	755	0.81	Translational Slide	N16W	Yes	Conglomerate, sandstone, siltstone	Ban Co formation	Mesozoic	Yes	No
165	107° 46' 9.889" E	15° 48' 57.550" N	372	307	0.10	Rotational Slide	N3W	Yes	Conglomerate, sandstone, siltstone	Ban Co formation	Mesozoic	Yes	No
166	107° 46' 28.871" E	15° 48' 45.509" N	837	494	0.20	Rotational Slide	N6W	Yes	Conglomerate, sandstone, siltstone	Ban Co formation	Mesozoic	Yes	No
167	107° 46' 30.477" E	15° 48' 50.779" N	649	135	0.13	Debris Slide	N5W	Yes	Conglomerate, sandstone, siltstone	Ban Co formation	Mesozoic	Yes	No
168	107° 46' 46.030" E	15° 48' 58.156" N	461	328	0.15	Rotational Slide	N20W	Yes	Conglomerate, sandstone, siltstone	Ban Co formation	Mesozoic	Yes	No
169	107° 46' 41.009" E	15° 48' 51.306" N	593	534	0.31	Translational Slide	N19W	Yes	Conglomerate, sandstone, siltstone	Ban Co formation	Mesozoic	No	No
170	107° 46' 52.117" E	15° 48' 47.284" N	1049	605	0.63	Translational Slide	N19W	Yes	Conglomerate, sandstone, siltstone	Ban Co formation	Mesozoic	No	No
171	107° 46' 58.395" E	15° 48' 24.723" N	1672	598	1.00	Translational Slide	N21W	Yes	Conglomerate, sandstone, siltstone	Ban Co formation	Mesozoic	No	No
172	107° 45' 34.964" E	15° 47' 49.933" N	291	178	0.05	Rotational Slide	W74S	No	Siltstone, sandstone	Huu Chanh formation	Mesozoic	No	No
173	107° 45' 40.448" E	15° 47' 46.162" N	942	317	0.29	Debris flow	W18.68S	No	Siltstone, sandstone	Huu Chanh formation	Mesozoic	No	No
174	107° 51' 44.558" E	15° 47' 43.660" N	784	592	0.50	Rotational Slide	S44E	No	Sandstone, siltstone, conglomerate	Nong Son formation – Upper Subformation	Mesozoic	No	No
175	107° 52' 20.458" E	15° 48' 17.828" N	686	593	0.34	Rotational Slide	S54E	No	Sandstone, siltstone, conglomerate	Nong Son formation – Upper Subformation	Mesozoic	No	No
176	107° 47' 0.204" E	15° 47' 17.207" N	285	537	0.15	Translational Slide	S0.5E	No	Siltstone, sandstone	Huu Chanh formation	Mesozoic	No	No
177	107° 46' 44.536" E	15° 47' 10.680" N	656	235	0.15	Rotational Slide	S11.5E	No	Siltstone, sandstone	Huu Chanh formation	Mesozoic	No	No
178	107° 46' 52.905" E	15° 47' 0.120" N	526	216	0.12	Rotational Slide	W52.6S	No	Siltstone, sandstone	Huu Chanh formation	Mesozoic	No	No
179	107° 46' 35.299" E	15° 47' 3.233" N	472	180	0.09	Rotational Slide	S36E	No	Siltstone, sandstone	Huu Chanh formation	Mesozoic	No	No
180	107° 46' 31.684" E	15° 46' 55.010" N	206	247	0.02	Rotational Slide	S87E	No	Siltstone, sandstone	Huu Chanh formation	Mesozoic	No	No
181	107° 46' 18.165" E	15° 46' 54.582" N	349	80	0.04	Rotational Slide	W0.5S	No	Siltstone, sandstone	Huu Chanh formation	Mesozoic	No	No
182	107° 46' 20.589" E	15° 46' 42.090" N	360	150	0.05	Debris flow	W43.41S	No	Siltstone, sandstone	Huu Chanh formation	Mesozoic	No	No
183	107° 46' 10.646" E	15° 46' 38.416" N	222	169	0.03	Rotational Slide	S60.87E	No	Siltstone, sandstone	Huu Chanh formation	Mesozoic	No	No
184	107° 46' 7.621" E	15° 46' 27.093" N	132	202	0.02	Translational Slide	W81.5S	No	Siltstone, sandstone	Huu Chanh formation	Mesozoic	No	No
185	107° 46' 19.688" E	15° 46' 31.526" N	524	167	0.10	Debris flow	W36.78S	No	Siltstone, sandstone	Huu Chanh formation	Mesozoic	No	No
186	107° 47' 28.703" E	15° 46' 36.752" N	217	208	0.04	Translational Slide	W17.22S	No	Siltstone, sandstone	Khe Ren formation	Mesozoic	No	No
187	107° 47' 50.066" E	15° 46' 36.403" N	212	143	0.03	Translational Slide	S48.7E	No	Siltstone, sandstone	Khe Ren formation	Mesozoic	No	No
188	107° 47' 32.085" E	15° 46' 25.473" N	178	104	0.02	Rotational Slide	E8.75N	No	Siltstone, sandstone	Khe Ren formation	Mesozoic	No	No
189	107° 47' 37.474" E	15° 46' 10.769" N	225	333	0.07	Rotational Slide	E15N	Yes	Conglomerate, sandstone, siltstone	Ban Co formation	Mesozoic	No	No
190	107° 47' 42.982" E	15° 46' 13.777" N	238	308	0.06	Rotational Slide	W21S	Yes	Conglomerate, sandstone, siltstone	Ban Co formation	Mesozoic	No	No
191	107° 48' 24.779" E	15° 46' 5.559" N	302	319	0.08	Rotational Slide	E15.47N	Yes	Sandstone, siltstone, conglomerate	Nong Son formation – Upper Subformation	Mesozoic	No	No
192	107° 48' 37.494" E	15° 45' 45.719" N	293	137	0.04	Rotational Slide	E41.4N	Yes	Sandstone, siltstone, conglomerate	Nong Son formation – Upper Subformation	Mesozoic	No	No

(1)	(2)	(3)	(4)	(5)	(6)	(7)	(8)	(9)	(10)	(11)	(12)	(13)	(14)
193	107° 48' 4.176" E	15° 45' 44.105" N	1249	400	0.24	Compound slide	N40W	Yes	Sandstone, siltstone, conglomerate	Nong Son formation – Upper Subformation	Mesozoic	No	No
194	107° 47' 54.160" E	15° 45' 50.172" N	230	302	0.06	Rotational Slide	E51N	No	Conglomerate, sandstone, siltstone	Ban Co formation	Mesozoic	No	No
195	107° 47' 41.439" E	15° 45' 43.383" N	1426	1027	1.28	Debris Slide	N7W	Yes	Conglomerate, sandstone, siltstone	Ban Co formation	Mesozoic	No	No
196	107° 47' 18.458" E	15° 45' 58.712" N	750	615	0.44	Debris Slide	E76N	Yes	Conglomerate, sandstone, siltstone	Ban Co formation	Mesozoic	No	No
197	107° 46' 53.873" E	15° 45' 59.374" N	552	682	0.33	Debris Slide	E59N	Yes	Siltstone, sandstone	Khe Ren formation	Mesozoic	No	No
198	107° 46' 51.465" E	15° 45' 48.437" N	1310	2155	1.30	Debris Slide	E88N	Yes	Conglomerate, sandstone, siltstone	Ban Co formation	Mesozoic	No	No
199	107° 46' 21.466" E	15° 45' 48.761" N	1292	561	0.64	Debris Slide	N26W	Yes	Siltstone, sandstone	Khe Ren formation	Mesozoic	No	No
200	107° 46' 11.599" E	15° 45' 33.279" N	962	352	0.35	Debris Slide	N16W	Yes	Conglomerate, sandstone, siltstone	Ban Co formation	Mesozoic	No	No
201	107° 45' 38.060" E	15° 45' 31.308" N	461	443	0.18	Debris Slide	N70W	Yes	Conglomerate, sandstone, siltstone	Ban Co formation	Mesozoic	No	No
202	107° 45' 30.800" E	15° 45' 19.508" N	406	426	0.15	Debris Slide	N76W	Yes	Conglomerate, sandstone, siltstone	Ban Co formation	Mesozoic	No	No
203	107° 45' 19.840" E	15° 45' 11.333" N	181	231	0.04	Debris Slide	N52W	Yes	Conglomerate, sandstone, siltstone	Ban Co formation	Mesozoic	No	No
204	107° 46' 43.311" E	15° 45' 15.285" N	466	518	0.21	Debris Slide	W73S	No	Sandstone, siltstone, conglomerate	Nong Son formation – Upper Subformation	Mesozoic	No	No
205	107° 46' 14.945" E	15° 44' 42.593" N	660	1102	0.59	Debris Slide	S20E	Yes	Sandstone, siltstone, conglomerate	Nong Son formation – Upper Subformation	Mesozoic	No	No
206	107° 46' 44.033" E	15° 44' 50.769" N	833	610	0.55	Debris Slide	S19E	Yes	Sandstone, siltstone, conglomerate	Nong Son formation – Upper Subformation	Mesozoic	No	No
207	107° 47' 1.071" E	15° 44' 55.176" N	857	510	0.46	Debris Slide	S18E	Yes	Sandstone, siltstone, conglomerate	Nong Son formation – Upper Subformation	Mesozoic	No	No
208	107° 47' 18.523" E	15° 44' 47.901" N	852	724	0.51	Debris Slide	S9E	Yes	Sandstone, siltstone, conglomerate	Nong Son formation – Upper Subformation	Mesozoic	No	No
209	107° 47' 18.806" E	15° 45' 11.495" N	520	246	0.28	Debris Slide	W86S	No	Sandstone, siltstone, conglomerate	Nong Son formation – Upper Subformation	Mesozoic	No	No
210	107° 47' 42.582" E	15° 44' 52.066" N	799	756	0.48	Debris Slide	S17E	Yes	Sandstone, siltstone, conglomerate	Nong Son formation – Upper Subformation	Mesozoic	No	No
211	107° 47' 47.613" E	15° 45' 7.748" N	361	428	0.13	Debris Slide	S34E	No	Sandstone, siltstone, conglomerate	Nong Son formation – Upper Subformation	Mesozoic	No	No
212	107° 47' 59.893" E	15° 45' 8.572" N	505	213	0.09	Debris Slide	S47E	No	Sandstone, siltstone, conglomerate	Nong Son formation – Upper Subformation	Mesozoic	No	No
213	107° 48' 14.839" E	15° 45' 6.878" N	1077	341	0.41	Debris Slide	S15E	Yes	Sandstone, siltstone, conglomerate	Nong Son formation – Upper Subformation	Mesozoic	No	No
214	107° 48' 45.571" E	15° 45' 17.617" N	1207	255	0.42	Debris Slide	S82E	Yes	Sandstone, siltstone, conglomerate	Nong Son formation – Upper Subformation	Mesozoic	No	No
215	107° 48' 37.791" E	15° 45' 25.517" N	212	205	0.04	Debris Slide	S31E	No	Sandstone, siltstone, conglomerate	Nong Son formation – Upper Subformation	Mesozoic	No	No
216	107° 52' 18.907" E	15° 46' 30.376" N	468	270	0.11	Rotational Slide	S80E	No	Conglomerate, sandstone, siltstone	Nong Son formation – Lower Subformation	Mesozoic	No	No
217	107° 52' 11.993" E	15° 46' 24.346" N	169	181	0.03	Rotational Slide	S74E	No	Conglomerate, sandstone, siltstone	Nong Son formation – Lower Subformation	Mesozoic	No	No
218	107° 52' 17.873" E	15° 46' 12.175" N	441	510	0.20	Rotational Slide	N26W	No	Conglomerate, sandstone, siltstone	Nong Son formation – Lower Subformation	Mesozoic	No	No
219	107° 51' 39.803" E	15° 46' 17.187" N	254	303	0.07	Rotational Slide	E60N	No	Biotit schist, Biotit gneiss	Kham Duc formation - Middle Subformation	Mesozoic	No	No
220	107° 50' 48.873" E	15° 45' 40.228" N	695	269	0.18	Rotational Slide	S59E	No	Biotit schist, Biotit gneiss	Kham Duc formation - Middle Subformation	Mesozoic	No	No
221	107° 50' 49.633" E	15° 45' 30.834" N	441	93	0.03	Debris Slide	S64E	No	Biotit schist, Biotit gneiss	Kham Duc formation - Middle Subformation	Mesozoic	No	No
222	107° 50' 40.918" E	15° 45' 27.712" N	400	215	0.07	Debris Slide	S35E	No	Biotit schist, Biotit gneiss	Kham Duc formation - Middle Subformation	Mesozoic	No	No
223	107° 50' 56.018" E	15° 45' 4.276" N	388	276	0.12	Rotational Slide	E72N	No	Biotit schist, Biotit gneiss	Kham Duc formation - Middle Subformation	Mesozoic	No	No

(1)	(2)	(3)	(4)	(5)	(6)	(7)	(8)	(9)	(10)	(11)	(12)	(13)	(14)
224	107° 50' 42.440" E	15° 45' 4.141" N	329	143	0.06	Debris Slide	E60N	No	Biotit schist, Biotit gneiss	Kham Duc formation - Middle Subformation	Mesozoic	No	No
225	107° 50' 45.662" E	15° 44' 59.773" N	319	139	0.03	Debris Slide	E90N	No	Biotit schist, Biotit gneiss	Kham Duc formation - Middle Subformation	Mesozoic	No	No
226	107° 50' 31.044" E	15° 44' 51.196" N	325	220	0.07	Debris Slide	W30S	Yes	Biotit schist, Biotit gneiss	Kham Duc formation - Middle Subformation	Mesozoic	No	No
227	107° 50' 35.292" E	15° 44' 45.352" N	372	205	0.07	Debris Slide	W29S	Yes	Biotit schist, Biotit gneiss	Kham Duc formation - Middle Subformation	Mesozoic	No	No
228	107° 52' 25.547" E	15° 44' 37.307" N	600	275	0.17	Debris Slide	W30S	No	Conglomerate, sandstone, siltstone	Nong Son formation – Lower Subformation	Mesozoic	No	No
229	107° 52' 31.375" E	15° 44' 29.364" N	471	274	0.09	Debris Slide	W10S	No	Conglomerate, sandstone, siltstone	Nong Son formation – Lower Subformation	Mesozoic	No	No
230	107° 52' 23.166" E	15° 44' 13.555" N	505	291	0.13	Debris Slide	W37S	Yes	Conglomerate, sandstone, siltstone	Nong Son formation – Lower Subformation	Mesozoic	No	No
231	107° 52' 15.197" E	15° 44' 14.585" N	246	182	0.03	Debris Slide	W50S	Yes	Conglomerate, sandstone, siltstone	Nong Son formation – Lower Subformation	Mesozoic	No	No
232	107° 51' 52.823" E	15° 44' 28.845" N	417	304	0.13	Debris Slide	W50S	No	Conglomerate, sandstone, siltstone	Nong Son formation – Lower Subformation	Mesozoic	No	No
233	107° 52' 3.888" E	15° 43' 43.140" N	255	312	0.07	Rotational Slide	E60N	Yes	Conglomerate, sandstone, siltstone	Nong Son formation – Lower Subformation	Mesozoic	No	No
234	107° 51' 45.024" E	15° 43' 52.307" N	458	358	0.13	Debris Slide	E50N	Yes	Conglomerate, sandstone, siltstone	Nong Son formation - Lower Subformation	Mesozoic	No	No
235	107° 51' 42.136" E	15° 43' 46.197" N	546	389	0.05	Debris Slide	E54N	Yes	Conglomerate, sandstone, siltstone	Nong Son formation – Lower Subformation	Mesozoic	No	No
236	107° 51' 50.170" E	15° 43' 46.607" N	596	487	0.28	Debris Slide	E57N	Yes	Conglomerate, sandstone, siltstone	Nong Son formation – Lower Subformation	Mesozoic	No	No
237	107° 51' 21.732" E	15° 43' 47.347" N	520	289	0.13	Debris Slide	E35N	No	Conglomerate, sandstone, siltstone	Nong Son formation – Lower Subformation	Mesozoic	No	No
238	107° 50' 37.037" E	15° 43' 45.404" N	459	454	0.18	Debris Slide	N2W	Yes	Conglomerate, sandstone, siltstone	Nong Son formation – Lower Subformation	Mesozoic	No	No
239	107° 50' 4.387" E	15° 43' 18.372" N	668	150	0.10	Debris Slide	W11S	Yes	Granite	Cha Val complex – Phase 1	Mesozoic	No	No
240	107° 46' 54.110" E	15° 44' 24.991" N	323	190	0.06	Debris Slide	S44E	Yes	Sandstone, siltstone, conglomerate	Nong Son formation – Upper Subformation	Mesozoic	No	No
241	107° 46' 40.649" E	15° 44' 15.834" N	331	555	0.16	Debris Slide	S38E	Yes	Conglomerate, sandstone, siltstone	Nong Son formation – Lower Subformation	Mesozoic	No	No
242	107° 47' 4.316" E	15° 44' 20.141" N	393	222	0.10	Debris Slide	N51W	Yes	Conglomerate, sandstone, siltstone	Nong Son formation – Lower Subformation	Mesozoic	No	No
243	107° 46' 59.982" E	15° 44' 15.798" N	200	295	0.05	Debris Slide	E71N	Yes	Conglomerate, sandstone, siltstone	Nong Son formation – Lower Subformation	Mesozoic	No	No
244	107° 47' 6.583" E	15° 44' 7.587" N	850	861	0.62	Rotational Slide	N53W	Yes	Conglomerate, sandstone, siltstone	Song Bung formation – Lower Subformation	Mesozoic	No	No
245	107° 47' 37.169" E	15° 43' 57.765" N	504	297	0.16	Debris Slide	S22E	Yes	Conglomerate, sandstone, siltstone	Song Bung formation – Lower Subformation	Mesozoic	No	No
246	107° 47' 34.062" E	15° 43' 46.790" N	668	492	0.31	Debris Slide	S46E	Yes	Conglomerate, sandstone, siltstone	Song Bung formation – Lower Subformation	Mesozoic	No	No
247	107° 47' 6.552" E	15° 43' 45.265" N	238	330	0.06	Rotational Slide	W85S	No	Conglomerate, sandstone, siltstone	Song Bung formation – Lower Subformation	Mesozoic	No	No
248	107° 47' 6.703" E	15° 43' 41.747" N	482	506	0.22	Debris Slide	S23E	No	Conglomerate, sandstone, siltstone	Song Bung formation – Lower Subformation	Mesozoic	No	No
249	107° 47' 6.016" E	15° 43' 29.101" N	185	280	0.05	Rotational Slide	S23E	Yes	Conglomerate, sandstone, siltstone	Song Bung formation – Lower Subformation	Mesozoic	No	No
250	107° 46' 56.460" E	15° 43' 12.375" N	491	157	0.11	Debris Slide	N32W	No	Conglomerate, sandstone, siltstone	Song Bung formation – Lower Subformation	Mesozoic	No	No
251	107° 46' 47.240" E	15° 43' 10.555" N	163	209	0.03	Debris Slide	N31W	No	Conglomerate, sandstone, siltstone	Song Bung formation – Lower Subformation	Mesozoic	No	No
252	107° 46' 43.035" E	15° 43' 7.477" N	130	116	0.01	Debris Slide	N35W	No	Conglomerate, sandstone, siltstone	Song Bung formation – Lower Subformation	Mesozoic	No	No
253	107° 47' 16.537" E	15° 43' 6.932" N	118	171	0.02	Debris Slide	W20S	No	Conglomerate, sandstone, siltstone	Song Bung formation – Lower Subformation	Mesozoic	No	No

(1)	(2)	(3)	(4)	(5)	(6)	(7)	(8)	(9)	(10)	(11)	(12)	(13)	(14)
254	107° 47' 11.338" E	15° 43' 3.170" N	309	358	0.10	Debris Slide	S6E	No	Conglomerate, sandstone, siltstone	Song Bung formation – Lower Subformation	Mesozoic	No	No
255	107° 46' 54.108" E	15° 42' 54.616" N	215	237	0.04	Debris Slide	W41S	No	Conglomerate, sandstone, siltstone	Song Bung formation – Lower Subformation	Mesozoic	No	No
256	107° 46' 57.798" E	15° 42' 48.290" N	175	177	0.03	Debris Slide	W36S	No	Conglomerate, sandstone, siltstone	Song Bung formation – Lower Subformation	Mesozoic	No	No
257	107° 46' 48.205" E	15° 42' 35.121" N	230	342	0.07	Debris Slide	W60S	Yes	Conglomerate, sandstone, siltstone	Song Bung formation – Lower Subformation	Mesozoic	No	No
258	107° 46' 58.714" E	15° 42' 18.603" N	261	257	0.06	Debris Slide	S39E	Yes	Conglomerate, sandstone, siltstone	Song Bung formation – Lower Subformation	Mesozoic	No	No
259	107° 50' 28.377" E	15° 42' 45.858" N	433	497	0.19	Rotational Slide	W39S	Yes	Granite	Cha Val complex – Phase 1	Mesozoic	No	No
260	107° 50' 34.072" E	15° 42' 54.665" N	481	512	0.34	Rotational Slide	W60S	Yes	Granite	Cha Val complex – Phase 1	Mesozoic	No	No
261	107° 50' 40.542" E	15° 42' 34.643" N	416	353	0.15	Debris Slide	W24S	Yes	Granite	Cha Val complex – Phase 1	Mesozoic	No	No
262	107° 50' 49.882" E	15° 42' 49.779" N	424	330	0.14	Rotational Slide	S2E	No	Granite	Cha Val complex – Phase 1	Mesozoic	No	No
263	107° 51' 0.480" E	15° 42' 43.628" N	413	251	0.10	Debris Slide	W63S	No	Granite	Cha Val complex – Phase 1	Mesozoic	No	No
264	107° 51' 51.457" E	15° 42' 2.436" N	1253	545	0.60	Rotational Slide	W2S	No	Conglomerate, sandstone, siltstone	Nong Son formation – Lower Subformation	Mesozoic	No	No
265	107° 51' 57.642" E	15° 42' 10.662" N	232	568	0.12	Debris Slide	W83S	No	Conglomerate, sandstone, siltstone	Nong Son formation – Lower Subformation	Mesozoic	No	No
266	107° 52' 10.039" E	15° 41' 39.787" N	803	613	0.45	Debris Slide	W38S	No	Conglomerate, sandstone, siltstone	Nong Son formation – Lower Subformation	Mesozoic	No	No
267	107° 51' 49.964" E	15° 41' 31.938" N	285	289	0.07	Debris Slide	W81S	No	Conglomerate, sandstone, siltstone	Nong Son formation – Lower Subformation	Mesozoic	No	No
268	107° 47' 35.605" E	15° 42' 11.527" N	677	340	0.21	Translational Slide	N62W	No	Granite	Ben Giang – Que Son complex– Phase 2	Paleozoic	No	No
269	107° 47' 25.261" E	15° 41' 50.748" N	358	421	0.13	Rotational Slide	E88N	Yes	Conglomerate, sandstone, siltstone	Nong Son formation – Lower Subformation	Mesozoic	No	No
270	107° 47' 31.468" E	15° 41' 39.359" N	648	407	0.29	Rotational Slide	E88N	No	Conglomerate, sandstone, siltstone	Nong Son formation – Lower Subformation	Mesozoic	No	No
271	107° 47' 42.739" E	15° 41' 44.600" N	221	355	0.07	Rotational Slide	E81N	No	Conglomerate, sandstone, siltstone	Nong Son formation – Lower Subformation	Mesozoic	No	No
272	107° 48' 25.135" E	15° 41' 46.084" N	340	211	0.07	Debris Slide	W16S	No	Conglomerate, sandstone, siltstone	Nong Son formation – Lower Subformation	Mesozoic	No	No
273	107° 48' 11.835" E	15° 41' 46.738" N	396	360	0.13	Rotational Slide	N90W	No	Conglomerate, sandstone, siltstone	Nong Son formation – Lower Subformation	Mesozoic	No	No
274	107° 47' 56.098" E	15° 41' 47.836" N	199	182	0.04	Debris Slide	N84W	No	Conglomerate, sandstone, siltstone	Nong Son formation – Lower Subformation	Mesozoic	No	No
275	107° 47' 55.114" E	15° 41' 43.507" N	154	97	0.00	Debris Slide	N77W	No	Conglomerate, sandstone, siltstone	Nong Son formation – Lower Subformation	Mesozoic	No	No
276	107° 47' 58.974" E	15° 41' 49.970" N	1536	491	0.60	Debris Slide	N85W	No	Conglomerate, sandstone, siltstone	Nong Son formation – Lower Subformation	Mesozoic	No	No
277	107° 48' 59.035" E	15° 41' 48.734" N	679	293	0.19	Debris Slide	N82W	No	Conglomerate, sandstone, siltstone	Nong Son formation – Lower Subformation	Mesozoic	No	No
278	107° 48' 26.542" E	15° 41' 34.975" N	439	98	0.04	Debris Slide	W35S	No	Conglomerate, sandstone, siltstone	Nong Son formation – Lower Subformation	Mesozoic	No	No
279	107° 48' 33.034" E	15° 41' 30.064" N	407	156	0.06	Debris Slide	W38S	No	Conglomerate, sandstone, siltstone	Nong Son formation – Lower Subformation	Mesozoic	No	No
280	107° 48' 26.554" E	15° 41' 26.631" N	752	382	0.31	Debris Slide	W65S	No	Conglomerate, sandstone, siltstone	Nong Son formation – Lower Subformation	Mesozoic	No	No
281	107° 47' 33.856" E	15° 41' 3.889" N	750	350	0.30	Debris Slide		Yes	Granite	Hai Van complex– Phase 1	Mesozoic	Yes	No
282	107° 47' 45.294" E	15° 41' 13.381" N	450	236	0.11	Debris Slide	W63S	No	Granite	Hai Van complex– Phase 1	Mesozoic	No	No
283	107° 47' 56.186" E	15° 41' 7.967" N	523	175	0.09	Debris Slide	W85S	No	Granite	Hai Van complex– Phase 1	Mesozoic	No	No

(1)	(2)	(3)	(4)	(5)	(6)	(7)	(8)	(9)	(10)	(11)	(12)	(13)	(14)
284	107° 48' 21.533" E	15° 41' 1.274" N	503	194	0.11	Debris Slide	W80S	No	Granite	Hai Van complex– Phase 1	Mesozoic	No	No
285	107° 48' 34.935" E	15° 41' 11.700" N	203	116	0.03	Debris Slide	W75S	No	Granite	Hai Van complex– Phase 1	Mesozoic	No	No
286	107° 48' 50.823" E	15° 41' 12.375" N	1371	291	0.56	Debris Flow	S22E	Yes	Conglomerate, sandstone, siltstone	Nong Son formation – Lower Subformation	Mesozoic	No	No
287	107° 48' 30.394" E	15° 40' 49.997" N	923	640	0.53	Debris Slide	W71S	Yes	Granite	Hai Van complex– Phase 1	Mesozoic	No	No
288	107° 49' 16.361" E	15° 41' 15.427" N	488	400	0.21	Rotational Slide	W87S	No	Conglomerate, sandstone, siltstone	Nong Son formation – Lower Subformation	Mesozoic	No	No
289	107° 49' 15.321" E	15° 41' 5.309" N	521	439	0.17	Rotational Slide	W83S	No	Conglomerate, sandstone, siltstone	Nong Son formation – Lower Subformation	Mesozoic	No	No
290	107° 49' 12.550" E	15° 40' 53.647" N	557	338	0.19	Rotational Slide	W82S	Yes	Conglomerate, sandstone, siltstone	Nong Son formation – Lower Subformation	Mesozoic	No	No
291	107° 48' 45.980" E	15° 40' 38.700" N	577	301	0.21	Debris Slide	N30W	Yes	Conglomerate, sandstone, siltstone	Nong Son formation – Lower Subformation	Mesozoic	No	No
292	107° 49' 12.333" E	15° 40' 28.510" N	304	218	0.06	Rotational Slide	N29W	No	Conglomerate, sandstone, siltstone	Nong Son formation – Lower Subformation	Mesozoic	No	No
293	107° 46' 47.258" E	15° 38' 27.725" N	1445	1339	2.01	Rotational Slide	W9S	No	Schist	A Vuong formation – Lower Subformation	Paleozoic	No	No
294	107° 47' 33.297" E	15° 38' 57.803" N	651	884	0.52	Debris Slide	W86S	No	Schist	A Vuong formation – Lower Subformation	Paleozoic	No	No
295	107° 47' 46.780" E	15° 39' 23.762" N	685	393	0.30	Debris Slide	E56N	No	Granite	Hai Van complex– Phase 1	Mesozoic	No	No
296	107° 48' 1.086" E	15° 38' 47.214" N	389	295	0.11	Debris Slide	S21E	Yes	Granite	Hai Van complex– Phase 1	Mesozoic	No	No
297	107° 47' 57.733" E	15° 38' 35.267" N	421	489	0.16	Debris Slide	N42W	Yes	Schist	A Vuong formation – Lower Subformation	Paleozoic	No	No
298	107° 48' 11.031" E	15° 38' 37.573" N	561	350	0.17	Debris Slide	N32W	Yes	Schist	A Vuong formation – Lower Subformation	Paleozoic	No	No
299	107° 48' 21.173" E	15° 38' 25.232" N	330	195	0.06	Debris Slide	N44W	No	Granite	Ben Giang – Que Son complex– Phase 1	Paleozoic	No	No
300	107° 49' 8.805" E	15° 39' 53.296" N	731	425	0.35	Debris Slide	W29S	No	Conglomerate, sandstone, siltstone	Nong Son formation – Lower Subformation	Mesozoic	No	No
301	107° 48' 50.978" E	15° 39' 38.561" N	486	185	0.08	Debris Slide	N90W	Yes	Granite	Ben Giang – Que Son complex– Phase 1	Paleozoic	No	No
302	107° 48' 55.574" E	15° 39' 26.084" N	327	324	0.10	Rotational Slide	W82S	No	Granite	Ben Giang – Que Son complex– Phase 1	Paleozoic	No	No
303	107° 49' 10.681" E	15° 39' 24.691" N	524	197	0.10	Debris Flow	W45S	No	Granite	Ben Giang – Que Son complex– Phase 1	Paleozoic	No	No
304	107° 49' 12.082" E	15° 39' 12.076" N	715	264	0.17	Debris Flow	W38S	No	Granite	Ben Giang – Que Son complex– Phase 1	Paleozoic	No	No
305	107° 49' 28.539" E	15° 38' 56.538" N	631	258	0.20	Debris Slide	W81S	Yes	Granite	Ben Giang – Que Son complex– Phase 1	Paleozoic	No	No
306	107° 49' 42.362" E	15° 39' 18.044" N	821	597	0.42	Translational Slide	S18E	No	Conglomerate, sandstone, siltstone	Nong Son formation – Lower Subformation	Mesozoic	No	No
307	107° 49' 49.867" E	15° 39' 30.666" N	301	189	0.05	Translational Slide	N60W	No	Conglomerate, sandstone, siltstone	Nong Son formation – Lower Subformation	Mesozoic	No	No
308	107° 49' 59.651" E	15° 39' 36.222" N	410	353	0.12	Debris Slide	S38E	No	Conglomerate, sandstone, siltstone	Nong Son formation – Lower Subformation	Mesozoic	No	No
309	107° 49' 52.679" E	15° 39' 41.967" N	459	401	0.22	Debris Slide	S59E	No	Conglomerate, sandstone, siltstone	Nong Son formation – Lower Subformation	Mesozoic	No	No
310	107° 50' 12.262" E	15° 39' 44.472" N	395	281	0.10	Debris Slide	S21E	No	Conglomerate, sandstone, siltstone	Nong Son formation – Lower Subformation	Mesozoic	No	No
311	107° 50' 1.242" E	15° 39' 50.027" N	578	297	0.19	Debris Slide	S69E	No	Conglomerate, sandstone, siltstone	Nong Son formation – Lower Subformation	Mesozoic	No	No
312	107° 50' 10.192" E	15° 39' 53.502" N	235	250	0.04	Debris Slide	W88S	No	Conglomerate, sandstone, siltstone	Nong Son formation – Lower Subformation	Mesozoic	No	No
313	107° 49' 59.343" E	15° 39' 58.050" N	276	342	0.08	Debris Slide	S3E	No	Conglomerate, sandstone, siltstone	Nong Son formation – Lower Subformation	Mesozoic	No	No

(1)	(2)	(3)	(4)	(5)	(6)	(7)	(8)	(9)	(10)	(11)	(12)	(13)	(14)
314	107° 50' 5.117″ E	15° 39' 46.427″ N	785	728	1.89	Debris Slide	W78S	No	Conglomerate, sandstone, siltstone	Nong Son formation – Lower Subformation	Mesozoic	No	No
315	107° 50' 3.062″ E	15° 39' 12.931″ N	379	632	0.22	Translational Slide	S30E	Yes	Conglomerate, sandstone, siltstone	Nong Son formation – Lower Subformation	Mesozoic	No	No
316	107° 50' 15.075″ E	15° 39' 23.376″ N	661	355	0.22	Debris Slide	S34E	Yes	Conglomerate, sandstone, siltstone	Nong Son formation – Lower Subformation	Mesozoic	No	No
317	107° 50' 29.056″ E	15° 39' 27.121″ N	288	321	0.09	Rotational Slide	S39E	No	Conglomerate, sandstone, siltstone	Nong Son formation – Lower Subformation	Mesozoic	No	No
318	107° 50' 36.137″ E	15° 39' 32.604″ N	150	160	0.03	Rotational Slide	S12E	No	Conglomerate, sandstone, siltstone	Nong Son formation – Lower Subformation	Mesozoic	No	No
319	107° 50' 31.742″ E	15° 39' 36.438″ N	239	204	0.04	Rotational Slide	S14E	No	Conglomerate, sandstone, siltstone	Nong Son formation – Lower Subformation	Mesozoic	No	No
320	107° 50' 39.897″ E	15° 39' 40.957″ N	294	196	0.06	Rotational Slide	S39E	No	Conglomerate, sandstone, siltstone	Nong Son formation – Lower Subformation	Mesozoic	No	No
321	107° 50' 44.827″ E	15° 39' 44.912″ N	214	181	0.04	Rotational Slide	S35E	No	Conglomerate, sandstone, siltstone	Nong Son formation – Lower Subformation	Mesozoic	No	No
322	107° 50' 31.680″ E	15° 39' 14.674″ N	736	242	0.19	Debris Slide	N51W	No	Conglomerate, sandstone, siltstone	Nong Son formation – Lower Subformation	Mesozoic	No	No
323	107° 50' 18.681″ E	15° 39' 11.994″ N	193	365	0.07	Debris Slide	N25W	Yes	Conglomerate, sandstone, siltstone	Nong Son formation – Lower Subformation	Mesozoic	No	No
324	107° 50' 26.474″ E	15° 39' 5.741″ N	779	366	0.29	Debris Slide	N57W	Yes	Conglomerate, sandstone, siltstone	Nong Son formation – Lower Subformation	Mesozoic	No	No
325	107° 50' 8.342″ E	15° 39' 4.131″ N	382	333	0.12	Debris Slide	N43W	Yes	Granite	Ben Giang – Que Son complex– Phase 1	Paleozoic	No	No
326	107° 50' 0.048″ E	15° 39' 0.539″ N	315	216	0.06	Debris Slide	N55W	Yes	Granite	Ben Giang – Que Son complex– Phase 1	Paleozoic	No	No
327	107° 49' 51.279″ E	15° 38' 51.101″ N	356	302	0.10	Rotational Slide	W18S	Yes	Granite	Ben Giang – Que Son complex– Phase 1	Paleozoic	No	No
328	107° 49' 58.818″ E	15° 38' 37.645″ N	801	1113	0.76	Rotational Slide	S17E	Yes	Granite	Ben Giang – Que Son complex– Phase 1	Paleozoic	No	No
329	107° 50' 27.348″ E	15° 38' 37.000″ N	588	695	0.46	Rotational Slide	S15E	No	Conglomerate, sandstone, siltstone	Nong Son formation – Lower Subformation	Paleozoic	No	No
330	107° 50' 43.566″ E	15° 38' 45.050″ N	692	417	0.28	Rotational Slide	W29S	No	Conglomerate, sandstone, siltstone	Nong Son formation – Lower Subformation	Mesozoic	No	No
331	107° 50' 53.037″ E	15° 38' 58.376″ N	491	306	0.16	Debris Slide	W70S	No	Conglomerate, sandstone, siltstone	Nong Son formation – Lower Subformation	Mesozoic	No	No
332	107° 51' 6.618″ E	15° 38' 37.840″ N	424	323	0.12	Debris Slide	W18S	No	Conglomerate, sandstone, siltstone	Nong Son formation – Lower Subformation	Mesozoic	No	No
333	107° 51' 7.527″ E	15° 38' 45.686″ N	605	538	0.29	Debris Slide	W25S	No	Conglomerate, sandstone, siltstone	Nong Son formation – Lower Subformation	Mesozoic	No	No
334	107° 52' 11.209″ E	15° 39' 56.596″ N	763	477	0.31	Debris Slide	N31W	No	Sandstone, siltstone, conglomerate	Nong Son formation – Upper Subformation	Mesozoic	No	No
335	107° 52' 12.158″ E	15° 39' 31.295″ N	424	503	0.19	Debris Slide	W40S	No	Sandstone, siltstone, conglomerate	Nong Son formation – Upper Subformation	Mesozoic	No	No
336	107° 52' 0.761″ E	15° 39' 25.649″ N	959	573	0.43	Debris Slide	N4W	No	Sandstone, siltstone, conglomerate	Nong Son formation – Upper Subformation	Mesozoic	No	No
337	107° 52' 40.454″ E	15° 39' 20.290″ N	1466	1669	1.96	Debris Slide	N28W	No			Mesozoic	No	No
338	107° 52' 8.610″ E	15° 38' 46.297″ N	1139	636	0.51	Debris Slide	N88W	No	Conglomerate, sandstone, siltstone	Ban Co formation	Mesozoic	No	No
339	107° 52' 5.592″ E	15° 38' 41.562″ N	381	312	0.09	Debris Slide	W3S	No	Conglomerate, sandstone, siltstone	Ban Co formation	Mesozoic	No	No
340	107° 51' 34.338″ E	15° 38' 36.125″ N	956	295	0.30	Debris Slide	W74S	No	Sandstone, siltstone, conglomerate	Nong Son formation – Upper Subformation	Mesozoic	No	No
341	107° 52' 1.680″ E	15° 38' 27.098″ N	441	535	0.16	Debris Slide	W61S	No	Conglomerate, sandstone, siltstone	Ban Co formation	Mesozoic	No	No
342	107° 52' 17.299″ E	15° 38' 23.984″ N	859	441	0.29	Debris Slide	W50S	No	Conglomerate, sandstone, siltstone	Ban Co formation	Mesozoic	No	No
343	107° 52' 21.457″ E	15° 38' 7.638″ N	829	361	0.22	Debris Slide	W10S	No	Conglomerate, sandstone, siltstone	Ban Co formation	Mesozoic	No	No
344	107° 52' 1.354″ E	15° 37' 54.083″ N	787	608	0.52	Debris Slide	W32S	No	Conglomerate, sandstone, siltstone	Ban Co formation	Mesozoic	No	No

(1)	(2)	(3)	(4)	(5)	(6)	(7)	(8)	(9)	(10)	(11)	(12)	(13)	(14)
345	107° 51' 59.861" E	15° 37' 43.819" N	240	129	0.03	Debris Slide	S0E	No	Conglomerate, sandstone, siltstone	Nong Son formation – Lower Subformation	Mesozoic	No	No
346	107° 52' 8.703" E	15° 37' 46.334" N	541	255	0.17	Debris Slide	W25S	No	Conglomerate, sandstone, siltstone	Nong Son formation – Lower Subformation	Mesozoic	No	No
347	107° 52' 13.181" E	15° 38' 10.036" N	1796	958	1.81	Debris Slide	W35S	No	Conglomerate, sandstone, siltstone	Ban Co formation	Mesozoic	No	No
348	107° 52' 14.135" E	15° 37' 28.788" N	645	646	0.49	Translational Slide	W86S	No	Conglomerate, sandstone, siltstone	Nong Son formation – Lower Subformation	Mesozoic	No	No
349	107° 52' 30.783" E	15° 37' 34.162" N	761	344	0.27	Debris Slide	W42S	No	Conglomerate, sandstone, siltstone	Nong Son formation – Lower Subformation	Mesozoic	No	No
350	107° 52' 35.789" E	15° 37' 27.836" N	585	335	0.17	Debris Slide	W25S	No	Conglomerate, sandstone, siltstone	Nong Son formation – Lower Subformation	Mesozoic	No	No
351	107° 52' 7.137" E	15° 37' 17.805" N	318	314	0.09	Debris Slide	E80N	No	Conglomerate, sandstone, siltstone	Nong Son formation – Lower Subformation	Mesozoic	No	No
352	107° 52' 5.545" E	15° 37' 3.636" N	408	143	0.06	Debris Slide	W74S	No	Granite	Ben Giang – Que Son complex– Phase 1	Paleozoic	No	No
353	107° 52' 18.182" E	15° 37' 10.443" N	501	288	0.12	Debris Slide	W76S	No	Conglomerate, sandstone, siltstone	Nong Son formation – Lower Subformation	Mesozoic	No	No
354	107° 52' 25.572" E	15° 37' 2.397" N	151	210	0.03	Rotational Slide	S18E	No	Granite	Ben Giang – Que Son complex– Phase 1	Paleozoic	No	No
355	107° 52' 11.408" E	15° 37' 24.446" N	2433	1491	2.79	Debris Slide	W30S	No	Conglomerate, sandstone, siltstone	Nong Son formation – Lower Subformation	Mesozoic	No	No
356	107° 51' 39.826" E	15° 37' 42.100" N	478	449	0.17	Debris Slide	S2E	No	Sandstone, siltstone, conglomerate	Nong Son formation – Upper Subformation	Mesozoic	No	No
357	107° 52' 21.930" E	15° 36' 52.679" N	333	319	0.08	Debris Slide	W16S	No	Granite	Ben Giang – Que Son complex– Phase 1	Paleozoic	No	No
358	107° 52' 20.498" E	15° 36' 43.833" N	675	338	0.18	Debris Slide	N47W	No	Conglomerate, sandstone, siltstone	Nong Son formation – Lower Subformation	Paleozoic	No	No
359	107° 52' 0.722" E	15° 36' 37.142" N	433	181	0.06	Debris Slide	N25W	No	Granite	Ben Giang – Que Son complex– Phase 1	Paleozoic	No	No
360	107° 51' 46.188" E	15° 36' 48.760" N	489	346	0.15	Rotational Slide	N6W	No	Granite	Ben Giang – Que Son complex– Phase 1	Paleozoic	No	No
361	107° 51' 40.434" E	15° 36' 55.112" N	228	202	0.04	Rotational Slide	E8N	No	Granite	Ben Giang – Que Son complex– Phase 1	Paleozoic	No	No
362	107° 51' 33.316" E	15° 36' 39.814" N	375	294	0.08	Rotational Slide	W9S	No	Granite	Ben Giang – Que Son complex– Phase 1	Paleozoic	No	No
363	107° 51' 21.972" E	15° 37' 7.273" N	365	175	0.06	Rotational Slide	E76N	Yes	Granite	Ben Giang – Que Son complex– Phase 1	Paleozoic	No	No
364	107° 50' 44.380" E	15° 37' 27.390" N	211	178	0.03	Rotational Slide	E88N	Yes	Conglomerate, sandstone, siltstone	Nong Son formation – Lower Subformation	Mesozoic	Yes	No
365	107° 50' 35.521" E	15° 37' 24.881" N	319	240	0.07	Rotational Slide	E78N	No	Conglomerate, sandstone, siltstone	Nong Son formation – Lower Subformation	Mesozoic	No	No
366	107° 50' 28.083" E	15° 37' 20.456" N	307	148	0.04	Rotational Slide	E28N	No	Conglomerate, sandstone, siltstone	Nong Son formation – Lower Subformation	Mesozoic	No	No
367	107° 50' 31.531" E	15° 37' 13.104" N	148	102	0.02	Rotational Slide	W76S	No	Conglomerate, sandstone, siltstone	Nong Son formation – Lower Subformation	Mesozoic	No	No
368	107° 50' 34.227" E	15° 37' 12.251" N	173	65	0.01	Debris Slide	W70S	No	Conglomerate, sandstone, siltstone	Nong Son formation – Lower Subformation	Mesozoic	No	No
369	107° 50' 35.788" E	15° 37' 11.234" N	161	49	0.01	Debris Slide	W65S	No	Conglomerate, sandstone, siltstone	Nong Son formation – Lower Subformation	Mesozoic	No	No
370	107° 50' 37.106" E	15° 37' 9.579" N	129	73	0.01	Debris Slide	W57S	No	Conglomerate, sandstone, siltstone	Nong Son formation – Lower Subformation	Mesozoic	No	No
371	107° 50' 48.875" E	15° 37' 14.218" N	454	482	0.17	Rotational Slide	S75E	Yes	Conglomerate, sandstone, siltstone	Nong Son formation – Lower Subformation	Mesozoic	Yes	No
372	107° 50' 47.031" E	15° 36' 55.012" N	275	132	0.03	Rotational Slide	E9N	No	Granite	Ben Giang – Que Son complex– Phase 1	Paleozoic	Yes	No
373	107° 50' 42.550" E	15° 36' 58.278" N	601	224	0.11	Rotational Slide	E5N	No	Granite	Ben Giang – Que Son complex– Phase 1	Paleozoic	Yes	No
374	107° 50' 32.529" E	15° 37' 3.687" N	338	218	0.05	Rotational Slide	E26N	No	Granite	Ben Giang – Que Son complex– Phase 1	Paleozoic	No	No

(1)	(2)	(3)	(4)	(5)	(6)	(7)	(8)	(9)	(10)	(11)	(12)	(13)	(14)
375	107° 50' 25.946" E	15° 36' 57.551" N	454	276	0.09	Debris Slide	E45N	No	Granite	Ben Giang – Que Son complex– Phase 1	Paleozoic	No	No
376	107° 50' 22.653" E	15° 37' 7.105" N	664	358	0.20	Debris Slide	E1N	No	Granite	Ben Giang – Que Son complex– Phase 1	Paleozoic	No	No
377	107° 50' 8.400" E	15° 37' 16.193" N	290	138	0.04	Rotational Slide	N6W	No	Conglomerate, sandstone, siltstone	Nong Son formation – Lower Subformation	Mesozoic	No	No
378	107° 50' 0.009" E	15° 36' 45.519" N	935	608	0.59	Translational Slide	S23E	No	Granite	Ben Giang – Que Son complex– Phase 1	Paleozoic	No	No
379	107° 50' 43.786" E	15° 36' 48.509" N	230	129	0.03	Translational Slide	S70E	No	Granite	Ben Giang – Que Son complex– Phase 1	Paleozoic	No	No
380	107° 50' 45.687" E	15° 36' 38.179" N	302	159	0.04	Rotational Slide	E8N	No	Granite	Ben Giang – Que Son complex– Phase 1	Paleozoic	No	No
381	107° 50' 39.420" E	15° 36' 44.470" N	809	357	0.23	Translational Slide	S82E	No	Granite	Ben Giang – Que Son complex– Phase 1	Paleozoic	Yes	No
382	107° 50' 57.103" E	15° 36' 28.596" N	339	527	0.14	Translational Slide	S88E	No	Granite	Ben Giang – Que Son complex– Phase 1	Paleozoic	Yes	No
383	107° 50' 43.093" E	15° 36' 19.089" N	256	117	0.03	Debris Slide	W83S	No	Granite	Ben Giang – Que Son complex– Phase 1	Paleozoic	Yes	No
384	107° 50' 39.024" E	15° 36' 23.096" N	355	195	0.06	Translational Slide	W69S	No	Granite	Ben Giang – Que Son complex– Phase 1	Paleozoic	No	No
385	107° 50' 31.747" E	15° 36' 28.716" N	364	375	0.14	Debris Slide	W62S	No	Granite	Ben Giang – Que Son complex– Phase 1	Paleozoic	No	No
386	107° 50' 35.885" E	15° 36' 11.858" N	218	327	0.07	Translational Slide	S43E	Yes	Granite	Ben Giang – Que Son complex– Phase 2	Paleozoic	Yes	No
387	107° 50' 29.677" E	15° 36' 18.942" N	360	334	0.10	Translational Slide	E47N	No	Granite	Ben Giang – Que Son complex– Phase 2	Paleozoic	No	No
388	107° 50' 20.372" E	15° 36' 19.393" N	556	179	0.10	Debris Slide	E59N	No	Granite	Ben Giang – Que Son complex– Phase 2	Paleozoic	No	No
389	107° 50' 17.848" E	15° 36' 24.389" N	398	106	0.04	Debris Slide	E54N	No	Granite	Ben Giang – Que Son complex– Phase 1	Paleozoic	No	No
390	107° 50' 10.419" E	15° 36' 22.905" N	321	176	0.05	Translational Slide	E75N	No	Granite	Ben Giang – Que Son complex– Phase 1	Paleozoic	No	No
391	107° 49' 58.053" E	15° 36' 24.904" N	509	246	0.10	Rotational Slide	E37N	No	Granite	Ben Giang – Que Son complex– Phase 1	Paleozoic	No	No
392	107° 49' 45.437" E	15° 36' 37.748" N	362	119	0.04	Debris Slide	S86E	No	Granite	Ben Giang – Que Son complex– Phase 1	Paleozoic	No	No
393	107° 49' 31.228" E	15° 36' 26.180" N	361	183	0.06	Rotational Slide	E12N	No	Granite	Ben Giang – Que Son complex– Phase 1	Paleozoic	No	No
394	107° 49' 27.016" E	15° 36' 31.792" N	535	205	0.10	Rotational Slide	S85E	No	Granite	Ben Giang – Que Son complex– Phase 1	Paleozoic	No	No
395	107° 49' 7.834" E	15° 36' 35.167" N	635	802	0.44	Translational Slide	S74E	No	Granite	Ben Giang – Que Son complex– Phase 1	Paleozoic	No	No
396	107° 45' 42.282" E	15° 37' 7.577" N	630	341	0.16	Rotational Slide	N90W	No	Schist	A Vuong formation – Lower Subformation	Paleozoic	No	No
397	107° 45' 41.158" E	15° 36' 31.931" N	174	105	0.02	Rotational Slide	E38N	Yes	Schist	A Vuong formation – Lower Subformation	Paleozoic	No	No
398	107° 46' 39.898" E	15° 35' 36.851" N	1076	204	0.20	Debris Slide	W65S	No	Schist	A Vuong formation – Lower Subformation	Paleozoic	No	No
399	107° 46' 46.940" E	15° 35' 34.574" N	1371	193	0.26	Debris Slide	W52S	No	Schist	A Vuong formation – Lower Subformation	Paleozoic	No	No
400	107° 47' 30.827" E	15° 36' 18.428" N	657	280	0.15	Rotational Slide	S89E	No	Schist	A Vuong formation – Lower Subformation	Paleozoic	No	No
401	107° 47' 49.466" E	15° 36' 7.017" N	705	390	0.22	Rotational Slide	E5N	No	Granite	Ben Giang – Que Son complex– Phase 1	Paleozoic	No	No
402	107° 48' 32.471" E	15° 36' 10.047" N	420	195	0.07	Debris Slide	S47E	No	Granite	Ben Giang – Que Son complex– Phase 1	Paleozoic	No	No
403	107° 48' 17.415" E	15° 35' 51.796" N	595	245	0.12	Translational Slide	E1.5N	No	Granite	Ben Giang – Que Son complex– Phase 1	Paleozoic	No	No
404	107° 48' 48.507" E	15° 35' 48.279" N	358	165	0.06	Debris Slide	S15E	No	Granite	Ben Giang – Que Son complex– Phase 1	Paleozoic	No	No

(1)	(2)	(3)	(4)	(5)	(6)	(7)	(8)	(9)	(10)	(11)	(12)	(13)	(14)
405	107° 49' 17.436″ E	15° 35' 43.928″ N	433	276	0.10	Rotational Slide	S50E	No	Granite	Ben Giang – Que Son complex– Phase 2	Paleozoic	No	No
406	107° 49' 42.372″ E	15° 35' 59.935″ N	367	193	0.07	Rotational Slide	S45E	No	Granite	Ben Giang – Que Son complex– Phase 2	Paleozoic	No	No
407	107° 49' 54.234″ E	15° 35' 56.655″ N	461	312	0.13	Translational Slide	S43E	No	Granite	Ben Giang – Que Son complex– Phase 2	Paleozoic	No	No
408	107° 50' 0.449″ E	15° 36' 8.214″ N	269	129	0.11	Debris Slide	S31E	No	Granite	Ben Giang – Que Son complex– Phase 2	Paleozoic	No	No
409	107° 50' 8.251″ E	15° 36' 3.690″ N	311	188	0.05	Rotational Slide	W39S	No	Granite	Ben Giang – Que Son complex– Phase 2	Paleozoic	No	No
410	107° 50' 0.812″ E	15° 35' 47.800″ N	213	124	0.02	Rotational Slide	S64E	No	Granite	Ben Giang – Que Son complex– Phase 2	Paleozoic	No	No
411	107° 50' 12.813″ E	15° 35' 52.387″ N	165	438	0.07	Rotational Slide	W25S	No	Granite	Ben Giang – Que Son complex– Phase 2	Paleozoic	No	No
412	107° 50' 27.126″ E	15° 36' 4.725″ N	375	175	0.06	Rotational Slide	S42E	Yes	Granite	Ben Giang – Que Son complex– Phase 2	Paleozoic	Yes	No
413	107° 50' 23.605″ E	15° 36' 1.264″ N	374	160	0.05	Debris Slide	S68E	Yes	Granite	Ben Giang – Que Son complex– Phase 2	Paleozoic	Yes	No
414	107° 50' 23.862″ E	15° 35' 56.111″ N	327	155	0.05	Debris Slide	E17N	Yes	Granite	Ben Giang – Que Son complex– Phase 2	Paleozoic	Yes	No
415	107° 50' 39.143″ E	15° 36' 2.364″ N	176	165	0.02	Debris Slide	N63W	Yes	Granite	Ben Giang – Que Son complex– Phase 3	Paleozoic	No	No
416	107° 50' 34.710″ E	15° 35' 49.452″ N	318	305	0.08	Debris Slide	N88W	Yes	Granite	Ben Giang – Que Son complex– Phase 3	Paleozoic	No	No
417	107° 51' 33.105″ E	15° 35' 57.704″ N	178	147	0.02	Debris Slide	N26W	No	Granite	Ben Giang – Que Son complex– Phase 3	Paleozoic	No	No
418	107° 52' 21.265″ E	15° 36' 7.896″ N	493	261	0.11	Rotational Slide	S80E	No	Conglomerate, sandstone, siltstone	Nong Son formation – Lower Subformation	Mesozoic	No	No
419	107° 52' 22.764″ E	15° 35' 58.222″ N	287	131	0.03	Debris Slide	S41E	No	Conglomerate, sandstone, siltstone	Nong Son formation – Lower Subformation	Mesozoic	No	No
420	107° 52' 30.685″ E	15° 35' 30.748″ N	257	212	0.05	Rotational Slide	E86N	No	Granite	Ben Giang – Que Son complex– Phase 3	Paleozoic	No	No
421	107° 50' 36.846″ E	15° 35' 37.673″ N	290	172	0.04	Translational Slide	N84W	Yes	Granite	Ben Giang – Que Son complex– Phase 3	Paleozoic	No	No
422	107° 50' 42.086″ E	15° 35' 6.898″ N	233	293	0.06	Rotational Slide	W80S	No	Granite	Ben Giang – Que Son complex– Phase 3	Paleozoic	No	No
423	107° 50' 0.857″ E	15° 35' 39.964″ N	509	209	0.09	Translational Slide	S72E	No	Granite	Ben Giang – Que Son complex– Phase 2	Paleozoic	No	No
424	107° 50' 2.575″ E	15° 35' 25.069″ N	378	579	0.16	Rotational Slide	S59E	Yes	Granite	Ben Giang – Que Son complex– Phase 2	Paleozoic	No	No
425	107° 49' 57.353″ E	15° 35' 16.335″ N	134	161	0.02	Rotational Slide	S47E	No	Granite	Ben Giang – Que Son complex– Phase 2	Paleozoic	No	No
426	107° 49' 39.514″ E	15° 35' 13.100″ N	337	150	0.05	Rotational Slide	E36N	No	Granite	Ben Giang – Que Son complex– Phase 2	Paleozoic	No	No
427	107° 49' 48.748″ E	15° 35' 8.310″ N	523	247	0.11	Rotational Slide	E28N	No	Granite	Ben Giang – Que Son complex– Phase 2	Paleozoic	No	No
428	107° 49' 46.458″ E	15° 35' 0.888″ N	141	65	0.01	Rotational Slide	E41N	No	Granite	Ben Giang – Que Son complex– Phase 2	Paleozoic	No	No
429	107° 49' 54.118″ E	15° 34' 59.767″ N	196	174	0.03	Rotational Slide	S64E	No	Granite	Ben Giang – Que Son complex– Phase 2	Paleozoic	No	No
430	107° 50' 10.947″ E	15° 34' 48.529″ N	326	422	0.11	Rotational Slide	N90W	Yes	Granite	Ben Giang – Que Son complex– Phase 2	Paleozoic	No	No
431	107° 49' 59.228″ E	15° 34' 46.410″ N	226	302	0.07	Rotational Slide	S54E	Yes	Granite	Ben Giang – Que Son complex– Phase 2	Paleozoic	Yes	No
432	107° 49' 49.252″ E	15° 34' 43.413″ N	314	171	0.05	Rotational Slide	S0E	No	Granite	Ben Giang – Que Son complex– Phase 2	Paleozoic	No	No
433	107° 50' 1.279″ E	15° 34' 38.168″ N	248	121	0.03	Rotational Slide	E66N	Yes	Granite	Ben Giang – Que Son complex– Phase 2	Paleozoic	Yes	No
434	107° 50' 4.687″ E	15° 34' 25.470″ N	190	181	0.03	Debris Slide	E9N	No	Granite	Ben Giang – Que Son complex– Phase 2	Paleozoic	No	No

(1)	(2)	(3)	(4)	(5)	(6)	(7)	(8)	(9)	(10)	(11)	(12)	(13)	(14)
435	107° 50' 0.117" E	15° 34' 18.477" N	262	198	0.05	Debris Slide	W84S	Yes	Granite	Ben Giang – Que Son complex– Phase 2	Paleozoic	Yes	No
436	107° 49' 54.283" E	15° 34' 21.952" N	337	179	0.05	Debris Slide	W87S	Yes	Granite	Ben Giang – Que Son complex– Phase 2	Paleozoic	Yes	No
437	107° 49' 48.000" E	15° 34' 23.606" N	416	172	0.07	Debris Slide	S3E	No	Granite	Ben Giang – Que Son complex– Phase 2	Paleozoic	Yes	No
438	107° 49' 28.472" E	15° 34' 35.493" N	255	309	0.07	Rotational Slide	W22S	No	Granite	Ben Giang – Que Son complex– Phase 2	Paleozoic	No	No
439	107° 49' 6.984" E	15° 35' 5.927" N	215	142	0.03	Rotational Slide	W32S	No	Granite	Ben Giang – Que Son complex– Phase 2	Paleozoic	No	No
440	107° 48' 46.067" E	15° 35' 20.344" N	384	229	0.08	Debris Slide	E1N	Yes	Granite	Ben Giang – Que Son complex– Phase 2	Paleozoic	No	No
441	107° 48' 48.738" E	15° 35' 14.528" N	326	145	0.04	Debris Slide	E16N	Yes	Granite	Ben Giang – Que Son complex– Phase 2	Paleozoic	No	No
442	107° 48' 51.541" E	15° 35' 9.523" N	268	159	0.04	Rotational Slide	E25N	No	Granite	Ben Giang – Que Son complex– Phase 2	Paleozoic	No	No
443	107° 48' 36.282" E	15° 35' 8.759" N	172	1155	0.17	Rotational Slide	W17S	No	Granite	Ben Giang – Que Son complex– Phase 2	Paleozoic	No	No
444	107° 48' 29.863" E	15° 35' 14.341" N	262	1146	0.24	Rotational Slide	E17N	No	Granite	Ben Giang – Que Son complex– Phase 2	Paleozoic	No	No
445	107° 48' 10.467" E	15° 35' 6.317" N	339	166	0.06	Debris Slide	S32E	No	Granite	Ben Giang – Que Son complex– Phase 1	Paleozoic	No	No
446	107° 47' 57.689" E	15° 35' 14.614" N	1449	367	0.48	Debris Slide	S21E	No	Granite	Ben Giang – Que Son complex– Phase 1	Paleozoic	No	No
447	107° 48' 10.753" E	15° 34' 51.725" N	331	209	0.06	Debris Slide	S10E	Yes	Schist	A Vuong formation – Lower Subformation	Paleozoic	No	No
448	107° 48' 58.779" E	15° 34' 40.890" N	245	115	0.03	Debris Slide	N44W	No	Granite	Ben Giang – Que Son complex– Phase 2	Paleozoic	No	No
449	107° 48' 29.742" E	15° 34' 39.555" N	278	144	0.04	Rotational Slide	E64N	No	Schist	A Vuong formation – Lower Subformation	Paleozoic	No	No
450	107° 48' 18.286" E	15° 34' 42.162" N	224	164	0.03	Rotational Slide	N7W	Yes	Granite	Ben Giang – Que Son complex– Phase 2	Paleozoic	No	No
451	107° 48' 49.348" E	15° 34' 50.330" N	229	165	0.14	Debris Slide	N4W	Yes	Schist	A Vuong formation – Lower Subformation	Paleozoic	No	No
452	107° 46' 37.576" E	15° 34' 47.761" N	550	643	0.26	Rotational Slide	E30N	No	Schist	A Vuong formation – Lower Subformation	Paleozoic	No	No
453	107° 46' 28.334" E	15° 34' 40.694" N	186	197	0.03	Rotational Slide	E22N	No	Sandstone, Schist	A Vuong formation – Middle Subformation	Paleozoic	No	No
454	107° 46' 10.645" E	15° 34' 44.069" N	828	461	0.33	Rotational Slide	E81N	No	Sandstone, Schist	A Vuong formation – Middle Subformation	Paleozoic	No	No
455	107° 47' 27.976" E	15° 34' 13.092" N	301	115	0.03	Debris Slide	S11E	No	Biotit schist, Biotit gneiss	Kham Duc formation - Middle Subformation	Precambrian	No	No
456	107° 47' 31.593" E	15° 34' 11.739" N	253	115	0.03	Debris Slide	W89S	No	Biotit schist, Biotit gneiss	Kham Duc formation - Middle Subformation	Precambrian	No	No
457	107° 47' 41.041" E	15° 33' 59.331" N	407	208	0.09	Rotational Slide	S7E	No	Biotit schist, Biotit gneiss	Kham Duc formation - Middle Subformation	Precambrian	No	No
458	107° 48' 6.293" E	15° 33' 49.812" N	351	186	0.07	Rotational Slide	W64S	No	Biotit schist, Biotit gneiss	Kham Duc formation - Middle Subformation	Precambrian	No	No
459	107° 48' 28.434" E	15° 33' 50.410" N	363	245	0.10	Rotational Slide	E39N	No	Biotit schist, Biotit gneiss	Kham Duc formation - Middle Subformation	Precambrian	No	No
460	107° 49' 15.904" E	15° 34' 20.545" N	282	158	0.04	Debris Slide	E47N	No	Schist	A Vuong formation – Lower Subformation	Paleozoic	No	No
461	107° 49' 16.729" E	15° 34' 7.429" N	178	71	0.01	Debris Slide	S57E	Yes	Schist	A Vuong formation – Lower Subformation	Paleozoic	Yes	No
462	107° 49' 12.975" E	15° 33' 57.085" N	282	138	0.04	Debris Slide	S60E	Yes	Schist	A Vuong formation – Lower Subformation	Paleozoic	Yes	No
463	107° 49' 12.439" E	15° 33' 49.309" N	209	68	0.01	Debris Slide	S83E	Yes	Schist	A Vuong formation – Lower Subformation	Paleozoic	Yes	No

(1)	(2)	(3)	(4)	(5)	(6)	(7)	(8)	(9)	(10)	(11)	(12)	(13)	(14)
464	107° 48' 54,850" E	15° 33' 32,057" N	160	192	0,03	Rotational Slide	W53S	No	Biotit schist, Biotit gneiss	Kham Duc formation - Middle Subformation	Precambrian	No	No
465	107° 49' 1,186" E	15° 33' 38,336" N	203	175	0,04	Rotational Slide	E88N	Yes	Biotit schist, Biotit gneiss	Kham Duc formation - Middle Subformation	Precambrian	No	No
466	107° 49' 7,015" E	15° 33' 36,774" N	258	167	0,04	Rotational Slide	E65N	Yes	Biotit schist, Biotit gneiss	Kham Duc formation - Middle Subformation	Precambrian	No	No
467	107° 49' 11,853" E	15° 33' 33,513" N	292	112	0,03	Debris Slide	N22W	Yes	Biotit schist, Biotit gneiss	Kham Duc formation - Middle Subformation	Precambrian	No	No
468	107° 48' 58,461" E	15° 33' 16,703" N	511	364	0,16	Debris Slide	E73N	No	Biotit schist, Biotit gneiss	Kham Duc formation - Middle Subformation	Precambrian	No	No
469	107° 49' 25,098" E	15° 33' 9,070" N	427	208	0,08	Rotational Slide	E27N	No	Biotit schist, Biotit gneiss	Kham Duc formation - Middle Subformation	Precambrian	No	No
470	107° 49' 36,412" E	15° 33' 12,560" N	289	265	0,04	Rotational Slide	S78E	Yes	Biotit schist, Biotit gneiss	Kham Duc formation - Middle Subformation	Precambrian	Yes	No
471	107° 50' 36,732" E	15° 33' 31,277" N	401	360	0,13	Rotational Slide	W55S	No	Schist	Nui Vu formation – Lower Subformation	Precambrian	No	No
472	107° 50' 54,029" E	15° 33' 22,230" N	378	222	0,09	Rotational Slide	W35S	No	Schist	Nui Vu formation – Lower Subformation	Precambrian	No	No
473	107° 51' 18,549" E	15° 33' 41,594" N	368	106	0,04	Debris Slide	E70N	No	Schist	Nui Vu formation – Lower Subformation	Precambrian	No	No
474	107° 51' 21,551" E	15° 33' 28,431" N	338	135	0,05	Debris Slide	W18S	No	Schist	Nui Vu formation – Lower Subformation	Precambrian	No	No
475	107° 51' 24,497" E	15° 33' 24,410" N	291	120	0,04	Debris Slide	W11S	No	Schist	Nui Vu formation – Lower Subformation	Precambrian	No	No
476	107° 52' 16,806" E	15° 33' 12,318" N	852	887	0,84	Rotational Slide	S8E	No	Schist	Nui Vu formation – Lower Subformation	Precambrian	No	No
477	107° 52' 14,905" E	15° 32' 41,305" N	457	208	0,09	Debris Slide	E45N	No	Granite	Dieng Bong complex	Precambrian	No	No
478	107° 48' 16,524" E	15° 33' 15,179" N	568	992	0,42	Rotational Slide	E46N	No	Biotit schist, Biotit gneiss	Kham Duc formation - Middle Subformation	Precambrian	No	No
479	107° 48' 6,560" E	15° 33' 0,356" N	310	147	0,04	Debris Slide	N19W	No	Biotit schist, Biotit gneiss	Kham Duc formation - Middle Subformation	Precambrian	No	No
480	107° 47' 58,428" E	15° 32' 58,886" N	1165	412	0,46	Debris Slide	E88N	No	Biotit schist, Biotit gneiss	Kham Duc formation - Middle Subformation	Precambrian	No	No
481	107° 47' 54,708" E	15° 33' 15,173" N	800	327	0,23	Debris Slide	E54N	No	Biotit schist, Biotit gneiss	Kham Duc formation - Middle Subformation	Precambrian	No	No
482	107° 47' 44,020" E	15° 33' 22,922" N	615	314	0,17	Debris Slide	E68N	No	Biotit schist, Biotit gneiss	Kham Duc formation - Middle Subformation	Precambrian	No	No
483	107° 47' 34,388" E	15° 33' 34,105" N	425	276	0,11	Translational Slide	S50E	No	Biotit schist, Biotit gneiss	Kham Duc formation - Middle Subformation	Precambrian	No	No
484	107° 47' 32,989" E	15° 33' 24,640" N	575	257	0,16	Rotational Slide	E85N	No	Biotit schist, Biotit gneiss	Kham Duc formation - Middle Subformation	Precambrian	No	No
485	107° 47' 23,667" E	15° 33' 23,322" N	374	238	0,07	Rotational Slide	N2W	No	Biotit schist, Biotit gneiss	Kham Duc formation - Middle Subformation	Precambrian	No	No
486	107° 47' 15,949" E	15° 33' 26,519" N	275	236	0,05	Rotational Slide	N9W	No	Biotit schist, Biotit gneiss	Kham Duc formation - Middle Subformation	Precambrian	No	No
487	107° 47' 12,212" E	15° 33' 19,426" N	245	255	0,06	Rotational Slide	N88W	No	Biotit schist, Biotit gneiss	Kham Duc formation - Middle Subformation	Precambrian	No	No
488	107° 47' 14,187" E	15° 32' 59,850" N	577	324	0,16	Translational Slide	W24S	No	Biotit schist, Biotit gneiss	Kham Duc formation - Middle Subformation	Precambrian	No	No
489	107° 47' 8,586" E	15° 32' 45,647" N	396	227	0,08	Translational Slide	W38S	No	Biotit schist, Biotit gneiss	Kham Duc formation - Middle Subformation	Paleozoic	No	No
490	107° 47' 11,714" E	15° 32' 39,949" N	410	195	0,07	Translational Slide	W36S	No	Biotit schist, Biotit gneiss	Kham Duc formation - Middle Subformation	Precambrian	No	No
491	107° 48' 16,132" E	15° 32' 47,718" N	487	345	0,15	Rotational Slide	E18N	No	Biotit schist, Biotit gneiss	Kham Duc formation - Middle Subformation	Precambrian	No	No

(1)	(2)	(3)	(4)	(5)	(6)	(7)	(8)	(9)	(10)	(11)	(12)	(13)	(14)
492	107° 48' 23,595" E	15° 32' 42,561" N	450	263	0,10	Rotational Slide	E55N	No	Biotit schist, Biotit gneiss	Kham Duc formation - Middle Subformation	Precambrian	No	No
493	107° 48' 53,677" E	15° 32' 25,601" N	216	137	0,03	Rotational Slide	S1E	No	Biotit schist, Biotit gneiss	Kham Duc formation - Middle Subformation	Precambrian	No	No
494	107° 48' 49,158" E	15° 32' 20,183" N	350	484	0,13	Rotational Slide	S84E	No	Biotit schist, Biotit gneiss	Kham Duc formation - Middle Subformation	Precambrian	No	No
495	107° 48' 41,072" E	15° 32' 28,955" N	280	270	0.08	Rotational Slide	E9N	No	Biotit schist, Biotit gneiss	Kham Duc formation - Middle Subformation	Precambrian	No	No
496	107° 48' 29,455" E	15° 32' 23,792" N	370	234	0.08	Rotational Slide	S19E	No	Biotit schist, Biotit gneiss	Kham Duc formation - Middle Subformation	Precambrian	No	No
497	107° 48' 18,602" E	15° 32' 29,388" N	247	243	0,05	Debris Slide	W79S	No	Biotit schist, Biotit gneiss	Kham Duc formation - Middle Subformation	Precambrian	No	No
498	107° 48' 5,249" E	15° 32' 34,175" N	267	154	0,04	Rotational Slide	S41E	No	Biotit schist, Biotit gneiss	Kham Duc formation - Middle Subformation	Precambrian	No	No
499	107° 47' 58,836" E	15° 32' 34,126" N	275	103	0,04	Rotational Slide	S69E	No	Biotit schist, Biotit gneiss	Kham Duc formation - Middle Subformation	Precambrian	No	No
500	107° 47' 32,837" E	15° 32' 31,682" N	665	300	0.16	Debris Slide	W10S	No	Biotit schist, Biotit gneiss	Kham Duc formation - Middle Subformation	Precambrian	No	No
501	107° 47' 41,105" E	15° 32' 24,511" N	785	343	0,21	Debris Slide	W2S	No	Biotit schist, Biotit gneiss	Kham Duc formation - Middle Subformation	Precambrian	No	No
502	107° 47' 26,934" E	15° 32' 12,118" N	703	238	0.15	Debris Slide	W41S	No	Biotit schist, Biotit gneiss	Kham Duc formation - Middle Subformation	Precambrian	No	No
503	107° 47' 27,489" E	15° 32' 3,135" N	1232	349	0,45	Debris Slide	W30S	No	Biotit schist, Biotit gneiss	Kham Duc formation - Middle Subformation	Precambrian	No	No
504	107° 47' 24,549" E	15° 31' 45,668" N	351	178	0.06	Debris Slide	W37S	No	Schist and gneiss	Kham Duc formation - Upper Subformation	Precambrian	No	No
505	107° 47' 55,407" E	15° 32' 2,272" N	621	272	0,17	Debris Slide	S31E	No	Biotit schist, Biotit gneiss	Kham Duc formation - Middle Subformation	Precambrian	No	No
506	107° 48' 0,090" E	15° 32' 10,859" N	907	430	0,44	Debris Slide	W83S	No	Biotit schist, Biotit gneiss	Kham Duc formation - Middle Subformation	Precambrian	No	No
507	107° 48' 14,719" E	15° 32' 15,039" N	287	230	0.05	Rotational Slide	S76E	No	Biotit schist, Biotit gneiss	Kham Duc formation - Middle Subformation	Precambrian	No	No
508	107° 48' 20,674" E	15° 32' 20,311" N	165	183	0.03	Rotational Slide	E37N	No	Biotit schist, Biotit gneiss	Kham Duc formation - Middle Subformation	Precambrian	No	No
509	107° 48' 41,166" E	15° 32' 8,030" N	506	372	0.16	Rotational Slide	E26N	No	Biotit schist, Biotit gneiss	Kham Duc formation - Middle Subformation	Precambrian	No	No
510	107° 48' 50,073" E	15° 31' 58,485" N	579	476	0,25	Rotational Slide	E23N	No	Biotit schist, Biotit gneiss	Kham Duc formation - Middle Subformation	Precambrian	No	No
511	107° 48' 54,480" E	15° 31' 42,423" N	486	385	0,18	Rotational Slide	E10N	No	Biotit schist, Biotit gneiss	Kham Duc formation - Middle Subformation	Precambrian	Yes	No
512	107° 48' 57,836" E	15° 31' 31,254" N	195	112	0.02	Rotational Slide	E50N	No	Biotit schist, Biotit gneiss	Kham Duc formation - Middle Subformation	Precambrian	No	No
513	107° 48' 9,919" E	15° 31' 43,172" N	382	407	0.14	Rotational Slide	W39S	No	Biotit schist, Biotit gneiss	Kham Duc formation - Middle Subformation	Precambrian	No	No
514	107° 48' 18,290" E	15° 31' 33,343" N	390	363	0,12	Rotational Slide	W45S	No	Biotit schist, Biotit gneiss	Kham Duc formation - Middle Subformation	Precambrian	No	No
515	107° 48' 34,783" E	15° 31' 33,713" N	331	174	0,05	Rotational Slide	S77E	No	Biotit schist, Biotit gneiss	Kham Duc formation - Middle Subformation	Precambrian	No	No
516	107° 48' 22,632" E	15° 31' 18,223" N	731	205	0,17	Debris Slide	W75S	No	Biotit schist, Biotit gneiss	Kham Duc formation - Middle Subformation	Precambrian	No	No
517	107° 48' 34,418" E	15° 31' 19,479" N	522	252	0,13	Rotational Slide	S6E	No	Biotit schist, Biotit gneiss	Kham Duc formation - Middle Subformation	Precambrian	No	No
518	107° 48' 41,208" E	15° 31' 22,728" N	255	148	0,03	Rotational Slide	S0E	No	Biotit schist, Biotit gneiss	Kham Duc formation - Middle Subformation	Precambrian	No	No

(1)	(2)	(3)	(4)	(5)	(6)	(7)	(8)	(9)	(10)	(11)	(12)	(13)	(14)
519	107° 48' 53.206″ E	15° 31' 6.341″ N	341	169	0.05	Rotational Slide	E0N	Yes	Biotit schist, Biotit gneiss	Kham Duc formation - Middle Subformation	Precambrian	Yes	No
520	107° 47' 52.368″ E	15° 31' 27.130″ N	875	245	0.21	Debris Slide	S1E	No	Schist and gneiss	Kham Duc formation – Upper Subformation	Precambrian	No	No
521	107° 49' 31.314″ E	15° 32' 22.494″ N	288	201	0.05	Rotational Slide	N60W	Yes	Biotit schist, Biotit gneiss	Kham Duc formation - Middle Subformation	Precambrian	No	No
522	107° 49' 26.401″ E	15° 32' 13.203″ N	238	171	0.03	Rotational Slide	N82W	Yes	Biotit schist, Biotit gneiss	Kham Duc formation - Middle Subformation	Precambrian	No	No
523	107° 49' 25.158″ E	15° 32' 6.925″ N	308	203	0.06	Rotational Slide	W4S	Yes	Biotit schist, Biotit gneiss	Kham Duc formation - Middle Subformation	Precambrian	No	No
524	107° 49' 36.159″ E	15° 32' 9.487″ N	312	155	0.04	Rotational Slide	N40W	Yes	Biotit schist, Biotit gneiss	Kham Duc formation - Middle Subformation	Precambrian	No	No
525	107° 49' 56.835″ E	15° 32' 20.839″ N	252	129	0.03	Debris Slide	N67W	No	Biotit schist, Biotit gneiss	Kham Duc formation - Middle Subformation	Precambrian	No	No
526	107° 50' 2.630″ E	15° 32' 17.122″ N	283	136	0.04	Debris Slide	E74N	No	Biotit schist, Biotit gneiss	Kham Duc formation - Middle Subformation	Precambrian	No	No
527	107° 50' 11.935″ E	15° 32' 15.037″ N	486	339	0.09	Rotational Slide	E87N	No	Biotit schist, Biotit gneiss	Kham Duc formation - Middle Subformation	Precambrian	No	No
528	107° 50' 37.731″ E	15° 32' 11.188″ N	610	169	0.09	Debris Slide	N79W	No	Biotit schist, Biotit gneiss	Kham Duc formation - Middle Subformation	Precambrian	No	No
529	107° 51' 7.683″ E	15° 31' 58.932″ N	357	123	0.04	Debris Slide	N5W	No	Biotit schist, Biotit gneiss	Kham Duc formation - Middle Subformation	Precambrian	No	No
530	107° 51' 11.489″ E	15° 31' 59.768″ N	451	130	0.05	Debris Slide	N27W	No	Biotit schist, Biotit gneiss	Kham Duc formation - Middle Subformation	Precambrian	No	No
531	107° 50' 15.585″ E	15° 31' 52.002″ N	276	196	0.06	Rotational Slide	W39S	No	Biotit schist, Biotit gneiss	Kham Duc formation - Middle Subformation	Precambrian	No	No
532	107° 49' 26.849″ E	15° 31' 24.023″ N	598	220	0.12	Rotational Slide	E0N	Yes	Biotit schist, Biotit gneiss	Kham Duc formation - Middle Subformation	Precambrian	No	No
533	107° 49' 58.966″ E	15° 31' 29.043″ N	451	205	0.09	Rotational Slide	W84S	No	Biotit schist, Biotit gneiss	Kham Duc formation - Middle Subformation	Precambrian	No	No
534	107° 50' 19.142″ E	15° 31' 24.425″ N	327	163	0.05	Rotational Slide	E38N	No	Biotit schist, Biotit gneiss	Kham Duc formation - Middle Subformation	Precambrian	No	No
535	107° 50' 20.425″ E	15° 31' 14.226″ N	118	212	0.03	Rotational Slide	W65S	No	Biotit schist, Biotit gneiss	Kham Duc formation - Middle Subformation	Precambrian	No	No
536	107° 50' 34.012″ E	15° 31' 11.499″ N	137	182	0.02	Rotational Slide	W87S	No	Biotit schist, Biotit gneiss	Kham Duc formation - Middle Subformation	Precambrian	No	No
537	107° 46' 59.030″ E	15° 31' 38.631″ N	491	577	0.27	Rotational Slide	S72E	No	Sandstone, Schist	A Vuong formation – Middle Subformation	Paleozoic	No	No
538	107° 45' 40.862″ E	15° 33' 5.831″ N	996	785	0.70	Rotational Slide	E82N	No	Sandstone, Schist	A Vuong formation – Middle Subformation	Paleozoic	No	No
539	107° 45' 6.886″ E	15° 32' 38.940″ N	2666	1254	1.74	Rotational Slide	N86W	No	Sandstone, Schist	A Vuong formation – Middle Subformation	Paleozoic	No	No
540	107° 45' 35.453″ E	15° 32' 36.575″ N	456	276	0.11	Rotational Slide	N58W	No	Sandstone, Schist	A Vuong formation – Middle Subformation	Paleozoic	No	No
541	107° 46' 19.732″ E	15° 31' 23.491″ N	2238	3127	5.75	Debris Slide	E4N	No	Sandstone, Schist	A Vuong formation – Middle Subformation	Paleozoic	No	No
542	107° 45' 49.298″ E	15° 31' 55.639″ N	1073	332	0.40	Debris Slide	W88S	No	Sandstone, Schist	A Vuong formation – Middle Subformation	Paleozoic	No	No
543	107° 46' 0.079″ E	15° 32' 1.678″ N	881	220	0.18	Debris Slide	W89S	No	Sandstone, Schist	A Vuong formation – Middle Subformation	Paleozoic	No	No
544	107° 46' 6.770″ E	15° 32' 0.117″ N	878	223	0.18	Debris Slide	W87S	No	Sandstone, Schist	A Vuong formation – Middle Subformation	Paleozoic	No	No
545	107° 46' 24.926″ E	15° 32' 5.161″ N	484	193	0.09	Debris Slide	S72E	No	Sandstone, Schist	A Vuong formation – Middle Subformation	Paleozoic	No	No
546	107° 46' 37.821″ E	15° 31' 54.343″ N	682	179	0.11	Debris Slide	S43E	No	Sandstone, Schist	A Vuong formation – Middle Subformation	Paleozoic	No	No

(1)	(2)	(3)	(4)	(5)	(6)	(7)	(8)	(9)	(10)	(11)	(12)	(13)	(14)
547	107° 46' 22.522" E	15° 32' 8.567" N	875	392	0.40	Debris Slide	S69E	No	Sandstone, Schist	A Vuong formation – Middle Subformation	Paleozoic	No	No
548	107° 46' 38.350" E	15° 31' 34.440" N	803	1126	0.80	Debris Slide	S66E	No	Sandstone, Schist	A Vuong formation – Middle Subformation	Paleozoic	No	No
549	107° 46' 4.927" E	15° 31' 17.129" N	1165	420	0.63	Debris Slide	S17E	No	Sandstone, Schist	A Vuong formation – Middle Subformation	Paleozoic	No	No
550	107° 45' 51.240" E	15° 31' 26.269" N	1173	281	0.35	Debris Slide	S18E	No	Sandstone, Schist	A Vuong formation – Middle Subformation	Paleozoic	No	No
551	107° 45' 52.757" E	15° 31' 11.677" N	312	103	0.03	Debris Slide	S65E	No	Sandstone, Schist	A Vuong formation – Middle Subformation	Paleozoic	No	No
552	107° 45' 46.643" E	15° 31' 6.394" N	275	165	0.05	Debris Slide	E0N	No	Sandstone, Schist	A Vuong formation – Middle Subformation	Paleozoic	No	No
553	107° 45' 53.271" E	15° 31' 1.207" N	563	320	0.15	Rotational Slide	E18N	No	Sandstone, Schist	A Vuong formation – Middle Subformation	Paleozoic	No	No
554	107° 46' 4.899" E	15° 30' 48.967" N	870	332	0.28	Rotational Slide	E26N	No	Sandstone, Schist	A Vuong formation – Middle Subformation	Paleozoic	No	No
555	107° 46' 12.646" E	15° 30' 43.470" N	624	289	0.18	Rotational Slide	E58N	No	Sandstone, Schist	A Vuong formation – Middle Subformation	Paleozoic	No	No
556	107° 45' 31.099" E	15° 30' 39.431" N	656	469	0.25	Debris Slide	W4S	No	Sandstone, Schist	A Vuong formation – Middle Subformation	Paleozoic	No	No
557	107° 45' 35.605" E	15° 30' 27.512" N	713	360	0.22	Debris Slide	W14S	No	Sandstone, Schist	A Vuong formation – Middle Subformation	Paleozoic	No	No
558	107° 48' 13.982" E	15° 30' 18.222" N	528	716	0.33	Rotational Slide	E0N	No	Schist and gneiss	Kham Duc formation – Upper Subformation	Precambrian	No	No
559	107° 48' 33.919" E	15° 30' 23.282" N	272	126	0.21	Rotational Slide	E0N	No	Biotit schist, Biotit gneiss	Kham Duc formation – Middle Subformation	Precambrian	No	No
560	107° 50' 38.155" E	15° 30' 31.100" N	478	273	0.11	Debris Slide	N10.3W	No	Biotit schist, Biotit gneiss	Kham Duc formation - Middle Subformation	Precambrian	No	No
561	107° 51' 9.820" E	15° 30' 15.951" N	253	209	0.05	Debris Slide	E0N	No	Biotit schist, Biotit gneiss	Kham Duc formation - Middle Subformation	Precambrian	No	No
562	107° 51' 15.982" E	15° 30' 21.433" N	241	336	0.07	Rotational Slide	E0N	No	Biotit schist, Biotit gneiss	Kham Duc formation - Middle Subformation	Precambrian	No	No
563	107° 51' 26.471" E	15° 30' 20.258" N	272	126	0.03	Rotational Slide	E0N	No	Biotit schist, Biotit gneiss	Kham Duc formation - Middle Subformation	Precambrian	No	No
564	107° 51' 28.253" E	15° 30' 16.277" N	202	161	0.03	Rotational Slide	E0N	No	Biotit schist, Biotit gneiss	Kham Duc formation - Middle Subformation	Precambrian	No	No
565	107° 51' 12.475" E	15° 30' 1.659" N	405	303	0.10	Rotational Slide	S30E	No	Biotit schist, Biotit gneiss	Kham Duc formation - Middle Subformation	Precambrian	No	No
566	107° 50' 0.761" E	15° 30' 10.591" N	291	135	0.03	Debris Slide	N14.03W	No	Biotit schist, Biotit gneiss	Kham Duc formation - Middle Subformation	Precambrian	No	No
567	107° 49' 54.066" E	15° 30' 11.262" N	599	241	0.11	Debris Slide	N30.38W	No	Biotit schist, Biotit gneiss	Kham Duc formation - Middle Subformation	Precambrian	No	No
568	107° 49' 43.675" E	15° 30' 18.079" N	538	320	0.14	Debris Slide	N35.83W	No	Biotit schist, Biotit gneiss	Kham Duc formation - Middle Subformation	Precambrian	No	No
569	107° 49' 35.704" E	15° 30' 14.831" N	437	206	0.11	Debris Slide	N12.09W	No	Biotit schist, Biotit gneiss	Kham Duc formation - Middle Subformation	Precambrian	No	No
570	107° 49' 50.522" E	15° 29' 38.982" N	1025	783	0.73	Debris Slide	W69.1S	Yes	Schist and gneiss	Kham Duc formation – Upper Subformation	Precambrian	No	No
571	107° 49' 29.330" E	15° 29' 46.460" N	584	497	0.27	Rotational Slide	W42.82S	Yes	Schist and gneiss	Kham Duc formation – Upper Subformation	Precambrian	No	No
572	107° 49' 5.525" E	15° 29' 56.523" N	321	332	0.08	Rotational Slide	W33.11S	Yes	Schist and gneiss	Kham Duc formation – Upper Subformation	Precambrian	No	No
573	107° 49' 9.412" E	15° 30' 10.721" N	513	576	0.25	Rotational Slide	N74.22W	Yes	Schist and gneiss	Kham Duc formation – Upper Subformation	Precambrian	No	No
574	107° 48' 53.394" E	15° 29' 55.795" N	443	385	0.15	Rotational Slide	E9.66N	Yes	Gneissogranite	Dai Loc complex – Phase 1	Precambrian	No	No
575	107° 47' 41.870" E	15° 29' 56.275" N	292	167	0.04	Rotational Slide	E57.5N	No	Schist and gneiss	Kham Duc formation – Upper Subformation	Precambrian	No	No

(1)	(2)	(3)	(4)	(5)	(6)	(7)	(8)	(9)	(10)	(11)	(12)	(13)	(14)
576	107° 47' 25.237" E	15° 29' 55.094" N	287	300	0.07	Rotational Slide	N73.05W	No	Schist and gneiss	Kham Duc formation – Upper Subformation	Precambrian	No	No
577	107° 47' 28.822" E	15° 29' 42.573" N	651	426	0.26	Rotational Slide	N63.71W	No	Schist and gneiss	Kham Duc formation – Upper Subformation	Precambrian	No	No
578	107° 46' 41.001" E	15° 29' 44.036" N	826	595	0.39	Rotational Slide	N34.19W	No	Sandstone, Schist	A Vuong formation – Middle Subformation	Paleozoic	No	No
579	107° 45' 57.603" E	15° 29' 31.769" N	347	176	0.05	Debris Slide	E87.4N	No	Sandstone, Schist	A Vuong formation – Middle Subformation	Paleozoic	No	No
580	107° 46' 47.183" E	15° 29' 13.871" N	576	231	0.12	Debris Slide	S2.15E	No	Sandstone, Schist	A Vuong formation – Middle Subformation	Paleozoic	No	No
581	107° 47' 2.843" E	15° 29' 32.954" N	556	337	0.17	Debris Slide	E33.4N	No	Sandstone, Schist	A Vuong formation – Middle Subformation	Paleozoic	No	No
582	107° 47' 17.612" E	15° 29' 28.813" N	475	337	0.16	Rotational Slide	E67.6N	No	Schist and gneiss	Kham Duc formation – Upper Subformation	Precambrian	No	No
583	107° 47' 29.623" E	15° 29' 25.040" N	729	386	0.18	Debris Slide	N33.36W	No	Schist and gneiss	Kham Duc formation – Upper Subformation	Precambrian	No	No
584	107° 48' 9.491" E	15° 29' 30.160" N	561	280	0.12	Debris Slide	N38.5W	No	Schist and gneiss	Kham Duc formation – Upper Subformation	Precambrian	No	No
585	107° 48' 22.184" E	15° 29' 26.773" N	155	246	0.04	Rotational Slide	S48E	No	Schist and gneiss	Kham Duc formation – Upper Subformation	Precambrian	No	No
586	107° 47' 33.165" E	15° 29' 3.486" N	539	289	0.12	Rotational Slide	N79.36W	No	Schist and gneiss	Kham Duc formation – Upper Subformation	Precambrian	No	No
587	107° 48' 41.132" E	15° 29' 4.446" N	415	213	0.07	Debris Slide	E43.69N	No	Schist and gneiss	Kham Duc formation – Upper Subformation	Precambrian	No	No
588	107° 49' 19.676" E	15° 29' 5.837" N	878	400	0.32	Debris Slide	N2.18W	No	Schist and gneiss	Kham Duc formation – Upper Subformation	Precambrian	No	No
589	107° 48' 2.814" E	15° 28' 47.395" N	216	150	0.03	Debris Slide	S43.73E	No	Schist and gneiss	Kham Duc formation – Upper Subformation	Precambrian	No	No
590	107° 46' 31.833" E	15° 28' 19.996" N	652	278	0.15	Debris Slide	W56.51S	No	Sandstone, Schist	A Vuong formation – Middle Subformation	Paleozoic	No	No
591	107° 46' 40.979" E	15° 28' 9.582" N	517	664	0.27	Rotational Slide	W17.2S	No	Sandstone, Schist	A Vuong formation – Middle Subformation	Paleozoic	No	No
592	107° 47' 2.586" E	15° 28' 24.491" N	460	229	0.08	Debris Slide	E1.33N	No	Sandstone, Schist	A Vuong formation – Middle Subformation	Paleozoic	No	No
593	107° 48' 14.076" E	15° 28' 31.049" N	333	151	0.05	Debris Slide	W30.16S	No	Schist and gneiss	Kham Duc formation – Upper Subformation	Precambrian	No	No
594	107° 48' 46.747" E	15° 28' 20.582" N	457	266	0.10	Debris Slide	W30.16S	No	Schist and gneiss	Kham Duc formation – Upper Subformation	Precambrian	No	No
595	107° 49' 9.197" E	15° 28' 13.427" N	556	372	0.18	Rotational Slide	S35.59E	No	Schist and gneiss	Kham Duc formation – Upper Subformation	Precambrian	No	No
596	107° 47' 44.310" E	15° 27' 46.966" N	126	124	0.01	Rotational Slide	N21.42W	No	Schist and gneiss	Kham Duc formation – Upper Subformation	Precambrian	No	No
597	107° 47' 36.992" E	15° 27' 43.422" N	98	70	0.01	Rotational Slide	N50.39W	No	Schist and gneiss	Kham Duc formation – Upper Subformation	Precambrian	No	No
598	107° 50' 3.797" E	15° 27' 36.738" N	320	287	0.08	Debris Slide	N1.1W	Yes	Schist and gneiss	Kham Duc formation – Upper Subformation	Precambrian	No	No
599	107° 49' 54.665" E	15° 27' 25.929" N	465	219	0.09	Debris Slide	W1.94S	Yes	Schist and gneiss	Kham Duc formation – Upper Subformation	Precambrian	No	No
600	107° 52' 8.593" E	15° 27' 42.390" N	538	303	0.16	Rotational Slide	W8S	No	Schist and gneiss	Kham Duc formation – Upper Subformation	Precambrian	No	No
601	107° 52' 2.714" E	15° 27' 31.805" N	251	307	0.07	Rotational Slide	E23.2N	No	Schist and gneiss	Kham Duc formation – Upper Subformation	Precambrian	No	No
602	107° 48' 37.161" E	15° 27' 5.558" N	148	140	0.02	Rotational Slide	W78.44S	Yes	Schist and gneiss	Kham Duc formation – Upper Subformation	Precambrian	No	No
603	107° 48' 44.806" E	15° 26' 58.661" N	271	282	0.07	Rotational Slide	N84.43W	Yes	Schist and gneiss	Kham Duc formation – Upper Subformation	Precambrian	No	No
604	107° 48' 44.145" E	15° 26' 47.316" N	264	382	0.09	Rotational Slide	W5.49S	Yes	Schist and gneiss	Kham Duc formation – Upper Subformation	Precambrian	No	No
605	107° 47' 18.116" E	15° 27' 5.744" N	250	151	0.03	Debris Slide	S27.2E	No	Biotit schist, Biotit gneiss	Kham Duc formation – Middle Subformation	Precambrian	No	No

(1)	(2)	(3)	(4)	(5)	(6)	(7)	(8)	(9)	(10)	(11)	(12)	(13)	(14)
606	107° 47' 4.875" E	15° 27' 7.437" N	280	171	0.04	Debris Slide	W83.19S	No	Biotit schist, Biotit gneiss	Kham Duc formation – Middle Subformation	Precambrian	No	No
607	107° 46' 25.417" E	15° 26' 58.486" N	718	255	0.16	Debris Slide	W64.09S	No	Biotit schist, Biotit gneiss	Kham Duc formation – Middle Subformation	Precambrian	No	No
608	107° 46' 33.442" E	15° 26' 51.471" N	283	109	0.02	Debris Slide	W57.99S	No	Biotit schist, Biotit gneiss	Kham Duc formation – Middle Subformation	Precambrian	No	No
609	107° 45' 12.983" E	15° 26' 34.422" N	234	184	0.04	Rotational Slide	W75.96S	Yes	Biotit schist, Biotit gneiss	Kham Duc formation – Middle Subformation	Precambrian	No	No
610	107° 45' 18.646" E	15° 26' 35.056" N	363	117	0.04	Debris Slide	W75.96S	Yes	Biotit schist, Biotit gneiss	Kham Duc formation – Middle Subformation	Precambrian	No	No
611	107° 45' 22.816" E	15° 26' 35.836" N	384	92	0.04	Debris Slide	W68.01S	Yes	Biotit schist, Biotit gneiss	Kham Duc formation – Middle Subformation	Precambrian	No	No
612	107° 46' 41.006" E	15° 26' 39.143" N	245	285	0.07	Debris Slide	W13.74S	No	Biotit schist, Biotit gneiss	Kham Duc formation – Middle Subformation	Precambrian	No	No
613	107° 47' 11.479" E	15° 26' 42.531" N	1087	517	0.45	Debris Slide	S75.2E	Yes	Biotit schist, Biotit gneiss	Kham Duc formation – Middle Subformation	Precambrian	No	Yes
614	107° 51' 8.280" E	15° 26' 23.733" N	395	234	0.07	Rotational Slide	S2.08E	Yes	Schist and gneiss	Kham Duc formation – Upper Subformation	Precambrian	Yes	No
615	107° 51' 17.580" E	15° 26' 23.274" N	301	230	0.06	Rotational Slide	S15.59E	Yes	Schist and gneiss	Kham Duc formation – Upper Subformation	Precambrian	Yes	No
616	107° 51' 29.930" E	15° 26' 28.527" N	493	283	0.12	Rotational Slide	W87.18S	Yes	Schist and gneiss	Kham Duc formation – Upper Subformation	Precambrian	Yes	No
617	107° 51' 39.571" E	15° 26' 21.280" N	602	388	0.18	Rotational Slide	W89.09S	Yes	Schist and gneiss	Kham Duc formation – Upper Subformation	Precambrian	Yes	No
618	107° 51' 50.078" E	15° 26' 22.063" N	526	283	0.11	Rotational Slide	W79.61S	Yes	Schist and gneiss	Kham Duc formation – Upper Subformation	Precambrian	Yes	No
619	107° 51' 48.938" E	15° 26' 9.706" N	390	345	0.11	Rotational Slide	N20.66W	Yes	Schist and gneiss	Kham Duc formation – Upper Subformation	Precambrian	Yes	No
620	107° 49' 28.020" E	15° 26' 6.629" N	783	836	0.46	Rotational Slide	N24.06W	Yes	Gneissogranite	Chu Lai complex	Precambrian	No	No
621	107° 48' 9.491" E	15° 26' 2.327" N	232	95	0.02	Debris Slide	W76.46S	No	Schist and gneiss	Kham Duc formation – Upper Subformation	Precambrian	Yes	No
622	107° 48' 6.658" E	15° 25' 56.485" N	185	349	0.05	Debris Slide	S41.82E	No	Schist and gneiss	Kham Duc formation – Upper Subformation	Precambrian	Yes	No
623	107° 47' 42.173" E	15° 25' 49.820" N	136	93	0.01	Rotational Slide	E4.48N	No	Basalt	Dai Nga formation	Quaternary	No	No
624	107° 47' 44.905" E	15° 25' 47.097" N	141	107	0.01	Rotational Slide	S80.54E	No	Basalt	Dai Nga formation	Quaternary	No	No
625	107° 47' 35.904" E	15° 25' 39.416" N	444	533	0.21	Rotational Slide	S24.62E	Yes	Basalt	Dai Nga formation	Quaternary	No	No
626	107° 47' 23.090" E	15° 25' 33.705" N	397	415	0.17	Rotational Slide	S22.52E	Yes	Basalt	Dai Nga formation	Quaternary	No	No
627	107° 47' 16.149" E	15° 25' 28.115" N	339	122	0.04	Rotational Slide	S51.47E	Yes	Basalt	Dai Nga formation	Quaternary	No	No
628	107° 47' 3.712" E	15° 25' 25.911" N	115	159	0.02	Rotational Slide	W21.8S	No	Biotit schist, Biotit gneiss	Kham Duc formation – Middle Subformation	Precambrian	Yes	No
629	107° 47' 11.115" E	15° 25' 20.363" N	255	154	0.03	Rotational Slide	S17.65E	Yes	Biotit schist, Biotit gneiss	Kham Duc formation – Middle Subformation	Precambrian	No	No
630	107° 48' 3.579" E	15° 25' 42.128" N	203	267	0.05	Rotational Slide	N20.7W	Yes	Basalt	Dai Nga formation	Quaternary	No	No
631	107° 47' 48.169" E	15° 25' 34.332" N	478	763	0.27	Rotational Slide	N17.86W	Yes	Basalt	Dai Nga formation	Quaternary	No	No
632	107° 47' 32.088" E	15° 25' 27.772" N	330	224	0.06	Rotational Slide	N21.14W	Yes	Basalt	Dai Nga formation	Quaternary	No	No
633	107° 47' 25.009" E	15° 25' 23.520" N	420	298	0.11	Rotational Slide	N56.6W	Yes	Basalt	Dai Nga formation	Quaternary	No	No
634	107° 47' 21.435" E	15° 25' 17.152" N	330	152	0.04	Rotational Slide	N74.52W	Yes	Basalt	Dai Nga formation	Quaternary	No	No
635	107° 47' 22.020" E	15° 25' 8.915" N	375	255	0.08	Rotational Slide	W22.91S	Yes	Basalt	Dai Nga formation	Quaternary	No	No
636	107° 47' 37.456" E	15° 25' 4.680" N	297	501	0.15	Rotational Slide	W84.35S	Yes	Basalt	Dai Nga formation	Quaternary	No	No
637	107° 47' 46.591" E	15° 24' 51.522" N	384	340	0.09	Rotational Slide	W0.68S	Yes	Basalt	Dai Nga formation	Quaternary	No	No
638	107° 47' 37.858" E	15° 24' 44.175" N	2230	272	0.06	Rotational Slide	N34.99W	Yes	Basalt	Dai Nga formation	Quaternary	No	No
639	107° 46' 25.620" E	15° 24' 54.144" N	307	168	0.05	Debris Slide	N21.8W	Yes	Basalt	Dai Nga formation	Quaternary	No	No
640	107° 45' 15.372" E	15° 24' 52.721" N	430	308	0.11	Rotational Slide	N37.9W	No	Schist and gneiss	Kham Duc formation – Upper Subformation	Precambrian	No	No
641	107° 45' 37.881" E	15° 24' 16.911" N	318	206	0.06	Debris Slide	W72.3S	No	Schist and gneiss	Kham Duc formation – Upper Subformation	Precambrian	No	No
642	107° 46' 45.408" E	15° 24' 30.428" N	205	121	0.02	Debris Slide	W14.93S	No	Basalt	Dai Nga formation	Quaternary	No	No
643	107° 47' 8.140" E	15° 24' 26.120" N	175	162	0.02	Debris Slide	S74.58E	Yes	Basalt	Dai Nga formation	Quaternary	No	No
644	107° 47' 14.094" E	15° 24' 28.878" N	168	244	0.04	Rotational Slide	N58.74W	Yes	Basalt	Dai Nga formation	Quaternary	No	No
645	107° 46' 52.140" E	15° 24' 17.444" N	316	218	0.06	Rotational Slide	S30.87E	Yes	Basalt	Dai Nga formation	Quaternary	No	No
646	107° 46' 53.613" E	15° 24' 10.429" N	302	415	0.10	Rotational Slide	N35.6W	Yes	Basalt	Dai Nga formation	Quaternary	No	No

(1)	(2)	(3)	(4)	(5)	(6)	(7)	(8)	(9)	(10)	(11)	(12)	(13)	(14)
647	107° 46' 50.569″ E	15° 23' 51.359″ N	299	360	0.11	Rotational Slide	N66.95W	Yes	Basalt	Dai Nga formation	Quaternary	No	No
648	107° 46' 49.191″ E	15° 23' 41.881″ N	350	295	0.10	Rotational Slide	N79.15W	Yes	Basalt	Dai Nga formation	Quaternary	No	No
649	107° 45' 16.888″ E	15° 23' 38.744″ N	249	172	0.04	Rotational Slide	E80.75N	No	Granite	Hai Van complex – Phase 1	Mesozoic	Yes	No
650	107° 48' 49.935″ E	15° 25' 29.065″ N	337	255	0.08	Rotational Slide	E77.22N	Yes	Biotit schist, Biotit gneiss	Kham Duc formation – Middle Subformation	Precambrian	No	No
651	107° 49' 15.959″ E	15° 25' 35.241″ N	364	205	0.06	Rotational Slide	W13.35S	Yes	Biotit schist, Biotit gneiss	Kham Duc formation – Middle Subformation	Precambrian	No	No
652	107° 49' 14.627″ E	15° 25' 29.582″ N	198	200	0.03	Rotational Slide	W5S	Yes	Biotit schist, Biotit gneiss	Kham Duc formation – Middle Subformation	Precambrian	No	No
653	107° 51' 47.161″ E	15° 25' 35.014″ N	348	213	0.07	Rotational Slide	E72.86N	No	Gneissogranite	Chu Lai complex	Precambrian	No	No
654	107° 51' 59.482″ E	15° 25' 37.195″ N	206	188	0.04	Rotational Slide	E52.3N	Yes	Gneissogranite	Chu Lai complex	Precambrian	No	No
655	107° 52' 5.047″ E	15° 25' 28.011″ N	634	407	0.24	Rotational Slide	E66.8N	Yes	Gneissogranite	Chu Lai complex	Precambrian	No	No
656	107° 52' 16.510″ E	15° 25' 44.728″ N	358	159	0.05	Rotational Slide	N39.29W	No	Gneissogranite	Chu Lai complex	Precambrian	No	No
657	107° 52' 28.508″ E	15° 25' 23.244″ N	335	201	0.06	Rotational Slide	N57.01W	No	Gneissogranite	Chu Lai complex	Precambrian	No	No
658	107° 52' 25.844″ E	15° 25' 14.828″ N	210	287	0.05	Rotational Slide	W77.32S	Yes	Gneissogranite	Chu Lai complex	Precambrian	No	No
659	107° 51' 48.878″ E	15° 25' 16.267″ N	780	353	0.22	Debris Slide	E86.75N	No	Gneissogranite	Chu Lai complex	Precambrian	No	No
660	107° 51' 41.315″ E	15° 25' 18.887″ N	742	321	0.22	Debris Slide	E39N	No	Gneissogranite	Chu Lai complex	Precambrian	No	No
661	107° 52' 33.713″ E	15° 25' 5.458″ N	370	230	0.08	Rotational Slide	N33.15W	Yes	Gneissogranite	Chu Lai complex	Precambrian	No	No
662	107° 52' 25.202″ E	15° 25' 3.023″ N	783	336	0.25	Rotational Slide	N0.6W	Yes	Gneissogranite	Chu Lai complex	Precambrian	No	No
663	107° 51' 12.635″ E	15° 25' 6.262″ N	565	206	0.10	Debris Slide	W32.88S	No	Gneissogranite	Chu Lai complex	Precambrian	No	No
664	107° 50' 57.695″ E	15° 24' 59.685″ N	733	189	0.18	Debris Slide	E47.86N	No	Gneissogranite	Chu Lai complex	Precambrian	No	No
665	107° 51' 24.609″ E	15° 24' 50.977″ N	585	224	0.12	Debris Slide	W5.55S	No	Gneissogranite	Chu Lai complex	Precambrian	No	No
666	107° 51' 31.776″ E	15° 24' 19.368″ N	743	678	0.12	Rotational Slide	S68.71E	No	Biotit schist, Biotit gneiss	Kham Duc formation – Middle Subformation	Precambrian	No	No
667	107° 49' 55.763″ E	15° 25' 3.280″ N	750	282	0.19	Debris Slide	W53.28S	No	Biotit schist, Biotit gneiss	Kham Duc formation – Middle Subformation	Precambrian	No	No
668	107° 49' 27.423″ E	15° 24' 59.271″ N	518	650	0.24	Rotational Slide	W25.94S	Yes	Biotit schist, Biotit gneiss	Kham Duc formation – Middle Subformation	Precambrian	No	No
669	107° 49' 32.643″ E	15° 24' 44.348″ N	230	185	0.03	Rotational Slide	N77.56W	Yes	Biotit schist, Biotit gneiss	Kham Duc formation – Middle Subformation	Precambrian	No	No
670	107° 49' 33.886″ E	15° 24' 39.195″ N	295	203	0.05	Rotational Slide	N87.32W	Yes	Biotit schist, Biotit gneiss	Kham Duc formation – Middle Subformation	Precambrian	No	No
671	107° 49' 42.700″ E	15° 24' 41.683″ N	333	194	0.04	Rotational Slide	W8.97S	No	Biotit schist, Biotit gneiss	Kham Duc formation – Middle Subformation	Precambrian	No	No
672	107° 49' 42.502″ E	15° 24' 29.984″ N	461	333	0.14	Rotational Slide	W43.34S	Yes	Biotit schist, Biotit gneiss	Kham Duc formation – Middle Subformation	Precambrian	No	No
673	107° 50' 8.296″ E	15° 24' 5.583″ N	832	837	0.62	Rotational Slide	W38.78S	Yes	Biotit schist, Biotit gneiss	Kham Duc formation – Middle Subformation	Precambrian	No	No
674	107° 50' 8.444″ E	15° 24' 20.820″ N	193	206	0.03	Rotational Slide	W40.49S	No	Biotit schist, Biotit gneiss	Kham Duc formation – Middle Subformation	Precambrian	No	No
675	107° 50' 20.665″ E	15° 24' 20.369″ N	156	250	0.08	Rotational Slide	S59.98E	No	Schist and gneiss	Kham Duc formation – Upper Subformation	Precambrian	No	No
676	107° 49' 22.754″ E	15° 24' 22.018″ N	743	678	0.49	Rotational Slide	S68.71E	Yes	Biotit schist, Biotit gneiss	Kham Duc formation – Middle Subformation	Precambrian	No	No
677	107° 50' 14.470″ E	15° 23' 1.444″ N	262	276	0.07	Rotational Slide	E90N	No	Biotit schist, Biotit gneiss	Kham Duc formation – Middle Subformation	Precambrian	No	No
678	107° 50' 7.817″ E	15° 22' 52.318″ N	352	615	0.17	Rotational Slide	W6.52S	Yes	Biotit schist, Biotit gneiss	Kham Duc formation – Middle Subformation	Precambrian	No	No
679	107° 50' 32.735″ E	15° 22' 41.944″ N	332	240	0.07	Rotational Slide	N85.49W	No	Biotit schist, Biotit gneiss	Kham Duc formation – Middle Subformation	Precambrian	No	No
680	107° 50' 50.934″ E	15° 22' 29.355″ N	333	248	0.07	Rotational Slide	W30.36S	No	Biotit schist, Biotit gneiss	Kham Duc formation – Middle Subformation	Precambrian	No	No
681	107° 52' 19.188″ E	15° 22' 46.934″ N	279	179	0.04	Rotational Slide	N80W	No	Biotit schist, Biotit gneiss	Kham Duc formation – Middle Subformation	Precambrian	No	No
682	107° 52' 44.221″ E	15° 39' 9.538″ N	361	295	0.09	Debris Slide	N26W	No	Conglomerate, sandstone, siltstone	Ban Co formation	Mesozoic	No	No
683	107° 52' 51.666″ E	15° 39' 18.890″ N	376	208	0.08	Debris Slide	N31W	No	Conglomerate, sandstone, siltstone	Ban Co formation	Mesozoic	No	No
684	107° 53' 22.407″ E	15° 39' 20.452″ N	787	297	0.20	Debris Slide	N2W	No	Conglomerate, sandstone, siltstone	Ban Co formation	Mesozoic	No	No

(1)	(2)	(3)	(4)	(5)	(6)	(7)	(8)	(9)	(10)	(11)	(12)	(13)	(14)
685	107° 53' 5,121" E	15° 39' 31,960" N	709	515	0,36	Rotational Slide	W7S	No	Conglomerate, sandstone, siltstone	Ban Co formation	Mesozoic	No	No